Investigation of the metabolic changes in the haematopoietic stem cell compartment in response to stress

By

Jayna Jaymani Natwarlal Mistry, BSc

A thesis submitted for the degree:

Doctor of Philosophy

Norwich Medical School
Department of Molecular Haematology
The University of East Anglia, Norwich, UK
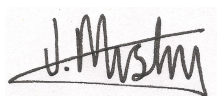
Date of submission: 13th January 2021

Declaration

I declare that the contents of this thesis entitled "Investigation of the metabolic changes in the haematopoietic stem cell compartment in response to stress" was undertaken and completed by myself, unless otherwise acknowledged and has not been submitted in an application for another degree or qualification in this or any other university or institution.

This thesis is approximately 71 000 words in length

Parts of this research have been published prior to submission and is referenced in the List of Publications.

Jayna Jaymani Natwarlal Mistry

Acknowledgement

The long and winding road towards achieving a PhD has been a fun, rewarding and a life-changing experience. There have been a multitude of supportive and inspiring people who have been an instrumental part of my doctoral journey. First and foremost, I would like to express my sincere gratitude to my supervisors, Stuart and Kris, whose expertise and mentorship have been second to none. When I started my PhD journey, I never imagined that I would be so fortunate to have the most supportive and encouraging supervisors. Without their invaluable advice, guidance, enthusiasm and patience, this PhD would not have been achievable. Seriously guys, you rock!

I would also like to thank my secondary supervisor Federica Di Palma for her support and Iain Macaulay for his help facilitating access to the sorter. A special thanks to Naiara Beraza who assisted me with the *Salmonella* work. Importantly, I would like to express thanks to the patients who generously donated research samples and the staff at the NNUH, without who, this study would not have been possible. I would also like to acknowledge the University of East Anglia and the Earlham Institute for the studentship that allowed me to conduct this research.

To my team Charlotte, Jamie, Aisha, Chris, Becky and Adam without whom I would not have been able to complete my PhD. It has been a thoroughly enjoyable experience to be part of this lab group. A special mention to Charlotte for her ongoing friendship, support, endless proofreading and the most fantastic baked goods. I would also like to thank everyone at the BCRE especially Dan, Adam, Martyn and Vaisakh who were always there for a chat and never failed to make me laugh.

To my friends, you have been awesome. To my best friend Alpa for always cheering me on and who, in her own words will always be my hype girl. To the Uni girls; Emma, Danni, Monique and Zoe whose traffic light quotes and jokes care pack got me through writing. To all my Norwich friends, especially Imogen and Mairead whose Friday night drinks, and crazy antics provided a happy distraction from the research. I am grateful for all of you, you really are the best of people.

Finally, to my mum, dad and sister, who have seen me through this long journey- I got there in the end! Thank you for your never-ending love, support and encouragement, I consider myself to be extremely lucky to have you as my family.

Abstract

Haematopoietic stem cells (HSCs) exist in a fine balance between self-renewal and differentiation. The maintenance of this balance is critical for sustaining long term multilineage haematopoietic reconstitution. Quiescent HSCs heavily rely on glycolysis over oxidative phosphorylation (OXPHOS) to produce adenosine triphosphate (ATP). This is thought to be an adaptation to the hypoxic bone marrow (BM) microenvironment and reflects the low metabolic demands of quiescent HSCs, but also may allow for long-term survival. The transition from quiescent to active HSCs is accompanied by a metabolic switch towards OXPHOS which is essential for HSC differentiation. Stress stimuli such as infection initiate rapid expansion and differentiation of HSCs, which requires extensive ATP production. The underlying mechanisms involved in this process remain largely unknown. Here I examine the immuno-metabolic processes which facilitate HSC expansion in response to acute infection.

This research shows that infection drives an increase in mitochondrial mass in HSCs, resulting in a metabolic switch from glycolysis towards OXPHOS. The initial mitochondrial mass increase occurred as a result of mitochondrial transfer from BM stromal cells (BMSCs) to the HSCs. This process was mediated by macrophage derived NADPH oxidase 2 (NOX2) reactive oxygen species facilitating the opening of connexin-43 channels. Moreover, mitochondrial transfer was regulated by activation of phosphoinositide3-kinase and this process occurred before the cells transcriptional program to generate new mitochondria. Furthermore, following infection HSCs also take up free fatty acids (FFA) and subsequently have an increased dependency on β-oxidation. Mechanistically, CD36 upregulation mediates FFA uptake into HSCs, enabling CPT1A to transport fatty acyl chains into the mitochondria. Without uptake of FFA HSC expansion is reduced, leading to increased susceptibility and enhanced mortality in response to infection. Together, these findings provide mechanistic understanding of the interplay between HSCs and the BM microenvironment which supports the metabolic demands of HSCs during pathogenic stress.

Access Condition and Agreement

Table of Contents

9

List of publications and conference papers

First author publications

Mistry, J., Moore, J., Kumar, P., Marlein, C., Hellmich, C., Pillinger, G., Jibril, A., Di Palma, F., Collins, A., Bowles, K. and Rushworth, S. (**2020**). Daratumumab inhibits acute myeloid leukaemia metabolic capacity by blocking mitochondrial transfer from mesenchymal stromal cells. *Haematologica*, pp.haematol.2019.242974.

Mistry, J., Bowles, K. and Rushworth, S. (**2020**). Powering up the emergency response to infections. *TheScienceBreaker* 06(02). Lay Outreach Journal

Mistry, J., Marlein, C., Moore, J., Hellmich, C., Wojtowicz, E., Smith, J., Macaulay, I., Sun, Y., Morfakis, A., Patterson, A., Horton, R., Divekar, D., Morris, C., Haestier, A., Di Palma, F., Beraza, N., Bowles, K. and Rushworth, S. (**2019**). ROS-mediated PI3K activation drives mitochondrial transfer from stromal cells to hematopoietic stem cells in response to infection. *Proceedings of the National Academy of Sciences*, 116(49), pp.24610-24619.

Conference papers

Enhanced Free Fatty Acid Uptake Via CD36 Promotes a Metabolic Switch to B-Oxidation within Hematopoietic Stem Cells in Response to Acute Infection. **Oral presentation. American Society for Haematology Annual Meeting 2020.**

Superoxide drives PI3K kinase mediated mitochondria transfer from the bone marrow microenvironment to hematopoietic stem cells in response to infection. **Oral presentation. 6th conference on mitochondria, apoptosis and cancer 2019, Prague, Czech Republic.**

Investigating the Dual Targeting of BCL-2 and CD38 in Models of Acute Myeloid Leukemia. **Poster presentation. American Society for Haematology Annual Meeting 2020.**

Targeting CD38 inhibits metabolic capacity of acute myeloid leukemia in the tumour microenvironment. **Poster presentation. American Association for Cancer research Annual Meeting 2020.**

Superoxide Drives PI3 Kinase Mediated Mitochondria Transfer from the Bone Marrow Microenvironment to Hematopoietic Stem Cells in Response to Salmonella Typhimurium **Poster presentation. American Society for Haematology Annual Meeting 2019, Orlando, USA.**

Free Fatty Acid Uptake By Hematopoietic Stem and Progenitor Cells Drives Immune Cell Expansion in Response to Salmonella Typhimurium infection. **Poster presentation. American Society for Haematology Annual Meeting 2019, Orlando, USA.**

Daratumumab Inhibits AML Metabolic Capacity and Tumor Growth through Inhibition of CD38 Mediated Mitochondrial Transfer from Bone Marrow Stromal Cells to Blasts in the Leukemic Microenvironment. **Poster presentation. American Society for Haematology Annual Meeting 2019, Orlando, USA.**

Stressed Hematopoiesis Induces Mitochondrial Trafficking to Hematopoietic Stem Cells. **Poster presentation. American Society for Haematology Annual Meeting 2018 San Deigo, USA.**

Other relevant publications

Marlein, C., Piddock, R., **Mistry, J.,** Zaitseva, L., Hellmich, C., Horton, R., Zhou, Z., Auger, M., Bowles, K. and Rushworth, S. (**2019**). CD38-Driven Mitochondrial Trafficking Promotes Bioenergetic Plasticity in Multiple Myeloma**.** *Cancer Research*, 79(9), pp.2285-2297.

Abdul-Aziz, A., Sun, Y., Hellmich, C., Marlein, C., **Mistry, J**., Forde, E., Piddock, R., Shafat, M., Morfakis, A., Mehta, T., Di Palma, F., Macaulay, I., Ingham, C., Haestier, A., Collins, A., Campisi, J., Bowles, K. and Rushworth, S. (**2019**). Acute myeloid leukemia induces protumoral p16INK4a-driven senescence in the bone marrow microenvironment. *Blood*, 133(5), pp.446-456.

List of figures

List of tables

List of abbreviations

Acsl	Acyl CoA synthetase
ALL	Acute lymphoblastic leukaemia
AML	Acute myeloid leukaemia
ATGL	Adipose triglyceride lipase
ATP	Adenosine triphosphate
BM	Bone marrow
BMAT	Bone marrrow adipose tissue
BMDM	BM derived macrophages
BMSC	BM mesenchymal stromal cell
BMSC	Bone marrow stromal cells
BODIPY 493/503	4- difluoro-1,3,5,7,8-pentamethyl-4-bora-3a,4a-diaza-s-indacene
BSA	Bovine serum albumin
BSO	Buthionine sulfoximine
CAR	CXCL12-abundant reticular
CBX	Carbenoxolone
CFC	Colony forming cell
CGD	Chronic granulomatous diseases
CLL	Chronic lymphoblastic leukaemia
CLP	Common lymphoid progenitor
CML	Chronic myeloid leukaemia
CMP	Common myeloid progenitor
CNS	Central nervous system
CoA	Coenzyme A
CPT1	Carnitine palmitoyl transferase 1
CPT2	Carnitine palmitoyl transferase 2
CT	Cycle threshold
CX43	Connexin 43
CXCR4	C-X-C chemokine receptor type 4
CytoB	Cytochalasin B
DCF	2', 7' –dichlorofluorescin
DMEM	Dulbecco's Modified Eagle's Medium
DMSO	Dimethyl sulfoxide
E. coli	*Escherichia coli*
ECAR	Extracellular acidification rates
ECL	Enhanced chemiluminescence
EoBP	Eosinophil-basophil progenitor
ETX	Etomoxir
FA	Fatty acids
FABP	FA binding protein

FACS	Fluorescence activated cell sorting
FADH$_2$	Flavin adenine nucleotide
FAO	Fatty acid β-oxidation
FATP	Fatty acid transport protein
FCS	Foetal calf serum
FFA	Free fatty acids
FLT-3	Flt-3 ligand
FMO	Fluorescence minus one
G-CSF	Granulocyte colony stimulating factor
gDNA	Genomic DNA
GFP	Green fluorescent protein
GM-CSF	Granulocyte-macrophage colony stimulating factor
GMP	Granulocyte-macrophage progenitors
GPX1	Glutathione peroxidase 1
GSH	L-glutathione
HEK	Human embryonic kidney
HPC	Haematopoietic progenitor cells
HRP	Horseradish peroxidase
HSC	Haematopoietic stem cells
HSL	Hormone sensitive lipase
HSPC	Haematopoietic stem and progenitor cells
IL	Interleukin
IL2rg^{nul}	IL2 receptor common gamma chain
IP	Intraperitoneal
IV	Intravenous
LB	Luria Bertani
LIF	Leukaemia inhibitory factor
LIMP II	Lysosomal integral membrane protein II
Lin	Lineage
Lin-	Lineage negative
LK	Lineage negative, CD117+
LMPP	Lymphoid-primed multipotent progenitors
LPS	Lipopolysaccharide
LSC	Leukaemic stem cells
LT-HSC	Long term HSCs
MACS	Magnetic-activated sorting
mCSF	Macrophage colony stimulating factor
MEM	Minimum Essential Medium Eagle
MEP	Megakaryocyte-erythrocyte progenitors
MFI	Mean fluorescence intensity
MM	Multiple myeloma
MPP	Multipotent progenitors

MSCs	Mesenchymal stromal cells
MSL	Monolglyceride lipase
Msr1	Macrophage scavenger receptor 1
mtDNA	Mitochondrial DNA
MTG	Mitotracker Green
NAC	N-acetyl cysteine
NAD	Nicotinamide adenine dinucleotide
NADPH	Nicotinamide adenine dinucleotide phosphate
NK	Natural killer
NOD	Non-obese diabetic
NOX	Nicotinamide adenine dinucleotide phosphate oxidase
NOX2	NADPH oxidase 2
NSG	NOD SCID gamma
OCR	Oxygen consumption rates
OXPHOS	Oxidative phosphorylation
pAKT	Phosphorylated AKT
pCMV	Cytomegalovirus promoter
PCR	Polymerase chain reaction
PGE2	Prostaglandin E2
PI	Propidium iodide
PI3K	Phosphoinositide 3-kinase
PIP$_3$	Phosphoinositide-3,4,5-trisphosphate
PPARs	Peroxisome proliferator-activated receptors
PPARδ	PML-Peroxisome proliferator-activated receptor delta
PRR	Pattern recognition receptors
PVDF	Polyvinyladine fluoride
qPCR	Quantitative PCR
RIPA	Radioimmunoprecipitation assay
RISC	RNA-induced silencing complex
ROI	Reactive oxidant intermediates
ROS	Reactive oxygen species
S. typhimurium	*Salmonella typhimurium*
S.aureus	*Staphylococcus aureus*
SASP	Senescence-associated secretory phenotype
SCF	Stem cell factor
SCID	Severe combined immunodeficient
SDS-PAGE	Sodium dodecyl sulfate polyacrylamide gel electrophoresis
shRNA	Short hairpin RNA
SNP	Single-nucleotide polymorphisms
SOD2	Superoxide dismutase 2
SSO	Sulfosuccinimidyl oleate

ST-HSC	Short term HSCs
TAE	Tris Acetate EDTA
TCA	Tricarboxylic acid
TGF-B1	Transforming growth factor- b1
TLR4	Toll-like receptor 4
TMRM	Tetramethylrhodamine, methyl ester
TNF-α	Tumour necrosis factor- alpha
TNTs	Tunnelling nanotubules
TPO	Thrombopoietin
UPR^{mt}	Unfolded protein response
VCAM-1	Vascular cell adhesion molecule 1
VSMCs	Vascular smooth muscle cells
VSV-G	Vesicular stomatitis virus glycoprotein
β-oxidation	Beta oxidation

1   Introduction

1.1   Haematopoiesis

On average, a healthy individual (70 kg in weight) is estimated to produce around 8×10^{11} mature blood cells daily (1). The process in which new blood cells are made is known as haematopoiesis. This can be broken down into various cell types including red cells, myeloid cells and lymphoid cells. It is estimated that we produce 2×10^{11} red cells, 1×10^{11} white cells and 4×10^{11} platelets per day (2). Moreover, this production is increased when needed, in situations such as infections, trauma and severe blood loss (3). Thus, an efficient process is essential to generate large volumes of cells. This upregulation in adverse conditions is termed stress haematopoiesis.

The bone marrow (BM) is the primary organ for haematopoiesis and bone formation (4). The BM not only contains haematopoietic cells, it also contains cells which contribute to bone homeostasis (5). Although the BM aims to maintain this homeostasis, the make-up of the BM can be displaced by aberrations such as malignancy or infection (6). The haematopoietic tissue comprises many different types of cells including; blood cells and precursor blood cells, barrier cells, adipocytes and macrophages. The arrangement of these cells is not arbitrary and show organisation within the BM (7).

Haematopoiesis is the continuous, active process involved in the production of blood cells within the BM (8). The process originates at the haematopoietic stem cell (HSC), which is a multipotent stem cell (9, 10) HSCs give rise to haematopoietic progenitor cells (HPCs) through a series of lineage commitments. HPCs include common lymphoid and myeloid progenitors which can then differentiate into many different immune cells (11). Despite its complexity, haematopoiesis is one of the best defined human systems due to seminal animal experimentation (12).

McCulloch and Till, 1960 were pioneers in first describing HSCs. Their research showed animals receiving a lethal dose of irradiation were rescued

from death via transplantation with unfractionated BM cells from non-irradiated mice (13). Interestingly, the transplanted irradiated mice developed small splenic lumps (14). They later went on to demonstrate that the colonies that formed in the spleen of the irradiated animals were formed by single cells capable of multilineage differentiation (15). These cells, now identified as HSCs, are regulated by many complex cellular and molecular signals at both a genetic and epigenetic level (16). Alterations to these highly regulated signals can lead to the dysfunction of haematopoietic cells causing them to become malignant stem cells (17). Thus, understanding more about the mechanisms behind how these highly regulated cells work is important in understanding the fundamentals of disease.

The isolation of HSCs and HPCs, using distinct cell surface markers, allowed for the complex classification of the hierarchical structure of haematopoiesis to be identified (18). HSCs give rise to common lymphoid and myeloid progenitors, which can then differentiate into numerous different immune cells (11). Myeloid progenitors ultimately differentiate into granulocytes, monocytes and megakaryocytes (11). Granulocytes and monocytes play a key role in pathogen immunity and megakaryocytes can form platelets (11). Lymphoid progenitors give rise to the T cells, natural killer (NK) cells, dendritic cells and B cells, which are responsible for cell mediated immunity (11). This, however, is a simplified model and there is increasing evidence to suggest that the HSC does not strictly follow the hierarchical organisation but rather gradually acquire lineage biases along multiple directions (Figure 1.1) (19).

Further analysis of the human haematopoietic system occurred after the emergence of severe combined immunodeficient (SCID) mice, these mice lack mature T and B cells (20). Transplanted human leukocytes from peripheral blood successfully engrafted into SCID mice and were able to produce functional human T and B cells (21). Furthermore, using a modified SCID model, the non-obese diabetic (NOD) SCID gamma (NSG) mouse allowed for more specific transplantation of HSCs isolated from human umbilical cord blood (22). Human CD45+ cells engrafted in the BM and the spleen of the

NSG mouse and mature human blood cells were found in the peripheral blood of the transplanted animal (23). Analysis of both human and murine haematopoietic systems has greatly aided in the understanding of haematopoiesis.

Ordinarily, the BM is the sole site of haematopoiesis however, extramedullary haematopoiesis can occur in the spleen, liver and lymph nodes when compensatory mechanisms in the BM are compromised (1). In order for normal haematopoiesis to occur, support from the BM microenvironment is needed (24). The microenvironment provides the growth factors, neurological stimuli and cytokines required to aid proliferation, differentiation and maturation of stem cells along the lineage commitments (25). The BM microenvironment also provides the energy required for the rapid production of new blood cells (26). The haematopoietic microenvironment comprises the cells of the BM (27). Together, the BM microenvironment and the HSCs and progenitor cells constantly interact to allow for demands of new blood cells to be made under normal and stressed haematopoiesis.
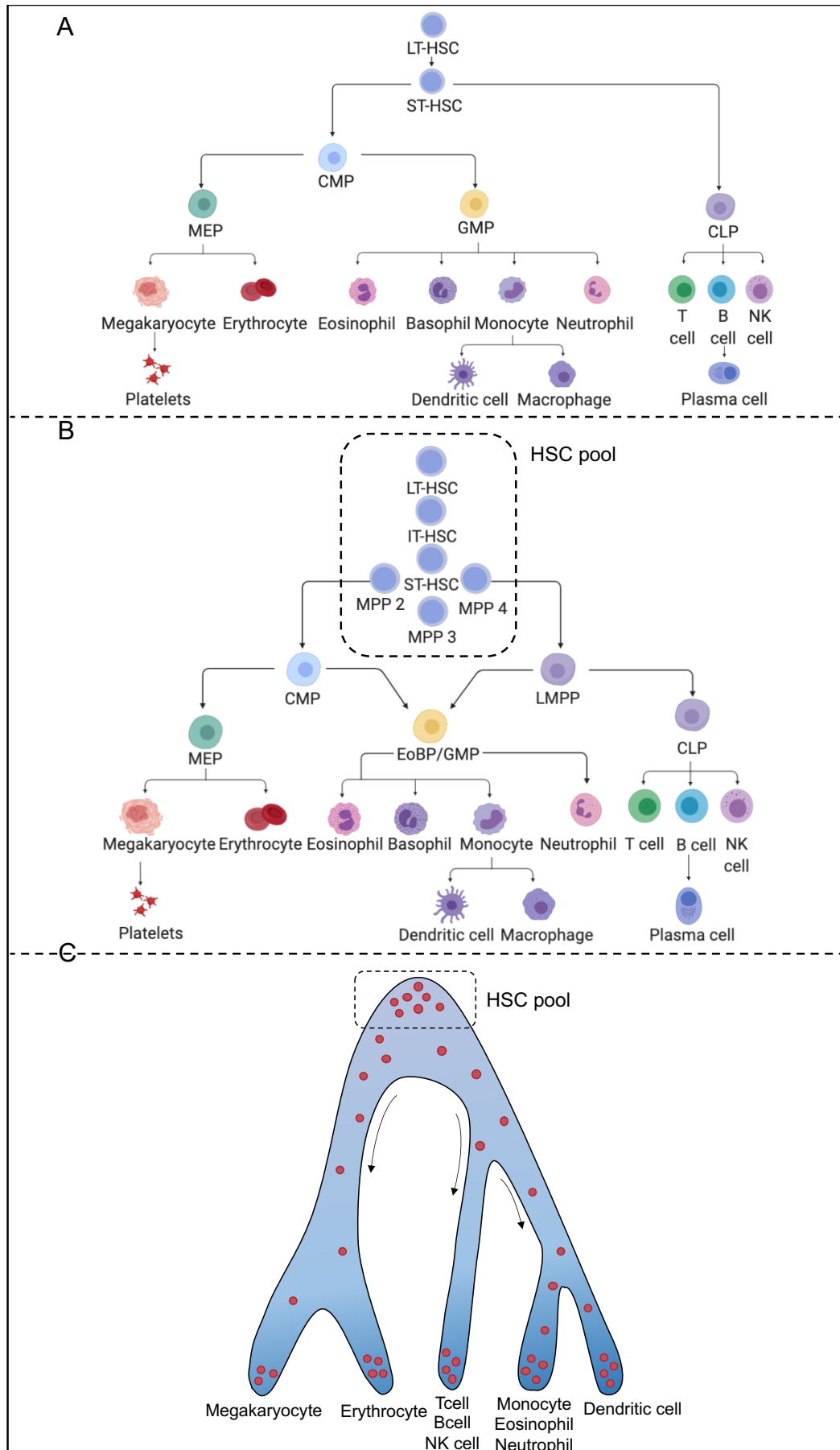
Figure 1.1. Hierarchical models of haematopoiesis.
(A) A visualisation of the haematopoiesis model from around 2000. Long term haematopoeitic stem cells (LT-HSC) give rise to short term HSCs (ST-HSC), which can either revert back to LT-HSCs or differentiate and give rise to haematopoietic progenitor cells (HPCs). The multipotent progenitors (MPP) are the next stage of differentiation, which gives rise to both the common myeloid progenitor (CMP) and the common lymphoid progenitor (CLP). Myeloid cells include megakaryocyte-erythrocyte progenitors (MEP) and the granulocyte-macrophage progenitors (GMP), which differentiate to form monocytes, macrophages, neutrophils, basophils, eosinophils, erythrocytes, and megakaryocytes. Whereas lymphoid cells include natural killer (NK) cells, T cells, and B cells. B cells also form the plasma cells (Created using BioRender.com). (B) From 2005 to 2015 the model expanded to incorporate new discoveries. The HSC pool is more heterogeneous and myeloid and lymphoid progenitors remain further down the hierarchy by the lymphoid-primed multipotent progenitors (LMPP) population. The eosinophil-basophil progenitor (EoBP)/ GMP population is fairly heterogeneous (28) (Created using BioRender.com). (C) From 2016, advances in single cell transcriptomics indicated cells gradually acquire lineage biases in a continuum of differentiation. The red dots represent a single cell. (Adapted from Laurenti and Göttgens, 2018 (29)).

1.2   The human bone marrow

The BM is an organ in which new blood cells are made in a process known as haematopoiesis (8). BM, found in the central cavities of the bone, is a sponge-like tissue. It is comprised of blood vessels and a heterogeneous population of cells (30). The BM itself is made up of red marrow, also referred to as myeloid tissue, and yellow marrow (31). At birth, the BM consists of mostly red marrow, however with age, this is slowly displaced by yellow marrow which has a much higher level of adipocytes. In response to certain stress stimuli such as severe blood loss yellow marrow has the ability to revert back to red marrow (32). Red marrow is typically located either at the ends of the long bones or in the flat bones including; the hip, breastbone, skull, ribs, vertebrae and shoulder blades (Figure 1.2). The red marrow comprises the parenchyma, the haematopoietic stem and progenitor cells and vascular components including the supporting stromal cells (33). The main function of the red marrow is haematopoiesis, which is estimated to produce around 8 x 10^{11} mature blood cells daily (1). Haematopoiesis is controlled by the central nervous system (CNS), which senses the body's blood requirement, and increases or decreases blood production accordingly by its control of haematopoietic stem and progenitor cells located in the red marrow (34). The yellow marrow is mostly composed of fat cells, and operates as an energy

store in times such as severe starvation (35). Together, the red and yellow marrow function to support haematopoiesis.

The human bone itself is comprised of the trabecular bone enclosed by a cortical bone layer and connective tissue (36). The BM cavity is comprised of at least four niches endosteal, subendosteal, central, and perisinusoidal (37). In terms of haematopoiesis histological and functional assays have shown that HSCs and multipotent progenitors preferentially reside in the endosteal and subendosteal regions, closely associated with the surface of the bone (27, 38). The more committed progenitors and mature cell types however colonise in the central and perisinusoidal regions, respectively. This complex organisation within the BM allows for efficient haematopoiesis.

The BM is connected to the peripheral blood through vascular sinuses; pools of mixed arterial and venous blood dispersed within a trabecular bone network, which surrounds haematopoietic tissue islands and adipose cells (33). The venous sinuses are flat, thin-walled endothelial cells typically lacking a basement membrane. The venous sinuses receive arterial blood from the arteries and capillary networks connected by the Haversian canals. Consequently, blood flows in a circular process from the centre of the BM cavity toward the edge of the cavity and then back towards the centre (39) (Figure 1.2). The cavities are lined with a monolayer of flat "bone-lining cells", which are reinforced with a thin layer of connective tissue (7). Neural innervation of bone, both myelinated and non-myelinated, permeates the BM through the nutrient foramina and is distributed similarly to the nutrient artery (40). The nerves run through the arterioles, innervating the vessels, and terminate at the haematopoietic tissue in the BM further suggesting blood production is regulated by the central nervous system. Taken together, this highlights the physiological complexity of the BM.
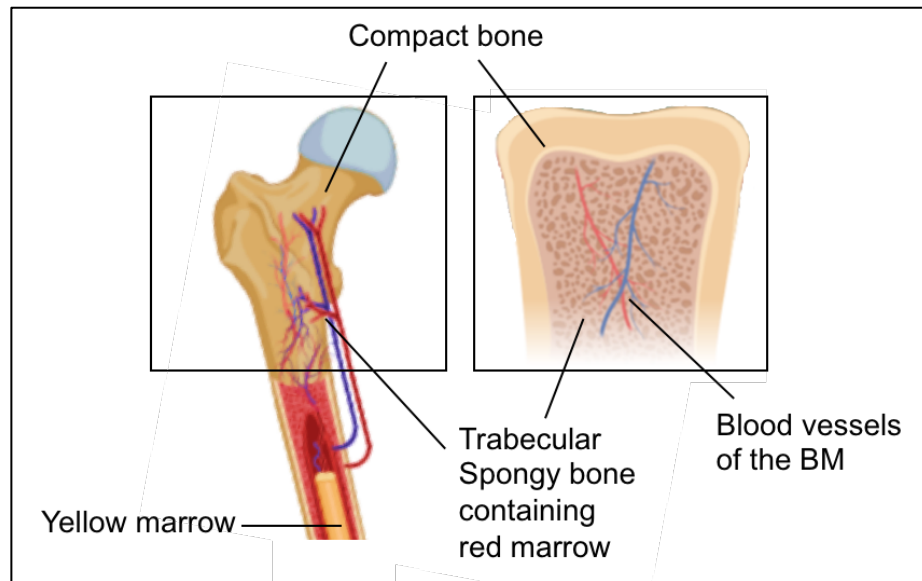
Figure 1.2. Cross section of the bone marrow.
Anatomy of the bone, the diagram shows the trabecular, the spongy bone located at the end of the bone with the red marrow and the yellow marrow filling the cavities of the bone. A cross section of the bone shows the compact bone and blood vessels, the vascular sinuses. (Created using BioRender.com).

1.3   Bone marrow microenvironment

The BM microenvironment and its role in disease has recently been a research focus for many scientists. Several studies have demonstrated interactions between haematological malignancies and the non-haematopoietic cells within the BM aid the survival of these malignant cells both *in vitro* and *in vivo* (27). Studies have also shown that leukaemic cells compete for the BM resources creating a favourable environment for the progression of the disease (17, 41, 42).

It has been theorised that the BM microenvironment can be categorised into compartments or niches which affect the differentiation and proliferation potential of HSCs (43). The two broad regions in the BM are the endosteal and the vascular niche (44). HSCs transition between the two niches. The endosteal niche maintains quiescence whereas the vascular niche enables differentiation and proliferation (45). This process ensures the HSC is in favourable microenvironment specific to its needs.

1.4   HSC niche

A stem cell niche is defined as the location in which HSCs reside in an undifferentiated and self-renewable state (46). The idea of a niche was first described by Schofield in 1978 (47). However, since then considerable progress has been made in defining the structure and components of the niche (48). The best characterised BM microenvironment is the niche that regulates the HSC (49). 3D imaging of the mouse BM show dense populations of HSCs in micro-domains or niches (50). In the niche, cells interact with the HSCs, and either maintain quiescence or promote differentiation (51). Many studies have collectively established that the niche is mainly perivascular therefore, blood vessels and perivascular stromal cells are the key components of the niche (52). In addition, numerous other cell types have been shown to be components of the niche including osteoblasts and blood vessels (53). Thus, the HSC niche is a vastly complex network of cells functioning collectively for the production of BM cells (Figure 1.3).

Within the niche, there is a relatively large number of maturing progenitor cells, for all lineages. This allows for prompt recruitment and reallocation of these cells under stressed conditions. The factors involved in the continuous turnover of mature cells in the BM are not well understood. There is however, evidence supporting the role of several growth factors and basic genetic controls in haematopoiesis regulation within the BM microenvironment (54). Together, the HSC niche is a highly organised microenvironment functioning to support the HSC.
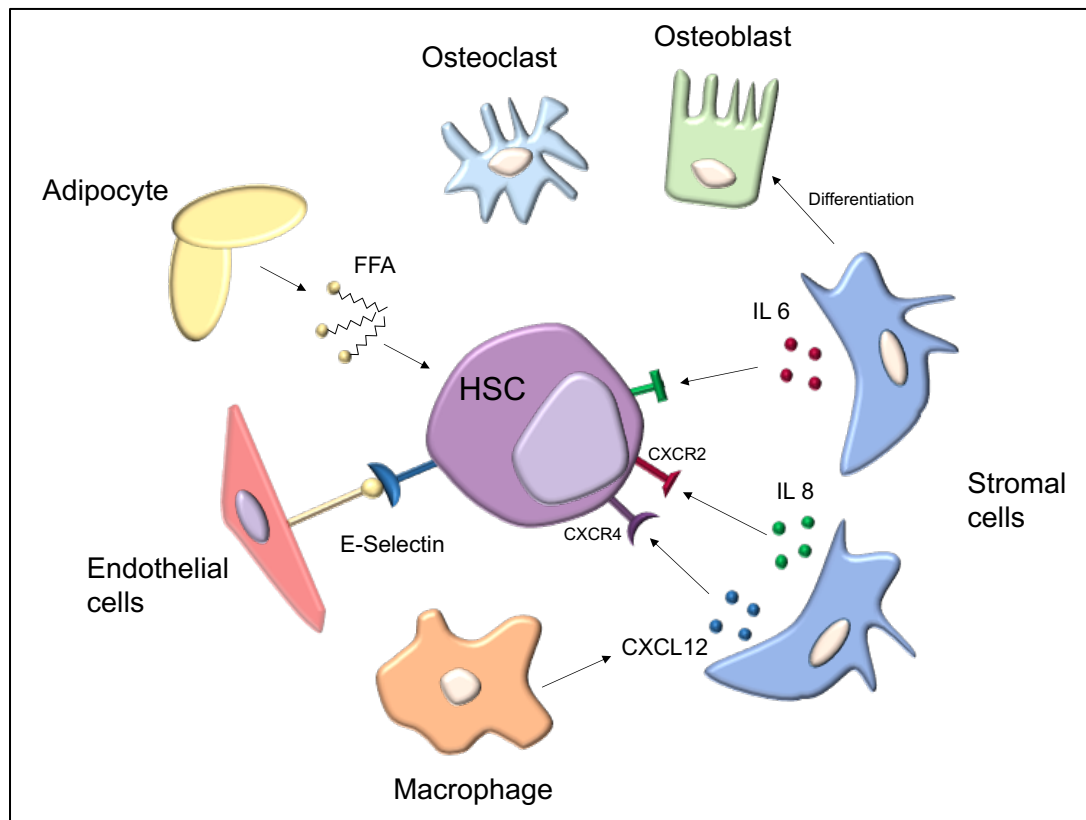
Figure 1.3. The HSC Niche.
Haematopoietic stem cells (HSCs) interaction with cells of the bone marrow (BM). The stromal cells release IL 6, IL 8 and CXCL12 which regulate the HSCs and can differentiate into the osteoblasts. The macrophage also can promote the release of CXCL12 from the stromal cells. The adipocytes release free fatty acids (FFA) which can provide the energy for HSC differentiation. The endothelial cells can regulate the quiescence of the HSC via E-selectin. (Adapted from Shafat *et al*. 2017 (30)).

1.5   Cell compartments of the BM microenvironment

1.5.1   Haematopoietic Cells

1.5.1.1   Haematopoietic stem cells

The key player in haematopoiesis is the HSC. McCulloch and Till findings introduced the two defining criteria of the HSC; self-renewal and differentiation. HSCs are the only cells of the haematopoietic system capable of both self-renewal and differentiation. Specifically, HSC self-renewal is the ability to give rise to identical daughter cells whilst maintaining an undifferentiated state and differentiation is the ability of the HSCs to differentiate into all functional mature blood cells (55-58) (Figure 1.1). HSCs are first formed in early embryogenesis and their location changes during development (59). HSCs are a rare population within the BM making up around 0.05% of the total mouse BM cells (60, 61). Under normal conditions HSC numbers remain relatively unchanged and the majority of the HSCs primarily reside in G0 phase of the cell cycle (62).

HSCs were first purified in 1988 from mouse BM cells using the then novel technology fluorescence activated cell sorting (FACS) and monoclonal antibodies (61). The enriched mouse HSC populations were sorted using the expression of two cell surface markers Thy-1^{low} lineage marker (Lin) and Sca 1, with HSCs being Lin negative (Lin-) and Sca 1 positive (60, 61). It was also demonstrated that these sorted Lin$^-$Sca 1$^+$ HSCs were the only mouse BM cells with the ability to reconstitute the entire haematopoietic system after transplantation into irradiated mice (61). It is important to note both Lin$^+$Sca 1$^+$ and Lin$^-$Sca 1$^-$ cells were unable to reconstitute the BM (63). Following these initial findings, identifying additional cell surface markers CD117/c-Kit and CD34 allowed for more extensive purification of HSCs (64, 65). In 1996, it was demonstrated that injection of a single HSC (mCD34-, CD117, Sca 1+, Lin-) alone resulted in long-term repopulation of the haematopoietic system in lethally irradiated recipients (66). These additional cell surface markers also highlighted at least three distinct isolated populations; long term HSCs (LT-

HSCs), short term HSCs (ST-HSCs) and multipotent progenitors (MPPs) (67). These cell populations are now well defined, with the additional cell surface markers, CD150 and CD48 (68).

LT-HSCs are a subset of HSCs capable of undergoing asymmetric cell division to self-renew sustaining the HSC pool, and additionally differentiate into ST-HSCs. (69). The ST-HSC is a multipotent HSC which is able to differentiate into the MPP. The MPP can differentiate to produce the common myeloid and lymphoid progenitors, which then differentiate further into mature, functional haematopoietic cells. LT-HSCs must sustain haematopoiesis for the lifespan of the organism, continually replenishing the haematopoietic system. However, the ST-HSCs and MPPs are only capable of maintaining haematopoiesis for a relatively short time of 6-8 weeks (70, 71). Taken together, HSCs play a key role in the regulation of haematopoiesis.

1.5.1.2   Macrophages

Macrophages are immune effector cells and play a significant defensive role in the immune response (72). They participate in the host defence by phagocytosing microbes and parasites they come into contact with (73). The role of the macrophage also includes rapid and efficient removal of cell debris produced by cells undergoing apoptosis or during tissue modifications (74). The BM is an active site of myelopoiesis, a process in which monocytes and macrophages are produced (11). Within the BM, macrophages have been identified as being a vital element in modulating the HSC niche (75). Studies have reported depletion of macrophages, using clodronate-loaded liposomes or by using macrophage-Fas-induced apoptosis transgenic mice, led to HSC reallocation to the blood and a reduced number of HSC niche factor encoding genes (76). Winkler *et al.* 2010 also reported that CD169^{+} macrophages promoted the release of CXCL12 from the stromal cells causing HSCs to remain in their niche in a quiescent state (76). Other studies however, have shown using models of conditional depletion of macrophages, that a decrease in the number of macrophages causes a reduction of CXCL12 which leads to HSC retention by down regulation of the retention genes in the

Nestin+ mesenchymal stem cells (MSC) (77). Macrophages, therefore, are essential in the regulation of the HSCs.

1.5.2   Non-haematopoietic Cells

1.5.2.1   Osteolineage cells

Alongside the haematopoietic system development, bone formation also occurs within the BM (78). Cells of the osteolineage include osteoblasts and osteoclasts which regulate bone formation. Osteoblasts are found at the surface of the new bone and are responsible for new bone formation (osteoid). They are phenotypically oval and elongated cells, stemmed from the MSCs (79). Osteoblast differentiation from MSCs is regulated by the transcription factor Runx2 (80). Both heterozygous and homozygous knockout of Runx2 in mice considerably disrupt osteogenesis, with homozygous knockout mice not surviving past birth (81). Mature osteoblasts form the bone by undergoing proliferation, matrix maturation and mineralisation (82). HSCs are found to be located close to osteoblasts whereas more mature progenitor cells are located further away (83). Initial studies into osteoblasts showed that osteoblasts promote the development of HPCs in culture (84). This was further reported by both Calvi *et al.* 2003 (85) and Zhang *et al.* 2003 (86). The authors showed activating osteolineage cells either pharmacologically or via genetic mutation, increased the number of HSCs in the BM. This suggests that osteoblasts have an important role in the maintenance of HSCs. An increase in the number of osteoblasts has also been positively correlated with an increased number of LT-HSCs *in vivo* (86, 87)*.* Furthermore, it has been shown that in a conditional osteoblast knockout model there is an inability of the BM to sustain haematopoiesis (88, 89). However, there have been studies which disprove this and imaging of the BM has shown no relationship between HSCs and osteoblasts (90, 91). This could be due to osteolineage cells only having an indirect role in HSC regulation (27). The osteoblast population is heterogenic and there are many stages of differentiation of the osteoblasts. However, it

remains unclear which population is important in the maintenance of HSCs (92).

Osteoclasts, on the other hand, are not derived from MSCs but do play an important role in the BM microenvironment. Osteoclasts are produced from the myeloid lineage specifically granulocyte macrophage progenitors (93). Bone formation is dynamic and relies on a balance between bone forming osteoblasts and bone resorbing osteoclasts (94). Osteoclasts are key in establishing a functional HSC niche. In an osteopetrotic (oc/oc) mouse, osteoclasts are not present and the BM of these mice lack any functional niches, which is thought to be due to the inability of HSC homing (95). There was also a reduced number of osteoblasts in the oc/oc mice. Overall, this suggests that the osteoclasts' role in the maintenance of HSCs is linked indirectly though osteoblasts.

1.5.2.2   Perivascular cells

The BM needs to be highly vascularised to supply oxygen and nutrients for haematopoiesis. Perivascular cells, including pericytes and vascular smooth muscle cells (VSMCs) enclose the inner endothelial lining, providing support and stabilisation (96). Perivascular cells also surround the blood vessels promoting maturation of the vessel. This helps deter haemorrhaging or leaky vessels (97, 98). It is reported that the perivascular cells not only sustain the BM but also express high levels of major HSC niche factors making them a key component of the HSC niche (99, 100).

1.5.2.3   Endothelial cells

Endothelial cells make up the lining of the blood vessels and they have also been shown to modulate the trafficking of HPCs and HSCs in the HSC niche (101). Endothelial cells are derived from mesenchymal stem/stromal cells (MSC). Endothelial cells cultured *in vitro* have been shown to promote proliferation and differentiation of human CD34$^+$ progenitor cells (102). They also regulate quiescence of HSCs via E-selectin, which is only expressed on

endothelial cells and activated by cytokines (103). Moreover, initial studies on endothelial cells with conditionally deleted gp130 receptor showed that this lead to a reduction of the HSC cell count in the HSC niches within the BM (104). Endothelial cells also release critical cytokines involved in HSC maintenance, including granulocyte colony stimulating factor (G-CSF), granulocyte-macrophage colony-stimulating factor (GM-CSF) and interleukin (IL) 6 when stimulated with the proinflammatory cytokines IL 1 or tumour necrosis factor-alpha (TNF-α) (102). Additionally, vascular cell adhesion molecule 1 (VCAM-1) is expressed on endothelial cells (105). VCAM-1 binds to the leukocyte ligand VLA-4 present on HSCs causing HSC retention in the niche. Endothelial cells can also synthesise stem cell factor (SCF) in both its forms, soluble and membrane bound. Moreover, there is a depletion of HSCs when SCF is knocked out (106). Arterial vessels also promote HSC quiescence due to them being less permeable, thus maintaining the HSCs in a low reactive oxygen species (ROS) environment. High levels of ROS augment the differentiation and migration ability of HSC population (107). Therefore, endothelial cells and arterial vessels play a crucial role in the regulation of the stem cell niche.

1.5.2.4   Adipocyte

Adipocytes, often regarded as fat cells, are derived from MSCs and predominantly compose the BM adipose tissue (BMAT) (108). BMAT is an interesting form of adipocyte tissue which composes more than 10% of the total fat mass in normal healthy humans (109). Recent advances in imaging of the BM has shown BMAT has unique features highlighting physiological specificity in the BMAT (110). Alongside ageing (111, 112) BMAT is increased in osteoporosis (113) and obesity (114, 115). With age, the haematopoietic tissue within the BM is gradually replaced with adipocytes. Adipocytes make up around 15% of the BM in young adults, however, by age 65 this is increased to 60% (116). Thus, the number of HSC is negatively correlated with the increase of adipocytes in the BM (117). Adipocytes importantly contain large levels of fat and therefore play a significant role in regulating bone metabolism

(118). These cells store fat in lipid droplets in the form of triglycerides, which can be broken down by a catabolic process known as lipolysis into free fatty acids (FFA) and glycerol (119, 120) (Figure 1.4). These studies suggest that BM adipocytes are not just space fillers but play a substantial role.

There have been many conflicting reports on adipocytes and whether they are directly involved in the maintenance of HSCs (78). These cells have been found to both generate and secrete SCF (121), they can also produce CXCL12, IL 8 and IL 3 (122), which are all key regulators in maintaining the HSC niche. Proteomic analysis of BM adipocytes showed, an upregulation of the pathways involved in sphingolipid signalling, arachidonic and cholesterol metabolism but a decrease in lipolytic enzymes compared to subcutaneous adipocytes (110). The physical location inside the niche may suggest BM adipocytes are an important energy source in response to stress. However, the full extent of the role of the adipocyte in the BM is not well established. This is due to the difficulties in isolating BM adipocytes from both humans and mice, which is partially due to the locality of the adipocyte. Additional studies need to be undertaken to further explore the roles of adipocytes in the HSC niche.
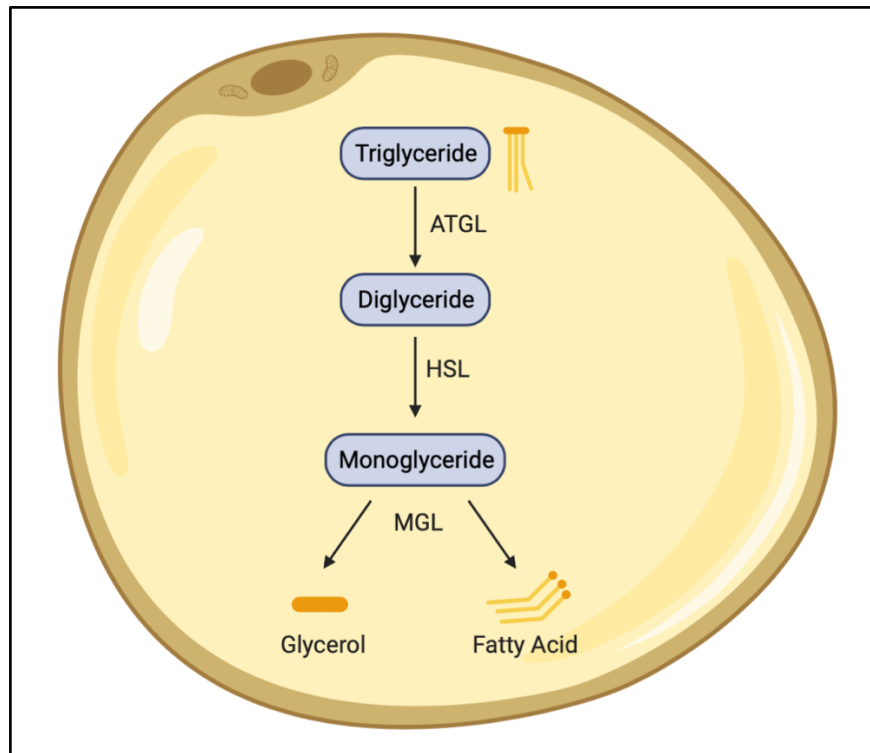
Figure 1.4. The biochemical pathway governing lipolysis in the adipocyte.
Triglycerides are broken down to glycerol and fatty acids in the adipocyte by the enzymes adipose triglyceride lipase (ATGL), hormone sensitive lipase (HSL) and monolglyceride lipase (MSL). (Created using BioRender.com).

1.5.2.5   Stromal cells

Another cell key to the establishment of the HSC niche is the BM mesenchymal stromal cell (BMSC). Often referred to as mesenchymal stem/stromal cells, the BMSC have the potential to differentiate into many different types of cells described above including adipocytes, osteoblasts, myocytes and chondrocytes (123, 124). The identification of the BMSC is one of the least understood areas in stem cell biology. Many studies have tried to define the role of the BMSC. However, they are universally recognised as connective tissue, which is phenotypically similar to skeletal progenitors and pericytes (30). Bianco *et al*. 2008, were the first to identify the progenitor to the BMSC and redefined them as a skeletal stem cell (124, 125). Saccehetti *et al*. 2016, then help further the understanding of the stem cells proving that BMSC are not universal but in fact have varying differentiating capacities for different tissues of different origin (126). BMSC culture *in vitro* are characterised by

their differentiation ability, adherence to plastic and expression of fibroblast surface markers (127). The BMSCs have many importantant roles in the supporting the HSCs and heamatopoisis, which is dicussed further in section 1.6.

1.6   BMSC and normal haematopoiesis

BMSC have been shown to release key cytokines and chemokines that regulate HSC maintenance (27). The potential of the HSCs to differentiate, self-renew, remain quiescent or proliferate is dependent on these factors secreted by adjacent cells in the BM microenvironment (128). BMSC specifically are a key source of SCF and CXCL12. Conditional deletion of the SCF (129) or CXCL12 (130) from stromal cells have also been shown to decrease the number of HSCs in the BM, solidifying the fact that BMSCs play a key role in the HSC niche compartment.

SCF is a cytokine crucial in regulating the HSC niche (131). SCF can be present in both soluble and membrane bound forms and is activated when bound to the tyrosine kinase receptor CD117 expressed by HSCs to regulate proliferation (132, 133). It was reported that a small alteration in CD117 has a large effect on the functionality of HSCs (134). Thus, when culturing HSCs *in vitro* SCF proves vital. It has also been shown that maintenance of haematopoiesis by the membrane bound SCF is fundamental, as Sl/Sl^d mutant mice which only express the soluble SCF lack HSCs and progenitor cells (135). This data shows that SCF is a vital cytokine in HSC regulation.

CXCL12 is a chemokine which regulates the HSC niche by promoting the retention of HSCs to maintain the HSC pool. CXLCL12 binds to and activates the C-X-C chemokine receptor type 4 (CXCR4) on the HSCs (136, 137). It has been shown that CXCL12 plays a key role in the regulation and reallocation of the HSC to the peripheral blood or spleen. The number of HSCs is reduced in the niche when there is a deletion of CXCL12 in MSCs (100, 138) or CXCR4 in HSCs (137). It has recently been found that BMSC secretion of CXCL12 can be controlled by circadian oscillations (139). The sympathetic nerve fibres

release noradrenaline and this causes a downregulation of CXCL12 secretion from the BMSCs leading to HSC migration from the BM. Together, CXCL12 plays a crucial role in the maintenance of haematopoiesis.

BMSCs also secrete a variety of other growth factors and chemokines such as; Flt-3 ligand (FLT-3), thrombopoietin (TPO), IL 6, IL 7, IL 11, macrophage colony stimulating factor (mCSF), TNF-α, transforming growth factor- b1 (TGF- B1) and leukaemia inhibitory factor (LIF) (140). These are all essential in the maintenance of haematopoietic homeostasis.

BMSCs are a diverse cell population and there is increasing evidence about the number of different types of stromal cells (141, 142), which have different functions in regulating HSCs (90). However, there are three distinct populations which have been widely studied; CXCL12-abundant reticular (CAR) cells, nestin-GFP^{+} stromal cells and leptin receptor^{+} stromal cells (131). These stromal cell populations have substantial similarities as they were first found by transgene expression of stromal cell promotors. To identify CAR cells, GFP was knocked in to the CXC12 locus, similarly for nestin-GFP^{+} stromal cells GFP was knocked in to the nestin promoter(143, 144). Leptin receptor^{+} stromal cells were first found by lineage mapping of leptin receptor elements using Cre-recombinase expression (106).

CAR cells are mesenchymal progenitors which can produce CXCL12 and can differentiate into adipocytes and osteoblasts (137, 145). Deletion of the CAR cells significantly decreases the amount of SCF and CXCL12 and also decreases the number of HSCs in the BM (145). BMSC express high levels Nestin-GFP[+] transgene and deletion of this gene increases the translocation of HSCs from the BM to the spleen (100). Nestin-GFP^{+} cells, however, express both CXCL12 and SCF, and deletion of these cells leads to a decrease in HSC numbers (131). Similarly, leptin receptor^{+} stromal cells also express CXCL12 and SCF and can differentiate into adipocytes however they are unable to differentiate into osteoblasts (145). HSC quiescence has been shown to be maintained by the NG2^{+} LepR^{−} cells which contribute to the arteriolar niches.

Whereas NG2−LepR+ cells are thought to form perisinusoidal niches and regulate the proliferation of HSCs within the BM. Conditional depletion of NG2 expressing cells has been found to induce HSC cycling (146). Whilst these 3 cell types may be distinct, they have commonalities, including the ability to produce CXCL12 and SCF, and therefore can be classified as BMSCs.

Intriguingly, intracellular HSC ROS levels can be reduced when in contact with BMSCs. This is via multiple mechanisms including CXCL12 and CXCR4 and ROS uptake via gap junctions (147). High levels of ROS enhance the differentiation ability and motility of the HSC population thus, BMSC are important in maintaining normal haematopoiesis (107).

1.7   Pathological diseases of the BM

An organism needs to achieve a balance between maintaining a sufficient HSC pool throughout its life span, whilst also consistently meeting the demand for replenishing the mature blood cells, many which only live for a short amount of time (58). The significance of maintaining this balance is highlighted by the many instances where abnormal HSC expansion causes severe disease. Examples of this are when HSC progenitors cannot fully differentiate into the more mature blood cell types or when HSCs do differentiate into more committed progenitors but do not lose their capacity for self-renewal (148). Examples of pathological diseases of the BM are discussed further in the sections below.

1.7.1   Ageing

Ageing is a process which affects all normal cells, tissues and organ systems; both the BM and the BM microenvironment are modified with age. Haematological changes within the BM are shown by a decrease in cellularity, a decline in adaptive immunity and a higher risk of developing myeloproliferative diseases (149) anaemia (150) autoimmune (151) and inflammatory disorders (152). The cellularity in the BM decreases dramatically

with age from 90% at birth to only 25% haematopoietic tissue at age 70 (153) (Figure 1.5). The haematopoietic tissue is replaced by adipocyte infiltration into the BM, which results in a decrease in the number of immune cells. These increased numbers of maturing adipocytes release factors that influence the neighbouring BMSC, driving further differentiation of the BMSCs towards adipocytes (154) creating a feedback loop and promoting ageing in the BM.

Whilst extrinsic factors including an inflammatory microenvironment can accelerate ageing (155), they also effect the HSC, causing cell-intrinsic changes that can alter the self-renewal and differentiation potential, triggering lineage skewing (156). With ageing, the number of HSCs are increased, however, there is a reduced production of lymphoid cells and a preferential skewing towards myeloid cell production (27, 157-159). This age related loss of HSC function is thought to be due to telomere shortening (160), the accrual of nuclear and mitochondrial DNA damage (161) and changes in gene expression. Aged HSCs have upregulation of genes associated with stress and inflammation, whilst DNA repair and chromatin silencing genes are downregulated compared to young HSCs (157, 159). Furthermore, transcriptome analysis of aged HSCs showed a reduction in TGFβ signalling and impairment of genes involved in HSC differentiation and proliferation. Aged HSCs also showed elevated DNA methylation specifically at transcription factor binding sites. This was associated with an increase in genes promoting differentiation and a decrease in genes in sustaining HSC maintenance (162). Taken together this shift in HSC gene expression reinforces the diminished capacity for self-renewal and differentiation in aged HSCs.

More recently it has been shown that the traits of HSC ageing and myeloid-biased haematopoiesis in mice are initiated in middle-age. Moreover, the middle-aged BM microenvironment induces these haematopoietic ageing phenotypes, through a decreased production of IGF1 which accelerates BM ageing and stimulation with IGF1 rescues haematopoietic ageing (163). These

results indicate that the functional decline from young to aged HSCs may occur during middle age.

Interestingly, although there are dramatic changes in the HSC niche with age, in the absence of disease HSCs are still able to repopulate the BM. When BM is transplanted from a 65-year-old donor into an HLA-matched younger recipient, the BM is still fully functional and maintains haematopoiesis, however, the only clinical change is an increased risk of rejection (164). Overall loss of HSC function with age majorly contributes to the decrease in function of the haematopoietic system and can lead to an impaired vaccination response, increased susceptibility to infection, clonal haematopoiesis and increased risk of developing haematological malignancies (163).
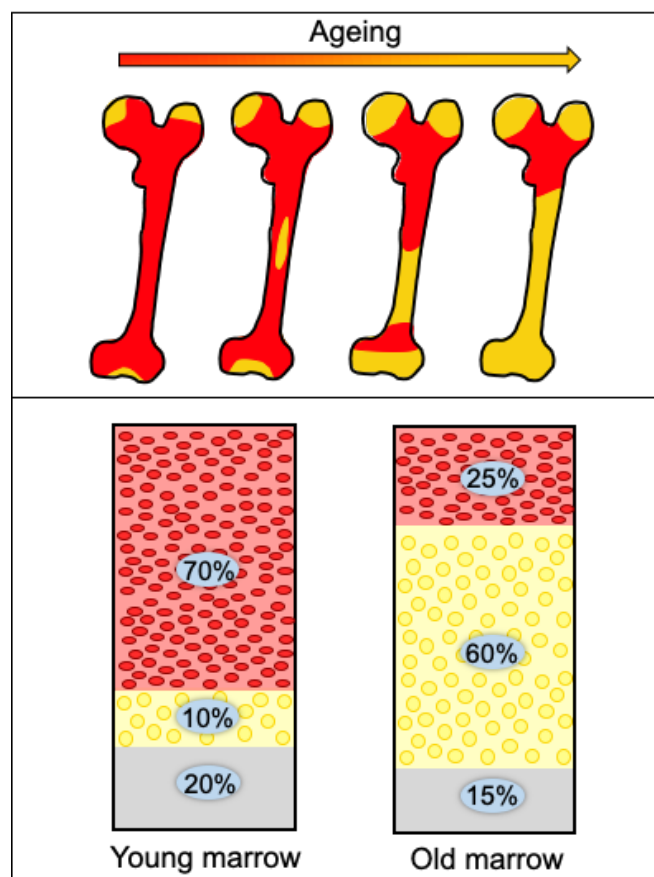
Figure 1.5. The ageing bone marrow.
Schematic diagram of decreased cellularity in the bone marrow with age. The red marrow is displaced by adipocyte rich yellow marrow with small changes percentage of trabecular bone volume (grey). (Adapted from Griffith 2017 (165)).

1.7.2   Haematological Malignancies

Although the BM microenvironment is involved in promoting normal haematopoiesis, it also plays a significant role in the development and progression of disease, including different types of haematological cancer. Many malignant disorders develop in the BM when blood cells become cancerous and proliferate uncontrollably. Haematological malignancies can be classified into three broad groups; leukaemia, myeloma and lymphoma (166). Leukaemia can be further subdivided into acute myeloid leukaemia (AML), chronic myeloid leukaemia (CML), acute lymphoblastic leukaemia (ALL) and chronic lymphoblastic leukaemia (CLL).

Acute leukaemias are defined by the proliferation and accrual of malignant immature myeloid (AML) or lymphoid (ALL) progenitor cells whilst in chronic leukaemias there is proliferation of more mature monoclonal myeloid (CML) and lymphoid (CLL) cells. The myeloid malignancies generally have a lower survival outcome than lymphoid malignancies (167). Furthermore, the acute conditions progress faster and are more severe than the slower chronic conditions. These haematological malignancies result in the failure of normal haematopoiesis. Multiple myeloma (MM) is a malignancy of the plasma cells in the BM which leads to the production of non-functional monoclonal intact immunoglobulins or immunoglobulin chains (168). MM and leukaemia are liquid cancers present in the BM and peripheral blood, lymphoma however is a solid tumour made up of lymphocytes and resides in the lymphatic system. Lymphoma can be subdivided into either Hodgkin or Non-Hodgkin lymphoma. Hodgkin lymphoma is defined by the presence of malignant Reed-Sternburg cells whereas Non-Hodgkin lymphoma includes all other lymphomas (169).

MM (170), AML (171), ALL (172), CLL (173) and CML (174) have all been shown to be heavily reliant on the BM microenvironment. The tumour microenvironment is vital for tumour cell proliferation, angiogenesis, invasion and metastasis. This is through its provision of survival signals, secretion of growth and pro-angiogenic factors and has been shown to provide a protective environment allowing malignant cells to evade

chemotherapy (43). Together, these studies demonstrate the significance of the BM microenvironment in the progression of haematological malignancies.

1.7.2.1   Acute Myeloid Leukeamia

AML is an aggressive malignancy defined by the proliferation and accrual of immature myeloid progenitors in the BM (175). AML is sustained by a pool of leukaemic stem cells (LSCs), which have the ability to evade chemotherapy and are often responsible for the relapse of this disease (176). AML is heterogeneous, there are many chromosomal translocations present in this disease (177). Similar to MM, AML primarily affects the older demographic with 71 being the average age at diagnosis (178).

In the HSC niche, interactions between the BM microenvironment and leukaemia promote the survival, proliferation and chemotherapy resistance of AML (179-181). Many studies have now shown that primary leukaemia cells are not able to proliferate outside its disease microenvironment (30, 173, 182, 183). Moreover, in many cases the interactions between the leukaemia and its microenvironment are hijacked from normal interactions between haematopoietic stem and progenitor cells (HSPCs) and the BM microenvironment. Thus, understanding the interactions between leukaemia cells and its BM microenvironment could also help us understand how normal HSPCs interact with the BM microenvironment. For example, AML has been shown to use the CXCR4/CXCL12 signalling axis to hone the BM (184) and blocking this interaction mobilises the AML into the peripheral blood (185). Discovering this mechanism in a malignant setting has allowed for the use of CXCR4 inhibitors to mobilise HSCs into the peripheral blood for isolation prior to stem cell transplantation (186, 187).

In our laboratory we have shown that the BM microenvironment plays a key role in this disease. Specifically, the BM adipocytes have been shown to support the proliferation of AML. AML blasts reprogram the metabolism of the adipocytes to induce lipolysis, releasing FFA, which in turn are taken up by the AML (42). We have also shown that BMSC play a key role in the growth of

these malignant cells by facilitating interactions between the BM microenvironment and the leukaemic cell. A potential reason for this interaction is the tumours' reliance on mitochondrial driven adenosine triphosphate (ATP) production which is provided by the microenvironment in the form of mitochondrial transfer (188). It has recently been reported that tumour derived nicotinamide adenine dinucleotide phosphate oxidase 2 (NOX2) stimulates the generation of superoxide, causing the BMSCs within the microenvironment to donate their mitochondria to the AML through tunnelling nanotubes (TNTs), promoting tumour survival (41). Moreover, this study also showed that CD34+ HPCs could acquire mitochondria from the BMSC, but only when stimulated with hydrogen peroxide. Understanding these processes in normal and stressed haematopoiesis is one of the main objectives of this study.

1.8 Stressed haematopoiesis

Stress at the cellular and organism level arises in numerous forms. Intrinsic stress is defined as intercellular metabolic changes such as; the amalgamation of waste products, damage caused by repeated cell division with age and production of toxic metabolites, including ROS (189). Environmental stress causing potentially harmful alterations in the biological system is referred to as extrinsic stress (190). Stresses such as bacterial infections, viral infections, ageing, trauma or severe blood loss can affect the haematopoietic response. The ability of the haematopoietic system to adapt in response to this stress is critical for survival (191).

1.8.1 Stress and ageing

Ageing exhibits characteristics of both extrinsic and intrinsic stresses and thus, can be construed as a stress itself (189). Biological ageing, also known as senescence, is described as adverse alterations leading to increased mortality (192). In cellular senescence, cells ensue distinct phenotypic alterations and no longer undergo the process of cell division or proliferation (193). With

cellular senescence there is a release of many pro-inflammatory cytokines, chemokines, proteases and growth factors, this is considered the senescence-associated secretory phenotype (SASP) (194). Senescence is thought to occur from the presence of alleles with harmful consequences, which manifest themselves as adverse phenotypes in later age (195). Immunosenescence is defined by a reduction of both innate and adaptive immunity in the peripheral blood and the BM (196). Both these processes are likely to have a significant impact on normal haematopoiesis.

With ageing there is also an accumulation of dysfunctional mitochondria (197, 198) oxidative stress (199), proteotoxic stress (200), and inflammation (201) these all can alter normal HSC function. As HSCs have the ability to self-renew throughout their lifetime they are one of the only blood cells that can truly age (202). Although HSC expansion increases with age, their functionality decreases over time. Subsequently, there is a decrease in the production of blood and engraftment after transplantation (203). However, the reason for this decline remains unknown (204).

During ageing, HSCs acquire mutations which are passed to daughter cells, some mutations have no effect (205), whilst others can lead to increased proliferation, self-renewal and disproportionate expansion at the expense of other clones (206). This survival advantage is a hallmark of clonal haematopoiesis. Clonal haematopoiesis is often initiated by a skewed X chromosome inactivation or somatic mutations, most commonly in the DNM3TA, TET2, and ASXL1 genes (206, 207). These mutations represent a permissive state for leukaemia development and are commonly associated with myeloproliferative disorders, myelodysplatic syndrome and AML (148, 208-210). Therefore, ageing itself is a stress, which can lead to functional decline of the haematopoietic system.

1.8.2   Response to infection

Alongside haematopoiesis, the BM is also an important site for granulopoiesis, erythropoiesis and lymphopoiesis which are all key to the response to infection. Microbial challenges, including acute infection, are linked to significant changes in the HSC compartment. This, in turn, has an impact on the differentiation and migration of HSCs (211). The BM has a central role in maintaining this immune homeostasis; in infection the haematopoietic system drives the immune response necessary for host survival. HSC differentiation can be influenced by a variety of stimuli, including contact with pathogens, to combat the cellular needs of the immune response resulting in physiological changes within the BM (212). Infection can therefore dysregulate the progenitor cells and interfere with normal homeostasis in the BM, including the availability of blood cells (213). Under pathogenic challenge, emergency granulopoiesis and rapid mobilisation of neutrophils out of the BM is key to overcome pathogen invasion (191). Erythropoiesis similarly is increased in response to acute inflammation upon pathogen detection. Under systemic challenges such as malaria and toxoplasmosis, there is a preferential increase of granulocytes in the BM. This is at the expense of the lymphocyte, erythrocyte, and megakaryocyte populations (214).

Increases in the number of progenitor or HSC populations within the BM is a trademark of infection (215). Immune challenges with *Plasmodium chabaudi* or *Pneumocystis carinii* increase the number of HPCs and HSCs in the BM and in the peripheral blood, which subsequently causes an increase in MPP cells (216). It has not been distinguished whether the changes in the BM are a consequence of the infection or part of the response to minimise the infection. It is also unclear whether the role of HSCs in infection includes immune sensing, however, it has been reported that the proliferation of HSCs could be a component of the primary response alongside replenishing depleted progenitors (217). Nevertheless, despite these drastic changes in the make-up of the BM microenvironment populations caused by infection, once cleared the BM returns to normal homeostasis.

The long-term effects of repeated infection on haematopoiesis and the function of life-long HSCs can however be detrimental. It has recently been shown that repeated inflammatory challenge with Poly IC results in depletion of functional HSCs and that these HSCs have an inability to self-renew. This depletion had no initial consequences on the mice however they developed clinically relevant features of ageing, comparable to elderly humans (218). Similarly, when mice were given daily low dose of lipopolysaccharide (LPS) for 1 month HSCs were unable to maintain quiescence, and following transplantation these HSCs skewed toward a myeloid lineage concurrent with ageing (219). Overall the haematopoietic system has an effective efficient reponse to immune challenges, however sustained or repeated infection can have an adverse effect and accelerate ageing.

1.8.3   LPS as a surrogate for bacterial infection

Bacterial LPS are a main component of the outer surface membrane of most gram-negative bacteria (220). They are strong activators of the innate and natural immune system in humans and murine models so are ideal in mimicking an infection (221). LPS comprises an oligosaccharide region which is attached to the outer membrane on the bacteria via a carbohydrate, lipid A (222). The main immunostimulatory effects of LPS is due to lipid A. In mammals, activation of the immune system with highly endotoxic forms of LPS have all been comprised of lipid A types of LPS (223). LPS can trigger a number of physiological immunostimulatory effects in mammals, however, if the dose is too high it can lead to the induction of septic shock (224).

Myeloid lineage cells have been shown to be the primary sensors for LPS in the immune system (223). Significant progress been made to understand the signalling cascade caused by LPS in mammalian phagocytes. It is thought that the LPS is first recognised by the LPS binding protein (LBP), CD14 either membrane bound or soluble form and Toll-like receptor 4 (TLR4) *MD-2 complex. This leads to the rapid activation of the intracellular signalling

network similar to the signalling of IL 1 and IL 18 (223). Whilst LPS alone activates the TLR4 immune response, whole bacterial cells secrete many virulence factors which activate numerous TLRs and pattern recognition receptors (PRR) that can modulate the immune response so LPS alone may not be truly representative of a bacterial infection. Whole bacterial cells also replicate and shed LPS, resulting in a more kinetic immune response rather than a direct activation of the immune system. However, to assess the effect of the host response to infection in a more standardised manner, *in vivo* and *in vitro* LPS can be used as a surrogate for simulating a bacterial infection.

1.8.4   *Salmonella*

Salmonella typhimurium (*S. typhimurium*) is the most common cause of invasive nontyphoidal *Salmonella* infection. Aggressive strains of non-typhoidal salmonellae have been the main cause of infection of the bloodstream in African children and adults, with a fatality rate of 20–25% (225). *S. typhimurium* infections cause acute inflammation of the intestine in both human and mice hosts. The *S. typhimurium* can survive in this inflammatory environment and therefore has a selective growth advantage over the gut microbiota (226). Following adherence to the intestine the *S. typhimurium* then invades and crosses the intestinal epithelium (227). Toll like receptors (TLRs) are the first pathogen recognition receptors to recognise the presence of *Salmonella* (228). *Salmonella* has been shown to activate several TLRs including TLR1/2/6 *in vitro* by its bacterial lipoproteins; TLR4 by its LPS, TLR5 by its flagellin and TLR9 by the CpG-rich repetitive elements in its DNA (226). When the ligands bind to the TLRs, MyD88 and TRIF signalling adaptors are activated initiating a signalling cascade in which transcriptional factors NFκB and IRF3 are also activated. This induces the production of several inflammatory cytokines including IL 8, IL 10, IL1β, IL 18 and type I interferon response (228). Mice infected with *S. typhimurium* have been shown to have upregulation of Sca 1 expression. Systemic infection with *S. typhimurium* also induced HSC activation and γH2AX$^+$ and 53BP1$^+$ foci formation indicating

proliferative stress caused by TLR4-TRIF signalling (229). *S. typhimurium* is the model of bacterial infection used in this study.

1.8.5 NOX2

It is interesting to note that, in some genetic diseases there exist a number of immunodefficiency syndromes (230). Nicotinamide adenine dinucleotide phosphate (NADPH) oxidase (NOX) isoforms have many important roles in the maintenance of normal functionality however, they have been connected to the pathogenesis of multiple diseases (231). NOX2 (Figure 1.6) is crucial in the host defence to microbes. One example of this inability to fight infection is NOX2 deficiency in several chronic granulomatous diseases (CGD), which are characterised by extreme inflammation and severe bacterial and fungal infection (232). This results from an inability of the phagocytes to produce ROS caused by a mutation in the genes encoding NOX2 (232, 233). The phagocytes, unable to produce reactive oxidant intermediates (ROI), have a low capability for phagocytosis. It has also been suggested that NOX2 plays a crucial role in the crosstalk between neutrophils and macrophages promoting neutrophilic apoptosis and clearance, to limit inflammation (231). NOX2-deficient mice developed pro-inflammatory cytokine responses and neutrophilic lung inflammation in response to zymosan a ligand found on the surface of fungi. Wild type and transgenic mice which had NOX2 reconstructed in the monocytic and dendritic linages exhibited self-limited responses (234). These data show that NOX2 plays a critical role in fighting infection. However, we need to further understand if and how NOX2 signalling is required for the expansion of the HSC compartment in response to infection.
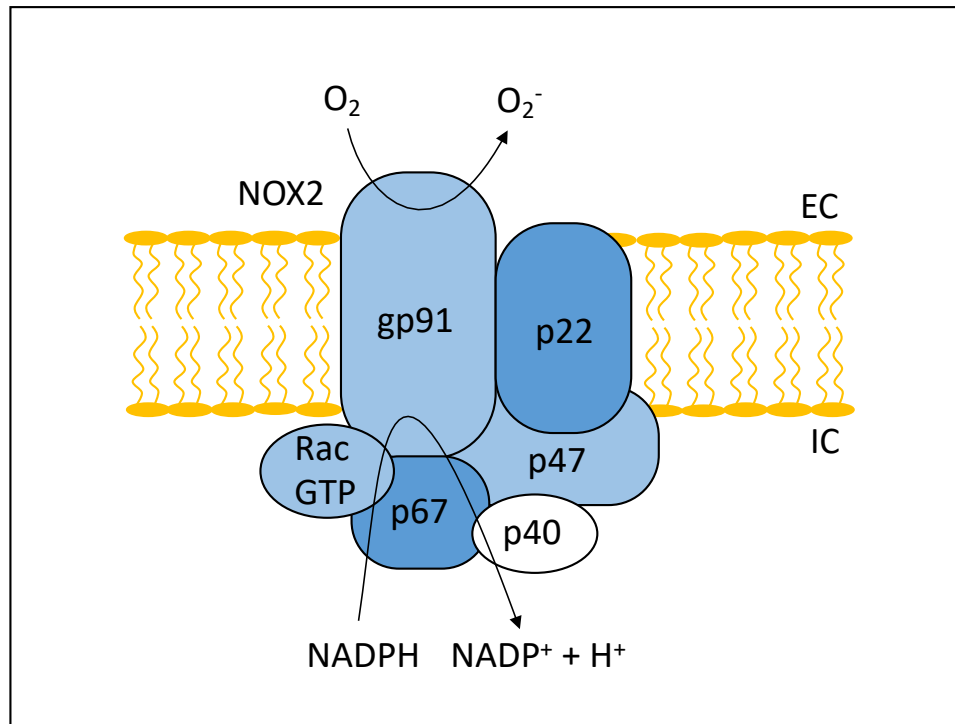
Figure 1.6. Diagram of NOX2.
Activated complex of NADPH oxidase 2 (NOX2) also known as gp91phox. NOX2 is activated on phagosomes of phagocytic cells. NOX2 is formed of heterodimeric complexes and has a p22phox chain which is regulated by p47phox a homologous organiser protein and p67phox an activator protein. NOX2 also requires Rac bound to a GTP. When activated the preassembled cytosolic subunits p67phox, p40phox and p47phox translocate to the complex. Superoxide anions are produced by NOX2 upon activation. (Adapted from Rada and Leto, 2008 (235)).

1.9   The energy requirements for normal and stressed haematopoiesis

1.9.1   Metabolism

The broad definition of metabolism is the sum of the biochemical processes which generate or consume energy in a living organism. This is a vast amount, more than 8,700 reactions and 16,000 metabolites (236). Pathways utilising abundant nutrients such as carbohydrates, fatty acids and amino acids are the basis of core metabolism and vital for energy homeostasis. Cells utilise these nutrients for energy in the form of ATP, primarily generated by aerobic respiration using glucose as the metabolite (237).

Glucose is converted into pyruvate which generates two molecules of ATP in a process known as glycolysis. Pyruvate can then feed the tricarboxylic acid (TCA) cycle for further ATP production (238). Glycolysis is an oxygen independent reaction. Interestingly, recent studies have shown that lactate can also feed the TCA cycle via its conversion back to pyruvate by lactate dehydrogenase (239) (Figure 1.7). Within the mitochondria pyruvate is converted to acetyl CoA reducing nicotinamide adenine dinucleotide (NAD+) to NADH, which is later used by the cell to generate ATP (240). Acetyl CoA enters the TCA cycle where one molecule of ATP is generated, however three molecules of NADH and one molecule of reduced flavin adenine nucleotide (FADH$_2$) are also produced (241). NADH and FADH$_2$ provide the high energy electrons for the next stage in the process, oxidative phosphorylation (OXPHOS).

OXPHOS is a process in which ATP is produced by electron transport from the NADH and FADH$_2$ along protein Complex I, II, III and IV situated on the inner mitochondrial membrane (237). Electrons are removed from NADH in mitochondrial Complex I and FADH$_2$ in Complex II and transferred to coenzyme Q (ubiquinone). Ubiquinone is reduced to ubiquinol in Complexes I and II transferring electrons to cytochrome C through Complex III. Electrons are removed from cytochrome C in Complex IV and transferred to oxygen molecules, generating water. As the electrons are transported through the complexes, mitochondrial matrix protons are passed across the inner mitochondrial membrane, creating an electrical potential gradient (242). This generates a proton-motive force, synthesising ATP from ADP and Pi by a rotation of the F$_0$ subunit (243). Four protons are necessary for one molecule of ATP to be produced (244). NADH releases 10 protons whereas FADH$_2$ releases only six protons (237). Consequently, during this process many ATP molecules can be produced and therefore, OXPHOS is the most efficient way to generate ATP.

1.9.2   Glycolysis vs Oxidative phosphorylation

The HSC niche in which the HSCs reside is known to be hypoxic, this maintains stem cell quiescence. Under normal conditions quiescent HSCs heavily rely on anaerobic glycolysis rather than OXPHOS to sustain ATP production (245). Metabolic analysis has shown that HSCs/HPCs have a different metabolic profile to that of the more committed cells (246). HSCs have been shown to have an increased pyruvate kinase activity and accrue high levels of fructose-1,6-bisphosphate, suggesting that the HSCs are metabolising by active glycolysis. They also have been shown to have high levels of pyruvate but low levels of phosphoenolpyruvate, which is the product and substrate of the glycolysis pathway (247). These data show that under normal conditions it is most likely that glycolysis is the metabolic pathway of choice for the HSCs.

As HSCs differentiates into progenitor cells, they exit the niche and many of these cycling cells are situated near the vascular endothelial cells. The oxygen levels increase to a more normoxic level and the progenitor cells start to use OXPHOS to generate ATP (248). However, under stressed haematopoiesis, the primary source of ATP was thought to be glycolysis. During stress the BM becomes acidic due to an increased lactate production, a by-product of glycolysis (249). The BM is also full of triglyceride containing adipocytes, which release FFA and glycerol in response to stress conditions (250). The next two sections introduce how lactate and FFA could be the primary source of energy for HSPC under stressed conditions.

1.9.3   Lactate

It is important to note that a by-product of glycolysis is lactate. It has recently been found that alongside pyruvate, glucose also feeds the TCA cycle through lactate produced in glycolysis (239). This study showed that in lung tumours circulating lactate was the primary substrate for the TCA cycle. Glucose is a vital nutrient which is broken down into pyruvate and lactate through glycolysis

or CO_2 via the TCA cycle. Previously it was assumed that pyruvate was the primary source of circulating carbon from glycolysis for the TCA cycle and the amount of carbon provided by lactate remains unknown. In this study, to quantify glucose and lactate concentrations, ^{13}C isotope labelled nutrients were administered intravenously to fasting mice. In the fasting mice, lactate had the highest flux of metabolites even when compared to glucose, indicating that in this model lactate was the primary source of carbon for the TCA cycle. Pyruvate was expended at a similar rate to lactate, however as it only exists in small quantities it did not have a substantial flux. It was previously presumed that the abundance of lactate over glucose was due to the interchange between pyruvate and lactate (Figure 1.7), which occurs under low oxygen conditions or when there is an large quantity of lactate (249). However, if this was the case the ^{13}C labels would not be altered after infusion or during the conversion of lactate to pyruvate, therefore the large flux measured is from the lactate itself. It has also been shown that lactate can feed the TCA cycle under malignant conditions specifically in non-small cell lung cancer (251). Therefore, it is thought the lactate produced in glycolysis can be fed into the TCA cycle for OXPHOS production of ATP (Figure 1.8).
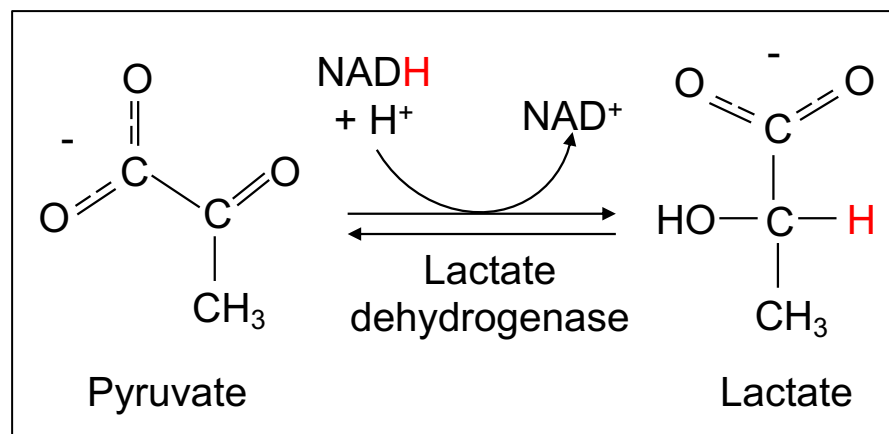
Figure 1.7. The conversion of pyruvate to lactate.
NAD+ is regenerated from NADH by reduction of pyruvate to lactate, it is a reversible reaction catalysed by the enzyme lactate dehydrogenase. This reaction occurs in cells when there is a limited supply of oxygen.

1.9.4 Fatty acid oxidation

Glucose and lactate contribute to around half of the carbon required for the TCA cycle. It is hypothesised that the remainder is provided by a combination of other amino acids and fat (239). Fatty acids (FAs) are released from the adipose tissue and are stored as triglycerides. Triglycerides are hydrolysed by lipolysis and secreted into the circulation as FFAs and glycerol (252). FFAs act as a substrate for beta (β)-oxidation and subsequent ATP production (253). Fatty acid β-oxidation (FAO) occurs in the both the mitochondria and peroxisomes and is the process by which FFAs are broken down to generate acetyl-CoA, which can feed the TCA cycle to produce energy in the form of ATP (Figure 1.8). The process of FAO can be broken down into four steps. Firstly, FFAs enter the cells and are activated by being coupled with coenzyme A (CoA) within the cytosol. This allows for the long-chain fatty-acyl-CoA to transfer the acyl group via carnitine palmitoyl transferase 1 (CPT1) producing acylcarnitine. It is then transported into the inner mitochondrial membrane by carnitine translocase. The final step is inside the mitochondria, the long chain acylcarnitine is oxidised by the carnitine palmitoyl transferase 2 (CPT2) and converted back to long-chain acyl-CoA which enters the TCA cycle for further ATP production (254). FAO is capable of providing a large amount of energy to fuel tumour growth by increasing production of ATP under metabolic stress (255). *In vitro* CPT1 has been shown to be upregulated in lung tumour models promoting tumour survival in metabolically stressed conditions (256). Previous studies have also shown cancer cells overexpress CTP1, which drives ATP production via FAO (257, 258). Taken together this data shows FAO could be an important source of energy under stressed conditions.
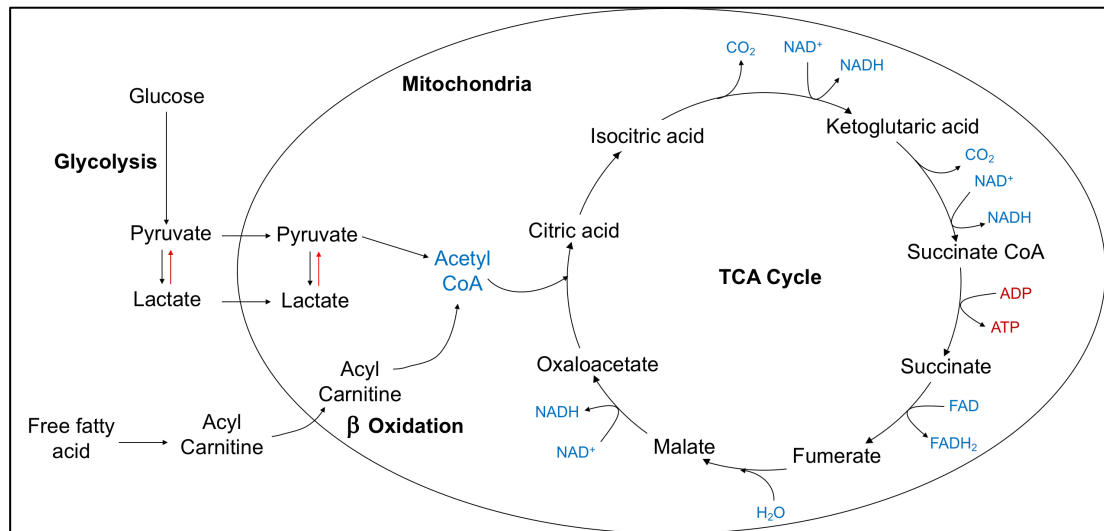
Figure 1.8. Glycolysis and Beta oxidation feed the TCA cycle.
Glucose is converted to pyruvate by a process called glycolysis. A by-product of this process is lactate which alongside pyruvate enters the mitochondria and is converted to acetyl CoA, which then feeds the tricarboxylic acid cycle (TCA) cycle. At the same time free fatty acids (FFA) are converted to acyl carnitine, which is then transported across the mitochondrial membrane and converted to acetyl CoA via beta (β) oxidation. The acetyl CoA produced during FAO is also used in the TCA cycle. The TCA cycle is a sequence of reactions which generates energy in the form of ATP during the process of aerobic respiration.

1.9.5 Fatty acid transporters

FAs not only serve as an energy source, but they also regulate the metabolism by transcriptional and enzymatic complexes which govern gene expression of many pathways such as cell survival, proliferation and metabolic responses (259-261). FA trafficking is a dynamic but complex process which affects many aspects of cell function (260). There are many transporters and receptors involved in FA transport including Macrophage scavenger receptor 1 (Msr1) (262), long chain acyl CoA synthetase (Acsl) (263), FA binding proteins (Fabp1, Fabp3, Fabp4, Fabp5) (264), fatty acid transporter proteins (Slc27a1, Slc27a4, Slc27a5) (265, 266) and fatty acid translocase (CD36) (267, 268) (Figure 1.9). FA binding proteins (FABPs) coordinate lipid trafficking and function in cells (261). It has been previously shown that AML can induces lipolysis in adipocytes releasing FFA which are transported into the cell by FABP4 (42). There are currently 9 distinctive isoforms of FABPs identified, and these are highly expressed in tissues with active lipid metabolism (269).

CD36 is a scavenger receptor which is expressed on many different types of cells. It is an integral membrane protein which is involved lipid metabolism, inflammation, thrombosis, atherogenesis and haemostasis (270). There are many members of the CD36 family of genes including lysosomal integral membrane protein II (LIMP II) and high-density lipoprotein receptor SR-B1. These all have a hairpin topology, which comprises two transmembrane domains a hydrophobic sequence adjacent to the COOH terminus and hydrophobic signal anchor adjacent to the NH_2 terminus (271). The COOH terminal half contains three disulphide bridges and is heavily glycosylated, which is key for CD36 membrane recruitment (272). CD36 has been shown to be expressed on haematopoietic cells including monocytes, megakaryocytes, platelets and erythroid progenitor cells. Whilst CD36 has many roles its primary role is suggested to be a FA transporter; it has a high affinity for binding long chain fatty acids. CD36 has been shown to be the primary facilitator of FA transport in cardiomyocytes, skeletal myocytes enterocytes and adipocytes (273-276). In a malignant setting CD36 has also been implicated in the progression of many types of cancers (17, 277-279). A subpopulation of LSCs have been shown to express CD36 and to have an altered metabolic profile with high levels of fatty acid oxidation. These CD36 expressing LSCs had a survival advantage and were able to evade chemotherapy (17). This study aims to elucidate the importance of CD36 for fatty acid transport in stressed haematopoiesis.
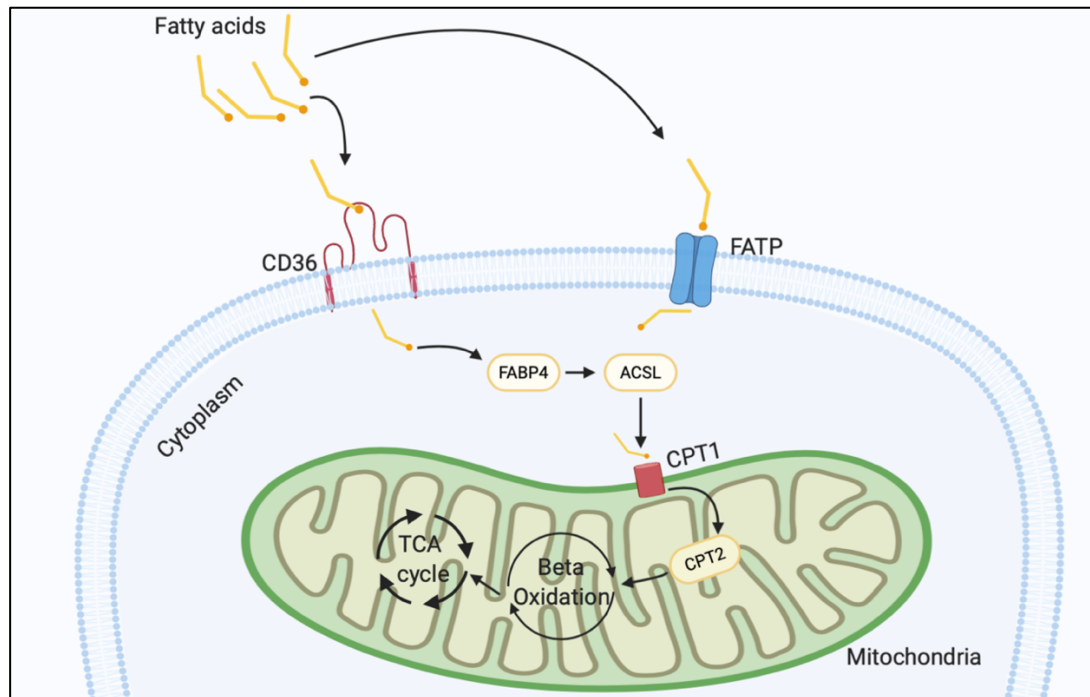
Figure 1.9. Transporters and receptors involved in FA transport.
A schematic diagram of fatty acid (FA) trafficking into the cell regulated by transport proteins and receptors. Extracellular FAs are transported into the cell across the plasma membrane by CD36 and fatty acid transport proteins (FATPs). Inside the cytoplasm FFAs bind to fatty acid binding protein 4 (FABP4) and then long chain acyl CoA synthetase. They are then transported across the mitochondrial membrane by carnitine palmitoyltransferase 1 (CPT1) and transported for further metabolism by carnitine palmitoyltransferase 2 (CPT2) to be utilised by β oxidation which then feeds into the TCA cycle to generate ATP. (Adapted from Masarwi *et al*. 2019 (280) and created using BioRender.com).

1.9.6   Mitochondria

Mitochondria are regarded as the powerhouse of the cell. They maintain homeostasis of the cells by regulating energy production, cell metabolism and calcium signalling (281). Endosymbiotic theory states that mitochondria originated from eubacteria engaging in a symbiotic relationship with the host cell (282). As such, mitochondria have conserved many bacterial characteristics including the double membrane, its own DNA and the ability to self-sustain by generating the majority of ATP for cells, either by OXPHOS or aerobic respiration (283). The inner mitochondrial membrane is folded and forms the cristae, this increases the surface area, for the electron transport chain to maximise ATP production. The mitochondria has its own distinct mitochondrial DNA (mtDNA) which differs from genomic DNA (gDNA) (284).

The 16 kilobase circular mtDNA genome is circular contains 37 genes, 13 of which encode protein subunits of Complex I, III, IV, and V (285).

Mitochondria are central to the metabolism of carbohydrates, lipids and amino acids in most cells including HSCs. Recent studies have shown that a key characteristic of HSCs is the maintenance of quiescence by limiting mitochondrial respiration (286). Although the role of mitochondria in stem cells is very complex, mitochondria in normal HSCs are somewhat inactive (287). ROS levels, related to mitochondrial activity, are also much lower in the HSCs compared to the committed progenitors (288) suggesting differentiation of HSCs requires a rapid burst of energy supplied via mitochondrial metabolism. As active cells require a different energy source to quiescent cells, the changes in cellular metabolism from dormant to cycling is important (59). Increasing ROS levels, as occurs with infection, promotes the differentiation of HSCs for repopulation, whereas low levels of ROS maintain quiescence (289).

This suggests reprogramming of HSC metabolism can occur dependent on the demand. For example, normal HSCs rely on the maintenance of quiescence via anaerobic glycolysis but can rapidly turn on mitochondrial OXPHOS to meet the energy demands of repopulation under stressed conditions (246, 290, 291). Understanding these underlying changes in HSC metabolism from quiescence to proliferation can aid in the understanding of the development of diseases and response to infection. This ultimately is the aim of my PhD study.

1.9.7 Mitochondrial transfer

Mitochondria were typically thought to reside in one cell for the entirety of their life, undergoing fusion and fission generating networks of mitochondria until degradation by mitophagy (292). However, it has now been proven this is not the case and mitochondria are able to move intercellularly. Multiple structures

have been found to potentially mediate this transfer such as tunnelling nanotubules (TNTs), extracellular vesicles and gap junctions (Figure 1.10).

Functional mitochondrial transfer was first described by Spees *et al*. 2006, where mitochondrial transfer between human stem cells and somatic cells *in vitro* rescued aerobic respiration of non-functional mitochondria-depleted recipient cells. A549 cells were treated long term with ethidium bromide to damage the mtDNA (ρ^0) causing dysfunctional or deleted mitochondria. When cultured alone these A549 ρ^0 cells did not survive monoculture. However, when co-cultured with human mesenchymal stem cells they obtained donor mitochondria and were able to respire aerobically (293). There was initial concern that intercellular mitochondrial transfer was not physiologically relevant as it was only observed *in vitro*. However, more recent studies disprove this and have reported that mitochondrial transfer does in fact also occur *in vivo* in tissue injury and cancer survival and proliferation (41, 294-297). Tan *et al.* 2015, showed mitochondrial transfer occurs *in vivo,* ρ^0 tumour cells acquired mtDNA from cells in the tumour microenvironment, leading to recovery of mitochondrial function in these tumour cells (298).

Intercellular mitochondria transfer has been shown to be crucial in the survival of cancer cells (299). Primary AML acquire functional mitochondria from the BMSC in a co-culture system increasing mitochondrial mass by 14%. Following co-culture, AML had a 1.5-fold increase in the production of mitochondrial ATP and were more resistant to mitochondrial depolarisation after chemotherapy, increasing cell survival. The mitochondrial transfer was cell to cell contact dependant (297).

Mitochondrial transfer may also affect normal processes including stem cell differentiation, activation of inflammatory signalling pathways or differentiated cellular reprogramming (300). Intercellular mitochondrial trafficking has been shown to protect against acute lung injury following infection. Mice were airway-instilled with LPS and mouse BMSC. The mouse BMSC released mitochondria-containing extracellular vesicles which were taken up by the

alveolar epithelium. This transfer of mitochondria caused an increase in ATP in the alveolar preventing acute lung injury in response to infection (295). Similarly, neurons have been shown to transfer their dysfunctional mitochondria to astrocytes for reprocessing and this process is bi-directional. In mice with transient focal cerebral ischaemia astrocytes release and transfer functional mitochondria to neurons increasing cell survival (296).

In a similar way, mitochondrial transfer occurs between MSC and human umbilical vein endothelial cells. Human umbilical vein endothelial cells were oxygen and glucose deprived and then reoxygenated, this stimulated mitochondrial trafficking from the MSC to the damaged endothelial cells resulting in rescued aerobic respiration and protection from apoptosis (301). Transfer of mitochondria from MSC to macrophages both *in vitro* and *in vivo* has been shown to enhance phagocytic capability of the macrophages in following Acute Respiratory Distress Syndrome and sepsis. Furthermore, inhibiting this process caused a decrease in macrophage functionality (302). These studies suggest intrinsic or extrinsic stress may be required to initiate intercellular mitochondrial transfer and that mitochondrial transfer is a fundamental process which occurs in both physiologically normal and malignant settings.
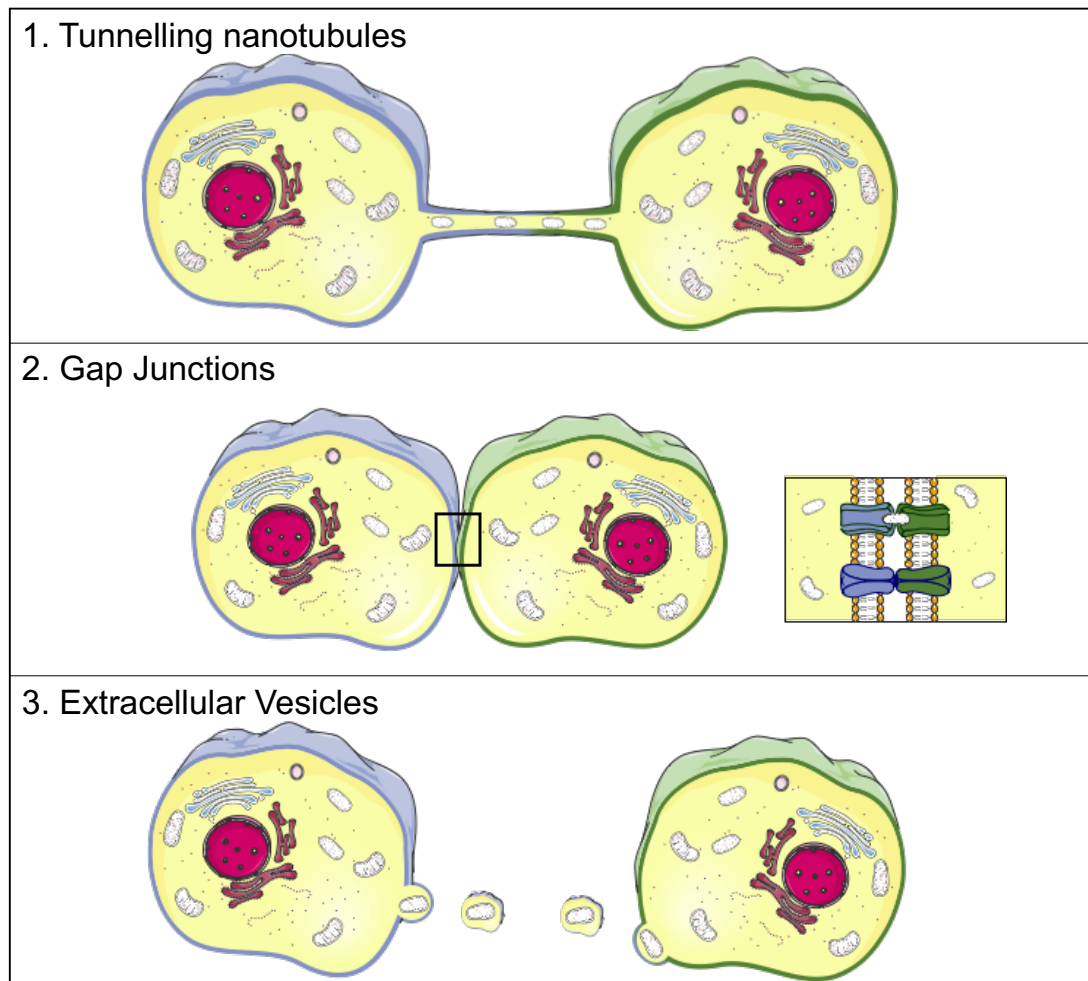
Figure 1.10. Mechanisms of mitochondrial transfer.
A schematic representation of the structure of the mechanism by which mitochondria can transfer intercellularly. 1. Tunnelling nanotubules 2. Gap junctions 3. Extracellular vesicles. (Created using Servier Medical ART).

1.9.7.1 Tunneling Nanotubules

One mediator of mitochondrial transfer are TNTs. TNTs have been shown to occur intercellularly both *in vitro* and *in vivo*. TNTs join the cytoplasm of two neighbouring cells directly via open tubes or channels (299). They enable the interchange of cellular organelles, membrane vesicles and small, cytoplasmic and membrane soluble molecules. A nanotubule is formed by the development of a membrane projection similar to the filopodium, which withdraws when it has reached the target cells leaving behind a very fine structure, separate to the substrate (300). TNTs are able to bidirectionally transport proteins, lipid droplets, ions, RNAs including miRNAs, organelles, and viruses over 150 mm

(303-305). There are two types of TNTs characterised by size, cytoskeletal design and functionality (306, 307). Type 1 TNTs tend to be longer and larger than type 2 TNTs and also have a clearer cytosolic tunnel. Interestingly, tubulin is not present in type 2 TNTs, however, type 1 TNTs are comprised of microfilaments and microtubules. Subsequently, organelle transporting only occurs by type 1 TNTs and this is therefore, the type of TNT utilised in mitochondrial transfer (306). TNTs are vital in some types of mitochondrial transfer, TNT impairment either chemically or with stress can reduce mitochondria trafficking (308). Intercellular mitochondrial transfer via TNTs is facilitated by Milton adaptor proteins and kinesin motors (309-311).

Stress agents have been shown to increase the formation of TNTs and subsequently induce mitochondrial transfer. Endothelial progenitors have increased mitochondrial transfer to mature endothelial cells when treated with doxorubicin (312). Similarly, ethidium bromide treatment increases TNT facilitated mitochondrial transfer from MSC to osteosarcoma cells (313). *In vivo* models of acute lung injury stimulated by rotenone or TNF-treatment also initiates mitochondrial transfer from the stem cells to lung epithelial cells via TNTs (294). Generally, mitochondrial transfer via TNTs is initiated by mitochondrial damage. However, serum starvation and hydrogen peroxide also promote TNT formation. Taken together, this signifies stress can induce the formation of TNTs and subsequently initiate mitochondrial transfer.

1.9.7.2   Extracellular vesicles

Another facilitator of intercellular mitochondrial transfer are extracellular vesicles. Most cell types release heterogeneous vesicles into the extracellular media. Extracellular vesicles range in size from 30 to 10000 nm and can be categorised into three broad subtypes microvesicles, exosomes and apoptotic bodies dependent on size, origin and composition (314). Extracellular vesicles also mediate intercellular communication in many physiological and pathological processes (315). These vesicles can move cellular materials and transport them over large distances (316). Mitochondrial proteins and DNA

have been found in extracellular vesicles and larger extracellular vesicles have been found to contain whole mitochondria.

For example, both MSCs (317) and astrocytes (296) have recently been found to release mitochondria containing extracellular vesicles. BMSC have also been reported to use this mechanism to remove the dysfunctional depolarised mitochondria and transport them to surrounding macrophages for degradation (317).

Extracellular vesicles have also been found to be considerably upregulated in the BM in haematological malignancies compared to their healthy counterparts (318). A recent study has shown isolation of extracellular vesicles from BMSC by ultracentrifugation, cocultured with CLL B cells decreased the amount of spontaneous apoptosis, increased migration capabilities and increased chemotherapy resistance to several drugs. The extracellular vesicles produced by the MSC in leukemic patients also protected the malignant cells from both spontaneous and drug induced apoptosis (173). Overall, these studies suggest that mitochondrial trafficking within extracellular vesicles is most likely the result of a cellular mechanism to rescue mitochondrial function.

1.9.7.3   Gap Junctions

Another intercellular transporter of mitochondria are gap junctions. Gap junctions are specialised intercellular channels directly connecting the cytoplasm of different cells (319). They allow for the interchange of ions and molecules smaller than ATP through a regulated gate (320). A gap junction consists of two connexons or half channels linked in the intercellular space forming a channel spanning both cell membranes (321). They were originally characterised as ion channels with low resistance, connecting nerve and muscle cells however, they have now been shown to be able to connect most cells. Gap junctions have evolved over time to have a range of different functions with many regulatory mechanisms (322).

Mitochondrial transfer by gap junctions was shown to protect against acute lung injury. This process of mitochondrial transfer was shown to be regulated by connexins specifically, connexin-43 (CX43), which promotes the connection between MSCs and LPS damaged alveolar epithelial cells. This then led to the MSCs releasing extracellular vesicles containing the mitochondria, which were engulfed by the alveolar epithelial cells. This establishment of the CX43 gap junction channel was essential, MSC with dysfunctional CX43 could not attach to the alveolar epithelium cells and subsequently, no mitochondrial transfer occurred (295). It has also been shown that BMSCs transfer mitochondria through gap junctions to oxygen-glucose deprivation injured neurons after spinal cord injury. The gap junction inhibitor 18β glycyrrhetinic acid reduced mitochondrial transfer from BMSCs to neurons whilst the gap junction potentiator retinoic acid enhanced the mitochondrial transfer (323). In the context of the haematopoietic system it has been shown that osteogenic BMSCs acquire mitochondria from the HSPC in a CX43 gap-junction dependent manner. This function of this process is to reduce ROS levels in the HSC to maintain quiescence (324).

Donor and acceptor cell connexin complementarity is essential in the mitochondrial transfer process (325). Previous studies have demonstrated that CX43 is key in the formation of gap junctions for TNTs (326). Connexin and gap junction channels have also been shown to be involved in the clathrin-dependent endocytosis of extracellular vesicles (327). This data indicates gap junctions are important in mediating all mechanisms of intercellular mitochondrial trafficking.

1.10 Rationale

The BM microenvironment regulates the production of both haematopoietic and non-haematopoietic cells for the maintenance of blood production under normal and stressed conditions. The ability to generate large amounts of energy in the form of ATP under stressed haematopoiesis is essential for the increase in proliferation of the required immune cells. Intercellular mitochondrial transfer has recently been reported in acute myeloid leukaemia as well as models of lung inflammation. In the context of bacterial infection, the haematopoietic system needs to drive the granulocytic response necessary for host survival. Whilst previous studies of the BM microenvironment have provided the foundation to characterise the interaction between haematopoietic stem and progenitor cells (HSPC) and their environment, this study aims to understand how mitochondrial transfer from the BM microenvironment to HSPC and, fatty acids as a substrate, facilitate the expansion of immune cells in response to infection. Understanding how the BM microenvironment responds to infection, will help broaden our understanding of the physiological processes that occurs after the disruption of BM homeostasis. Moreover, it is likely that these mechanisms, which support HSC metabolism are hijacked by haematological malignancies to support tumour growth and are a fundamental reason why blood cancers arising in the BM microenvironment are presently so difficult to treat. Developing our understanding of the effect of stress, on BM function in normal haematopoiesis may help improve treatments for haematological malignancies.

1.11 Hypothesis

I hypothesise that under stressed haematopoiesis mitochondria move from the non-haematopoietic cells of the BM microenvironment to the haematopoietic stem/progenitor cells to rapidly support and sustain the host response to bacterial infection. I also hypothesise that HSCs within the BM microenvironment utilise both OXPHOS and β-oxidation to provide the necessary energy for the expansion of HSCs under stressed conditions.

1.12   Aims and Objectives

1. To establish a model to track mitochondrial transfer *in vivo.*
2. To determine if intercellular mitochondria trafficking from the BM microenvironment to HSCs is essential for the immune response to infection and establish the mechanisms governing this.
3. To determine if fatty acids are transported to HSCs from the BM microenvironment and if fatty acid metabolism in the HSC is vital for generating cellular energy in response to bacterial infection.
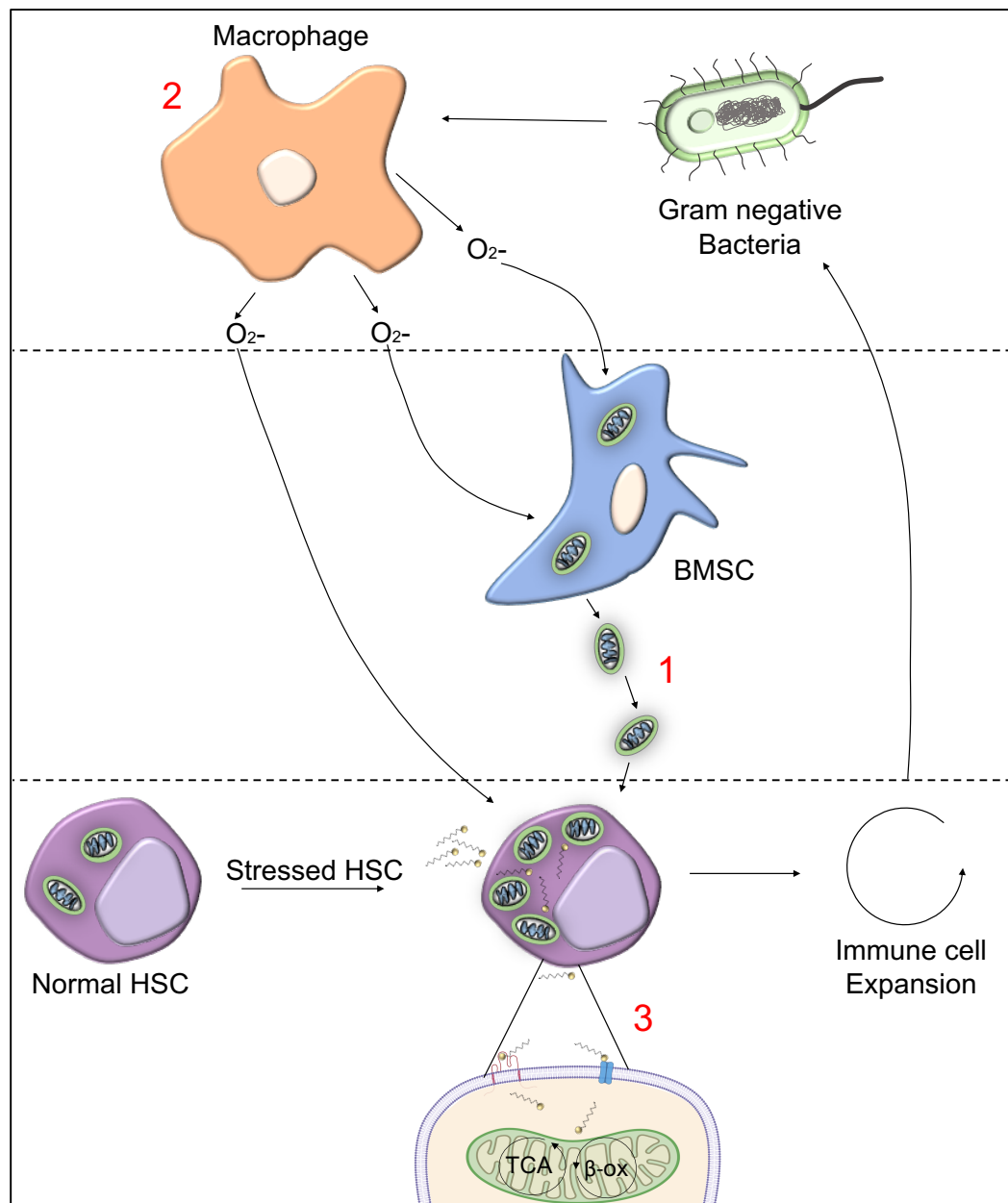
Figure 1.11. Graphical representation of aims/objectives.

2 Materials and methods

2.1 Materials

The reagents and materials used in this study are described in the methods below. All reagents were obtained from Sigma Aldrich (St Louis, MO, USA), unless otherwise specified in the text.

Table 2.1. Reagents used, with manufacturer and catalogue number.
Agilent (Santa Clara, CA, USA), BioLegend (San Diego, CA, USA), , Clontech Takara Bio, Saint-Germain-en-Laye, France), Fisher Scientific (Hampton, New Hampshire, USA), GE Healthcare (Little Chalfont, UK), Ibidi (Munich, Germany), Machery-Nagel, Duren, Germany), Merck Millipore (Burlington, MA, USA), Miltenyi Biotec (Bergisch Gladbach, Germany), New England BioLabs (Ipswich, MA, USA), PCR Biosystems (London, UK), Peprotech (Rocky Hill, NJ, Promega (Madison, WI, USA), USA), Qiagen (Hilden, Germany), Sigma Aldrich (St Louis, MO, USA), ThermoFisher (Waltham, MA, USA) and Vector Laboratories Ltd (Peterborough, UK).

Product	Manufacturer	Catalogue Number
100 Base pair DNA ladder	New England BioLabs	N3231S
10X RBC Lysis Buffer	ThermoFisher	00-4300-54
26G Butterfly Needles	Fisher Scientific	12349169
26G Needles	Fisher Scientific	12349189
30% Polyacrylamide/Bis Solution	Bio-Rad	1610154
4% Paraformaldehyde solution	Sigma Aldrich	1004968350
Ammonium Persulphate	Sigma Aldrich	A3678
Amplex Red Assay	ThermoFisher	A22188
AnnexinV Apoptosis Kit	ThermoFisher	88-8005-72
BL-Buthionine-sulfoximine	Sigma Aldrich	B2515
BODIPY™ 493/503	ThermoFisher	D3922
Bovine Serum Albumin	Fisher Scientific	BP1600-100
Bromophenol Blue	Sigma Aldrich	B0126
CAL101	Selleck Chemicals	S2226
Calcein	ThermoFisher	C1430
Carbenoxolone	Selleck Chemicals	S4368
CD117 MicroBeads, mouse	Miltenyi Biotec	130-091-224

Product	Manufacturer	Catalogue Number
D-Luciferin	Fisher Scientific	8829
DAPI	ThermoFisher	62248
DMEM Medium	ThermoFisher	10566016
DMSO	Fisher Scientific	BP231-100
EDTA	Sigma Aldrich	E9886
Etomoxir	Selleck Chemicals	S8244
Fetal Calf Serum	ThermoFisher	105000056
FIX & PERM Cell Fixation & Cell Permeabilization Kit	ThermoFisher	GAS004
FlouroBrite DMEM	ThermoFisher	A1896701
FLT 3	PeproTech	300-19
FuGENE	Promega	E2691
Gap 27	Sigma Aldrich	G1794
GeneJET Gel Extraction Kit	ThermoFisher	K0692
GenElute Mammalian Genomic DNA Miniprep Kit	Sigma Aldrich	G1N70
Glycine	Fisher Scientific	BP381-5
H2DCFDA	ThermoFisher	D399
H_2O_2	Sigma Aldrich	H1009
Heparin	Sigma Aldrich	H3393
Histopaque-1077	Sigma Aldrich	10771
Hoechst 33342 Solution	ThermoFisher	62249
Human CD105-FITC	Miltenyi Biotec	130-098-774
Human CD34 Microbead Kit	Miltenyi Biotec	130-046-702
Human CD34-VioBlue	Miltenyi Biotec	130-113-744
Human CD38-APC	Miltenyi Biotec	130-110-345
Human CD45-FITC	Miltenyi Biotec	130-110-770
Human CD45RA-PercyP	Miltenyi Biotec	130-113-920
Human CD49f-PeCy7	Miltenyi Biotec	130-107-832
Human CD73	Miltenyi Biotec	130-095-183
Human CD90-APC Cy7	Miltenyi Biotec	130-114-863
Human IL3	PeproTech	200-03
Human IL6	PeproTech	200-06
Human TPO	Miltenyi Biotec	130-094-011

Product	Manufacturer	Catalogue Number
Human/Mouse Ki67-FITC	Miltenyi Biotec	130-117-691
Immuno-Blot PVDF Membrane	Bio-Rad	1620177
L-Glutamine	Sigma Aldrich	G7513
Lipopolysaccharide	Sigma Aldrich	L2630
LS columns	Miltenyi Biotec	130-042-401
MEM Medium	ThermoFisher	11095080
MethoCult	STEMCELL Technologies	4434
Mitotracker Green FM	ThermoFisher	M7514
Mouse anti-connexin 43	ThermoFisher	13-8300
Mouse CD105-APC	BioLegend	120413
Mouse CD105-Pe	Miltenyi Biotec	130-102-548
Mouse CD115-APCVio770	BioLegend	135531
Mouse CD117-PeCy7	Miltenyi Biotec	130-108-355
Mouse CD140a-APCVio770	Miltenyi Biotec	130-105-117
Mouse CD150-BV510	BioLegend	115920
Mouse CD16/32-BV510	BioLegend	101333
Mouse CD31-PerCP	BioLegend	102522
Mouse CD34-PeCy5	BioLegend	103131
Mouse CD36-VioBright	Miltenyi Biotec	130-122-088
Mouse CD4-PeCy7	BioLegend	100527
Mouse CD45-VioBlue	Miltenyi Biotec	130-119-130
Mouse CD45.1-Pe	Miltenyi Biotec	130-103-009
Mouse CD45.2-VioGreen	Miltenyi Biotec	130-102-312
Mouse CD48-APC Cy7	BioLegend	103431
Mouse CD8-PeCy5	BioLegend	301009
Mouse F4/80-APC	Miltenyi Biotec	130-116-525
Mouse Gr1-PerCP	Miltenyi Biotec	130-119-794
Mouse IL3	PeproTech	213-13
Mouse IL6	PeproTech	216-16
Mouse Lineage Cell Depletion Kit	Miltenyi Biotec	130-110-470
Mouse Lineage Cocktail - Pacific blue	BioLegend	133310

Product	Manufacturer	Catalogue Number
Mouse mCSF	PeproTech	315-02
Mouse pAKT-PE	Miltenyi Biotec	130-105-343
Mouse Sca 1-APC	Miltenyi Biotec	130-102-343
Mouse SCF	PeproTech	250-03
Mouse Ter119-APC	Miltenyi Biotec	130-102-290
N-Acetyl-L-cysteine	Sigma Aldrich	A7250
ND1 Taqman Gene Expression Assay Human	ThermoFisher	4331182_Hs02596873
ND1 Taqman Gene Expression Assay Mouse	ThermoFisher	4331182_Mm04225274
Opti-MEM	ThermoFisher	31985062
OrangeG Gel Loading Dye	New England BioLabs	B7022S
Ovation® PicoSL WTA System V2	Tecan	3312-24
Penicillin-Streptomycin	GE-Healthcare	SV30010
PGE2	PeproTech	3632464
Pierce ECL Western Blotting Substrate	ThermoFisher	32106
Poly-D-Lycine Solution	Sigma Aldrich	A-003-E
Precision Plus Protien Standard Ladder	Bio-Rad	1610373
QBT Fatty Acid Uptake Assay	Molecular Devices	R8132
qPCRBIO SyGreen Mix	PCR Biosystems	PB20.12-51
RANKL	PeproTech	315-11C
ReliaPrep RNA Cell Miniprep System	Promega	Z6012
RIPA Buffer	ThermoFisher	89900
rLV.EF1.AcGFP-Mem9	Clontech	0019VCT
rLV.EF1.mCherry-Mito-9 lentivirus	Clontech	0024VCT
RPMI Medium	ThermoFisher	11875093
Seahorse Mito Stress Test	Agilent	103010-100
Seahorse XFp Base Medium	Agilent	1033335-100

Product	Manufacturer	Catalogue Number
Seahorse XFp Mito Fuel Flex Test	Agilent	103270-100
Serum/Plasma Fatty Acid Detection Kit	ZenBio Inc	GFA-1
Sodium Pyruvate	Fisher Scientific	11501871
StemMACS HSC expansion Medium	Miltenyi Biotec	130-101-526
Sulfosuccinimidyl Oleate	Cayman Chemical	11211
SYBR safe DNA Gel Stain	ThermoFisher	S33102
TaqMan Human Tert	ThermoFisher	4403316
Taqman Mouse Tert	ThermoFisher	4458368
TaqPath ProAmp MasterMix	ThermoFisher	A30865
TEMED	Sigma Aldrich	T9281
Tris Base	Fisher Scientific	BP152-1
Trypan Blue Solution	Sigma Aldrich	T8154
Trypsin-EDTA	ThermoFisher	25200056
Tween-20	Fisher Scientific	BP337-100
UltraPure Agarose	ThermoFisher	U3750
VECTASHIELD® mounting media	Vector Laboratories	H-1400-10
β-mercaptaethanol	Sigma Aldrich	M6250

2.2 Cell Culture

2.2.1 Primary cell isolation

2.2.1.1 Human cell isolation

Primary bone marrow (BM) aspirates and umbilical cord blood were obtained from patients at the Norfolk and Norwich University hospital under the approval of the UK NHS Health Research Authority (LCREref07/H0310/146) following informed consent. The aspirate was collected in sample tubes containing 5 mL Dulbecco's Modified Eagle's Medium (DMEM) supplemented with 100 units of Heparin. The cord blood was collected in sample tubes containing 15 mL DMEM supplemented with 500 units of Heparin.

2.2.1.1.1 BMSC

Primary human BM mesenchymal stromal cell (BMSC) were isolated by density gradient centrifugation using Histopaque-1077. Cells differentially migrate through the Histopaque-1077 allowing for viable fractionation of cell populations. 10 mL of Histopaque-1077 per 15-20 mL of BM was added to a 50 mL falcon tube. The BM aspirate was then gently layered on top of the Histopaque-1077 and centrifuged at 300 xg for 20 minutes with no brakes or acceleration, to allow for separation of the various BM components. Post centrifugation the red blood cells and heavy granulocytes are pelleted at the bottom of the tube, a layer of Histopaque-1077 sits atop. The 'buffy coat' containing mononuclear cells is formed on top of the Histopaque layer and finally the upper layer is the plasma (Figure 2.1).
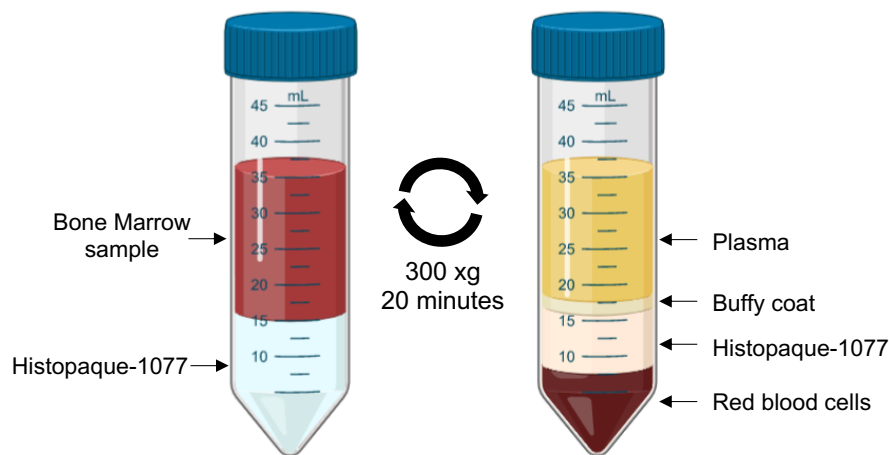
Figure 2.1. Schematic of density gradient centrifugation using Histopaque-1077.
Bone marrow aspirate was gently layered on top of Histopaque-1077 and centrifuged. Post centrifugation the BMSC of interest are located in the buffy coat. (Created using BioRender.com).

The buffy coat comprising the leukocytes and BMSC was isolated using a pasture pipette and washed twice using 1 X PBS. The cells were then cultured in DMEM supplemented with 10% foetal calf serum (FCS), and 100 U/mL penicillin and 10 µg/mL streptomycin (penstrep) for 24 hours. The non-adherent and non-viable cells were then washed off, fresh supplemented DMEM was added to the remaining adherent cells in the flask. The BMSC were situated in the adherent fraction. The media was replaced twice a week until BMSC colonies were visible. The BMSC were then passaged using the serine protease Trypsin-EDTA to allow for uniform coverage of BMSC in the flask. Briefly, the cells were washed with 15 mL of 1X PBS before addition of 3 mL of Trypsin. The flask was then placed in the incubator to ensure adherent cells were lifted from the flask surface. Next, 7 mL of DMEM was added to the flask to inactivate the Trypsin, the cells were then pelleted to remove any excess Trypsin, resuspended in DMEM and plated into a fresh flask. The BMSCs were then expanded until around 70-80% confluent prior to experimental use. The BMSCs were characterised by expression of the cell surface markers CD105, CD73 and CD90 but not the myeloid marker CD45.

2.2.1.1.2 CD34+ haematopoietic stem cells

CD34+ haematopoietic stem cells (HSC) were isolated from the umbilical cord from caesarean section. The cord blood was collected by Dr Charlotte Hellmich and Dr Genevra Pillinger at the Norfolk and Norwich University hospital. Briefly, 2X 25 mL of cord blood was gently layered on top of 2X 15 mL of Histopaque-1077 and separated by density centrifugation as described previously. The cells were then washed twice with 1X PBS and resuspended in MACS buffer (1X PBS pH 7.4 supplemented with 0.5% BSA and 1 mM EDTA). The CD34+ cells were then enriched using magnetic-activated sorting (MACS) and magnetically labelled CD34 microbeads. The CD34 magnetic microbeads were added to up to 200 million isolated cells and incubated at 4°C for 30 minutes. The cells were then centrifuged at 1400 rpm for 5 minutes and resuspended in 3 mL of MACS buffer. The cells were loaded onto a prewashed LS column (Miltenyi Biotec, Bergisch Gladbach, Germany) attached to a magnet. The column was washed a further three times with MACS buffer and the CD34+ cells were flushed from the LS column by removal from the magnet and firmly plunging the column. The cells were then used directly for experiments, cultured or cryopreserved (Section 2.2.2). CD34+ HSCs were injected into nonobese diabetic (NOD) severe combined immunodeficiency (SCID) Il2rg knockout NOD.Cg.Prkd^{scid}IL2rg^{tm1Wji}/SzJ (NSG) mice for the development of humanised mice or cultured in StemMACS™ HSC Expansion Medium (Miltenyi, Biotec, Bergisch Gladbach, Germany) supplemented with stem cell factor (SCF), Flt-3 ligand (FLT3), thrombopoietin (TPO), interleukin (IL) 3 and IL 6, all at 10 ng/mL concentration (PeproTech, Inc., Rocky Hill, NJ, USA).

2.2.1.2 Mouse primary cell isolation

The BM was extracted from the tibia, femur and hips of mice. Briefly, the bones were isolated, and all muscle were removed, the bone was the cut in half and placed in a perforated 0.5 mL Eppendorf tube. This was then placed in a 1.5 mL Eppendorf tube and centrifuged at max speed for 5 seconds. The BM collected in the 1.5 mL Eppendorf tube was then pooled and washed in PBS.

The extracted BM was then plated in different culture conditions dependent on cell type.

2.2.1.2.1　Mouse BMSC

The BM cells were cultured in Minimum Essential Medium Eagle (MEM) supplemented with 20% FCS, and 1% penstrep for 96 hours. The non-adherent and non-viable cells were then washed off, fresh supplemented MEM was added to the remaining adherent cells in the flask. The BMSC were situated in the adherent fraction. The media was replaced twice a week until BMSC colonies were visible. The BMSC were then passaged using the serine protease, Trypsin-EDTA as previously described for uniform coverage of BMSC in the flask. The BMSC were then expanded until around 70-80% confluent prior to experimental use. The BMSC were characterised by expression of the cell surface markers CD105 and CD140a but not the myeloid marker CD45 and the platelet endothelial cell marker CD31. The cells were then used directly for experiments.

2.2.1.2.2　Mouse lineage negative cells

The isolated BM cells were red cell lysed with remove any remaining red blood cells. The cells were centrifuged at 1400 rpm for 5 minutes the supernatant was removed and 1X red cell lysis buffer (1 mL) (ThermoFisher, Waltham, MA, USA) was added to the cell pellet. Following a 5-minute incubation 14 mL of PBS was added to the cells and the cells were centrifuged again at 1400 rpm for 5 minutes. The pellet was resuspended in MACS buffer and lineage depleted using direct lineage cell depletion kit, mouse (Miltenyi Biotec, Bergisch Gladbach, Germany), as previously described in section 2.2.1.1.2. The flow-through was collected which contained unlabeled cells representing the enriched lineage-negative (lin-) cells. The cells were then used directly for experiments or cultured in DMEM supplemented with 10% FCS, 1% penstrep, SCF (100 ng/mL), IL 3 (10 ng/mL) and IL 6 (10 ng/mL) (PeproTech, Inc., Rocky Hill, NJ, USA). Lin- cells were injected into mice for transplantation.

2.2.1.2.3   Mouse lineage negative, CD117 positive (LK) cells

Once the cells were lineage depleted (section 2.2.1.2.2) the cells were resuspended in MACS buffer and CD117 enriched using (MACS) and magnetically labelled CD117 microbeads. The enriched CD117+ cells were flushed from the LS column by removal from the magnet and firmly plunging the column. The lin-, CD117+ cells (LK) were then used directly for experiments or cultured in DMEM supplemented with 10% foetal calf serum (FCS), and 1% penstrep, SCF (100 ng/mL), IL 3 (10 ng/mL) and IL 6 (10 ng/mL) (PeproTech, Inc., Rocky Hill, NJ, USA). LK cells were injected into mice for transplantation.

2.2.1.2.4   Mouse osteoblasts

The isolated BM cells were red cell lysed to remove any remaining red blood cells. The pellet was resuspended in MEM containing 20% FCS and 1% penstrep supplemented with macrophage CSF (10 ng/mL) (PeproTech, Inc., Rocky Hill, NJ, USA) and Prostaglandin E2 (PGE2) (10^{-7}M) (PeproTech, Inc., Rocky Hill, NJ, USA) and plated at a density of 2 x 10^5 cells/well in a 24 well plate. After 3 days the media was changed to MEM containing 20% FBS plus 1% penicillin-streptomycin supplemented with macrophage CSF (10 ng/mL), PGE2 (10^{-7}M), and RANKL (10 ng/mL) (PeproTech, Inc., Rocky Hill, NJ, USA). The osteoblasts were visualised as a single layer of cuboidal or polygonal cells. The osteoblasts were then expanded until around 70-80% confluent prior to experimental use.

2.2.1.2.5   Mouse macrophages

The isolated BM cells were red cell lysed and the pellet resuspended in MEM containing 20% FCS and 1% penstrep supplemented with macrophage CSF (20 ng/mL) (PeproTech, Inc., Rocky Hill, NJ, USA). The cells were plated in at a density of 1 x 10^7 cells in a non-tissue culture treated 10cm dish. On day 3 the cells were washed with 1X PBS and detached using a cell scraper. The cells were centrifuged at 1400 rpm for 5 minutes and resuspended in MEM

containing 20% FCS plus 1% penstrep supplemented with macrophage CSF (10 ng/mL) (PeproTech, Inc., Rocky Hill, NJ, USA) at a density of 1×10^5 cells/well in a 24 well plate. The macrophages were characterised by adherence to tissue culture plastic and expression of the cell surface marker F4/80, intermediate CD115 expression but not the granulocyte marker GR1. The cells were then used directly for experiments.

2.2.2 Cryopreservation and recovery of primary cells

Continuous culturing causes cells to acquire genetic mutations and a higher risk of becoming senescent. To ensure cells are used at peak viability, cells are cryopreserved for long term storage. Aliquots of primary human BMSC were frozen after density separation (buffy coat), prior to plating and culturing. CD34+ HSC samples were directly preserved after MACS enrichment. The cells were pelleted and resuspended in freezing mix at a density of 5×10^6 cells/mL in Freezing mix (10% dimethyl sulfoxide (DMSO) in FCS). DMSO reduces the freezing point of the freezing mix to allow for a delayed rate of cooling. Cells were then transferred to cryotubes and slowly frozen in a Mr. Frosty™ Freezing Container (ThermoFisher, Waltham, MA, USA) in a -80˚C freezer. The Mr. Frosty™ Freezing Container cools as a steady rate of around -1˚C/minute, which is the optimum rate for cell cryopreservation.

To thaw, culture media was warmed to 37˚C, the cryotubes containing the cells were then removed from the -80˚C freezer. The cryotube was placed at 37˚C until partially defrosted. The cells were transferred into a 15mL falcon tube and 10 mL of warm culture media slowly was added dropwise to the tube to dilute the DMSO. The cells were then centrifuged at 1400 rpm for 5 minutes and supernatant discarded to completely remove the DMSO. The pellet was resuspended in the relevant media and cultured as per fresh primary cells.

2.3 Cell viability assays

2.3.1 Cell counting by trypan blue exclusion

The Trypan Blue exclusion assay is widely used to determine the number of viable cells. The non-viable cells do not have an intact cell membrane and therefore they take up the Trypan blue, but viable cells do not. 10 µL aliquot of the cell suspension was mixed in a 1:1 ratio with Trypan Blue. The cells were then pipetted onto a haemocytometer, and the healthy cells were counted. All four outer quadrants were counted and averaged, and cell/mL was calculated by the calculation below (Figure 2.2).

Cell number

$$\text{(cells/ mL)} = \left(\frac{\text{Number of viable cells}}{\text{Number of quadrants counted}} \right) \times \text{Trypan blue dilution factor} \times 10^4$$
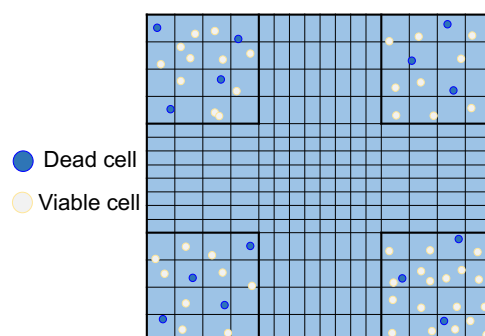
Figure 2.2. Cell number determination using Trypan Blue exclusion.

To calculate the number of cells required for a cell culture based experimental procedure the equation below was used.

$$\text{Volume of cells needed (mL)} = \left(\frac{\text{Number of required cells}}{\text{Cell number (cells/mL)}} \right)$$

For animal experiments the automated cell counter Cellometer T4 Bright field Viability Cell Counter (Nexcelom Bioscience LLC Lawrence, MA, USA) was

used. The automated cell counter uses bright field microscopy and patten recognition software to identify and count single live, dead, and total cells. Briefly, cells isolated from the BM cells were diluted 1 in 10 in MACS buffer. The cells were then further diluted a 1:1 ratio with Trypan Blue and 20 µL was loaded onto a cell counting chamber (Nexcelom Bioscience LLC Lawrence, MA, USA). The cell concentration was calculated accounting for dilution factors.

2.3.2   Annexin V/PI apoptosis assay

Cell viability of lin- cells was assessed using eBioscience™ Annexin V/PI detection kit (ThermoFisher, Waltham, MA, USA). The Annexin V FITC antibody preferentially bind to phosphatidylserine. Under normal condition this is located in the inner plasma membrane of the cell, however upon apoptosis the phosphatidylserine translocates across the lipid bilayer to the extracellular plasma membrane. This acts as a marker for cellular apoptosis and this phosphatidylserine can be detected by fluorescently labelled Annexin V. Propidium iodide (PI) is a viability dye which stains DNA. In late stage apoptosis, the cell membrane is no longer intact and PI stains the DNA, however in heathy cells the PI cannot cross the plasma membrane so is unable to stain the DNA. Annexin V allows for the detection of cells in early stage apoptosis and PI allows for the detection of cells which are in late stage apoptosis or necrotic. Early-stage apoptotic cells are Annexin V positive, PI negative, whereas late-stage apoptotic and necrotic cells are Annexin V positive, PI positive (Figure 2.3).
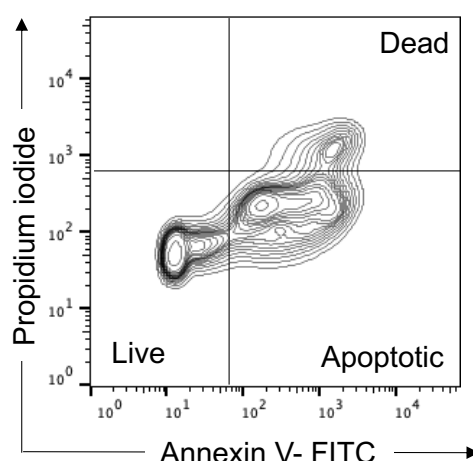
Figure 2.3. Representative flow cytometry plot of Annexin V/PI staining.
Cell were stained with Annexin V-FITC and PI and analysed by flow cytometry. Live cells (Annexin V- PI-), apoptotic cells (Annexin V+ PI-) and dead cells (Annexin V+ PI+).

In the assay 2×10^4 lin- cells were pelleted by centrifugation and resuspended in 800 µl of 1X annexin/PI binding buffer. 2 µl of annexin V FITC antibody and 4 µl of PI was then added to the buffer and left to incubate in the dark for 15 minutes. The cells were then washed in MACS buffer and analysed on the Sysmex Cube 6 flow cytometer. The results were analysed using BD FlowJo 10.7.0 software (FLowJo, LLC, Ashland, OR, USA).

2.4   Methylcellulose Mouse Colony Forming Cell (CFC) Assay

The methylcellulose assay or colony forming cell (CFC) assay can determine the differentiation capacity of the haematopoietic stem cells to progenitor cells. Haematopoietic progenitors can proliferate and differentiate into many different cell colonies, in this assay they are formed in a semi-solid media and can characterised by their specific morphologies and counted.

5×10^4 isolated BM cells were washed in 1X PBS and resuspended in 400 µl of 1X PBS. The cells were added to 5 mL of mouse MethoCult™ GF M3434 (Stemcell Technologies, Cambridge, UK) (a methylcellulose-based medium with recombinant cytokines) and briefly mixed by vortexing. Using a Pasteur pipette 1 mL of solution was dispensed into a 6-well plate. Each sample was

replicated 3 times. Sterile water was added to the spaces between the wells of the 6-well plate to maintain the correct humidity for colony development. The plate was then incubated undisturbed at 37°C and 5% CO_2 for 7-10 days to prevent colony shifts. Finally, the colonies were then assessed by light microscopy using a scoring grid.

2.5 Cell culture assays

Primary cells human BMSC (hBMSC), CD34+ HSCs, along with mouse BMSC (mBMSC), mouse BM osteoblast (mBM Osteoblast), mouse BM macrophages (mBM macrophages) and lin- or LK cells were cultured as described in section 2.2 before use in any cell culture assays.

2.5.1 Co-culture experiments

Coculture systems were used to determine mitochondrial transfer between different cell types of the BM microenvironment and the consequence of this during infection. mBMSCs, mBM osteoblasts, or mBM macrophages were seeded in a 24-well plate at a density of 5 x 10^5 in normal growth media. The media was refreshed 24 hours after seeding. Once the cells were 70% confluent the media was removed and primary 1 mL of 2 x 10^5 lin- cells were added to the plate and treated. Lin- cells were added at 4:1 ratio of lin- cells to adherent cells. Following coculture the two different cells types were then separated and analysed individually.

2.5.2 Mitochondrial DNA based transfer assay

A mitochondrial DNA (mtDNA) based transfer method was developed to show specific mtDNA movement from the BM cells to the lin- cells. There are 2 single-nucleotide polymorphisms (SNP) in the mitochondrial genome that can distinguish between murine strains, PepCboy and CBA. mBMSCs, mBM osteoblasts, or mBM macrophages were cocultured with the lin- cells in the absence or presence of 10 µM H_2O_2 for 24 hours. The lin- cells were then removed from the coculture and stained with CD45-FITC for 15 minutes in the

dark before washing and resuspending in MACS buffer. The lin- cells were then sorted into DNA cell lysis by fluorescence activated cell sorting (FACS) to ensure no BMSC remained. The DNA was extracted from these cells, and mtDNA quantification was performed using qPCR.

To assess the driver of mtDNA transfer C57BL/6J mBM macrophages were treated with LPS (10 µg/mL) for 1 hour. BMSC were cocultured with the lin-cells in the absence or presence of this conditioned media for 24 hours. The lin- cells were then removed from the coculture and stained with CD45 - FITC for 15 minutes in the dark before washing and resuspending in MACS buffer. The lin - cells were then sorted into DNA cell lysis by FACS to ensure no BMSC remained. The DNA was extracted from these cells, and mtDNA quantification was performed using qPCR.

The effects of pharmacological compounds on mtDNA transfer was assessed by comparing mtDNA transfer in the control, H_2O_2 alone and H_2O_2 with the drug (Table 2.2). These results are presented as mtDNA copy number of donor mtDNA compared to the non-drug treated baseline and H_2O_2 alone.

Table 2.2. Pharmacological agents used to assess mitochondrial transfer.

Pharmacological Agent	Target/effect	Concentration used
Carbenoxolone (CBX)	Gap junction inhibitor	50µM
CAL101	PI3K inhibitor	25µM
Calcein AM	Gap junction tracker	5µM
Gap27	CX43 peptide inhibitor	100µM
H_2O_2	ROS inducer	10µM
LPS	Bacterial mimic	5µg/mL

2.5.3   rLV.EF1.mCherry mitochondrial transfer assay

Mitochondrial transfer was also assessed using a stable lentiviral transduction of the BMSC mitochondria with a mCherry tag which fluoresces red. mBMSCs were isolated from the bone morrow and seeded at a density of 5×10^4 BMSCs

in 500 µL of penstrep free MEM supplemented with 10% FCS. 0.5 µL of the rLV.EF1.mCherry-Mito-9 lentivirus (Clontech Takara Bio Europe, Saint-Germain-en-Laye, France) (0.5×10^6 virus particles) was added to the BMSC. After 24 hours 1 mL of fresh MEM supplemented with 10% FCS was added, and mBMSCs were cultured for a further week to ensure that no residual lentivirus remained. Successful transduction was confirmed by mCherry fluorescence in the mBMSCs detected by fluorescent microscopy.

In addition, the rLV.EF1.AcGFP-Mem9 lentivirus was purchased from Clontech Takara Bio Europe, which allowed for stable tagging of the plasma membranes with a green fluorescent protein (GFP) fluorophore. Mouse lin- cells were depleted from mouse BM as previously described, and cells were transduced with rLV.EF1.AcGFP-Mem9 lentivirus. 24 hours later the cells were washed with DMEM and further cultured for 72 hours prior to use. Successful transduction was confirmed by GFP fluorescence in the lin- cells seen by fluorescent microscopy.

Following successful transduction, tissue culture coverslips coated with 1 µg/mL poly-D-lysine for 1 hour. The coverslips were washed with 1X PBS and placed in a 24-well plate. mBMSCs were seeded at 5×10^4 cells per well on the coverslips in the plate. The media was refreshed 24 hours after seeding and 2.5×10^5 transduced lin- cells were cocultured with the mBMSCs for 24 hours with or without of H_2O_2. Cells were then fixed using 4% paraformaldehyde and stained for 15 minutes in DAPI (ThermoFisher, Waltham, MA, USA). The coverslips were then washed 3 times with 1X PBS and mounted onto microscope slides with VECTASHIELD® mounting media (Vector Laboratories Ltd, Peterborough, UK).

2.5.4 Visualisation of mitochondrial transfer

To visualise the gap junctions formed between BMSC and the lin- cells, the gap junctions were stained with a CX43 antibody (ThermoFisher, Waltham, MA, USA). BMSCs successfully transduced with rLV.EF1.mCherry-Mito-9 lentivirus were seeded at a density of 5×10^4 on a black walled imaging plate

(Ibidi, Munich, Germany). Lin- cells were stained with CD45-APC (Miltenyi Biotec, Bergisch Gladbach, Germany), in 500 µL FluoroBrite DMEM medium (ThermoFisher, Waltham, MA, USA) supplemented with 10% FCS, for 20 minutes in the dark. The cells were then washed in 1X PBS and resuspended in DMEM supplemented with 10% FCS and 1% penstrep. 2.5 x 10^5 stained lin-cells were cocultured with the mBMSCs for 24 hours with H_2O_2 in the absence or presence of the CX43 peptide inhibitor Gap27. Cells were then fixed using 4% paraformaldehyde and stained with the primary CX43 antibody in for 1 hour. The plate was then washed 3 times with 1X PBS, and the cells were stained with secondary goat anti-mouse GFP and DAPI (ThermoFisher, Waltham, MA, USA) for 30 minutes in the dark. The plate was then washed a further 3 times with 1X PBS and 500 µL FluoroBrite DMEM medium was added to the wells. The plate was then imaged using confocal microscopy.

2.6   Analysis of reactive oxygen species

2.6.1   DCFDA / H2DCFDA (DCF) assay

To quantify the level of reactive oxygen species (ROS) in the specific BM populations the DCF assay (ThermoFisher, Waltham, MA, USA) was used. In this assay H_2DCFDA is added to the media containing cells and is internalised. Inside the cell the cellular esterases deacetylates the H_2DCFDA to H_2DCF, which is not fluorescent. H_2DCF is then oxidised by any cellular ROS to 2', 7' –dichlorofluorescin (DCF) which is a highly fluorescent compound (Figure 2.4). DCF emits a wavelength of 529 nm and therefore can be detected in the FITC channel by flow cytometry.
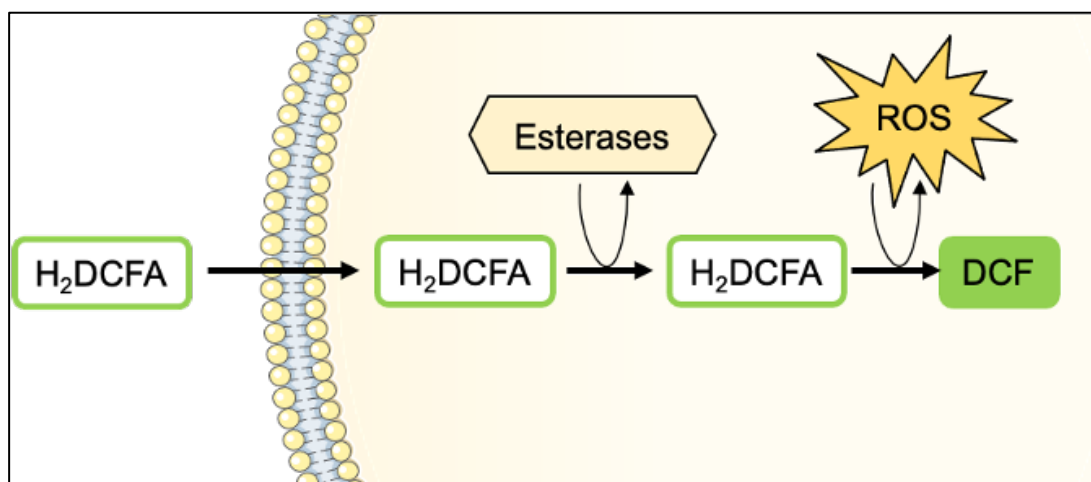
Figure 2.4. Schematic of the process occurring in DCF assay.
H₂DCFA is taken up by the cell and cellular esterases deacetylates the H₂DCFDA to H₂DCF. H₂DCF is then oxidised by ROS DCF.

To assess ROS in the in the specific BM populations 5×10^6 isolated BM cells were stained with 10 µM H₂DCFDA in 500 µl of MACS buffer for 20 minutes in the dark. Next, the cells were washed three times with 1X PBS and resuspended in 300 µl of MACS buffer. The cells were then stained with any other necessary antibodies and ran on the flow cytometer. The results were analysed using BD FlowJo 10.7.0 software (FLowJo, LLC, Ashland, OR, USA).

2.6.2 AmplexTM Red superoxide detection assay

The DCF assay whist cellular specific has the ability to measure total cellular ROS including peroxide, hydroxyl radicals, hydroxyl ions and superoxide. To specifically assess superoxide production the Amplex™ Red superoxide detection assay (ThermoFisher, Waltham, MA, USA) was utilised. The assay is a one-step reaction whereby the Amplex Red reagent (10-acetyl-3,7-dihydroxyphenoxazine) reacts with superoxide in the presence of horseradish peroxidase (HRP) to form resorifin (Figure 2.5). This reaction has an emission wavelength of 585nm which can be detected on a plate reader. The assay was carried out as per the manufacturer's instructions.
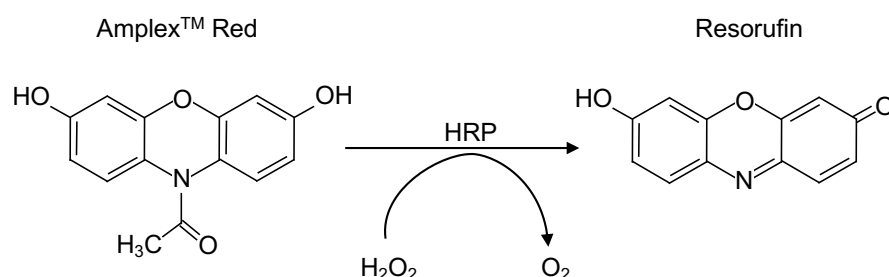
Figure 2.5. Overview of the Amplex™ Red superoxide detection assay.
In the presence of superoxide, the Amplex Red reagent is converted to fluorescent resorifin.

Briefly, 2 x 10^5 BM cells was resuspended in 50 µL FluoroBrite DMEM supplemented with 10% FCS and plated on a black 96-well plate with a transparent base. 0.5 µL Amplex Red reagent, 1 µL horseradish peroxidase, and 48.5 µL 1X reaction buffer was mixed per sample to create a master mix. 50 µL of master mix was then added to the BM cells. A standard curve was also performed on each 96-well plate for the hydrogen peroxide to ensure an accurate determination of superoxide concentration. The fluorescence was measured on the FLUOstar Omega microplate reader (BMG LABTECH, Ortenberg, Germany).

2.7   Confocal Microscopy

To visualise mitochondrial transfer between the BMSCs and HSCs and the mechanisms controlling this confocal microscopy was used. The microscope utilised was a Zeiss LSM 800 Axio Observer.Z1 confocal microscope with a 63X water objective (Carl Zeiss, Oberkochen, Germany). The cells were cocultured as previously described in section 2.5.2 and 2.5.3 and fixed on 24 well black walled imaging plate or coverslips on microscope slides. The plate or slide was placed on the culture plate or slide holder on the microscope. The ZEN Blue imaging software (Carl Zeiss) was used to acquire the images. Smart setup allowed for definition of the fluorophore wavelength acquisition parameters for mCherry, GFP, APC and DAPI. Relative mCherry positive lin-cells were calculated, multiple experiment and imaged were taken for

quantification. Fiji software was used to overlay, process and accurately quantify images.

Zeiss LSM 800 Axio Observer.Z1 confocal microscope was also used to visualise lipid levels within the cell. BM from treated animals was lineage depleted and CD117 enriched (LK) as previously described. These LK cells were then stained with 5μM Hoechst 33342 (ThermoFisher, Waltham, MA, USA) and 4- difluoro-1,3,5,7,8-pentamethyl-4-bora-3a,4a-diaza-s-indacene (BODIPY 493/503) (1μM) (ThermoFisher, Waltham, MA, USA) at room temperature for 20 minutes. The cells were then washed twice in 1X PBS by centrifugation at 1200rpm for 5 minutes. The cells were then stained with the cell surface antibody Sca 1-APC (Miltenyi Biotec, Bergisch Gladbach, Germany) for 20 minutes in the dark. The cell suspension was washed again with 1X PBS and resuspended in 200 μL of FluoroBrite DMEM medium supplemented with 10% FCS and plated in a black walled imaging plate. The cells were imaged using a 63X water objective, smart setup was performed for the fluorophore wavelength acquisition parameters for BODIPY 493/503, Hoechst and APC. Fiji software was used for image processing.

2.8   Flow cytometry

Flow cytometry was used for different purposes in this study:

- To identify cell populations by surface receptors with antibodies conjugated to a detectable fluorophore.
- To determine mitochondrial content, mitochondrial health, lipid content, ROS levels, pAKT and cell cycling in specific cell populations.
- To sort specific cell populations by the cell surface receptors.

To achieve these applications different flow cytometers were used dependent on the number of lasers determining the number fluorophores that can be detected in one sample and the ability to sort cells. Table 2.3 shows a comparison of the capabilities of the flow cytometers used in this study. Table 2.4 shows the antibodies and panels used to detect cell populations. All

antibodies were purchased from Miltenyi Biotech (Bergisch Gladbach, Germany) or BioLegend (San Diego, CA, USA).

2.8.1 Sysmex Cube 6

The Sysmex Cube 6 flow cytometer (Sysmex, Gorlitz, Germany) is a 2-laser flow cytometer (blue 488nm and Red 633nm) and is capable of detecting four fluorophores FITC, PE, PERCP and APC. Whist this flow cytometer can detect four fluorophores it lacks the ability to do colour compensations and therefore cannot account for cross-over of emission spectre. Consequently, this machine was only used for single colour flow cytometry. This flow cytometer enabled the analysis of engraftment using CD45.1 Antibody, anti-mouse on the FITC channel and Calcein AM (ThermoFisher, Waltham, MA, USA) to track movement through gap junctions which is also detected on the FITC channel.

The flow cytometer was primed prior to use ensuring the fluidics were clean and no blockages or air bubbles were present. 1×10^5 cells were stained with the either Calcein AM in 500 µL MACS buffer or CD45.1- FITC Antibody in 200 µL MACS buffer for 20 minutes in the dark. The cells were then washed by centrifugation at 1500 rpm for 5 minutes and re-suspended in 1mL of MACS buffer and transferred into a flow tube. The samples were then ran on the flow cytometer and 1×10^4 cells were analysed in a pre-defined gated region. The flow cytometer was the cleaned after use and data was exported as an FCS file data and analysed using BD FlowJo 10.7.0 software (FLowJo, LLC, Ashland, OR, USA).

2.8.2 Beckman Coulter CytoFLEX

The Beckman Coulter CytoFLEX (Brea, CA, USA) is a multi-channel flow cytometer which also has 2 lasers (488 and 633nm), but with the addition of bandpass filters. This allows for the detection of FITC, PE, PERCP/Pe Cy5, Pe Cy7, APC and APC Cy7. It also has the ability to calculate colour compensations, therefore can detect up to four fluorophores in one sample. This flow cytometer was used to detect <4 fluorophores within in the one

sample in this study. This flow cytometer enabled the detection hCD45-FITC and mCD45-APC in the peripheral blood to show CD34+ HSC engraftment into NSG mice.

The flow cytometer was cleaned and primed prior to use by a daily clean process on the cytometer. Before the samples were run, a compensation matrix was calculated using UltraComp eBeads™ Compensation Beads (ThermoFisher, Waltham, MA, USA) for each marker. This compensation calculation determines the cross-over of emission spectre and compensates to allow for any overlap. 1×10^5 cells were stained with the antibodies of interest or isotype controls for 20 minutes in the dark. The cells were then washed by centrifugation at 1500 rpm for 5 minutes and re-suspended in 400 µl of MACS buffer and transferred into a flow tube. The samples were then run on the flow cytometer and 1×10^4 cells were analysed in a pre-defined gated region. The flow cytometer was the cleaned after use and data was analysed using the CytExpert 1.2 software.

2.8.3   BD FACSCanto II

The FACSCanto II flow cytometer (BD, Franklin Lakes, NJ, USA) was located in the Pathology Laboratory at the Norfolk and Norwich University Hospital and is maintained by Dr Allyson Tyler. This flow cytometer has three-lasers, 488, 633 and 405nm and is therefore able to detect 7 fluorophores within the same sample including FITC, PE, PE Cy5, PE Cy7, APC, APC Cy7, BV421 and BV510. A compensation for each antibody panel was carried out to measure fluorophore emission cross-over using UltraComp eBeads™ Compensation Beads (ThermoFisher, Waltham, MA, USA) for each marker. The compensation was linked to each experiment before running the samples. This flow cytometer enabled the detection of mitochondrial content, mitochondrial potential, lipid content, ROS levels, pAKT, CD36, cell cycling and engraftment in various cell populations in mouse BM. The antibodies panels used to detect cell populations are shown in Table 2.4.

To analyse the mouse BM, 5 x 10^6 cells were used. For dyes including MitoTracker Green FM (200 nM) (ThermoFisher, Waltham, MA, USA) Tetramethylrhodamine, methyl ester (TMRM) (100 nM) (ThermoFisher, Waltham, MA, USA), H$_2$DCFDA (10 µM) (ThermoFisher, Waltham, MA, USA) and BODIPY 493/503 (1 µM) the cells were stained with the dyes in 500 µL MACS buffer for 20 minutes in the dark. The cells were then washed by centrifugation at 1500rpm for 5 minutes and re-suspended in 200 µL of MACS buffer. An antibody master mix was prepared containing 1 µL of each antibody per sample and was added to the cells. Following a 20-minute incubation at 4°C in the dark the cells were then centrifugation again at 1500rpm for 5 minutes and re-suspended in 200 µL of MACS buffer.

To analyse specific BM populations for antibody expression such as CD36 VioBright 515 mouse (Miltenyi Biotec, Bergisch Gladbach, Germany) and CD45.1 Antibody, anti-mouse FITC (Miltenyi Biotec, Bergisch Gladbach, Germany) or CD45.2 Antibody, anti-mouse PE (Miltenyi Biotec, Bergisch Gladbach, Germany) an antibody master mix was prepared containing 1µL of each antibody per sample and was added to 5 x 10^6 cells in 200 µL of MACS buffer. Following a 20-minute incubation at 4°C in the dark the cells were then centrifuged again at 1500rpm for 5 minutes and re-suspended in 200 µL of MACS buffer.

To analyse cell cycling by Ki67 expression and phospo AKT levels in the BM populations the cells required fixing and permeabilising. The FIX & PERM Cell Fixation & Cell Permeabilization Kit (ThermoFisher, Waltham, MA, USA) was used. Briefly, 5 x 10^6 isolated BM cells were stained with an antibody master mix containing 1 µL of each surface marker antibody per sample and was added to the cells. Following a 20-minute incubation at 4°C in the dark the cells were then centrifuged at 1500rpm for 5 minutes and re-suspended in 100µL of 1X PBS, 100 µL of Reagent A (Fixation Medium) was then added to the cell suspension and incubated at room temperature for 15 minutes in the dark. The cells were then washed with 3 mL 1X PBS and centrifuged at 1500rpm for 5 minutes. The pellet was resuspended in 100 µL of Reagent B (Permeabilisation Medium) and 1 µL of the intracellular antibodies, Anti-Ki-67

FITC human and mouse (Miltenyi Biotec, Bergisch Gladbach, Germany) or AKT pS473 Antibody, anti-human/mouse, PE-Vio® 770 mouse (Miltenyi Biotec, Bergisch Gladbach, Germany) was added. Following a 20 minutes incubation in the dark at room temperature, the cells were centrifuged again at 1500rpm for 5 minutes and re-suspended in 200µL of MACS buffer.

The samples were all run on the FACSCanto II utilising the automated carousel and data were analysed using BD FlowJo 10.7.0 software (FLowJo, LLC, Ashland, OR, USA). The gating was set by using fluorescence minus one (FMO) controls for every fluorophore to establish the positive and negative gates for each cell marker.

2.8.4 BD FACSMelody

The FACSMelody (BD, Franklin Lakes, NJ, USA) is located at the Earlham Institute (Norwich, UK) and has the same number of lasers and fluorophore capabilities as the FACSCanto II, however has the additional ability to sort cells. This flow cytometer was used to sort the CD45.1 and CD45.2 lin-populations from the NSGC57Bl/6 mice. It was also used to sort the human and mouse haematopoietic progenitor cells from mouse BM.

To sort the human and mouse haematopoietic progenitor cell populations the BM cells were isolated, and lineage depleted to isolate the lin- cells (section 2.2.1.2.2). The cells were then stained with the HSC or progenitor panels for 20-minute incubation at 4°C in the dark. The cells were centrifuged again at 1500 rpm for 5 minutes and re-suspended in 1mL of MACS buffer. The samples were then run on the FACSMelody and sorted into lysis buffer for RNA or DNA analysis by qPCR or into culture media for culture, transplantation or the Seahorse extracellular flux assay. The positive and negative gating for the sorting of the haematopoietic progenitor cell populations was set by using FMO controls for every fluorophore.

Table 2.3. Comparison of the capability of the flow cytometers used.

	Cube	CytoFlex	FACSCanto II	FACSMelody
Number of lasers	2	2	3	3
Fluorophore capability	1	4	7	7
Colour compensation	No	Yes	Yes	Yes
Automated	No	No	Yes	No
Cell sorting	No	No	Yes	Yes

Table 2.4. Antibody panels used in flow cytometry assays.

Antibody panel		Flourophore							
		FITC	APC	APC Cy7	Pe	PeCy7	PeCy5	BV421	BV510
Bodipy	HSC	Bodipy	Sca1	CD48		CD117	CD34	Lin Cocktail	CD150
CD36	HSC	CD36	Sca1	CD48		CD117	CD34	Lin Cocktail	CD150
DCF	HSC	DCF	Sca1	CD48		CD117	CD34	Lin Cocktail	CD150
	Progenitor	DCF	Sca1	CD48		CD117	CD34	Lin Cocktail	CD16/32
	BMSC	DCF	Ter119	CD140a	CD105		CD31		CD45
DsRed	Lin-				DsRed				
	HSC		Sca1	CD48	DsRed	CD117		Lin Cocktail	CD150
	BMSC		CD105	CD140a	DsRed		CD31		CD45
	Macrophage		F4/80	CD115	DsRed		Gr1		
Engraftment	CD45.1/HSC		Sca1	CD48	CD45.1	CD117	CD34	Lin Cocktail	CD150
	CD45.2/HSC	CD45.2	Sca1	CD48		CD117	CD34	Lin Cocktail	CD150
	Myeloid	CD45.2	CD45.1				Gr1		
	Lymphoid	CD45.2	CD45.1			CD4	CD8		
Humanised	HSC/Prog	MTG	hCD38	hCD90		hCD49f	hCD45RA	hCD34	mCD45
Ki67	HSC	Ki67	Sca1	CD48		CD117	CD34	Lin Cocktail	CD150
MTG	HSC	MTG	Sca1	CD48		CD117	CD34	Lin Cocktail	CD150
	Progenitor	MTG	Sca1	CD48		CD117	CD34	Lin Cocktail	CD16/32
	BMSC	MTG	Ter119	CD140a	CD105		CD31		CD45
pAKT	HSC		Sca1	CD48	pAKT	CD117	CD34	Lin Cocktail	CD150
	BMSC	CD105	Ter119	CD140a	pAKT		CD31		CD45
TMRM	HSC		Sca1	CD48	TMRM	CD117	CD34	Lin Cocktail	CD150

Invitrogen	Biolegend	Miltenyi

2.9 Free FA and glycerol detection

The level of free fatty acids (FFA) in the serum was detected using the Serum/Plasma Fatty Acid Detection Kit (ZenBio Inc., NC, USA). Serum or plasma levels of non-esterified fatty acids can be a sign of endogenous or induced adipocyte lipolysis. This assay detects non-Esterified Fatty Acids or FFA using a substrate to and causes a colorimetric change, which can be analysed using immunosorbance detection to calculate the concentration of FFA using a standard curve.

To assess the level of FFA in the serum it is a three-step coupled reaction. The first step is catalysed by acyl-CoA synthetase, CoA, FFA released by adipocytes, and ATP produce acyl-CoA thiol ester. The acyl-CoA thiol reacts with oxygen and is catalysed by acyl-CoA oxidase to produce hydrogen peroxide. 3-methyl-N-ethyl-N-(β- hydroxyethyl)- and aniline4-aminoantipyrine undertakes oxidative condensation due to the hydrogen peroxide and peroxidase. This forms a purple product which can absorb light at 550nm.
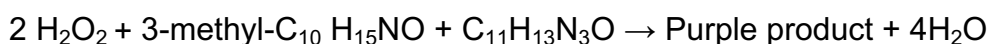
$$HCOOH \text{ (FFA)} + ATP + CoA \rightarrow Acyl\text{-}CoA + AMP + PP_i$$

$$Acyl\text{-}CoA + O_2 \rightarrow 2,3\text{-}trans\text{-}Enoyl\text{-}CoA + H_2O_2$$

$$2 H_2O_2 + 3\text{-}methyl\text{-}C_{10} H_{15}NO + C_{11}H_{13}N_3O \rightarrow Purple \text{ } product + 4H_2O$$

For this assay C57Bl/6J mice were left untreated or infected with *S.typhimurium* by oral gavage for 72 hours or injected with LPS 16 hours. The mice were anaesthetized and 600 µL of blood was taken by cardiac puncture. To isolate the serum, the blood was centrifuged at 1600 xg for 10 minutes to remove cells. The supernatant was then centrifuged again at 16000 xg for 5 minutes.

From each sample, 5 µL of serum was placed in a 96 well plate and 50 µL of dilution buffer was added to each sample. 100 µL of FFA reagent A was then added to the well and mixed. The plate was then placed at 37°C for 10 minutes. Post incubation 50 µL of FFA reagent B was then added mixed and the plate was left at room temperature for 5 minutes. The optical density of each well

was measured using a FLUOstar Omega plate reader (BMG Labtech, Offenburg, Germany). A standard curve was also performed and measured on the 96-well plate from known standard concentrations provided in the kit to ensure an accurate determination of FFA concentration.

2.10   Free Fatty Acid uptake assay

FFA uptake was measured using the QBT Fatty Acid Uptake Assay (Molecular Devices San Jose, CA, USA). The assay is a single step process which uses a BODIPY®-dodecanoic acid fluorescent fatty acid analog which acts like a natural FA. The BODIPY label is activated by attachment to acyl-CoA and is incorporated into both diglycerides and triglycerides. It also then accrues inside the cell as lipid droplets.

For this assay C57Bl/6J mice were left untreated or infected with *S.typhimurium* by oral gavage for 72 hours or injected with LPS 16 hours. The BM extracted, and the mouse lin- cells were depleted and CD117+ enriched (LK) as previously described. 5×10^4 LK cells were incubated with 4,4-Difluoro-5,7-Dimethyl-4-Bora-3a,4a-Diaza-s-Indacene-3-Dodecanoic Acid (BODIPY™ FL C_{12}) (1µM, Invitrogen) at room temperature for 20 minutes. The cells were then washed twice in 1X PBS and centrifuged at 1400rpm for 5 minutes. The cells resuspended in PBS and plated in a glass bottom 96 well plate. The absorbance was measured at 558/568 using a FLUOstar Omega plate reader (BMG Labtech, Offenburg, Germany). The cells were also visualised using Zeiss LSM 800 Axio Observer.Z1 confocal microscope and quantified fluorescence using Fiji software.

2.11   Seahorse Extracellular Flux Assay

To assess the metabolic activity of the LSK (Lin-, CD117+, Sca1+ cells) the Seahorse XFp Analyzer (Agilent Technologies, Santa Clara, CA, USA) was utilised with both the Seahorse XFp Cell Mito Stress Test Kit and the Seahorse XF Mito Fuel Flex Test.

For these assays C57Bl/6J mice were left untreated or infected with *S.typhimurium* by oral gavage for 72 hours or injected with LPS 16 hours. Prior

to the experiment day XFp flux cartridges were hydrated in XF Calibrant overnight at 37°C the Seahorse Extracellular Flux analyser was also switched on overnight to allow equilibration to 37°C. On the day of the experiment the Seahorse XFp cell culture plates were coated with Poly-D-Lysine for 2 hours and then washed thre times. The animals were sacrificed, and the BM extracted, the mouse lin- cells were depleted and the LSK cells were isolated by FACS into conventional Seahorse base media supplemented with pyruvate (1mM), L-Glutamine (2mM), Glucose (10mM) as previously described. The cells for each condition were pooled and 1×10^5 cells in 180 µl were plated into the wells of the coated Seahorse XFp culture plate. The plate was centrifuged briefly to achieve a uniform monolayer of cells. The plate was then equilibrated in a humidified non-CO_2 incubator until the start of the assay. All results were normalised to input cell number.

2.11.1   Seahorse XFp Cell Mito Stress Test

The quantification of mitochondrial respiration (oxidative phosphorylation (OXPHOS) measured by oxygen consumption rates (OCR)) and non-mitochondrial respiration (glycolysis measured by extracellular acidification rates (ECAR)) that a cell undertakes can be determined using this kit. In this study the assay was used to determine the differences in oxidative phosphorylation of the LSK before and after infection. This method can be used to quantify basal mitochondrial respiration rates maximum respiration, spare capacity of a cell, proton leak and ATP production. This is done by microinjection of Oligomycin an inhibitor of ATP synthase which reduces OCR, carbonyl cyanide-4-(trifluoromethoxy) phenylhydrazone (FCCP) which targets the inner mitochondrial membrane and increases OCR and Rotenone/Antimycin A which targets complex 1 and 3, leading to a reduced OCR (Figure 2.6). Basal and maximum respiration rates were of interest in this study.
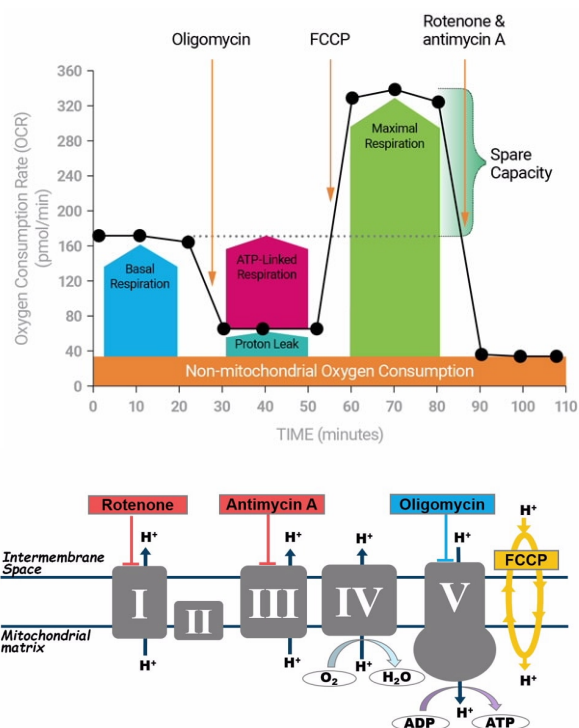
Figure 2.6. Mitostress test experimental profile.
Microinjection of Oligomycin an inhibitor of ATP synthase in Complex V of the mitochondria, FCCP which targets the inner mitochondrial membrane and Rotenone/Antimycin A which targets Complex 1 and III. (Source: Agilent Technologies (328)).

Once the cells were plated and the machine were equilibrated, Oligomycin (2 µM), FCCP (1 µM) and Rotenone/Antimycin A (0.5 µM) were loaded into the flux cartridges. The cartridge was then loaded into the Seahorse XFp Analyzer and the Mito Stress test protocol based on manufacturer's instructions. The sensors in the analyser were equilibrated for 20 minutes and the plate was loaded into the analyser. The results were analysed using GraphPad Prism software (Version 7.0, GraphPad Software, San Diego, CA, USA) and Microsoft Excel.

2.11.1.1   Seahorse XFp Mito Fuel Flex Test

For fatty acid fuel dependency flux cartridges were loaded according to manufacturer's instructions. Fatty acid dependency, capacity and flexibility values were obtained using the XFp Mito Fuel Flex Test Kit. Metabolic parameters were derived from calculations based on manufacturer's

instructions. The Mito Fuel Flex Test was used to measure mitochondrial fuel usage, specifically long chain fatty acids in the LSK after infection. The Fuel Flex Test has the ability to measure the cells capacity, dependency, and flexibility to oxidize glucose, glutamine and long chain fatty acids (Figure 2.7). This is determined by the oxidation consumption rate of cells with and without specific fuel pathway inhibitors, UK5099, BPTES and Etomoxir. UK5099 inhibits the glucose oxidation pathway by blocking the mitochondrial pyruvate carrier. BPTES inhibits the glutamine oxidation pathway by allosterically inhibiting glutaminase. Etomoxir inhibits long chain fatty acid oxidation specifically by inhibiting carnitine palmitoyl-transferase 1A (CPT1A). In the assay the pathway of interest is inhibited followed by the inhibition of the two alternative pathways, which allows for the determination of how dependent the cells are on a specific pathway to meet its basal energy requirements (Dependency). The dependency is the reliance of the cell on one pathway as the mitochondria is not able to compensate for the inhibition of the pathway by utilising other fuel sources. The two alternative pathways are also inhibited followed by the pathway of interest this allows for the determination of the cells mitochondrial capacity to meet energy requirements (capacity). The fuel flexibility is measured by subtracting the Fuel Dependency from the Fuel Capacity for the specific fuel pathway and demonstrates the cells are able to swich pathways to compensate for the inhibited pathway. If there is no flexibility this indicates the fuel pathway is required to maintain basal OCR. Only the fatty acid dependency, capacity and flexibility values were calculated for this study to show reliance on long chain fatty acids as a fuel source.
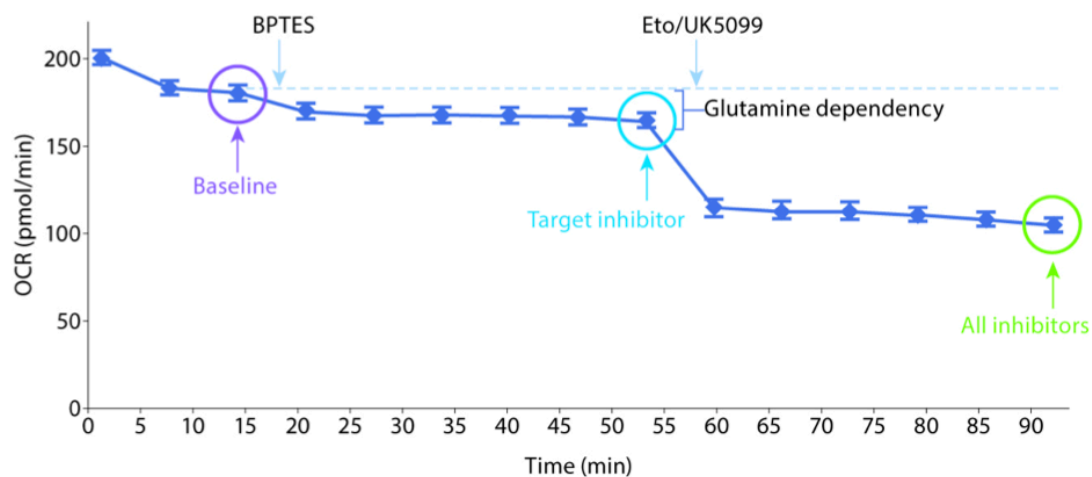
$$Dependency\ \% = \left[\frac{Baseline\ OCR - Target\ Inhibitor\ OCR}{Baseline\ OCR - All\ Inhibitors\ OCR} \right] * 100$$
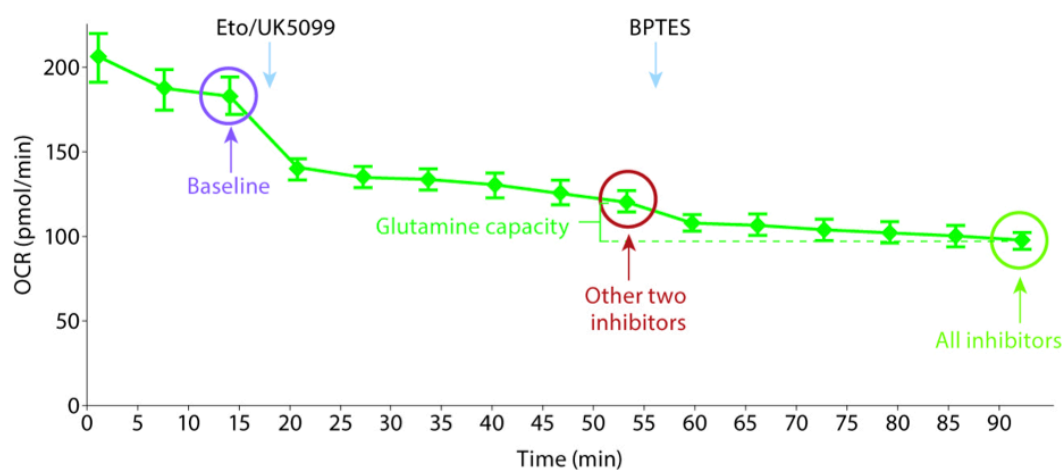
$$Capacity\ \% = \left[1 - \left[\frac{Baseline\ OCR - Other\ 2\ Inhibitors\ OCR}{Baseline\ OCR - All\ Inhibitors\ OCR} \right] \right] * 100$$

Figure 2.7. Mito Fuel Flex Test experimental profile.
Experimental profile and calculations to determine mitochondrial dependency and capacity for glutamine as a fuel source. Eto inhibits Fatty acid oxidation, BPTES inhibits glutamine oxidation and UK5099 inhibits glucose oxidation. (Source: Agilent Technologies (329)).

To perform the assay, once the cells were plates and the machine was equilibrated, UK5099 (2 µM), BPTES (3 µM) and Etomoxir (4 µM) were loaded into the correct wells of the flux cartridges. The cartridge was then loaded into the Seahorse XFp Analyzer and the Mito Stress test protocol based on manufacturer's instructions. The sensors in the analyser were equilibrated for 20 minutes and the plate was loaded into the analyser. The results were analysed using GraphPad Prism software (Version 7.0, GraphPad Software, San Diego, CA, USA) and Microsoft Excel.

2.12   Genetic knockdown of CPT1A

To analyse the effect of CPT1A on lipid uptake and response to infection it was genetically knocked down using short hairpin (shRNA) targeted to CPT1A using a lentivirus. In a lentiviral system the cell of interest is transduced with a lentivirus which contains RNA encoding shRNA targeting the gene of interest. The RNA incorporates into the cells genome and the shRNA begins to transcribe using RNA polymerase III. The shRNA acts like the pri-miRNA and is therefore modified by the enzymes Drosha and Dicer, which removes the short hairpin, producing double stranded RNA. The RNA is then transported into the RNA-induced silencing complex (RISC) and where Argonaute-2 degrades the sense strand. The anti-sense strand primes the RISC towards the complimentary mRNA. The mRNA is cleaved by the RISC and causes the gene of interest to be silenced. The lentiviral production process was carried out by Manar Shafat and is described below.

2.12.1   Lentiviral production

2.12.1.1   Plasmid preparation

pLKO.1-amp vector *Escherichia coli* (*E. coli*) glycerol stocks containing the shRNA specific to the gene of interest were purchased from MISSION® shRNA library (Sigma Aldrich, St Louis, MO, USA). The primary step in lentivirus preparation is pLKO.1-amp plasmid generation from *E. coli* stocks. Luria Bertani (LB) agar was made up containing 50 µg/mL ampicillin and

poured into plates. Once set the MISSION® glycerol stocks were aseptically streaked onto the plate to isolate single colonies and incubated at 37°C for 16 hours. A single colony was isolated and placed into 5 mL of sterile LB broth containing 50 µg/mL ampicillin and incubated in a shaker at 37°C for 24 hours. The culture was then centrifuged at 16000 xg for 10 minutes and the supernatant was discarded. The plasmid was purified by the NucleoSpin® Plasmid kit (Macherey-Nagel, Duren, Germany) as per manufacturer's instructions. The DNA was quantified, and purity confirmed using the A260/230 and A260/280 ratio on the Nanodrop spectrophotometer (ThermoFisher, Waltham, MA, USA). This process was carried out by Manar Shafat.

2.12.1.2 Transfection of packaging cells

The plasmid DNA concentration required for transfection was 180 ng/µl or higher.

293T packaging cells were used to produce the functional lentivirus encoding shRNA to target the CPT1A. 293T cells originated from the human embryonic kidney (HEK) 293 cells and were a kind gift from Dr Ariberto Fassati (University College London, UK). The cells were cultured tissue culture coated 10mm dishes in DMEM, supplemented with 10% FCS. They were split 90% confluency at a ratio of 1 in 3 using 0.25% Trypsin but were split 1 in 2 before transfection.

Three plasmids, pLKO.1-amp plasmid, Vesicular stomatitis virus glycoprotein (VSV-G) (envelope proteins) and cytomegalovirus promoter (pCMV) (packaging protein promoter, and a transfection reagent were required to produce a functional lentivirus. FuGENE® 6 (Promega, Fitchburg, WI, USA) was the transfection reagent utilised. A mastermix containing the three plasmids and transfection reagent was made. First 1.5 µg of pLKO.1-amp plasmid and 1 µg of VSVG and pCMV plasmids were mixed in 15 µl TE buffer. This was then added to 18 µl of FuGENE® 6 mixed with 200 µl of Opti-MEM media (ThermoFisher, Waltham, MA, US) and added dropwise to the cells. The cells were incubated for 24 hours and the media was replaced. The media

was then collected 48, 72 and 96 hours after transfection and stored at -80°C. This process was carried out by Manar Shafat.

2.12.1.3 Lentiviral knockdown

LK cells were seeded at a density of 2 x 10^5 cells in 500 µl of pen-strep free medium in a 24 well plates. 20 µl of lentivirus was added to the cells. As a control 20 µl of empty construct virus (ShE) was added to LK cells the cells were then incubated at 37°C for 24 hours. The cells were then topped up with 1 mL of fresh medium. The cells were then centrifuged at 1400rpm for 5 minutes and resuspended in 1X PBS before transplantation into mice. Knockdown efficiency of the gene of interest was assessed using qPCR, if the knockdown was successful the mice were used for further experiments.

2.13 Molecular biology

2.13.1 DNA extraction

To detect intraspecies and interspecies mitochondrial transfer, DNA was isolated from the relevant mice, the mtDNA was then quantified using qPCR. DNA was isolated using a GenElute Mammalian Genomic DNA Miniprep Kit (Sigma Aldrich, St Louis, MO, USA) as per manufacturer's instructions. Cells from the BM were extracted, washed in 1X PBS and stained with antibodies for FACS as previously described. The sorted cells were then re-suspended in 200 µL of Resuspension solution. 20 µL of Proteinase K was then added for cell lysis, prior to addition of 200 µL of Lysis Solution C. The lysate was then vortexed followed by a 10 minutes incubation at 70℃. 200 µL of absolute ethanol was added to the lysate post incubation. The column was pre-treated with column preparation solution to enable maximum yield. The lysate was loaded onto the column and centrifuged at 12000 xg for 1 minute. The flow though was discarded and 500 µL of Wash Solution was added to the column. This was then centrifuged again at 12000 xg for 1 minute. A second wash was carried out with 500 µL of Wash Solution and further centrifugation step for 3 minutes and 16000 xg. To elute the DNA, 50 µL of Elution Solution was added

to the column and incubated for 5 minutes at room temperature. Finally, the column was centrifuged for 1 minute at 12000 xg. The DNA was stored at -20°C until use.

2.13.2   RNA extraction

The gene expression levels in the HSC and LSK were also determined using qPCR. To extract the RNA from these cells for analysis the ReliaPrep™ RNA Cell Miniprep Kit (Promega, Fitchburg, WI, USA) was used as following the manufacturer's instructions. The BM from animals were extracted, washed in 1X PBS and stained with antibodies for FACS as previously described. The cells were sorted into 250 µl of BL+TG buffer and mixed thoroughly and 85µl of Isopropanol was then added and vortexed to mix. The cell lysate was then loaded onto the ReliaPrep™ mini-column and centrifuged at 13000 xg for 30 seconds. The flow through was discarded and 200 µl of column wash solution was added to the column. The column was centrifuged at 13000 xg for 30 seconds and 500 µl of RNA wash solution was then added. The column was centrifuged again using the same parameters before a second wash step with 300 µl of RNA wash solution. The column was then centrifuged at 16000 xg for 3 minutes. To elute the RNA, 20 µL of nuclease free water was added to the column and centrifuged for 1 minute at 12000 xg. The RNA was stored at -80°C until use.

2.13.3   Quantification of extracted DNA/RNA

DNA and RNA yield were quantified using the NanoDrop spectrophotometer (ThermoFisher, Waltham, MA, USA). Breifly, the NanoDrop was blanked using 1 µL of nuclease free water in which the RNA was eluted. 1 µL of sample was then measured, referenced to the blank sample and RNA or DNA concentration (ng/µL) determined. The sample with an A260/230 ratio between 1.7 and 2.3 was considered sufficiently pure.

2.13.4   cDNA synthesis

To assess gene expression in the HSC and LSK the RNA extracted from section 2.13.2 it had to be synthesised to cDNA. This is by a process called reverse transcription and the RNA was synthesised using the qPCRBIO cDNA synthesis kit (PCR Biosystems, London, UK). The reaction occurs in 10 µl, a master mix was made with 2 µl of 5X cDNA Synthesis Mix and 0.5 µl of 20X RTase per sample. 300 ng of RNA was then added to each PCR tube and nuclease free water was added to make the sample up to 10 µl. The PCR tubes were then centrifuged and loaded into a Thermocycler (Bio-Rad, Watford, UK). A pre-defined program was run which consisted of 42°C incubation for 30 minutes followed by an 85°C incubation for 10 minutes. The reaction was held for 4°C for less than 3 hours and stored at -20°C until further use.

2.13.5   RNA amplification and cDNA synthesis

A high concentration of RNA was required to be able to assess gene expression. For isolation of RNA from sorted HSCs the RNA yield could be low as the frequency of HSCs in the BM is low. Therefore, the Ovation® PicoSL WTA System V2 (Tecan, Männedorf, Switzerland) was used to amplify cDNA from RNA for gene expression analysis. The Ovation® PicoSL WTA System V2 is a three-step process. The first step is generation of first strand cDNA, which is a reverse transcription process producing a hybrid cDNA/mRNA molecule containing a unique RNA tag sequence (SPIA tag) at the 5 prime end of the cDNA. The next step is a synthesis of a DNA/RNA heteroduplex double strand cDNA with the SPIA tag at one end. Finally, there is a SPIA® amplification which results in an amplification of cDNA. The Thermocycler (Bio-Rad, Watford, UK) was used for the reaction sand the program cycles are shown in the table below (Table 2.5). Breifly, 2 µL of First Strand Primer Mix and 5 µL of RNA was added to a PCR tube and mixed. This was then loaded on Thermocycler (Bio-Rad, Watford, UK) and program 1 was run. The first strand master mix was then prepared using 2.5 µL Buffer Mix and 0.5 µL Enzyme Mix per sample and mixed well. 3 µL of the master mix

was added to each tube and loaded onto the thermocycler using program 2. The second strand cDNA was then synthesised by preparing the second strand master mix with 9.7 µL Buffer Mix B1 and 0.3 µL Enzyme Mix per

Program 1 Primer Annealing	65°C – 2 min, hold at 4°C
Program 2 First Strand Synthesis	4°C – 2 min, 25°C – 30 min, 42°C – 15 min, 70°C – 15 min, hold at 4°C
SECOND STRAND cDNA SYNTHESIS	
Program 3 Second Strand Synthesis	4°C – 1 min, 25°C – 10 min, 50°C – 30 min, 80°C – 20 min, hold at 4°C
SPIA AMPLIFICATION	
Program 4 SPIA Amplification	4°C – 1 min, 47°C – 75 min, 95°C – 5 min, hold at 4°C

The cDNA was then purified using the QIAGEN MinElute Reaction Cleanup Kit (Qiagen, Hilden, Germany) as per manufacturer's instructions. Briefly, the cDNA was added to 300 µL of Buffer ERC and vortexed. The sample was then loaded onto MinElute spin column and centrifuged at 16000 xg for 1 minute. The flow through was discarded and 750 µL of Buffer PE was added to the column. It was then centrifuged again at 16000 xg for 1 minute and the flow through discarded. The column was centrifuged again at maximum speed for 2 minutes to removed residual ethanol. The column was then placed into a

clean 1.5 mL microcentrifuge tube and eluted in 20 µL of Nuclease-free Water. The purified cDNA was stored at -20°C until use.

2.13.6 Polymerase chain reaction

In order to analyse the genetic sequence to confirm SNP between the DNA extracted in section 2.13.1 polymerase chain reaction (PCR) was performed using ND4 primers COX3 and ND3 primers (Details of PCR primers used provided in Appendix Table 8.3)

A master mix was created using 5 µL TaqPath ProAmp enzyme (ThermoFisher, Waltham, MA, USA) 2.5 µL water and 1 µL forward and reverse primers. The mitochondrial primers used were ND4, COX3 and ND3. The 1.5 µL of DNA was mixed with 8.5 µL of master mix in PCR tubes, centrifuged and loaded into a Thermocycler (Bio-Rad, Watford, UK). The PCR was run using a pre-defined method as seen below:

- **Pre-amplification** (98 °C for 1 minute).

- **Amplification** over 25 cycles (98 °C for 30 seconds, 58 °C for 30 seconds and 72 °C for 30 seconds).

- **Cooling** (72 °C for 7 minutes and infinite hold at 4 °C).

The samples were stored at -20 °C until further use.

2.13.7 Agarose gel electrophoresis

Agarose gel electrophoresis was utilised to isolate and analyse PCR product for sequencing. To cast a 60 mL 1.25% agarose gel, 0.75g of agarose was dissolved in 60 mL of 1X Tris Acetate EDTA (TAE) buffer and 6 µL of SYBR Safe (ThermoFisher, Waltham, MA, USA) was added to the solution. This was then microwaved for 60 seconds on full power to ensure all agarose was dissolved and left to cool slightly prior to pouring into gel casts. A well comb was added to create lane divides to allow for loading of the samples. Following setting, the gel was placed into an agarose gel running tank, the gel was then submerged in 1X TAE and the comb was removed. 2 µL of 6X Orange G loading dye was added to 10 µL of PCR products from section 2.13.6 and the

sample was loaded into the wells. 5 µL of 1KB DNA ladder (New England Biolabs, Ipswich, MA, USA) was also loaded into a well for PCR product size determination. The gel was run at 100V for 1 hour and imaged on the Chemdoc-It2 Imager (UVP, LLC, Upland, CA, USA) using the UV function (filter 1).

2.13.8 Agarose gel isolation and purification

PCR bands from 2.13.7 were excised using the UV function (filter 1) of the Chemdoc-It2 Imager (UVP, LLC, Upland, CA, USA) to gauge where the DNA was located. The DNA was then purified using GeneJET Gel Extraction Kit (ThermoFisher, Waltham, MA, USA) following manufacturer's instructions. Briefly, the gel slice was excised close to the DNA. 1:1 volume of Binding Buffer was added to the gel slice and incubated at 50-60°C for 10 minute. The sample was vortexed and transferred into GeneJET purification column and centrifuged for 1 minute at 12000 xg and the flow though discarded. 100 µL of Binding Buffer to the column and centrifuged again for 1 minute at 12000 xg. The flow-through was discarded followed by the addition of 700 µL of Wash Buffer to the column and centrifuged for 1 minute at 12000 xg. The column was centrifuged for an additional 1 minute to completely remove residual wash buffer. The column was transferred to a fresh 1.5 mL Eppendorf and 50 µL of Elution Buffer was added to the centre of the column membrane. Finally, the column was centrifuged for 1 minute at 12000 xg.

2.13.9 DNA preparation for sequencing

The purified PCR product was re-quantified for DNA concentration the NanoDrop spectrophotometer (ThermoFisher, Waltham, MA, USA). 10ng/mL of purified PCR product was added to 3.2pmol/µL of ND4 or ND3 and COX3 primer and made up to 5µl per reaction with nuclease free water. The solution was then sent to Source Bioscience for sequencing. Sequencing traces, electropherograms, were analysed using Sequence Scanner Software.

2.13.9.1 Real time qPCR

Real time quantitative PCR (qPCR) was carried out on the Roche Lightcycler 480 (Roche, Basel, Switzerland). This technique was used to determine mitochondrial and fatty acid transporter gene expression and for detection of murine mtDNA transfer. Details of qPCR primers used provided in Appendix Table 8.1 and 8.2.

2.13.9.2 Gene Expression

To determine mitochondrial and fatty acid transporter gene expression in the LSK and HSC the synthesised cDNA was analysed by Sybr Green qPCR. In this reaction, when the cDNA is amplified the Sybr Green intercalates and becomes incorporated into the double stranded DNA. When the Sybr Green is bound it fluoresces and can be detected in real time of the qPCR machine.

The reactions took place on a 384 well Roche Lightcycler reaction plates (Roche, Basel, Switzerland) using qPCRBIO SyGreen Mix (PCR Biosystems, London, UK). To perform the reaction a master mix comprising 4 µl of SyGreen Mix, 1 µl of 10 µM forward and reverse primer and 1 µl nuclease free water per sample was created. 6 µl of the master mix was plated into each well of a 384 well plate and 4 µl of cDNA was then added to the wells. The plate was then sealed and briefly centrifuged for 1 minute at 1000rpm and loaded onto the Lightcycler 480. The PCR was run using the following pre-programmed method:

- **Pre-amplification** (95 $^{\circ}$C for 2 minutes).
- **Amplification** 45 cycles (95 $^{\circ}$C for 15 seconds, 60 $^{\circ}$C for 10 seconds and 72 $^{\circ}$C for 10 seconds).
- **Melting curve analysis** confirms specificity of the PCR product (95 $^{\circ}$C for 5 seconds, 65 $^{\circ}$C for 1 minute and 97 $^{\circ}$C continuous).
- **Cooling** (40 $^{\circ}$C for 30 seconds).

The raw values on the qPCR machine are known as the cycle threshold (Ct) value. The gene of interest was normalised to a housekeeping gene GAPDH

which was present in every cell and expression is not changed with genetic alternations. To analyse the results ΔCt values for a specific gene was quantified by Ct GOI – Ct housekeeping gene. The ΔΔCt could then be calculated by ΔCt control – ΔCt test. The fold change in expression was then determined relative to untreated cells by $2^{-\Delta\Delta Ct}$. Each sample was replicated at least four times.

2.13.9.3 Taqman® based mtDNA analysis

To confirm the SNP genotyping assay, COX3 and ND3 primer efficiency and to quantify the levels of mitochondrial transfer occurring between BM microenvironment and HSCs after LPS treatment a TaqMan qPCR was developed. In this assay a sequence specific probe, which contains both a VIC/FAM fluorophore and TAMRA® quencher bind to the gene of interest. During amplification of the DNA the probe is cleaved which releases the fluorophore and quencher and allows for fluorophore detection. Pre-designed Taqman® assays were obtained from ThermoFisher, encompassing mouse COX3 and ND3 mtDNA, mouse ND1 mtDNA, human ND1 mtDNA and human and mouse genomic DNA (gDNA).

2.13.9.3.1 Mouse SNP mtDNA detection

The mouse mtDNA Taqman® assay was run in simplex reactions, as the probes had both 2′-chloro-7′phenyl-1,4-dichloro-6-carboxy-fluorescein (VIC) and 6- Carboxyfluorescein (FAM) fluorophores. The mouse gDNA Taqman® assays were also ran in simplex reactions. For the master mix: 0.25 μL of Taqman® reagent, which contained primers and probe was added to 2.5 μL of TaqPath ProAmp enzyme (ThermoFisher, Waltham, MA, USA) and mixed with 1.25 μL water. This master mix (4 μL) was then loaded onto each well of a 384 PCR plate. 1 μL of extracted DNA was then added to the master mix in the PCR plate. The plate was then sealed and briefly centrifuged for 1 minute at 1000rpm and loaded onto the Lightcycler 480. The PCR was run using the following pre-programmed method:

- **Pre-amplification** (60 °C for 30 seconds and 95 °C for 5 minutes).
- **Amplification** over 50 cycles (95 °C for 15 seconds and 60 °C for 1 minute).
- **Cooling** (40 °C for 30 seconds).

The Ct value was determined for the PCR run and from the Ct values obtained mouse mtDNA copy numbers were generated. Mouse COX3 and ND3 mtDNA and were normalised against the mouse gDNA Ct to obtain the ΔCt. ΔCt values was determined by Ct mouse COX3 or ND3 mtDNA – Ct mouse gDNA. The ΔCt value was used to generate mitochondrial copy number (2-ΔCt).

The relative mtDNA:gDNA ratio was calculated using the ΔΔCt method described in section 2.13.9.2. The mitochondrial copy number values were used to determine the percentage of donor mouse mitochondria in recipient cells.

2.13.9.3.2 Human and mouse mtDNA detection

To assess mitochondrial transfer in the hu-NSG model a predesigned Taqman® assay which encompassing both human and mouse mtDNA and gDNA was used. The mtDNA Taqman assays for both human and mouse were ran in duplex reactions whereas the human and mouse gDNA were ran in simplex reactions.

The simplex master mix was made as described in section 2.13.6. For the duplex reactions a master mix was made by mixing 0.5 µL of each Taqman® assay (human and mouse mtDNA) with 2.5 µL of TaqPath ProAmp enzyme and 0.5 µL water.

This master mix (5 µL) was then added to the DNA (1 µL) on the PCR plate. The PCR plate was sealed, centrifuged at 1,000 xg for 1 minute and loaded into the Lightcycler 480 using the program previously described. mtDNA copy numbers were determined for both human and mouse mitochondria applying the ΔΔCt method, using human genomic telomerase reverse transcriptase to normalise results. These values were used to generate the percentage of mouse mitochondria in the human cells to quantify mitochondrial transfer. The

master mix (4 µl) was then loaded onto each well of a 384 PCR plate. 1 µL of extracted DNA was then added to the master mix. The plate was then sealed and briefly centrifuged for 1 minute at 1000rpm and loaded onto the Lightcycler 480. The PCR was run using the following pre-programmed method:

- **Pre-amplification** (60 °C for 30 seconds and 95 °C for 5 minutes).
- **Amplification** over 50 cycles (95 °C for 15 seconds and 60 °C for 1 minute).
- **Cooling** (40 °C for 30 seconds).

mtDNA copy number was determined for both human and mouse mitochondria and normalised to human gDNA. The Ct values for human and mouse were obtained and normalised against the human gDNA. The mouse genomic DNA should not have been detected to ensure no mouse cell contamination. To calculate the ΔCt = h/m mtDNA – Ct hgDNA. The copy number was then calculated by $2^{-\Delta Ct}$ this method was adapted from (330). These values were used to quantify the percentage of mouse mitochondria in the human cells to determine levels of mitochondrial transfer in the calculation below.

$$\% \text{ Mouse mitochondrial DNA} = \left(\frac{\text{Mouse mtDNA copy number}}{\text{m mtDNA copy number + h mtDNA copy number}} \right) \times 100$$

2.13.9.4 Protein extraction

To assess the protein levels in the lin- cells after coculture with BMSC the protein was extracted and analysed by western blotting. To extract the nuclear, cytoplasmic and membrane-bound protein, the whole cell lysate was isolated using radioimmunoprecipitation assay (RIPA) buffer, which was supplemented with protease and phosphatase inhibitors. The lin- cells we sorted after coculture and added to 30 µl of RIPA buffer. The solution was then incubated on ice for 20 minutes. The samples were then centrifuged at 16000 xg for 20 minutes at 4ºC. The supernatant containing the protein was collected and the cell pellet was discarded. The supernatant was stored at -20ºC until use.

2.13.9.5 SDS page and immunoblotting

A 12% polyacrylamide sodium dodecyl sulfate polyacrylamide gel electrophoresis (SDS-PAGE) gel was cast to quantify the presence of phosphorylated AKT. To make the SDS-PAGE gel 30% Polyacrylamide/Bis Solution (BioRad, Hercules, CA, USA) was added to 10% SDS, 10% ammonium persulphate, 1.5M Tris pH 8.8, TEMED and water. 5 mL of the gel mixture was added to the case and was left to set. The stacking gel was then prepared containing 30% Polyacrylamide/Bis Solution, 10% SDS, 10% ammonium persulphate, 1 M Tris, TEMED and water. The gel mix was then layer on top of the gel and a comb was added to create wells. The gel was left to set, and the protein sample was then prepared. 4x sample loading buffer, containing bromophenol blue, β-mercaptaethanol, glycine and a reducing agent was added to the samples. The samples were then incubated at 100°C for 5 minutes to denature the protein.

Table 2.6. Recipe for making a 12% polyacrylamide gel.

12% separating gel 20mL		12% stacking gel 10mL	
Reagent	**Volume (mL)**	**Reagent**	**Volume (mL)**
Water	6.6	Water	6.75
30% Polyacrylamide	8	30% Polyacrylamide	1.675
1.5M Tris	5	1.5M Tris	1.25
10% SDS	0.2	10% SDS	0.1
10% Ammonium persulphate	0.2	10% Ammonium persulphate	0.1
TEMED	0.008	TEMED	0.001

Once the polyacrylamide SDS-PAGE gel was set the gel was placed in the tank filled with running buffer containing 10% SDS, 20µM glycine and 157µM Tris-Base. 10 µl of sample was loaded into the well alongside 5µl of Precision Plus Protein All Blue Prestained Protein standard ladder (BioRad, Hercules, CA, USA). The gels were run at 190V for around 1 hour, the protein was then transferred from the gel onto methanol pre-treated polyvinyladine fluoride (PVDF) membranes. The gel and the PVDF membrane were layered in a cassette and transferred to a tank filled with transfer buffer, 20µM Glycine and 157µM Tris-Base. An ice pack was also placed in the tank to prevent

overheating and was left to transfer at 100v for 45 minutes. The PVDF membrane was then blocked in TBST (1X PBS and 0.01% Tween) with 5% bovine serum albumin (BSA) on a shaker for 1 hour. The blocked membrane was then incubated with primary antibody overnight at 4˚C. The membrane was then washed with TBST 5 times and secondary anti rabbit horseradish peroxidase (HRP) was added to the membrane. The membrane was incubated for 1 hour at room temperature and washed a further 5 times in TBST. The membranes were also probed for total AKT as a loading control.

2.13.9.6 Chemiluminescent detection of the western blot

The antibody stained membranes were visualised using enhanced chemiluminescence (ECL) reagent (GE healthcare, Little Chalfont, UK). The solution A and B were first mixed in equal quantities and 500 µl was then added to the membrane. The membrane was incubated for 45 seconds and any excess solution remained was poured off. The membrane was imaged using the filter set on 3 on the Chemdoc-It2 Imager (UVP, LLC, Upland, CA, USA).

2.14 Animal Procedures

All animal work used in this thesis was carried out in accordance with regulations set by the UK Home Office and the Animal Scientific Procedures Act 1986 under project license 70/8814 (Prof. Kristian Bowles). All procedures were carried out by myself, under UK Home Office personal license I2777C6D5, with the aid of Dr Chris Marlein (IBB43C002), Dr Charlotte Hellmich, Jamie Moore (ID99A0852) and Dr Stuart Rushworth (ICD3874DB). Full training was conducted by Mr Richard Croft (IGEBEFB87) and Mrs Anja Croft (L8A2ACED) before undertaking the techniques described below. Animals were housed in a pathogen free, containment level 3 laboratory in the Disease Modelling Unit (DMU) at the University of East Anglia.

2.14.1 Maintenance of animal colonies

Seven strains of mice were used in this study. C57BL/6J (originally purchased from stock at the DMU, UEA, UK), Non-obese diabetic (NOD) severe combined immunodeficiency (SCID) Il2rg knockout (NOD.Cg.Prkd^{scid}IL2rg^{tm1Wji}/SzJ) (NSG) mice, (originally purchased from the Jackson Laboratory, Bar Harbour, ME, USA), B6.SJL-Ptprca$^{Pep3b/BoyJ}$ (PepCboy) mice (originally purchased from Jackson Laboratory), C57BL/6N$^{su9-DsRed2}$ (DsRed) Mice (A kind gift from Professor Jiri Neuzil Institute of Biotechnology, Czech Academy of Sciences, Prague, Czech Republic), B6.129S-Cybb^{tm1Din}/J (Cybb) mice (originally purchased from Jackson Laboratory), CBA/J mice (originally purchased from stock at the DMU) and B6.129S1-Cd36^{tm1Mfe}/J (CD36 knockout) mice (originally purchased from Jackson Laboratory). The mice were all maintained and bred in the "barn" of the DMU. Breeding pairs were kept together for 6 months before separation and the offspring weaned 3 weeks post birth. Animals were used for experimentation at 8 to 12 weeks of age (with the exception of mice used for transplantation in which case 3 to 4-week-old mice were used). Both genders were used for experiments.

2.14.1.1 Wildtype C57BL/6J mice

The C57BL/6J is the most commonly used inbred mouse strain, it is widely used as an all-purpose strain and a background strain for the generation of mice with spontaneous and induced mutations. The C57BL/6J mice are long-lived and breed well. The C57BL/6J mice were used in this study to analyse the mitochondrial content, mitochondrial health, lipid content, ROS levels, pAKT and cell cycling in the HSC and progenitor populations after infection. The mice were also used for the generation of mouse BMSC, mouse macrophages, mouse osteoblasts and lin- or LK cells for *in vitro* experiments. To assess response to infection 1 mg/kg LPS or control PBS were injected IP into C57BL/6J mice. Following a 2 or 16 hours incubation the mice were sacrificed, and BM was extracted and analysed by flow cytometry, cell sorting and seahorse metabolic analysis. C57Bl/6J mice were also subjected to pre-treatment with 500 mg/kg N-acetyl cysteine (NAC), 100 mg/kg buthionine

sulfoximine (BSO), 25 mg/kg cytochalasin B (CytoB), 30 mg/kg CAL 101, 50 mg/kg carbenoxolone (CBX), 40 mg/kg sulfosuccinimidyl oleate (SSO) or 10 mg/kg Etomoxir all diluted in PBS for 1 hour followed by 1 mg/kg LPS. After 16 hours the mice were sacrificed, and the BM extracted for analysis. C57Bl/6J mice were also used to determine the HSC response to *Salmonella typhimurium* (*S.typhimurium* infection). C57Bl/6J mice were treated with streptomycin (20 mg/mL) 24 hours prior to *S.typhimurium* infection. Mice were then left untreated or infected with 100 μL of 1 x 10^8 CFU *S.typhimurium* (SL1344- JH3009) by oral gavage for 72 hours.

2.14.1.2   NSG mice

NSG mice have two mutations scid and an IL2 receptor common gamma chain (IL2rg^{nul}) null allele on the NOD/ShiLtJ background. The mice are deficient of B and T cell as the scid mutation is in the Prkdc, a DNA repair complex protein. They are also deficient in functional natural killer cells due to the IL2rg^{null} mutation, which inhibits multiple receptor cytokine signalling. This severe immune deficiency allows for the engraftment of human CD34+ haematopoietic stem cells to create humanized mice. These mice were used for allograft and xenograft transplantations in this study. The mice were treated with busulfan rather than irradiation before transplantation, so the animals were relatively healthy.

2.14.1.3   Wildtype PepCboy mice

The B6.SJL-Ptprca$^{Pep3b/BoyJ}$ (PepCboy) mouse is a C57BL/6J congenic strain which carries the differential pan leukocyte marker, Ptprc^a also known as CD45.1. Wildtype inbred C57BL/6J inbred mice express the Ptprc^b or CD45.2 allele. Therefore, these mice are commonly used for transplantation studies. These animals were used in this study to generate transplantation models in which a C57BL/6J or a CD36 mouse BM was transplanted into PepCboy mice. The mice were also used for the generation of mouse BMSC and lin- of LK cells for *in vitro* mtDNA transfer assay.

2.14.1.4 DsRed mice

C57BL/6N$^{su9\text{-}DsRed2}$ (DsRed) mice are transgenic mice which express a red fluorescent protein in the mitochondria of somatic cells (*CAG/su9-DsRed2* transgene). DsRed mice are based on a C57Bl/6 background and were generated at the Institute of Molecular Genetics (Prague, Czech Republic). DsRed mice were used in this study to assess mitochondrial transfer within the BM. DsRed mice were ear notched for phenotyping and identification and fluorescence was detected by fluorescent microscopy. Fluorescent microscopy was carried out on a Zeiss Axio Observer fluorescent microscope with 20X objectives (Carl Zeiss, Oberkochen, Germany). Tissue samples collected from ear notching were placed into 24 well plate and placed on the plate holder on the microscope. ZEN Blue imaging software was used to acquire fluorescent and bright field images. For characterisation of the DsRed animals, phenotypically positive animals were sacrificed, the BM was extracted and analysed by flow cytometry for specific cell populations. Phenotypically negative DsRed animals were used as a control. For mitochondrial transfer analysis 1 mg/kg LPS or PBS control were injected by intraperitoneal injection. After 2-hour of treatment the mice were sacrificed, and BM was extracted for flow cytometry analysis.

2.14.1.5 Cybb mice

B6.129S-Cybbt^{m1Din}/J (Cybb) mice also known as gp91phox- have a C57Bl/6J background with a null allele in the gene involved in X-linked CGD. This gene encodes the oxidase cytochrome b in the 91 kD subunit and hemizygous male which are affected lack the ability to produce phagocytic superoxide and have an increased susceptibility to infection. The Cybb mice were used to analyse mitochondrial content in the HSC and progenitor populations after infection. 1 mg/kg LPS or PBS control were interperitoneally injected. After 2 hours of treatment the mice were sacrificed, and BM was extracted for analysis. The mice were also used for the generation of mouse macrophages for *in vitro* experiments.

2.14.1.6 CBA mice

Wildtype inbred CBA/J mice are a commonly used as a general-purpose strain. CBA/J mice express the Ptprc[b] or CD45.2 allele similar to the WT C57BL/6J. These mice were used to assess mitochondrial transfer in *in vitro* mtDNA transfer assays. The mice were sacrificed, and the BM was extracted and used to generate mouse BMSC and lin- cells.

2.14.1.7 CD36 knockout mice

B6.129S1-Cd36[tm1Mfe]/J (CD36 knockout) mice have a number of lipid-related metabolic traits including an altered fatty acid uptake. The knockout mice have a targeted mutation a NEO cassette instead of exon 3 which encodes the translation initiation site and the first 40 amino acids. Homozygous mice are viable, tend to be smaller and have elevated fasting levels of non-esterified FFA compared wildtype controls. The CD36 knockout mice were used in this study to analyse the lipid content, and cell cycling in the HSC and progenitor populations after infection. The mice were also used in transplantation experiment. To assess response to infection 1 mg/kg LPS or control PBS were injected IP into CD36 knockout mice. Following a 16 hour incubation the mice were sacrificed and BM was extracted and analysed by flow cytometry and seahorse metabolic analysis. CD36 knockout mice were also used to determine the HSC response to *S.typhimurium* infection. CD36 knockout mice were treated with streptomycin (20 mg/mL) 24 hours prior to *S.typhimurium* infection. Mice were then left untreated or infected with 100 μL of 1 x 10^8 CFU *S.typhimurium* (SL1344- JH3009) by oral gavage for 72 hours. The mice were sacrificed, and BM was extracted and analysed by flow cytometry and seahorse metabolic analysis.

2.14.2 Intraperitoneal injections

Busulfan, LPS, NAC, BSO, etomoxir and D-luciferin were all administered using an intraperitoneal (IP) injection. The mice were restrained using a scruff technique and 200 μL for a 6-week old mouse and 100 μL for a 3-6-week-old mouse of the compounds were injected into the peritoneum with a sterile 26-

gauge needle. In the case of busulfan where daily IP injection or pre-treatment was needed, the animals were injected in alternate flanks.

2.14.3   Intravenous injections

For transplantation models the donor LK cells were administered to the busulfan treated recipient mice via intravenous (IV) tail vein injection. The recipient mice were placed in a 37℃ hot box for 10 minutes to vasodilate the tail vein, prior to injection. The mice were then placed in a benchtop restrainer and 200 µL of 2 x 10^5 LK cells suspended in PBS was injected into the lateral tail vein with a sterile 26-gauge needle. The mice were then placed into a new cage for a short recovery period before being returned to their home cage.

2.14.4   Blood Sampling

Blood was taken from the tail vein of mice for engraftment and serum fatty acid analysis. For engraftment analysis the tail vein was vasodilated by placing the animals in a 37 °C hot box for 10 minutes. The mice were then placed in a benchtop restrainer, using a trimmed 26-gauge butterfly needle 200 µL of blood was collected in a 1.5mL Eppendorf tube containing 25 µL of monosodium citrate. The red cells were then lysed using 1X red blood cells lysis buffer (ThermoFisher, Waltham, MA, USA) and specific antibodies were added to the collected blood and stained for 20 minutes. The blood was then analysed using flow cytometry. For serum FFA analysis cardiac puncture was used to isolate the blood.

Cardiac puncture was used as it is method which can obtain large quantities of good quality blood. The mice are placed under deep terminal anaesthesia and the blood samples were taken from the left ventricle of the heart using a 25-gauge needle. The blood was withdrawn slowly to prevent the heart from collapsing and placed into EDTA coated tubes ready for analysis.

2.14.5   Oral gavage

For the administration of live *S.typhimurium* to C57BL/6J or CD36 knockout mice, oral gavage was utilised, this procedure was carried out by Dr Naiara Bezera. Glycerol stocks of *S. typhimurium* were aseptically streaked onto Luria

Broth agar plates, to isolate single colonies and incubated at 37˚C for 16 hours. A single colony was isolated and placed into 5 mL of sterile LB broth containing 0.3 M NaCl (LBS) and incubated in a shaker at 37˚C for 24 hours. The overnight culture was diluted in LBS 1:100 and incubated until the culture reached the optical density (ΔOD_{600nm}) of 1.2 to 1.4 which is the late exponential phase. At this ΔOD_{600nm} the SPI1 invasion genes in the *S. typhimurium* are turned on. The culture was then centrifuged at 8000 xg for 7 min and washed twice in 1X PBS, the pellet was resuspended at concentration of 1 to 5 x 10^8 CFUs per 100 µL in sterile 1X PBS. The mice were infected with 100 µL of 1 x 10^8 CFUs of *S. typhimurium* by restraining the mouse in a scruff and administering the *S. typhimurium* down the oesophagus directly into the stomach of the mouse.

2.14.6   Live animal imaging

To assess fatty acid uptake in the haematopoietic compartment bioluminescent imaging of live mice was carried out. To ensure engraftment, the FFA-luciferase allograft mouse model was intraperitoneally injected with150mg/kg D-luciferin. The mice were then left for 15 minutes at room temperature for maximum detection of the luciferase signal. The mice were then anaesthetised using a chamber filled with isoflurane with a flow rate of 3%. The mice were then transferred to the Bruker In-Vivo Xtreme (Bruker, Coventry, UK) an imaged using a pre-set method of 1-minute exposure bioluminescent image, x-ray and light image. The mice were transferred to their home cage to recover. Once engraftment was confirmed and the mice had sufficiently recovered the mice were injected with 100 µL of 200 µM FFA-SS-luc (SwissLumix Sarl, Switzerland) (0.014 mg/mouse) bound to 0.1% (w/v) BSA in PBS, interperitoneally. The mice were imaged using the Bruker In-Vivo Xtreme with a 2-minute exposure. One week after the mice had recovered the animals were interperitoneally injected with 1 mg/kg LPS for 16 hours. The mice were injected with 100 µL of 200 µM FFA-SS-luc (0.014 mg/mouse) bound to 0.1% (w/v) BSA in PBS again and imaged using the Bruker In-Vivo Xtreme with a 2-minute exposure FFA uptake was visualised by light detection produced Oxyluciferin formation from luciferin. This reaction was catalysed by

the luciferase in the modified haematopoietic cells. The images were merged with the X-ray files and the densitometry was analysed using Fiji software.

2.14.7　Schedule 1

Mice were monitored daily and humanely sacrificed upon first sign of illness including; weight loss, reduced motility, signs of graft vs host disease, severe over grooming, hind limb paralysis, hunched posture and piloerection using schedule 1 methods. The mice were also sacrificed at the end point of the experiment. Mice were sacrificed by gradual CO_2 asphyxiation followed by dislocation of the neck.

2.14.8　Transplantation models

For transplantation experiments engraftment was checked by expression of human CD45 or mouse CD45.1/2 on differentiated cells by blood sampling 4, 8 and 12 weeks post transplantation (Appendix Figure 8.1 to 8.3). 12-16 weeks post transplantation animals were treated. Engraftment was also measured by expression of human CD45 or mouse CD45.1/2 detected in the BM after termination, if more than 40% donor cells were detected the cells were considered to be engrafted.

2.14.8.1　NSG^{C57} allograft mouse model

The NSG mouse model expressing the CD45.1 allele antigen was used in transplant experiments whereby isolated BM cells from C57Bl/6J mice expressing the CD45.2 allele was transplanted. 3-4-week-old NSG mice were treated with 25 mg/kg Busulfan interperitoneally every 24 hours over a 72-hour time period. 2×10^5 isolated BM cells from C57Bl/6J mice were lineage depleted then injected IV into the tail vein. Engraftment of the C57Bl/6 BM was analysed by flow cytometry through analysis of CD45.2 and CD45.2 cells in the peripheral blood. Once engrafted these animals were then treated with 1 mg/kg LPS or control PBS for 2 hours. These transplanted mice were termed NSG^{C57}. The BM was isolated and sorted for donor C57BL/6J LSK (Lin-, Sca 1+, CD117) and donor C57BL/6J HSC (Lin-, Sca 1$^+$ CD117 CD48$^-$CD150$^+$) and analysed for mtDNA transfer by qPCR.

2.14.8.2 CD34+ haematopoietic progenitor cell xenograft model

For the CD34+ haematopoietic progenitor cell xenograft model (hu-NSG), 3-4-week-old NSG mice were treated with 25 mg/kg Busulfan interperitoneally every 24 hours over a 72-hour time period. On the day of transplantation 2 x 10^5 isolated CD34+ cord blood cells were injected into the tail vein of the busulfan treated NSG mice. CD34+ cell engraftment was checked by levels of human CD45+ cells in the peripheral blood. Post engraftment, the hu-NSG mice were treated with 1 mg/kg LPS for 2 hours and sacrificed. The BM was extracted, and the human HSCs (hHSCs) (mCD45−, hCD34+, hCD38−, hCD45RA−, hCD90+, hCD49f+), hMPPs (mCD45-, hCD34+, hCD38−, hCD45RA−, hCD90−, hCD49f−), and hGMPs (mCD45−, hCD34+, hCD38+, hCD45RA+, hCD90−, hCD49f−) was isolated by FACS. The BM was also analysed for human cell engraftment by human CD45+ cells. If more than 40% of human CD45 cells was detected in the BM, the CD34+ cells were deemed to be engrafted.

2.14.8.3 FFA luciferase allograft mouse model

For the FFA-luciferase allograft mouse model C57BL/6J and CD36 knockout mice expressing the CD45.2 allele antigen was used in the transplant experiments. C57BL/6J and CD36 knockout mice were sacrificed, BM was isolated, lineage depleted followed by CD117 enrichment using CD117+ enrichment kit. The cells were then seeded at a density of 2 x 10^5 cells/well in DMEM supplemented with 10% FBS plus 1% penstrep with mSCF, mIL 3, mIL 6 (Peptrotech, NJ, USA). The cells were transduced with pCDH-luciferase-T2A-mCherry virus, which was kindly provided by Professor Irmela Jeremias, (Helmholtz Zentrum München, Munich, Germany). Following a 24-hour incubation a successful transduction was confirmed by detection of mCherry fluorescence on a fluorescent microscope. The transduced cells were then transplanted into the tail vein of 3-4-week-old PepCboy mice by intravenous injection which had been preconditioned with 25 mg/kg/day for 3 days prior to transplantation. FFA-luciferase allograft mouse engraftment was monitored by *in vivo* bioluminescent live animal imaging (Section 2.14.13).

2.14.8.4 CPT1A KD allograft mouse model

In the CPT1A KD allograft mouse model PepCboy mice expressing the CD45.1 allele antigen was used in the transplant experiments to determine the role of CPT1A in the response to infection. C57BL/6J and CD36 knockout mice were sacrificed, BM was isolated, lineage depleted followed by CD117 enrichment using CD117+ enrichment kit. The cells were then seeded at a density of 2 x 10^5 cells/well in DMEM supplemented with 10% FBS plus 1% penstrep with mSCF, mIL3, mIL6 (Peptrotech, NJ, USA). The cells were transduced with MISSION shRNA TRCN0000036279 (human carnitine palmitoyltransferase IA (CPT1A) shRNA). MISSION pLKO.1-puro Control Vector was used as the lentivirus control (control short hairpin RNA (shRNA)). The transduced cells were then transplanted into the tail vein of 3-4-week-old C57BL/6J mice by intravenous injection which had been preconditioned with 25 mg/kg/day for 3 days prior to transplantation. Successful transduction was assessed using qPCR, if the knockdown was successful the mice were used for further experiments. Post engraftment the animals were treated with 1 mg/kg LPS or control PBS for 16 hours and sacrificed. The BM was extracted and analysed by flow cytometry for cell cycling and lipid content. The BM was analysed for CD45.1 expression to determine cell engraftment.

2.14.8.5 PepCboy CD36 allograft mouse model

In the PepCboy CD36 allograft model PepCboy mice expressing the CD45.1 allele antigen was used in this transplant experiment to assess the recovery of the haematopoietic system in CD36 knockout mice in response to infection. PepCboy mice were sacrificed and the BM was isolated, lineage depleted followed by CD117 enrichment (LK cells). 2 x 10^5 isolated LK PepCboy cells were then injected into the tail vein of 3-4-week-old CD36 knockout mice by intravenous injection which had been preconditioned with 25 mg/kg/day for 3 days prior to transplantation. Post engraftment the animals were treated with 1 mg/kg LPS or control PBS for 16 hours and sacrificed. The BM was extracted and analysed by flow cytometry for CD36 expression, lipid uptake and cell cycling and CD45.1 cell engraftment. The LSK cells were also isolated and metabolic changes were assessed by seahorse metabolic flux analysis.

2.14.8.6 CD36 PepCboy allograft mouse model

In the CD36 PepCboy allograft model PepCboy mice expressing the CD45.1 allele antigen was used in this transplant experiment to assess the role CD36 in the haematopoietic system in response to infection. C57BL/6J (WT CD36$^{+/+}$) and CD36 knockout (CD36$^{-/-}$) mice were sacrificed, and the BM was isolated, lineage depleted followed by CD117 enrichment (LK cells). LK WT CD36$^{+/+}$ and LK CD36$^{-/-}$ were then injected into tail vein of 3-4-week-old PepCboy mice by intravenous injection which had been preconditioned with 25 mg/kg/day for 3 days prior to transplantation. These transplanted mice were termed WT$^{(CD36-/-)}$ for CD36 knockout into WT and WT$^{(CD36+/+)}$ for WT into WT. Post engraftment the animals were infected with *S. typhimurium* for 4 days. The BM was extracted and analysed by flow cytometry for lipid uptake, cell cycling and CD45.2 cell engraftment.

2.15   Quantification and Statistical Analysis

All data produced in this study was analysed using Prism software (Version 7.0, GraphPad Software, San Diego, CA, USA), BD FlowJo 10.7.0 software (FLowJo, LLC, Ashland, OR, USA), Fiji ImageJ 2.0.0. and Microsoft Excel (Albuquerque, NM, USA). Due data variability *in vivo* work, statistical comparison of two groups was performed without assumption of normal distribution using the Mann-Whitney U test. For comparison of more than two groups, One-way ANOVA followed by Tukey's multiple comparisons test or Kruskal-Wallis statistical test followed by Dunn's multiple comparisons or Two-way Anova was performed using Prism software (GraphPad, La Jolla, CA, USA). Differences between group means were determined significant when the probability value, p, was less than 0.05* 0.01** 0.001*** 0.0001****. The results represent the mean ± standard deviation of 4 or more independent experiments. Sample size (n) represents number of biological replicates. No statistical methods were used to predetermine sample size.

3 Mitochondrial transfer occurs from the bone marrow microenvironment to the HSC during acute infection

3.1 Introduction

The ability of the HSC to maintain the HSC pool and differentiate into the mature blood cells is vital for the maintenance of haematopoiesis throughout life (9, 331). The HSC whilst mostly quiescent, upon exposure to specific stimuli can rapidly become active and enter the cell cycle (332). The mammalian response to infection is reliant on this switch, initiating a rapid expansion of leukocytes to respond to the pathogen (11). This expansion requires large amounts of energy however, the mechanism underlying the regulation of HSC metabolism in response to the pathogenic challenge are not fully elucidated.

HSCs reside in the BM microenvironment, within a specialised niche which helps maintain the production of mature blood cells under physiological conditions (51, 131). The HSC niche is a hypoxic environment, which supports the HSC for retention or expansion out of the niche. HSC expansion requires large amounts of energy and quiescent HSCs are thought to rely on anaerobic glycolysis (245, 333). It has been shown that quiescent HSCs have a low mitochondrial mass (245, 247, 334), which is maintained by mitophagy. This active removal of mitochondria has been shown to be vital for the maintenance of HSCs (334, 335). Furthermore, HSC mitochondrial mass has been shown to be stable over their lifetime with a lower turnover capacity of mitochondria than the more differentiated progenitors (336). HSC quiescence is maintained by the regulation of mitochondrial mass and a limited mitochondrial respiration (286). Taken together, the regulation HSC quiescence is reliant on specific metabolic conditions maintained by the HSC niche.

It has previously been shown that intercellular mitochondrial transfer from BMSCs to AML blasts aids proliferation and survival of the malignant cell though an increase in OXPHOS (41, 297). Moreover, it has also been shown non-malignant cells can transfer mitochondria to rescue aerobic respiration.

Furthermore, it has been observed that under normal conditions human CD34+ haematopoietic progenitor cells do not obtain mitochondria from BMSCs, however under oxidative stress mitochondria can move between these cells (41). This suggests that the metabolic switch in AML, regulated by mitochondrial transfer could have originated from the normal physiological response of the HSC during infection.

Pathogenic stress including bacterial infection is a major cause of oxidative stress in the human body (337) and therefore could stimulate the transfer of mitochondria to the HSC. LPS is found on the outer membrane of most gram-negative bacteria and has been shown to initiate an immune response similar to a bacterial infection in mice (68). In this chapter of my thesis using *S. typhimurium* and LPS I will examine the mitochondrial change in HSCs and the metabolic consequences following acute bacterial infection. I also aim to determine if mitochondrial transfer from the BM microenvironment to the HSC occurs *in vivo* during LPS stimulation.

3.2 Acute bacterial infection increases mitochondrial content in HSCs

Firstly, to analyse the effect of acute bacterial infection on mitochondrial mass in HSCs, C57BL/6J mice were infected with *S. typhimurium* for 72 hours. At 72 hours of *S. typhimurium* infection there is a significant increase of IL 6 in the serum compared to mice treated for 48 and 120 hours (Figure 3.1A). At 72 hours the animals also begin to lose weight, a hallmark of *S. typhimurium* infection, this time point was therefore chosen as the endpoint (Figure 3.1B). The haematopoietic cell populations were analysed for mitochondrial levels with a panel of cell surface antibodies and MitoTracker Green (MTG) using flow cytometry (Figure 3.2A). This included all colour compensations and the gating strategy to isolate the specific cell populations of interest is shown in Figure 3.2B. All gating was determined using fluorescence minus one controls and based on the methods described by Walter *et al* 2015 (68).
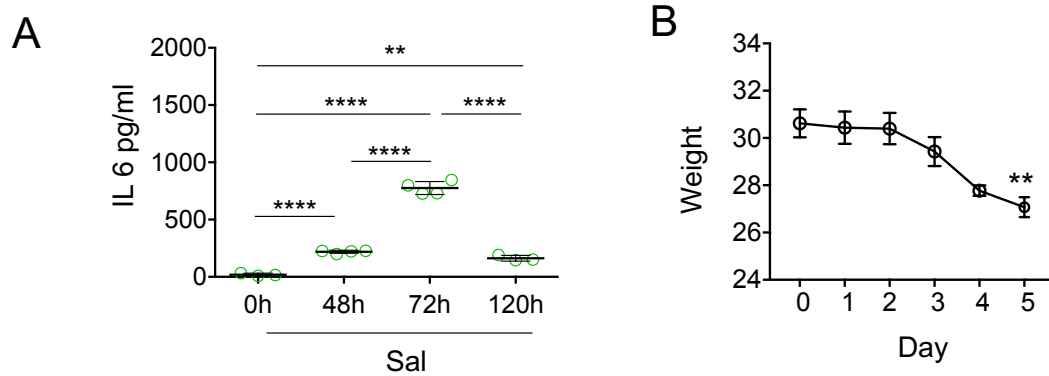
Figure 3.1. *S.typhimurium* infection induce an increase in IL 6 expression in the serum and weight loss.
(A) C57BL/6J mice were infected with *S.typhimurium* (Sal) for 48,72 or 120 hours. Blood was taken from the animals by cardiac puncture and the serum was assessed for IL 6. n>3 in each group. Experiment performed by Dr Stuart Rushworth. (B) C57BL/6J mice were infected with *S.typhimurium* (Sal) for 5 days, the animals were weighed daily. n=6 in each group. Data shown are means ± SD **P < 0.01 P< ****0.0001 Statistical test used was Kruskal-Wallis statistical test followed by Dunn's multiple comparisons.
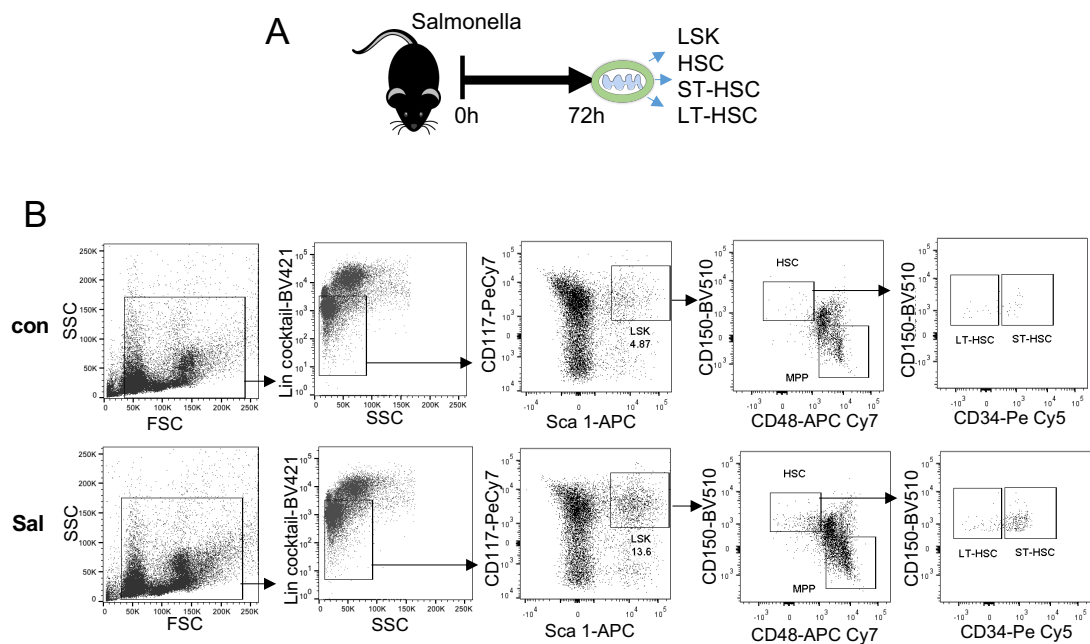
Figure 3.2. Gating strategy for mouse Lin-, LSK, HSC, MPP, ST-HSC and LT-HSC.
(A) C57BL/6J mice were infected with *S.typhimurium* (Sal) for 72 hours, the animals were sacrificed, and the bone marrow was extracted. The cells were stained with a panel of antibodies to analyse specific Lin-, LSK, HSC, MPP, ST-HSC and LT-HSC populations. (B) The gating strategy used is shown.

Figure 3.3A shows that HSPC populations within the BM increase their mitochondrial mass after treatment with LPS. Specifically the LSK (Lin- Sca 1+ CD117+), total HSCs (Lin- Sca 1+ CD117+ CD150+ CD48-), ST-HSC (Lin- Sca 1+ CD117+ CD150+ CD48- CD34+) and LT-HSCs (Lin- Sca 1+ CD117+ CD150+ CD48- CD34-) (68) populations all had a significant increase in mitochondrial fluorescence after *S.typhimurium* infection. In the other populations analysed Lin- and MPP (Lin- Sca 1+ CD117+ CD150- CD48+) there was no change in mitochondrial fluorescence after *S. typhimurium* infection (Figure 3.3A).

As with any dye it has been reported that there are limitations to MTG. MTG stains live mitochondria within a cell enabling the identification of mitochondrial localisation (338). MTG has also been used to quantify mitochondrial mass within a cell (339). However, it has been reported that MTG flourecence intensity can be affected by ROS levels or mitochondrial potential. Thus, taking these limitations into account, to further prove that the mitochondrial content increases in the HSC population in response to *S. typhimurium*, the HSC population was sorted from control and *S. typhimurium* treated mice and analysed for mtDNA. The increase in mitochondrial mass was confirmed in the HSC population by an increase in mtDNA following *S. typhimurium* infection (Figure 3.3B).
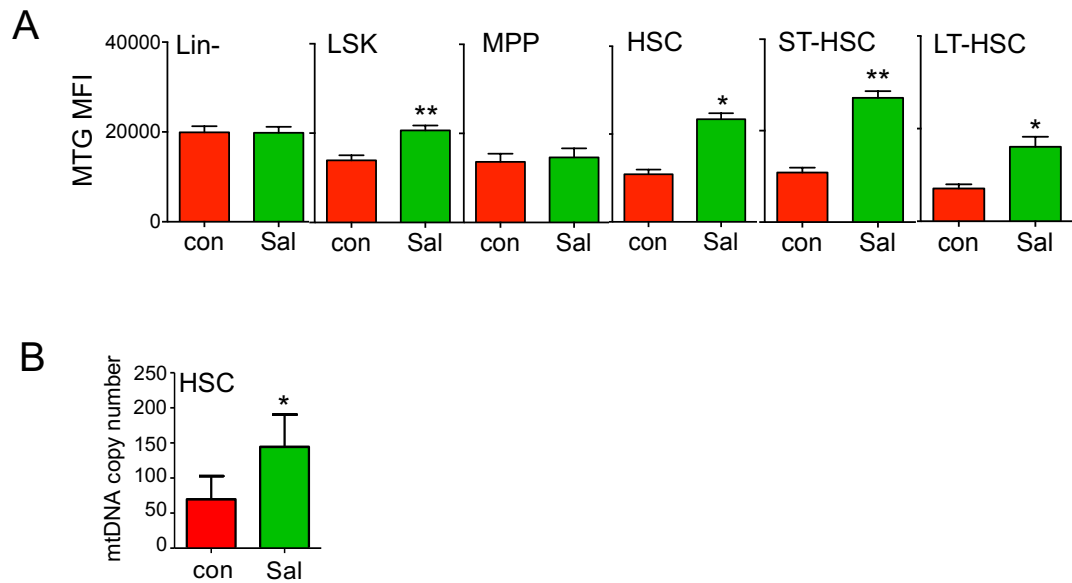
Figure 3.3. *S.typhimurium* **induces an increase in mitochondrial content in the heamatopoetic stem and progenitor populations.**
C57BL/6J mice were infected with *S. typhimurium* (Sal) for 72 hours, the animals were sacrificed, the bone marrow was extracted and stained with a panel of antibodies and Mitotracker green (MTG) to analyse mitochondrial content in specific Lin-, LSK, HSC, MPP, ST-HSC and LT-HSC populations. (A) Mitochondrial content (mitotracker green (mean fluorescence intensity (MFI)) in the specific populations of all animals examined. n=6. (B) The HSC (Lin-, Sca 1+, CD117+, CD48-, CD150+) population was sorted from control and *S. typhimurium* treated mice and analysed for mtDNA by qPCR. n=5 in each group. Data shown are means ± SD *P < 0.05 **P < 0.01

To examine mitochondrial content in the progenitor populations, C57BL/6J mice were infected with *S.typhimurium* by oral gavage for 72 hours. The mice were then sacrificed, and the haematopoietic progenitor populations were analysed for mitochondrial content (Figure 3.4A). The gating strategy shown in Figure 3.4B was determined using fluorescence minus one controls.
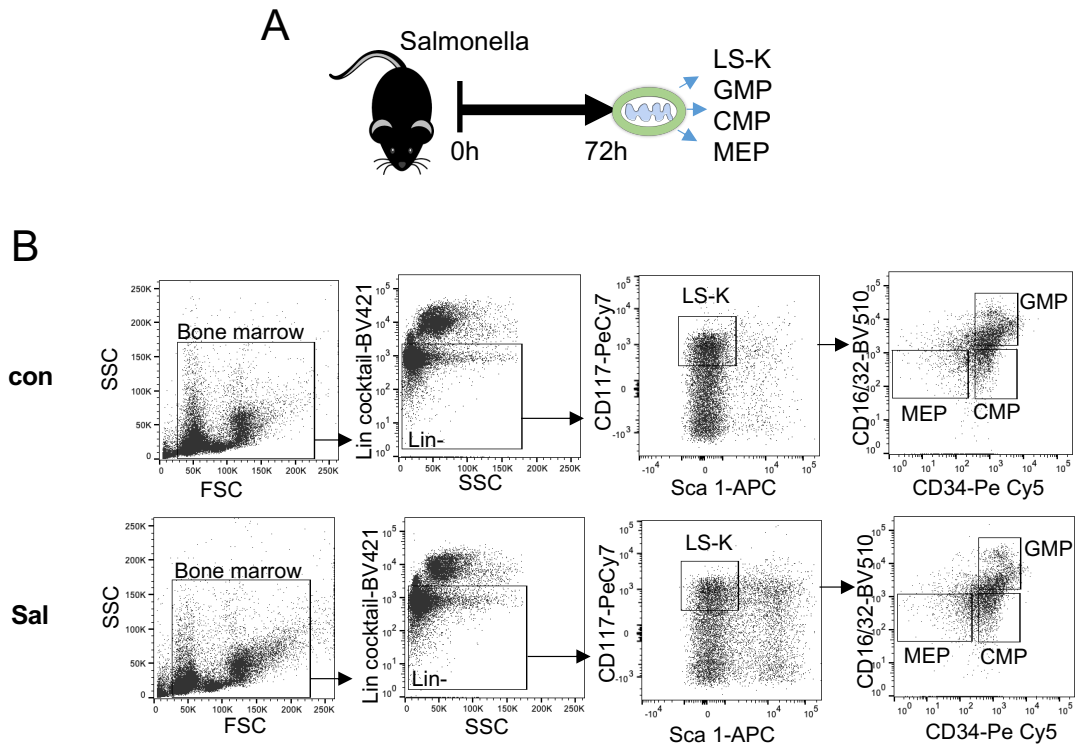
Figure 3.4. Gating strategy for mouse, LS-K, CMP, GMP and MEP.
(A) C57BL/6J mice were infected with S. typhimurium for 72 hours and were sacrificed. The bone marrow was extracted and cells were stained with a panel of antibodies to analyse specific LS-K, CMP, GMP and MEP populations. The gating strategy is shown.

The more lineage committed cells such as the LS-K, CMP, GMP and the MEP populations display no significant increase in mitochondrial mass following *S.ty* infection (Figure 3.5). Taken together, these data confirm that mitochondrial mass increases in the LSK and HSC populations in response to S. typhimurium but not in the downstream committed progenitor cells.
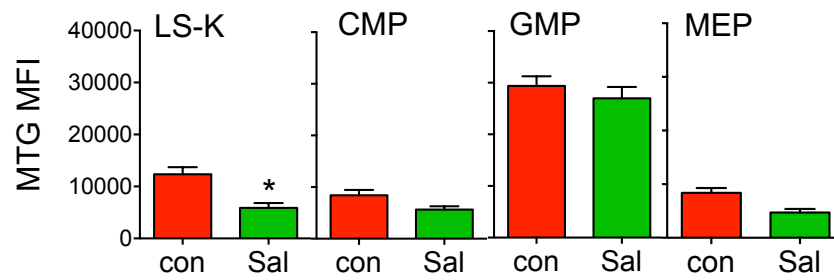
Figure 3.5. *S.typhimurium* does not induce an increase in mitochondrial content in the haematopoietic progenitor populations.
C57BL/6J mice were infected with *S.typhimurium* (Sal) for 72 hours, the animals were sacrificed, the bone marrow was extracted and stained with a panel of antibodies and Mitotracker green (MTG) to analyse mitochondrial content in specific LS-K, CMP, GMP and MEP populations. Mitochondrial content (mitotracker green mean fluorescence intensity (MFI)) in the specific populations of all animals examined. n=6 in each group. Data shown are means ± SD *P < 0.05

To understand the kinetics at which mitochondrial content increases I used LPS as a surrogate for bacterial infection. Firstly, to assess the inflammatory response to LPS treatment a time course kinetic experiment was performed. C57BL/6J mice were treated with LPS for 2, 16 and 48 hours, serum was isolated from these mice and assessed for IL 6 expression. There was a significant increase of IL 6 in the serum of mice treated with LPS for 16 hours compared to the other time point (Figure 3.6).
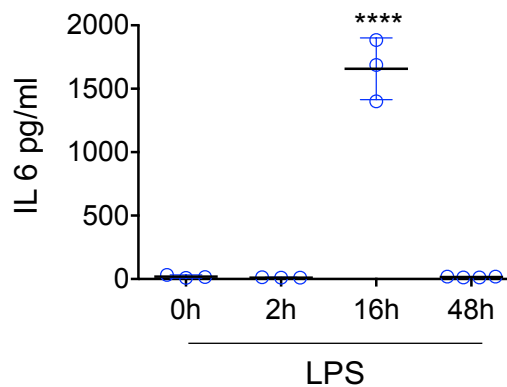
Figure 3.6. LPS treatment induce an increase in IL 6 expression in the serum.
C57BL/6J mice were treated with 1 mg/kg LPS for 2, 16 or 48 hours. Blood was taken from the animals by cardiac puncture and the serum was assessed for IL 6. n>3 in each group. Data shown are means ± SD P< ****0.0001 Statistical test used was Kruskal-Wallis statistical test followed by Dunn's multiple comparisons test.

C57BL/6J at 8 weeks of age were then treated with LPS for 2 and 16 hours and analysed for MTG fluorescence (Figure 3.7A). An increase in mitochondrial content was observed in the LSK, HSC, ST-HSC and LT-HSC at both 2 and 16 hours post LPS treatment. Similar to *Salmonella* there was no increase in mitochondrial mass in the Lin- and MPP population at both 2 and 16 hours post LPS treatment (Figure 3.7B and C).
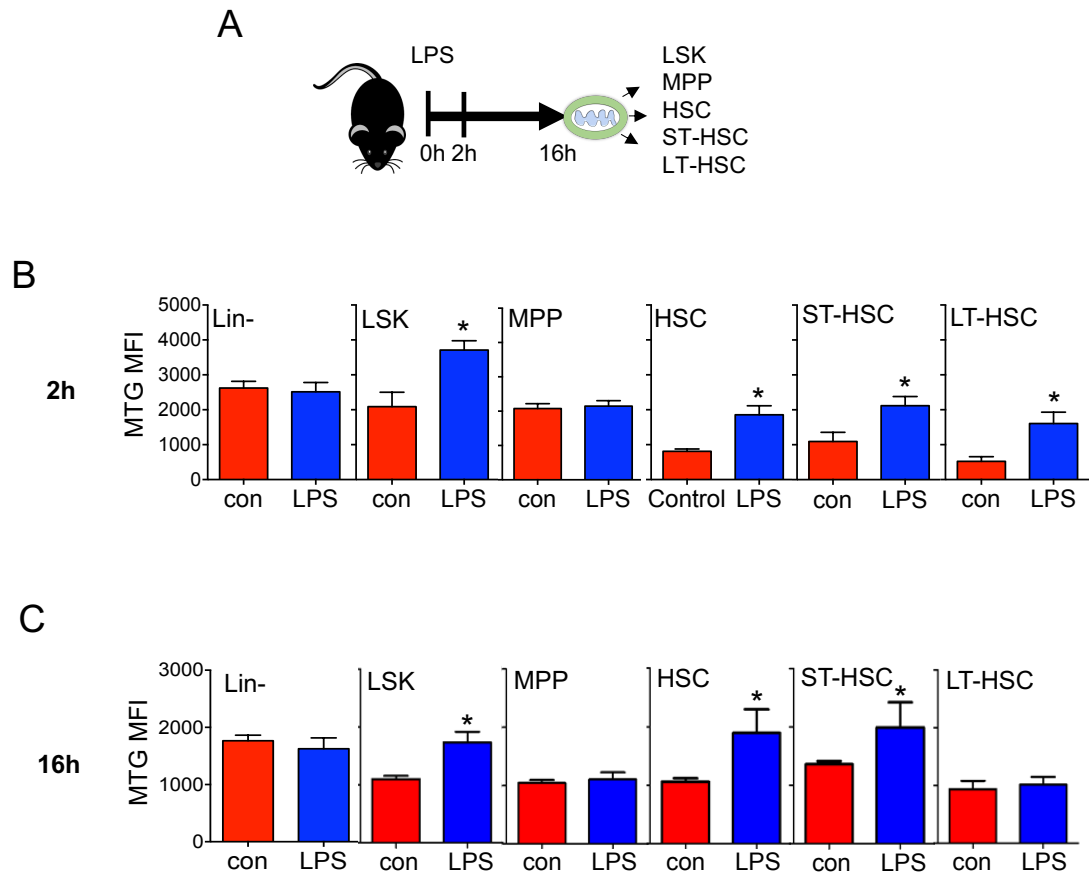
Figure 3.7. LPS induces an increase in mitochondrial content in the haematopoietic stem and progenitor populations.
(A) C57BL/6J mice were treated with 1 mg/kg LPS for 2 or 16 hours, the animals were sacrificed, the bone marrow was extracted and stained with a panel of antibodies and Mitotracker green (MTG) to analyse mitochondrial content in specific Lin-, LSK, HSC, MPP, ST-HSC and LT-HSC populations. (B) Mitochondrial content (mitotracker green (mean fluorescence intensity (MFI)) in the specific populations of all animals examined after 2 hours of LPS treatment. n=5. (C) Mitochondrial content in the specific populations of all animals examined after 16 hours of LPS treatment. n=5 in each group Data shown are means ± SD *P <0.05

Next, to determine if the increase mitochondrial mass in the HSCs was due to mitochondrial biogenesis, we examined the expression of the genes known to be involved with mitochondrial biogenesis fission and fusion. Figure 3.8 shows that mRNA expression of the biogenesis genes PCG1 β, NRF1, NRF2, TFAM, tfb1m and tfb1m were not upregulated in response to LPS at 2 hours. Expression of these genes did increase at 16 hours post LPS infection. PGC1α was upregulated in the HSC after 2 and 16 hours of LPS treatment, however, upregulation of PGC1α alone cannot establish the cell's ability to undertake mitochondrial biogenesis. Interestingly, expression of the fusion genes Opa1 and MFN1 were also upregulated at both 2 and 16 hours following LPS infection. MFN2 another gene regulating mitochondrial fusion was only upregulated at 16 hours post LPS treatment. The mitochondrial fission gene DNM1I was only upregulated at 16 hours following infection. This data suggests that the increase in mitochondrial mass in the HSC 2 hours post LPS infection is not associated with mitochondrial biogenesis. The 2-hour LPS time point was used in the following experiments to try to specifically detect changes in the HSC not caused by mitochondrial biogenesis.
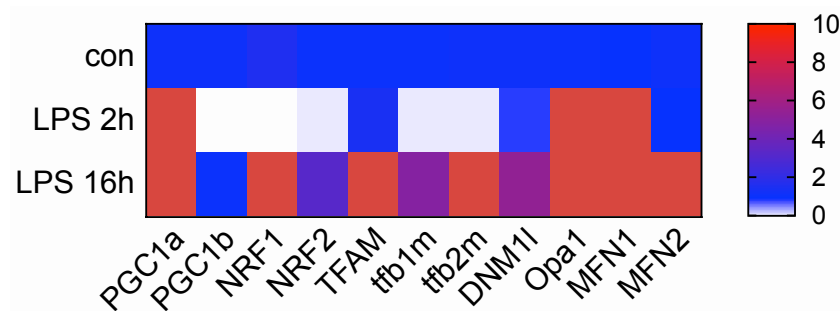
Figure 3.8. Mitochondrial biogenesis fission and fussion gene expression in response to LPS stimulation in the HSC.
C57BL/6J mice were treated with LPS for 2 or 16 hours, the animals were sacrificed, the bone marrow was extracted and stained with a panel of antibodies to isolate the HSC population by FACS. RNA was analysed for gene expression of mitochondrial biogenesis, fission and fusion genes by qPCR. n=5 in each group.

The xenobiotic efflux pumps in the HSC have high activity and this can lead to MTG dye extrusion (340). To ensure the mitochondrial mass increase was not affected by dye extrusion C56BL/6 mice were treated with LPS for 2 hours and the animals were sacrificed. The BM was extracted and stained with a panel of cell surface antibodies and combination of MTG with the addition of efflux inhibitor verapamil. Figure 3.9A and B show there is a significant increase in mitochondrial content in the LSK, HSC ST-HSC and LT-HSC populations, but not in the MPP population which is consistent with previous results. There were no differences observed between verapamil and non-verapamil treated cells. However, to ensure no dye leakage occurred after staining, verapamil was added to the panels when MTG was used in any future experiments.

A

B

+Verapamil
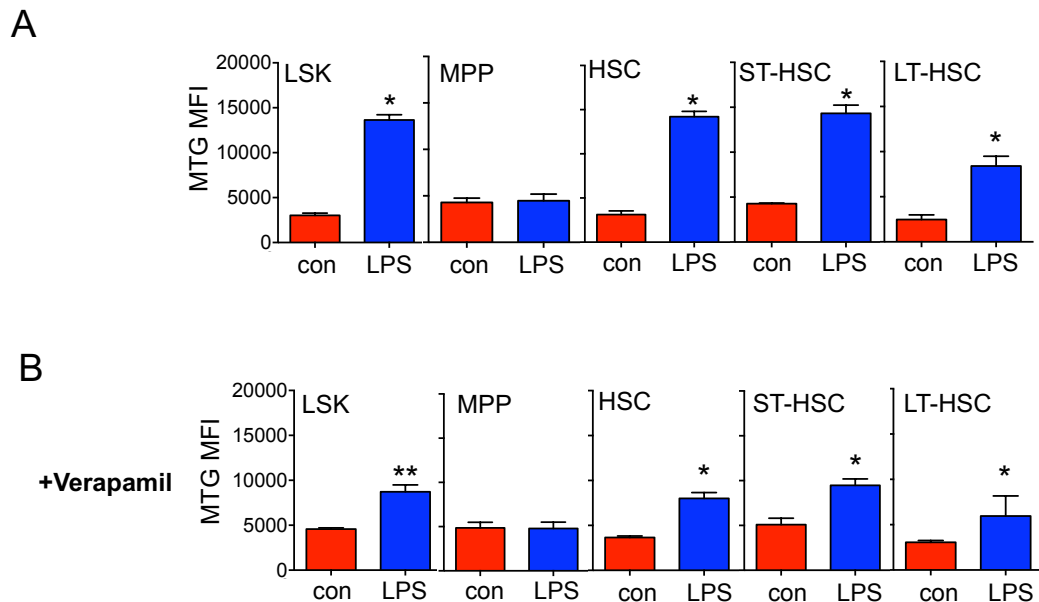
Figure 3.9. MTG fluorescence intensity does report mitochondrial mass. C57BL/6J mice were treated with LPS for 2 hours, the animals were sacrificed, the bone marrow was extracted and stained with a panel of antibodies and Mitotracker green (MTG) to analyse mitochondrial content in specific Lin-, LSK, HSC, MPP, ST-HSC and LT-HSC populations. (A) Mitochondrial content (mitotracker green (mean fluorescence intensity (MFI)) in the specific populations of all animals examined after 2 hours of LPS treatment. n=5. (B) The calcium channel inhibitor Verapamil was added to the cells prior to staining with MTG and antibodies. Mitochondrial in the specific populations after 2 hours of LPS treatment. n=5 in each group. Data shown are means ± SD *P < 0.05 **P < 0.01

Expansion of the haematopoietic cells is a hallmark of the immune response to acute infection. Figure 3.10A and B confirms a significant increase in cell number of LSK, HSC, MPP, ST-HSC and LT-HSC populations per 100 000 BM cells following both *S.typhimurium* and LPS treatment. There was no change in cell number observed in the Lin- population.
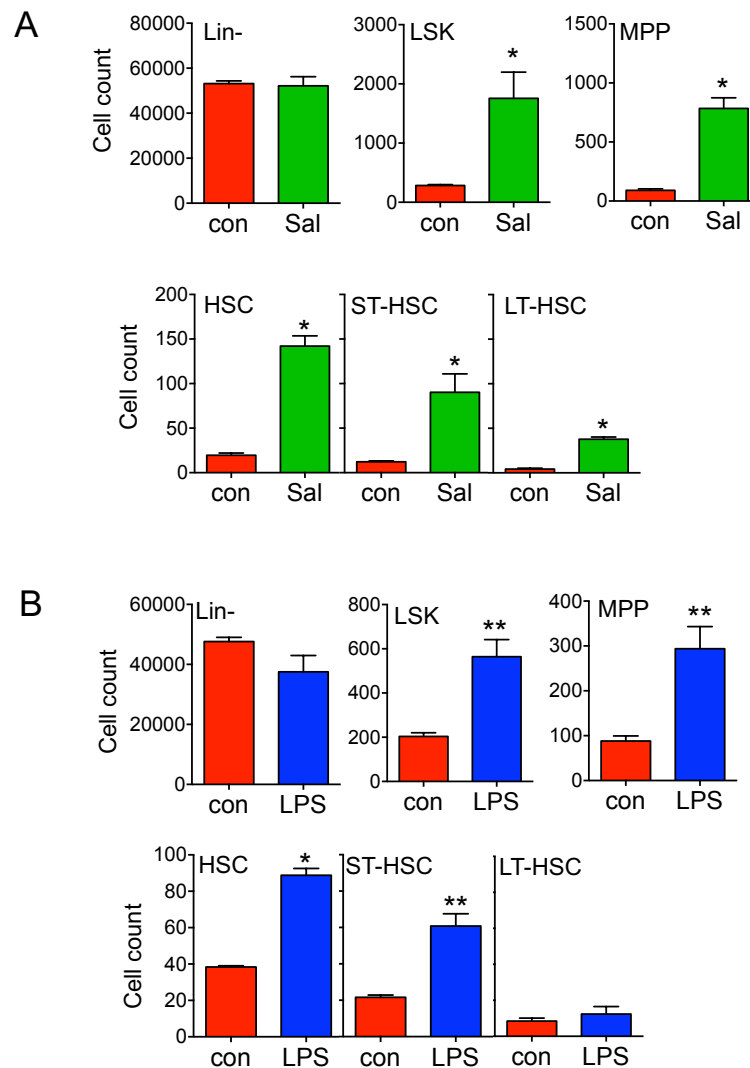
Figure 3.10. *S.typhimurium* or LPS increases HSC numbers per 100 000 BM cells counted.
(A) C57BL/6J mice were infected with *S.typhimurium* (Sal) for 72 hours, the animals were sacrificed, the bone marrow was extracted and stained with a panel of antibodies to analyse cell number in specific Lin-, LSK, HSC, MPP, ST-HSC and LT-HSC populations (B) C57BL/6J mice were treated with LPS for 2 hours, the animals were sacrificed, the bone marrow was extracted and stained with a panel of antibodies to analyse cell number in specific Lin-, LSK, HSC, MPP, ST-HSC and LT-HSC populations. n=5 in each group. Data shown are means ± SD *P < 0.05 **P < 0.01

Interestingly, there is no change in the number of progenitor cells per 100 000 BM cells (CMP, GMP and MEP) in the *S.typhimurium* or LPS treated animals compared to the control (Figure 3.11A and B). There is a trend towards a decrease in the number of GMPs after both *S.typhimurium* infection or LPS treatment compared to the control. This has previously been shown following infection (341, 342) and could be due to the 2-hour time point. As the GMPs produce granulocytes, the GMPs could be migrating to the spleen or peripheral blood to fight the infection. Taken together, following acute infection there is an increased number of the HSCs but no significant change in the downstream progenitor cells.
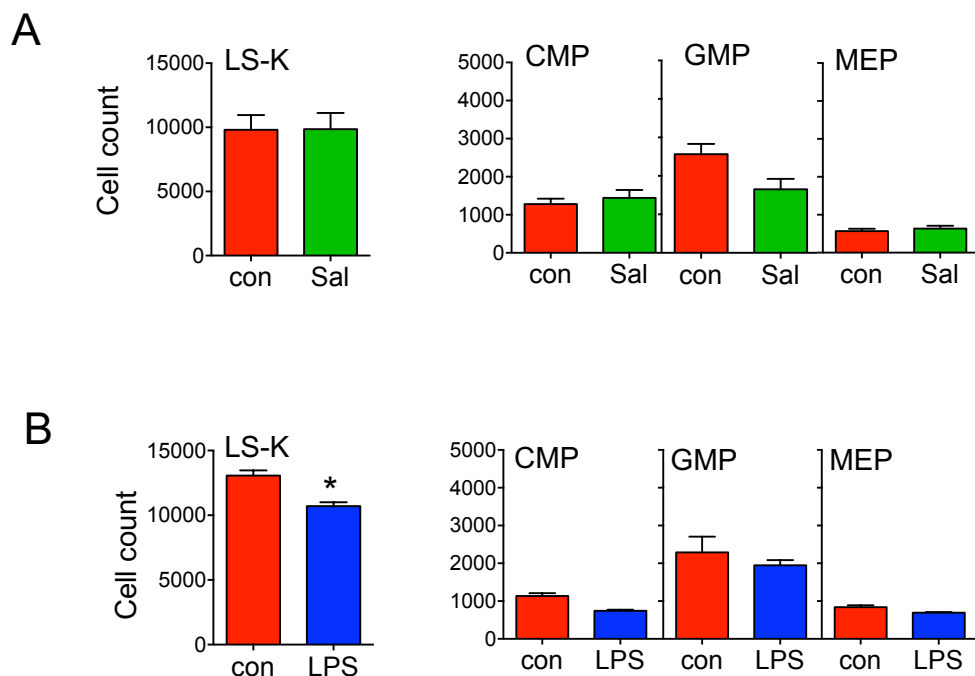
Figure 3.11. *S.typhimurium* or LPS does not increase progenitor population numbers.
(A) C57BL/6J mice were infected with *S.typhimurium* (Sal) for 72 hours, the animals were sacrificed, the bone marrow was extracted and stained with a panel of antibodies to analyse cell number in specific LS-K, CMP, GMP and MEP populations. (B) C57BL/6J mice were treated with LPS for 2 hours, the animals were sacrificed, the bone marrow was extracted and stained with a panel of antibodies to analyse cell number in specific LS-K, CMP, GMP and MEP populations. n=5 in each group. Data shown are means ± SD *P < 0.05

To determine if infection induced HSC cell cycling, C57BL/6J mice were treated with LPS for 16 hours. HSC cell cycle transit time is around 14 hours therefore the 16-hour time point was chosen as 2 hours post infection is too early for cell cycling to occur (343). The animals were then sacrificed, the BM extracted, and the cells were stained with the HSC panel of antibodies and Ki67. Ki67 is a protein in the cells which increases with cell division, therefore, the higher the levels of Ki67 the more quicky the cells are dividing. Ki67 staining can be used in combination with DAPI to identify the specific phase of the cell cycle the cells are in. Unfortunately, due to the lack of an ultraviolet or violet laser on the flow cytometers available I was unable to detect DAPI staining and therefore, used Ki67 alone to identify cycling cells. Following 16 hours of LPS treatment there was a significant increase in the percentage of cycling LSKs, HSC, ST-HSC and LT-HSCs (Figure 3.12A and B).

Figure 3.12. LPS induces increase in Ki67 positive cells in haematopoietic stem and progenitor populations.
C57BL/6J mice were treated with LPS for 16 hours, the animals were sacrificed, the bone marrow was extracted and stained with a panel of antibodies to analyse Ki67 positive cells in the LSK, HSC, ST-HSC and LT-HSC populations. n=5 in each group. Data shown are means ± SD *P < 0.05

To understand the colony forming ability of the haematopoietic compartment after LPS treatment, C57BL/6J mice were treated with control PBS or LPS for 2 hours. The animals were sacrificed, the BM was extracted, the cells were seeded in a semisolid Methocult for 7 days. There was a significant expansion of the granulocyte monocyte progenitor population (GM) in the BM cells from LPS treated animals compared to the control (Figure 3.13).
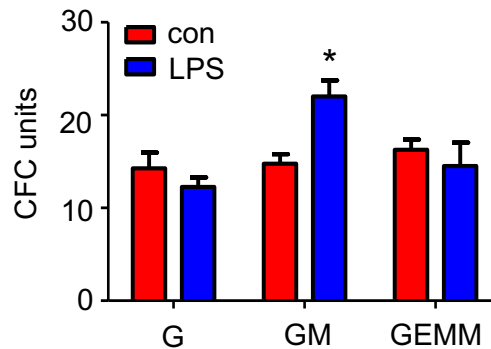
Figure 3.13. LPS increases CFCU in the granulocyte monocyte progenitor populations.
C57BL/6J mice were treated with control PBS or LPS for 2 hours, the animals were sacrificed, the bone marrow was extracted. 1×10^4 bone marrow cells were seeded in a semisolid Methocult for 7 days. Granulocytic progenitor (G), granulocyte monocyte progenitor (GM), and granulocyte monocyte megakaryocyte progenitor (GEMM) colonies were then counted. Data shown are means ± SD of n=5 *P < 0.05

3.3 Bacterial infection causes an increase in mitochondrial membrane potential and OCR

To determine the functional consequences of the increase in mitochondrial content after acute infection, C57BL/6J mice were first treated with control PBS or LPS for 2 hours. The animals were sacrificed, and the BM was extracted and analysed for mitochondrial membrane potential by flow cytometry. Figure 3.14 shows an increase in tetramethylrhodamine methyl ester (TMRM) staining as measured by mean flourecence intensity (MFI) in LPS treated LSK, HSCs and ST-HSCs. There was no change in mitochondrial potential observed in the LT-HSCs.
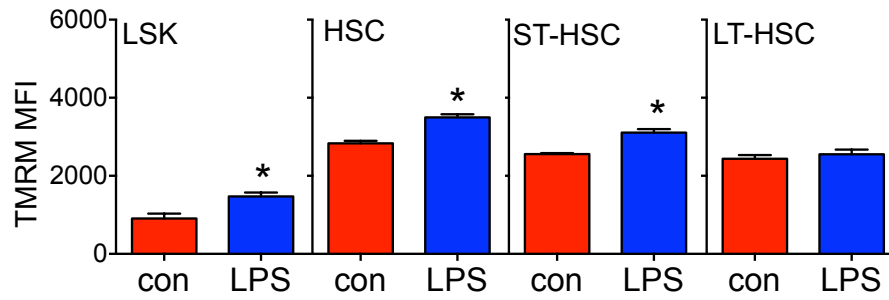
Figure 3.14. LPS treatment increases mitochondrial membrane potential in HSCs.
C57BL/6J mice were treated with LPS for 2 hours, the animals were sacrificed, the bone marrow was extracted and stained with a panel of antibodies and Tetramethylrhodamine, methyl ester (TMRM) to analyse mitochondrial potential in specific Lin-, LSK, HSC, ST-HSC and LT-HSC populations. n=5 in each group. Data shown are means ± SD *P < 0.05

Next, to better understand the metabolic changes in the HSC after bacterial infection I used the mitochondrial extracellular flux assay which measures oxygen consumption rate (OCR). I first sorted HSCs from the BM of control and LPS treated mice. Unfortunately, the proportion of HSCs in the BM is very low, and a high number of cells is needed for this assay. As a result it was not possible to sort sufficient cells from the BM and the time taken to sort greater numbers of cells affected cell viability. Therefore, there was no measurable level of OCR or extracellular acidification rate (ECAR) observed using sorted HSCs in this assay. Following optimisation this issue persisted and I therefore sorted the LSK population to represent the haematopoietic progenitor populations, as they are more abundant in the BM. LSKs isolated from *S. typhimurium* and LPS treated animals had an increased basal and maximal respiration compared to the control LSK cells (Figure 3.15A and B).
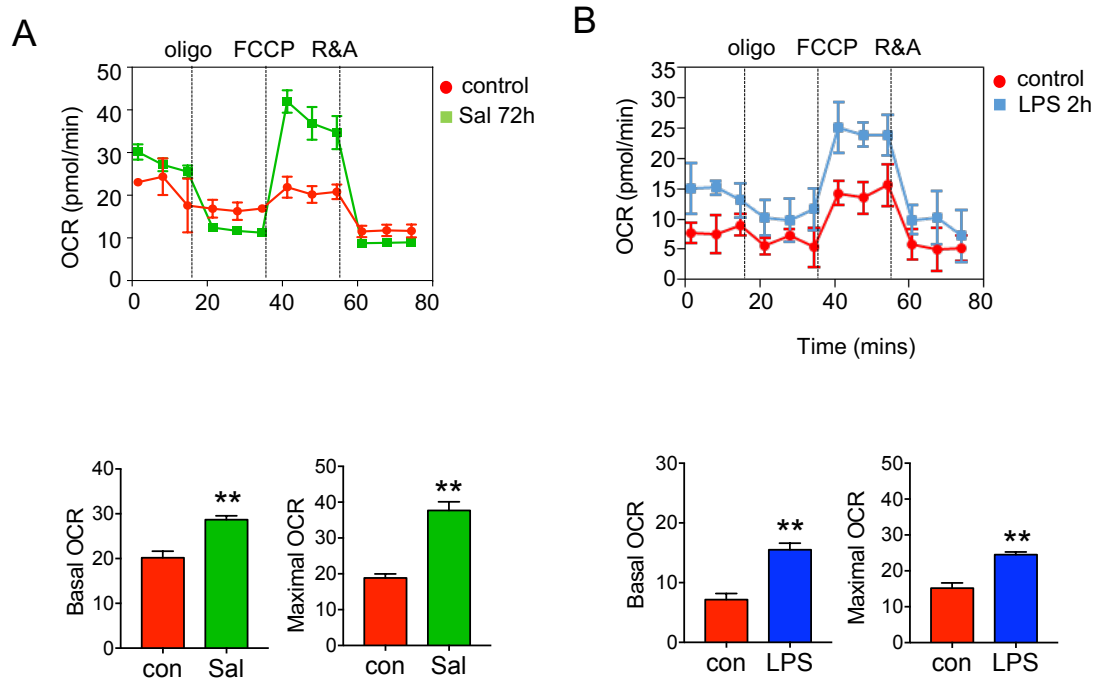
Figure 3.15. LSK have increased OCR after LPS and *S.typhimurium* infection.
(A) C57BL/6J mice were infected with *S.typhimurium* (Sal) for 72 hours, the animals were sacrificed, the bone marrow was extracted and stained with a panel of antibodies to isolate the LSK population by FACS. OCR was measured in the LSK n=5. (B) C57BL/6J mice were treated with PBS or LPS for 2 hours, the animals were sacrificed, the bone marrow was extracted and stained with a panel of antibodies to isolate the LSK population by FACS. OCR was measured in the LSK n=5. Data shown are means ± SD **P< 0.01

In addition to measuring OCR the mitochondrial extracellular flux assay also analyses ECAR as a measure of glycolysis. Glycolysis is not significantly upregulated in the LSKs from *S. typhimurium* and LPS treated animals (Figure 3.16).
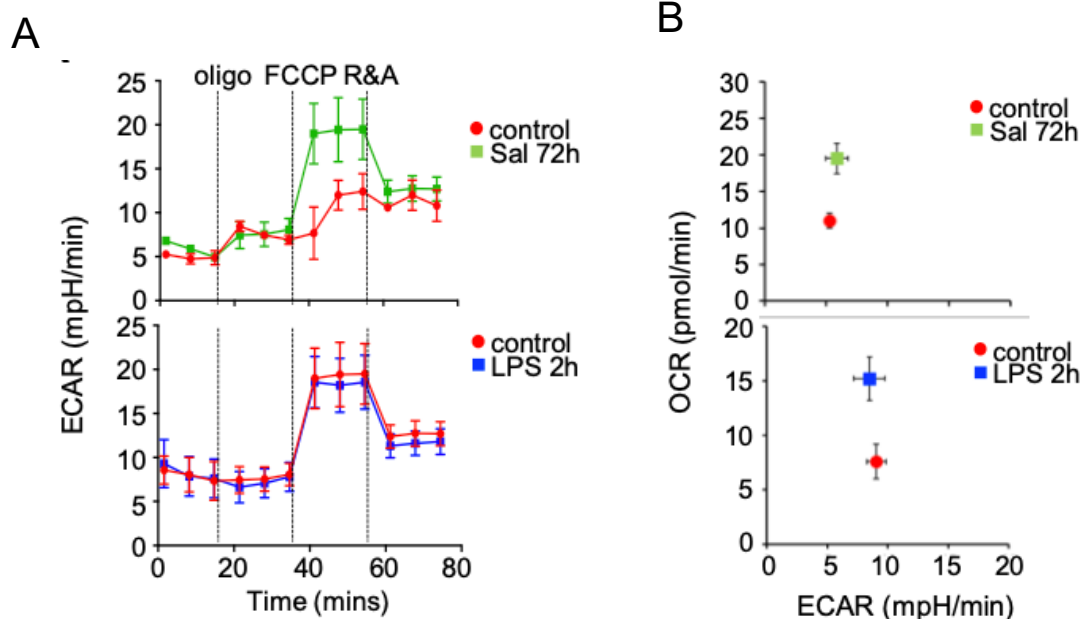
Figure 3.16. LSK have no change in ECAR after LPS and *S.typhimurium* infection.
(A) C57BL/6J mice were infected with *S. typhimurium* (Sal) for 72 hours or LPS for 2 hours, the animals were sacrificed, the bone marrow was extracted and stained with a panel of antibodies to isolate the LSK population by FACS. Glycolysis levels were measured by ECAR. (B) Basal OCR (normalised to rotenone) vs Basal ECAR of LSK after *S. typhimurium* and LPS treatment. n=5 in each group. Data shown are means ± SD

Taken together these data show infection with gram negative bacteria causes an increase in mitochondrial content and function in the HSC population. This increase in mitochondria, however, was not associated with a change in mitochondrial biogenesis in HSCs, with the exception of PGC1α. Moreover, the increased mitochondrial mass was associated with an increased OCR in the LSK population. This suggests that the cells require energy derived from increased mitochondria content for cellular proliferation and expansion to differentiate into the critically needed immune cells for host defence.

3.4   Development of a humanised mouse model to study mitochondrial transfer

To determine if the increase in mitochondrial content was a result of intercellular mitochondrial transfer to HSCs during infection, three models were developed to specifically track the movement of mitochondria *in vivo*. The first model utilised was a humanised nonobese diabetic (NOD) severe combined immunodeficiency (SCID) Il2rg knockout NOD.Cg.Prkd^{scid}IL2rg^{tm1Wji}/SzJ (NSG) mouse model (hu-NSG). In this model human umbilical cord blood CD34+ stem and progenitor cells were transplanted into 3-4-week-old NSG mice (huNSG). Once engrafted the hu-NSG were treated with 1 mg/kg LPS or PBS for 2 hours, the animals were sacrificed and the BM was extracted. The haematopoietic cell populations were analysed using flow cytometry and the human common myeloid progenitor (CMP), granulocyte macrophage progenitors (GMPs) multipotent progenitors (MPPs) and HSCs were isolated and analysed (Figure 3.17). The model utilises species-specific mitochondrial DNA (mtDNA) detection as a tracker for intercellular mitochondrial transfer based on a similar method used by Dong *et al.* (344).
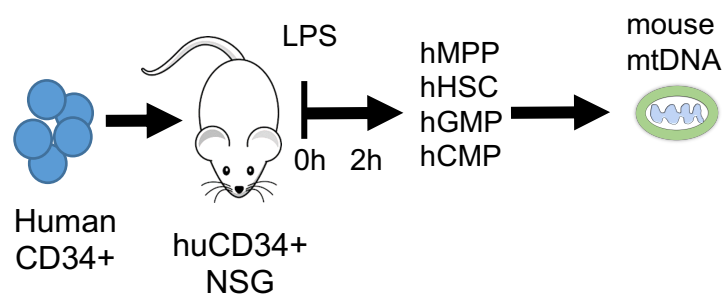
Figure 3.17. Schematic diagram of experimental design.
Recipient 3-4-week-old NSG mice were treated with 25 mg/kg busulfan for 3 days prior to tail-vein injections of human CD34+ donor cells. Post engraftment mice were treated with 1mg/kg LPS or vehicle PBS for 2 hours. BM was isolated and sorted for human CMP (mCD45−, hCD34+, hCD38+, hCD45RA-, hCD90−, hCD49f−), human GMP (mCD45−, hCD34+, hCD38+, hCD45RA+, hCD90−, hCD49f−), human MPP (mCD45−, hCD34+, hCD38−, hCD45RA−, hCD90−, hCD49f−), and human HSC (mCD45−, hCD34+, hCD38−, hCD45RA−, hCD90+, hCD49f+) using FACS. The sorted human cells were analysed for species-specific mtDNA using Taqman qPCR.

To assess the engraftment of the humanised mice peripheral blood was analysed monthly after transplantation to detect human CD45+ cells. Figure 3.18 confirms engraftment of human CD45+ cells in the huNSG mice. Around 3% engraftment was seen at 1-month post transplantation, the level of human CD45+ cells present in the peripheral blood increased to around 40% after 3 months post transplantation confirming humanisation.
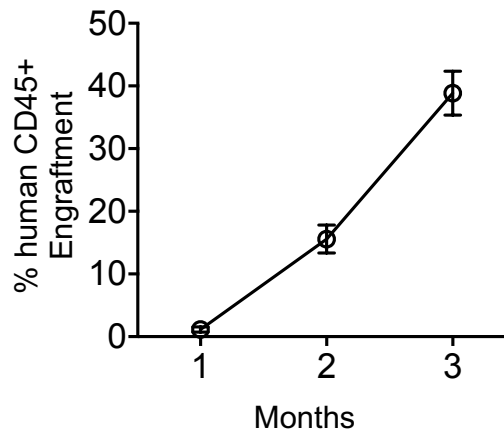
Figure 3.18. Human CD45+ cells are present in the peripheral blood of huNSG mice.
NSG mice were treated with 25 mg/kg busulfan for 3 days prior to tail-vein injections of human CD34+ cord blood donor cells. Engraftment was determined by CD45 expression in the peripheral blood detected by flow cytometry analysis. The peripheral blood was monitored monthly for 3 months, prior to experimentation. n=6

HuNSG mice produced were treated with either 1 mg/kg LPS or control PBS for 2 hours. A 2-hour time point was used in this assay to detect specific changes in mitochondrial content due to intercellular mitochondrial transfer rather than the cells own transcriptional mechanism to increase mitochondria. The mice were then sacrificed, the BM was extracted, and analysed for the presence of human CD45 using flow cytometry. Figure 3.19 confirms equal engraftment of human CD34+ HSCs in recipient NSG mice within both treatment groups.
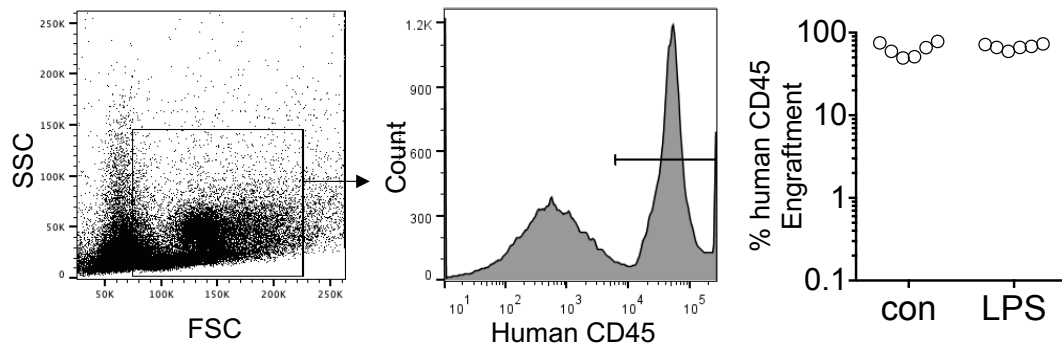
Figure 3.19. Human CD45+ engraftment is seen in the bone marrow of huNSG mouse model.
NSG mice were treated with 25 mg/kg busulfan for 3 days prior to tail-vein injections of human CD34+ cord blood donor cells. The mice were subjected to 1 mg/kg LPS or PBS intraperitoneal injections. After 2 hours the mice were sacrificed, and the bone marrow was extracted. Engraftment was determined by CD45 expression in the bone marrow detected by flow cytometry analysis. n=6 in each group.

In addition to engraftment the BM was also stained with a panel of antibodies to detect the human CMP (mCD45−, hCD34+, hCD38+, hCD45RA-, hCD90−, hCD49f−), human GMP (mCD45−, hCD34+, hCD38+, hCD45RA+, hCD90−, hCD49f−), human MPP (mCD45−, hCD34+, hCD38−, hCD45RA−, hCD90−, hCD49f−), and human HSC (mCD45−, hCD34+, hCD38−, hCD45RA−, hCD90+, hCD49f+) populations. This was carried out using 7 colour flow cytometry for the detection of six cell surface antibodies and a mitochondrial dye MTG. This included all colour compensations and the gating strategy to isolate the specific cell populations of interest is shown in Figure 3.20. All gating was determined using fluorescence minus one controls.
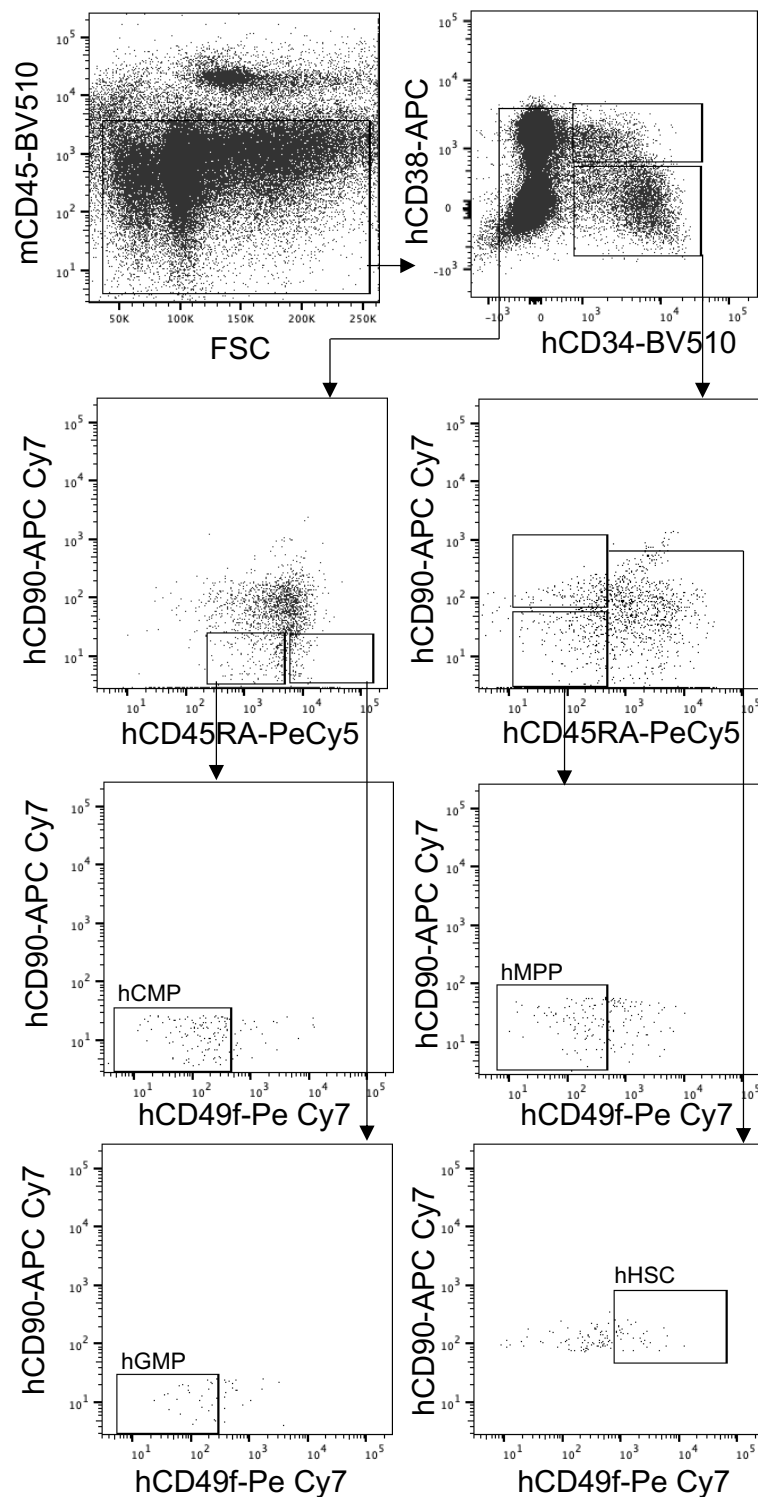
Figure 3.20. Gating strategy for human CMP, GMP, MPP, and HSC cell populations in huNSG mice.
After 2 hours of 1 mg/kg LPS or PBS the huNSG mice were sacrificed, and the bone marrow was extracted and stained with a panel of antibodies to analyse specific HSC, MPP, CMP and GMP populations. The gating strategy used is shown.

To determine whether the LPS had an effect on mitochondrial content, the hu-NSG BM was stained with MTG and the antibody panel. There was a significant increase in mitochondrial content within the human HSC and MPP populations after LPS treatment. There were no observed mitochondrial changes in the human CMP or GMP populations (Figure 3.21)
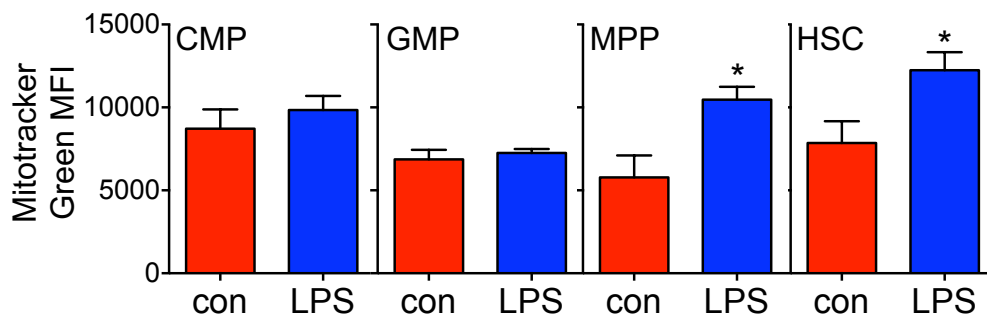
Figure 3.21. Mitochondria content is increased in the human HSC and MPP from huNSG mice after LPS treatment.
HuNSG were subjected to 1 mg/kg LPS or PBS intraperitoneal injections. After 2 hours the mice were sacrificed and the bone marrow was extracted, cells were stained with a panel of antibodies to analyse specific HSC, MPP, CMP and GMP populations. Mitochondrial levels (mitotracker green (mean fluorescence intensity (MFI)) in specific populations of all animals examined. n=6 in each group *P < 0.05

Finally, to determine if this observed increase in mitochondrial content was due to intercellular mitochondrial transfer from the mouse BM microenvironment, species specific mitochondrial analysis was performed. After LPS treatment the BM was extracted and the human CMP, human GMP, human MPP and human HSC population were sorted by FACS using the gating strategy shown in Figure 3.20. The DNA was extracted and duplex Taqman qPCR analysis was carried out using species specific probes targeting mitochondrial gene ND1. The Ct values were normalised to human genomic DNA (Tert). Figure 3.22 shows that in the LPS-treated huNSG mice, mouse mtDNA is significantly increased in the human MPPs and HSCs but not in human GMPs or CMPs. These data show mtDNA is transferred from the BM microenvironment to the HSCs after LPS treatment in a humanised mouse model.
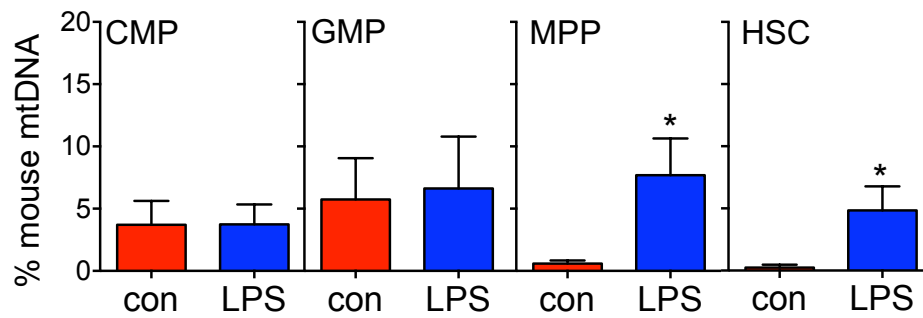
Figure 3.22. Mitochondrial DNA is transferred from the BM microenvironment to the HSC and MPP populations in the huNSG mice in response to LPS treatment.
Human CMP, GMP, MPP and HSC populations were sorted from the BM of huNSG treated with either LPS or PBS. The DNA was isolated and analysed using species specific Taqman probes targeting ND1 and Tert by qPCR. Mouse or human mitochondrial DNA was measured by ΔΔCt and normalised to human tert. Data shows the percentage of mouse mitochondria detected in the isolated human cells. Data shown are means ± SD of n = 5 mice in each group. *P < 0.05.

3.5 Development of a strain specific model to study mitochondrial transfer

As a second model to confirm transfer of mtDNA, I used a transplant model whereby NSG, CD45.1 recipient animals were transplanted with C57BL/6J CD45.2 donor lineage-negative cells. The model developed was using the difference in CD45 antigen which is known to be commonly expressed on all haematopoietic cells. The CD45 antigen is made up of 2 differing allelic variants CD45.1 or CD45.2 (345). The CD45.1 allele antigen is expressed on NSG mice and CD45.2 is expressed on C57Bl/6J mice. The functionality of both these alleles are identical and have previously been recognised as a marker identifying haematopoietic cells after BM transplants in mice (346). Next, I needed to establish a method to detect the mtDNA changes between these two mice after transplantation. Yu *et al*. 2009 reported that there was a single nucleotide polymorphism (SNP) in the COX3 region of the mtDNA whereby in BalbC mice had adenine (A) in the 9348 nucleotide position, this was displaced by guanine (G) in the C57Bl/6J mice (347), a potential probability for a SNP change in the ND4 region of mtDNA between BalbC and C57Bl/6J was also observed. They also found a SNP in the ND3 region of the

mtDNA, BalbC mice had a cytosine (C) in the 9461-nucleotide position, which was displaced by thymine (T) in the C57Bl/6J mice (Table 3.1). I therefore, designed primers to amplify and sequence the COX3 and ND3 region and ND4 transcripts from NSG and C57BL/6J DNA (Figure 3.23A and B).

Table 3.1. SNP differences in mtDNA between NSG mice and C57Bl/6 mice.
(347).

Nucleotide position	Protein	Nucleic acid change	Balb/c	C57BL/6
9348	mt-COX3	G/A	A	G
10623	mt-ND4	T/T	T	T
9461	mt-ND3	C/T	C	T
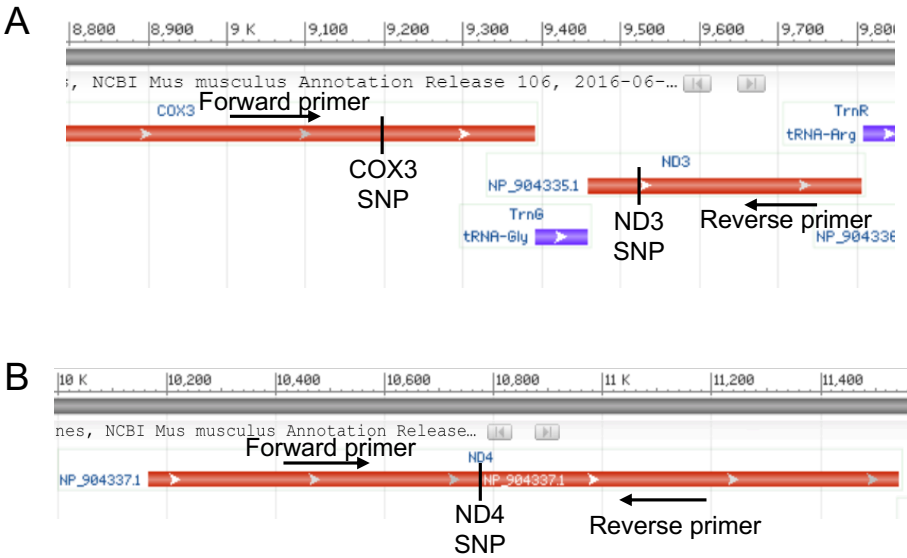
Figure 3.23. Genomic regions and primer targets for mitochondrial DNA.
(A) Genomic region for mitochondrial NADH dehydrogenase 3 (mt-ND3) and mitochondrial cytochrome c oxidase 3 (mt-COX3) with primer targets (B) Genomic region for mitochondrial NADH dehydrogenase 3 (mt-ND4) with primer targets.

To determine the efficiency of the primers, NSG or C57BL/6J mice were sacrificed, and the BM was extracted. The DNA was isolated and qPCR with the specific primers targeted to COX3, ND3 and ND4 mtDNA was carried out. The PCR products were then visualised by using agarose gel electrophoresis. Figure 3.24 show that PCR amplicon was detected in both NSG and C57BL/6J mice using both COX3/ND3 and the ND4 primer.
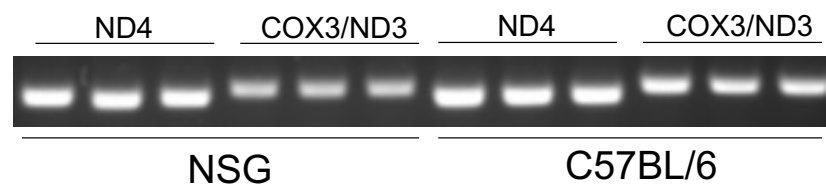
Figure 3.24. ND3, COX3 and ND4 PCR amplicons.
DNA from NSG and C57BL6/J bone marrow cells was isolated and quantified. After isolation, DNA was analysed using qPCR with ND4 primers or COX3 and ND3 primers. PCR products were detected by agarose gel electrophoresis and is presented in this figure. n=3.

Protein	Nucleic acid change	NSG	C57BL/6
mt-COX3	G/A	A	G
mt-ND3	C/T	C	T
mt-ND4	T/T	T	T

Figure 3.25. Sanger sequencing analysis to confirm SNP in mtDNA between C57 and NSG.
PCR bands were excised, and DNA purified using GenElute Mammalian Genomic DNA Miniprep Kit. Isolated DNA was then sent to Source Bioscience alongside the primers for sequencing. Sequencing traces were analysed using Sequence Scanner Software.

A TaqMan SNP genotyping assay was then designed to detect this difference in ND3 and COX3 mtDNA between NSG mice and C57BL/6J mice. TaqMan SNP PCR analysis of NSG DNA and C57BL/6J DNA with ND3 SNP Taqman probes show positive fluorescence on FAM for NSG cells but negative for C57BL/6J cells (Figure 3.26) confirming the effectiveness of the probe. Whereas, the COX3 show positive fluorescence on VIC for C57BL/6J cells but negative for NSG cells (Figure 3.26). This confirms that the COX3 SNP probe is effective at targeting the 'A' in the COX3 mtDNA from NSG mice but does not bind to the 'G' in the COX3 mtDNA region in the C57BL/6J mice.
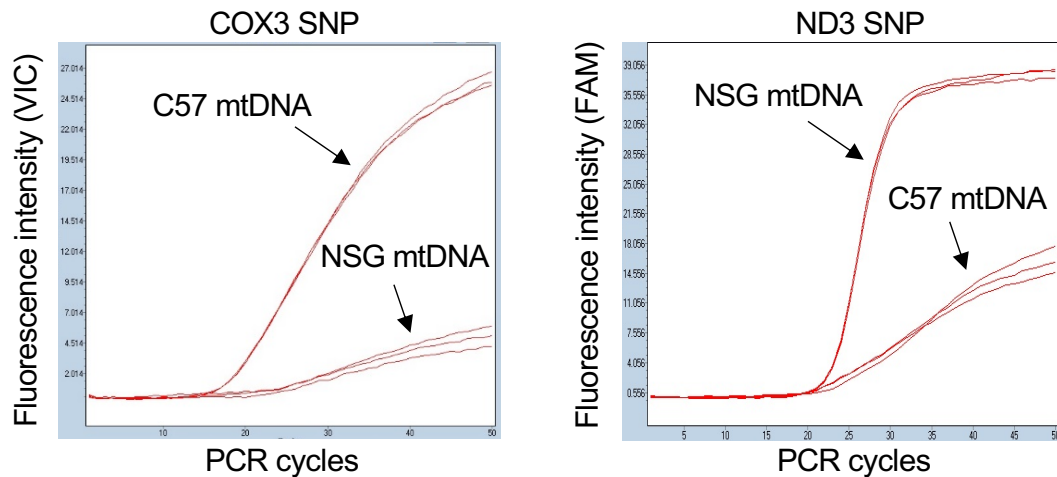
Figure 3.26. TaqMan RT-qPCR analysis of NSG and C57BL/6 DNA.
PCR using COX3 primer show positive fluorescence on VIC for C57Bl/6 DNA but negative for NSG DNA. Analysis with ND3 primer on FAM show positive fluorescence for NSG DNA but negative for C57BL/6 DNA.

Subsequently, I transplanted isolated BM cells from C57BL/6J mice expressing the CD45.2 allele into non-irradiated bulsulfan treated NSG mice expressing the CD45.1 allele. Due to the fact that the donor C57BL/6J and the recipient NSG mice differ in their CD45 allele, the cells origin and the mitochondria within these cells can be characterised by cell surface staining for specific CD45.1 or CD45.2 markers which can be analysed by flow cytometry. C57BL/6J expressing CD45.2 mice were sacrificed, the BM extracted, and lineage depleted. The cells were then intravenously injected through the tail vein into recipient NSG CD45.1 mouse. Once the C57BL/6J engraftment into NSG was confirmed the animals were treated with LPS for 2 hours. The BM was extracted and the C57BL/6J HSC and LSK populations were isolated and assessed for the presence of the NSG SNPs in the mtDNA (Figure 3.27).
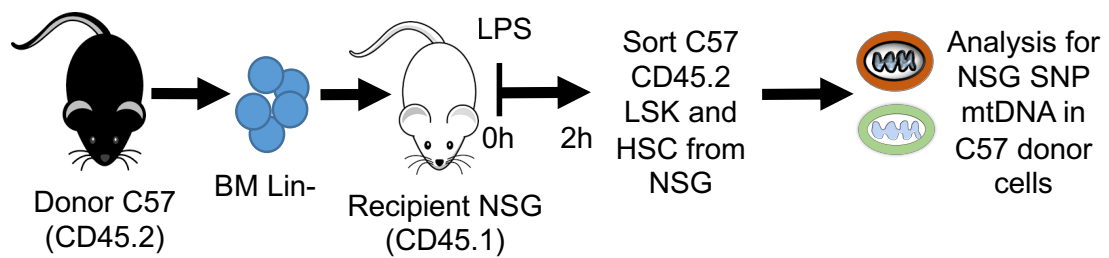
Figure 3.27. Schematic diagram of experimental design.
Recipient CD45.1 NSG mice were treated with 25 mg/kg busulfan for 3 days prior to tail-vein injections of lineage-negative CD54.2 C57BL/6J donor cells. Post engraftment mice were treated with 1 mg/kg LPS or vehicle PBS for 2 hours. BM was isolated and sorted for donor LSK (Lin-, Sca 1+, CD117+) and donor HSC (Lin-, Sca 1+, CD117+, CD48−, CD150+) cell populations expressing CD45.2 using FACS. The sorted donor cells were analysed for specific donor or host mtDNA by TaqMan PCR using ND3 or COX3 probes designed to detect strain-specific SNPs in the mitochondrial genome.

To determine engraftment, 12 weeks after transplantation recipient NSG mice were sacrificed and the BM was extracted and stained with CD45.1 PE and CD45.2 FITC conjugated antibody for flow cytometry analysis. The 12-week time point was chosen as at 12 weeks it has been shown there is stable engraftment and haematopoietic reconstitution (348). Figure 3.28 shows CD45.2 positive cells present in the NSG BM. This confirms engraftment of the C57BL/6J BM into the NSG mice. These transplanted mice were termed NSG[C57].
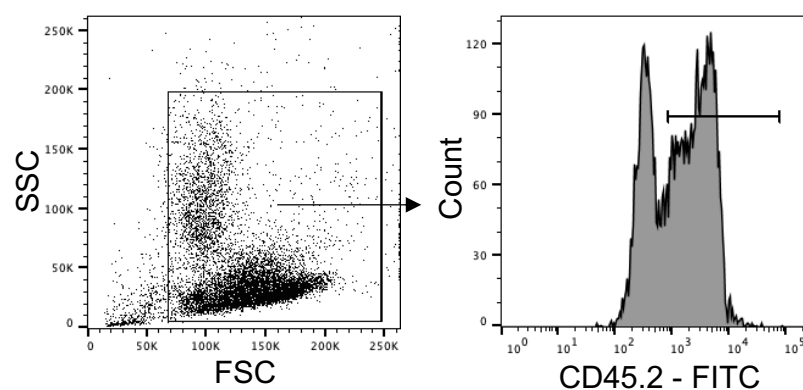
Figure 3.28. Engraftment data for NSG[C57] mouse model.
C57Bl/6J lineage negative cells were transplanted into NSG mice. The mice were subjected to 1 mg/kg LPS or PBS intraperitoneal injections. After 2 hours the mice were sacrificed, and the bone marrow was extracted, and cells were stained with CD45.2-FITC and analysed using flow cytometry to assess bone marrow engraftment.

Next, NSG[C57] mice generated were treated with either 1 mg/kg LPS or control PBS for 2 hours. The mice were then sacrificed, the BM was extracted, and stained with CD45.2 FITC lineage cocktail-pacific blue, Sca 1-APC, CD117-PeCy7, CD48-APC Cy7 and CD150-BV510 to monitor engraftment in the lineage positive (lin+), lineage negative (lin-), LSK and HSC populations. Figure 3.29 confirms equal engraftment of CD45.2 cells in recipient NSG mice within both treatment groups.
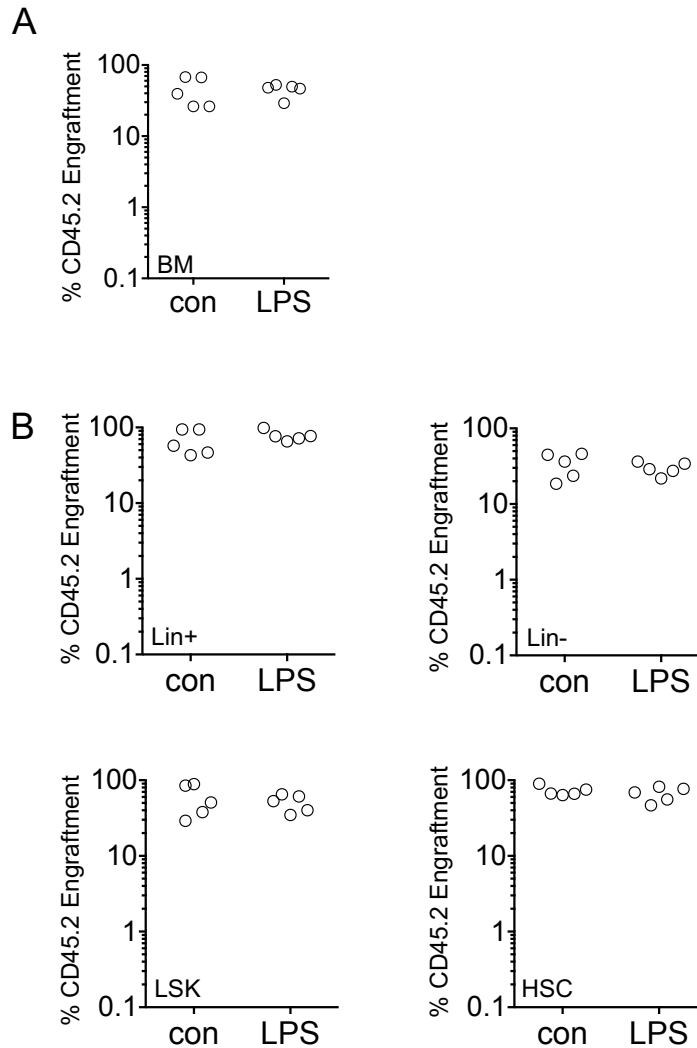
Figure 3.29. Engraftment data for NSG[C57] mouse model.
(A) C57Bl/6J lineage negative cells were transplanted into NSG mice. The mice were subjected to 1 mg/kg LPS or PBS intraperitoneal injections. After 2 hours the mice were sacrificed, the bone marrow was extracted and cells were stained with CD45.2 FITC and analysed using flow cytometry to assess bone marrow engraftment. (B) The cells were also stained with lineage cocktail-BV421, Sca 1-APC, CD117-PeCy7, CD48-APC Cy7 and CD150-BV510 to monitor engraftment in the lineage positive (lin+), lineage negative (lin-), LSK and HSC populations.

In addition to engraftment the BM was also stained with a panel of antibodies to assess intercellular mitochondrial transfer from the mouse BM microenvironment by strain specific mitochondrial analysis was performed. After LPS treatment the BM was extracted and the CD45.2 C57BL/6J HSC and LSK cell populations were sorted by FACS using the gating strategy shown in Figure 3.30.
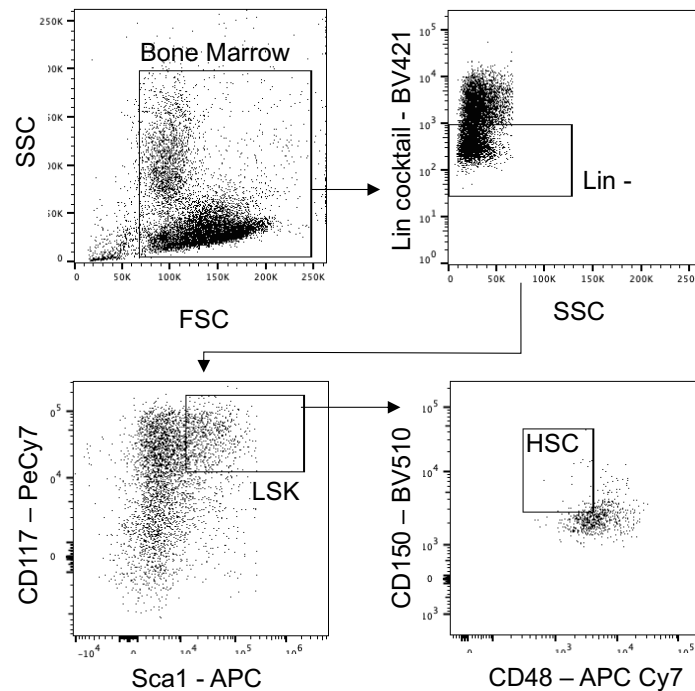
Figure 3.30. Gating strategy for the sorted LSK and HSC cell populations.
NSG[C57] mice were subjected to 1 mg/kg LPS or PBS intraperitoneal injections. After 2 hours the mice were sacrificed and the bone marrow extracted. Cells were stained with lineage cocktail-BV421, Sca 1-APC, CD117-PeCy7, CD48-APC Cy7 and CD150-BV510 to isolate the sort the LSK population and HSC populations

After the cells were sorted the DNA was extracted and analysed by qPCR using the COX3 SNP Taqman probe to detect the NSG SNP in the C57Bl/6J HSC and LSK CD45.2 C57BL/6J cell population. CD45.2 C57BL/6J donor cells from untreated mice had detectable mtDNA from CD45.1 NSG recipient-derived mitochondria, with a significant increase in CD45.1 NSG mtDNA in the CD45.2 C57BL/6J HSC and LSK populations upon LPS treatment (Figure 3.31). This suggests that mitochondria are being transferred from the host microenvironment into the donor cells under normal conditions, but when stimulated with LPS this transfer is significantly increased. The Ct values were

normalised to CD45.2 C57BL/6J genomic DNA and was used to determine a percentage of mtDNA transferred from CD45.1 NSG to CD45.2 C57BL/6J cells.
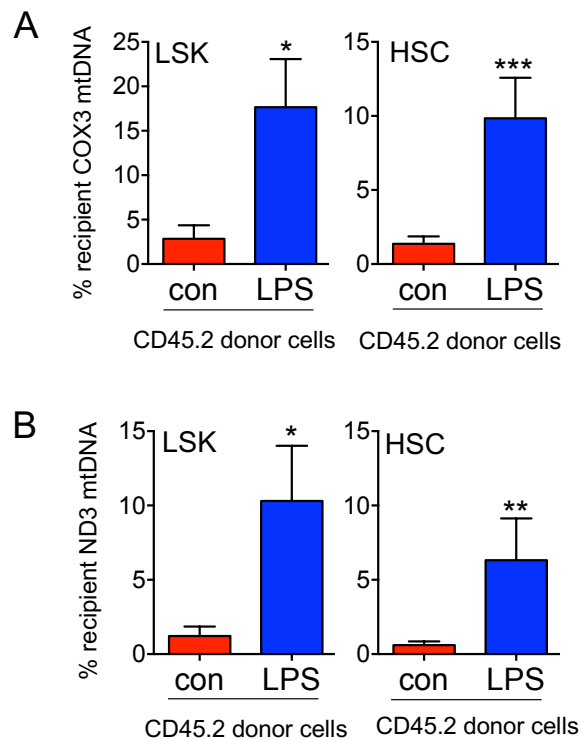
Figure 3.31. Mitochondria are transferred from the BM microenvironment to the HSC populations *in vivo* in response to LPS.
NSG[C57] mice were subjected to 1 mg/kg LPS or PBS intraperitoneal injections. After 2 hours the mice were sacrificed, and the bone marrow extracted. The LSK and HSC CD45.2 population was sorted by FACS and analysed for SNP differences by qPCR (A) The percentage of recipient mtDNA in isolated donor cells after a 2-hour treatment with 1 mg/kg LPS compared to control (untreated) cells using the COX3 TaqMan probe. (B) The percentage of recipient mtDNA in isolated donor cells after a 2-hour treatment with LPS versus control (untreated) cells using the ND3 TaqMan probe. Donor genomic DNA was used to standardise mtDNA copy number. Data shown are means ± SD of n=5 mice in each group. *P < 0.05 **P < 0.01 ***P < 0.001.

These data support the hypothesis that mitochondria are transferred from the BM microenvironment to the progenitor cells, a process shown to occur normally but significantly amplified in moments of stress, such as stimulation with LPS. This process occurs when an increased immune response is needed, and the HSCs require more energy for differentiation into immune cells.

3.6 Characterisation of the C57BL/6N$^{su9\text{-}DsRed2}$ model to study mitochondrial transfer

To further show that transfer from the BM microenvironment to the HSCs occurs within the BM in response to LPS, the C57BL/6N$^{su9\text{-}DsRed2}$ (DsRed) mouse model was the third model used (344). First, to establish detection of DsRed labelled mitochondria in living cells, I ear notched the animals for phenotype analysis. Fluorescent microscopy imaging highlighted the presence of DsRed within the cell populations of some animals (Figure 3.32). The animals positive for DsRed flourecence were used in the following experiments and the negative phenotype animals were used as a control.
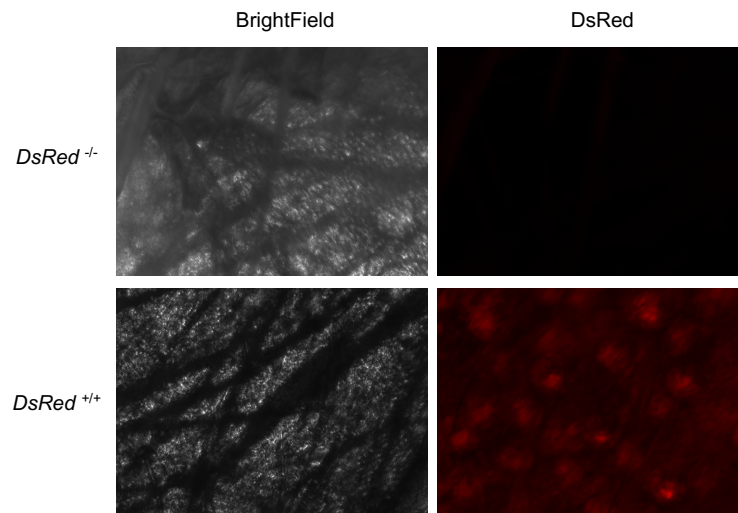
Figure 3.32. Phenotype analysis of DsRed animals.
DsRed mice were notched for phenotyping and identification of DsRed expression in the mitochondria of the mice. Representative fluorescent microscopy images of DsRed$^{-/-}$ and DsRed $^{+/+}$ to detect DsRed mitochondria (Red).

The DsRed model was used to characterise which cell populations have the DsRed mitochondria and to demonstrate where in the microenvironment the acquired mitochondria originated. The cell populations I chose to characterise was the lineage negative, stromal and macrophage cell populations as previous studies have shown these cells have been key in mitochondrial transfer within the BM microenvironment (41, 302, 324, 349).

DsRed mice, with both positive (DsRed $^{+/+}$) and negative (DsRed $^{-/-}$) phenotype, were sacrificed and the BM extracted. The first population I characterised was the lineage negative cells (Figure 3.33). Cells were stained with lineage cocktail pacific blue and analysed for DsRed fluorescence (Ex 561nM) by flow cytometry. Results showed that there was no difference in the DsRed fluorescence level between the DsRed$^{-/-}$ and DsRed $^{+/+}$ mice in the lineage negative cell population (Figure 3.33).
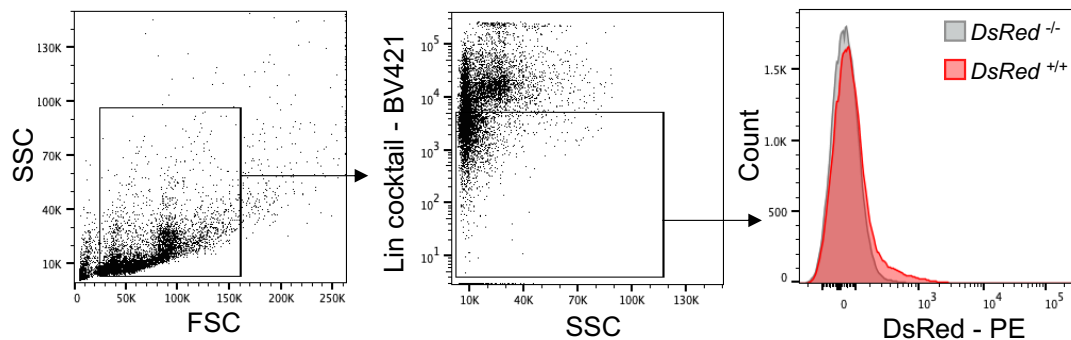
Figure 3.33. Characterisation of the DsRed in the lineage negative cell population.
DsRed$^{-/-}$ and DsRed $^{+/+}$ mice were sacrificed and the bone marrow extracted. Cells were stained with lineage cocktail-pacific blue. Data shows the level of mitochondrial DsRed fluorescence (Ex 561nM) in the lineage negative cell population.

The next population that was characterised was the stromal cell population. DsRed$^{-/-}$ and DsRed$^{+/+}$ mice were sacrificed the BM was extracted. The cells were stained with CD45-BV510, CD105-APC, CD140a-APC Cy7 and CD31-PeCy5 and analysed by flow cytometry (Figure 3.34). However, again it was unclear if there was DsRed mitochondria in the stromal cell population as both the DsRed$^{-/-}$ and DsRed $^{+/+}$ mice showed similar DsRed florescence (Figure 3.34).
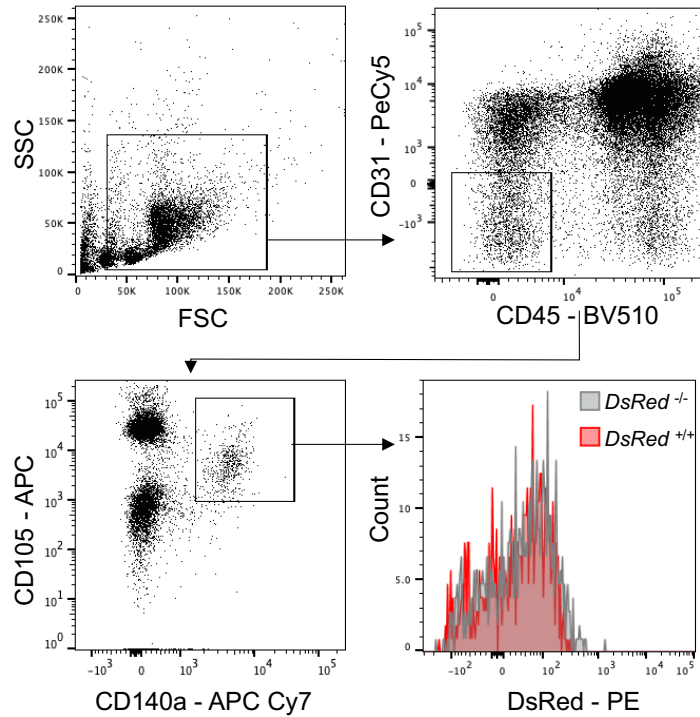
Figure 3.34. Characterisation of the DsRed in the stromal cell population.
DsRed$^{-/-}$ and DsRed $^{+/+}$ mice were sacrificed and the bone marrow extracted. Cells were stained with CD45-BV510, CD105-APC, CD140a-APC Cy7 and CD31-PeCy5 for analysis by flow cytometry. DsRed expression (Ex 561nM) in the stomal cell population CD45-, CD31-, CD105+ and CD140a+.

Finally, the last population I characterised was the macrophage cell population. Cells were stained with the macrophage markers GR1+, CD115 and F4/80+ as established previously (77) (Figure 3.35). The DsRed fluorescence level between the DsRed$^{-/-}$ and DsRed$^{+/+}$ again remained relatively unchanged in the macrophage population (Figure 3.35). Thus, it remained unclear which cells contained the DsRed phenotype.
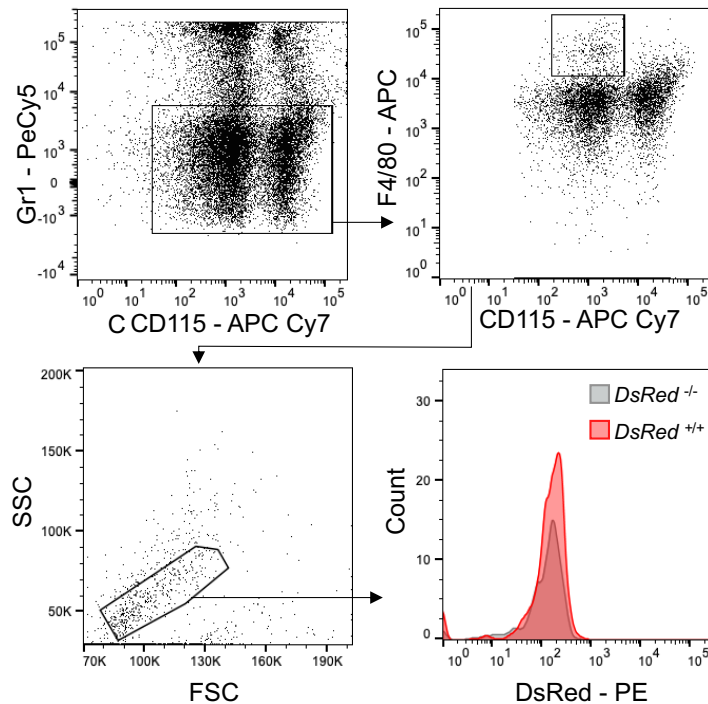
Figure 3.35. Characterisation of the DsRed in the macrophage cell population.
DsRed$^{-/-}$ and DsRed$^{+/+}$ mice were sacrificed and the bone marrow extracted. Cells were stained with with GR1-PeCy5, CD115-APC Cy7 and F4/80-APC for analysis by flow cytometry. DsRed expression (Ex 561nM) in the macrophage cell population GR1-, CD115^{int} and F4/80+.

Next, as the lineage negative cells showed no DsRed flourecence I performed an assay using the DsRed mice to determine if HSPC acquire DsRed fluorescence in response to LPS. DsRed$^{-/-}$ and DsRed$^{+/+}$ mice were treated with 1 mg/kg LPS or control PBS intraperitoneal injections. After 2 hours the mice were sacrificed, and the BM extracted. BM cells were stained with a lineage cocktail - pacific blue, Sca 1-APC, CD117-PeCy7, CD48-APC Cy7 and CD150-BV510. This enabled the detection the DsRed mean fluorescence intensity in the lineage negative, LSK, MPP and HSC populations by flow cytometry analysis (Figure 3.36 A). DsRed fluorescence in the specific cell populations which do not show fluorescence in the control mice, indicates transfer of DsRed mitochondria into the cells.

Figure 3.36A shows that lineage negative, LSK, MPP and HSC populations within the BM of the DsRed mice do not have an increase in mitochondrial content (as measured by DsRed mean fluorescence intensity) after treatment with LPS. The number of cells increased in the LPS treated DsRed mice in the lineage negative, LSK and HSC cell populations however the number of MPPs decreased in response to LPS (Figure 3.36B).
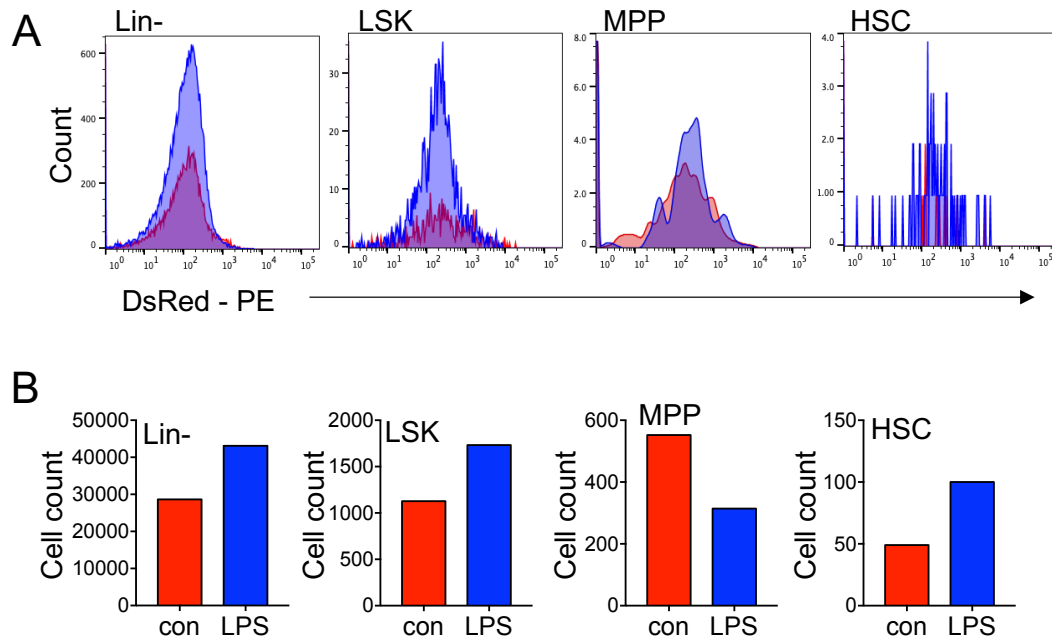
Figure 3.36. No DsRED was detected in HSPC population *in vivo* in response to LPS.
DsRed$^{+/+}$ mice were subjected to 1 mg/kg LPS or PBS intraperitoneal injections. After 2 hours the mice were sacrificed and the bone marrow was extracted, cells were stained with lineage cocktail-pacific blue, Sca 1-APC, CD117-FITC, CD48-APC Cy7 and CD150-BV510 and analysed using flow cytometry. (A) Representative histogram plots of the defined populations presenting DsRed fluorescence (Ex561nM) and cell counts. (B) Cell counts of specific populations after LPS treatment. (n=1)

There was no observed increase in DsRed fluorescence in all cell populations after LPS treatment. Moreover, it is unclear which specific cell populations within the BM contain the DsRed tag. Therefore, this model was not taken forward and I need to conduct this transfer assay in another model to identify which cell of the BM the mitochondria are acquired from in response to infection.

3.7 Summary

Taken together, in this chapter I have investigated intercellular mitochondrial transfer in a non-malignant haematological system. I have shown that mitochondrial content is increased in response to infection. This leads to a metabolic shift from baseline quiescent glycolytic HSCs towards utilisation of OXPHOS to generate ATP which is subsequently followed by HSC expansion into the immune cells. Importantly I have discovered that mitochondrial transfer occurs before the transcriptional changes needed for mitochondrial biogenesis to occur in a system which has evolved in mammals to support the required rapid granulocytic response to acute bacterial infection. Moreover, using two different models I have shown using LPS to simulate bacterial infection that mitochondrial transfer occurs from the BM microenvironment to the HSC. This transfer is specific to the early stem and progenitor populations MPP, LSK and HSCs, there was no transfer observed to the more differentiated CMP or GMP population. These data show mitochondrial transfer to the HSC is a fundamental process which underlies the mammalian response to infection, which has been hijacked by the malignant cells for a survival advantage.

4 Macrophage derived NOX2 ROS mediated PI3K activation drives mitochondrial transfer from the BMSC to the HSC

4.1 Introduction

In the previous chapter I have shown that mitochondrial DNA moves from the BM microenvironment to the HSC during infection and this transfer results in increased mitochondrial mass and increased levels of OXPHOS.

In response to stress, such as infection, it is known quiescent HSCs rapidly shift towards OXPHOS with an increase ATP production (350). This increased ATP allows for rapid cycling of the HSCs to differentiate into the more mature progenitor cells required to fight the infection (351). The metabolic changes in the cells from quiescent to cycling is key in regulating HSC fate (59, 290, 291). Differentiation of the HSC is promoted by increased levels of ROS in response to the infection while low ROS levels maintain HSC quiescence (289). This suggests that the rapid burst of energy required for HSC differentiation is reliant on both oxidative stress and OXPHOS.

HSCs interact with the cells of the BM microenvironment and the niche which can influence HSC quiescence, differentiation and lineage determination. Many of these cells have been shown to be vital in mitochondrial transfer including BMSC (301, 323) and macrophages (302, 352). In the second chapter of my thesis using *S. typhimurium* and LPS I will examine the specific cell of the BM that transfer their mitochondria to HSCs and the underlying mechanisms which regulate the transfer.

4.2 Superoxide drives mitochondrial transfer to HSCs during infection

Marlein *et al.* 2017 showed mitochondrial transfer to the AML is stimulated by AML derived NOX2 superoxide (41). To establish if there are elevated levels of superoxide in the BM of *S.typhimurium* and LPS treated C57BL/6J mice I used the Amplex red assay. Amplex red reacts with H_2O_2 and produces a fluorescent signal. There was an increase in H_2O_2 production in the BM of *S.typhimurium* (72 hours) (Figure 4.1A) or LPS (2 hour) (Figure 4.1B) treated mice.
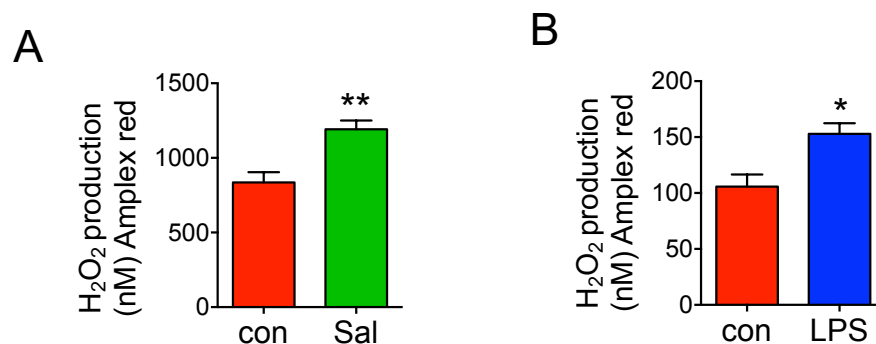
Figure 4.1. *S.typhimurium* and LPS induces an increase in H_2O_2 in the bone marrow.
(A) C57BL/6J mice were infected with *S.typhimurium* (Sal) for 72 hours, the animals were sacrificed, the bone marrow was extracted. 1×10^6 cells were analysed by Amplex Red assay n=5. (B) C57BL/6J mice were treated with 1 mg/kg LPS for 2 hours, the animals were sacrificed, the bone marrow was extracted. 1×10^6 cells were analysed by Amplex Red assay. n=5 in each group. Data shown are means ± SD *P < 0.05 **P < 0.01

Next, to determine if the elevated H_2O_2 in the BM caused an increase in ROS in the HSPC populations, ROS levels were measured using the DCF assay. Following inoculation of C57BL/6J mice with *S. typhimurium* for 72 hours, ROS levels (measured by DCF fluorescence) were elevated in the HSC, ST-HSC and LT-HSC populations (Figure 4.2A). Similarly, there was an increase in DCF fluorescence in the LSK, HSC, ST-HSC and LT-HSC in the LPS (2 hours) treated mice compared to control animals (Figure 4.2B).
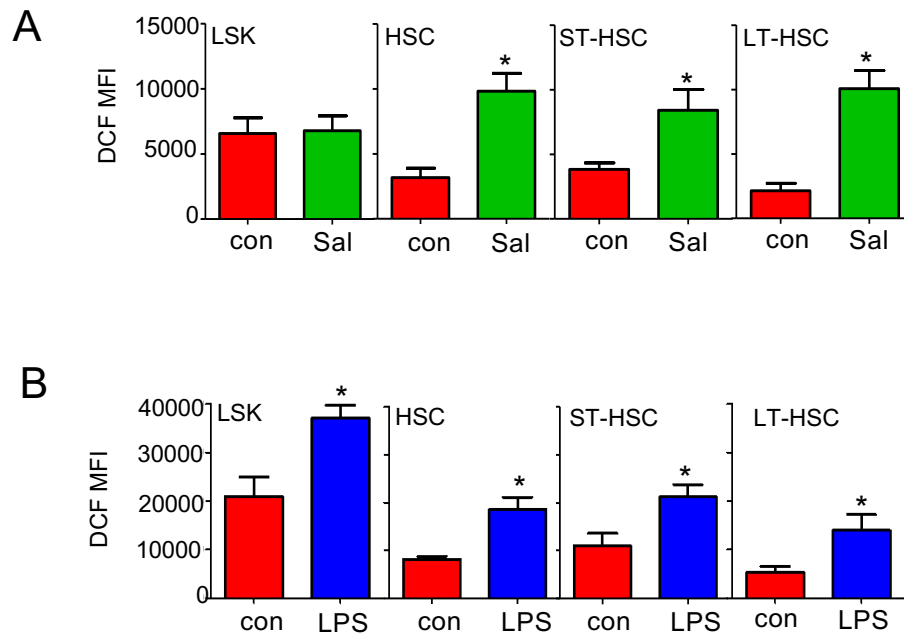
Figure 4.2. *S.typhimurium* and LPS induce an increase in ROS in the haematopoietic stem and progenitor populations.
(A) C57BL/6J mice were infected with *S.typhimurium* (Sal) for 72 hour, the animals were sacrificed, the bone marrow was extracted and stained with a panel of antibodies and H2DCFDA (DCF) to analyse ROS in specific LSK, HSC, ST-HSC and LT-HSC populations. n=6. (B) C57BL/6J mice were treated with 1 mg/kg LPS for 2 hours, the animals were sacrificed, the bone marrow was extracted stained with a panel of antibodies and H2DCFDA (DCF) to analyse ROS in specific populations. n=5 in each group. Data shown are means ± SD *P < 0.05

Next, to examine if there was elevated ROS in the more downstream populations, ROS levels were again measured using the DCF assay. There was no increase in ROS production observed in the LS-K, CMP, GMP and MEP populations following *S. typhimurium* (Figure 4.3A) or LPS treatment (Figure 4.3B).
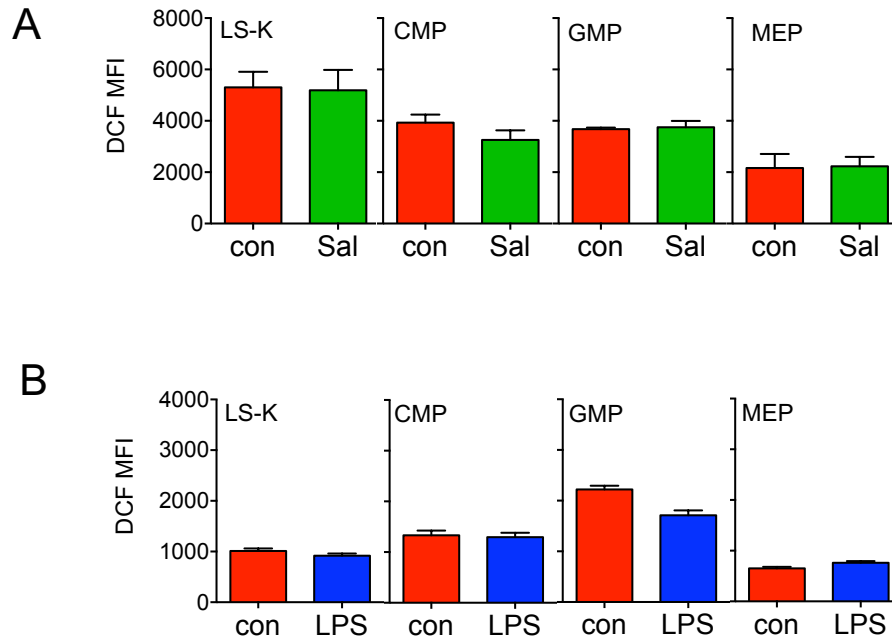
Figure 4.3. *S.typhimurium* **and LPS does not induce an increase in ROS in the more differentiated progenitor populations.**
(A) C57BL/6J mice were infected with *S.typhimurium* (Sal) for 72 hours, the animals were sacrificed, the bone marrow was extracted and stained with a panel of antibodies and H2DCFDA (DCF) to analyse ROS in specific LS-K, CMP, GMP and MEP populations n=6. (B) C57BL/6J mice were treated with 1 mg/kg LPS for 2 hours, the animals were sacrificed, the bone marrow was extracted stained with a panel of antibodies and H2DCFDA (DCF) to analyse ROS in specific populations. n=5 in each group. Data shown are means ± SD

Next, to investigate if ROS alone caused an increase in mitochondrial content within the HSC, C57BL/6J mice were treated with L-buthionine-sulfoximine (BSO) for 2 hours (Figure 4.4A). BSO blocks the rate-limiting step of L-glutathione (GSH) biosynthesis and therefore can be used to induce an increase in intracellular ROS *in vivo* (3). The dose of BSO used was confirmed to cause an increase in DCF fluorescence in the LSK, HSC, ST-HSC and LT-HSC populations similar to the increase observed in LPS and S. typhimurium treated animals (Figure 4.4B).
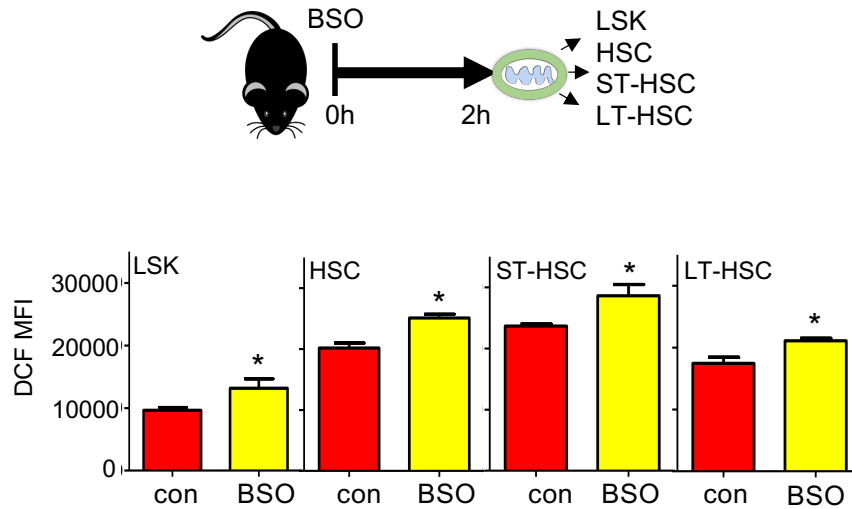
Figure 4.4. BSO induces an increase in ROS in the haematopoietic stem and progenitor populations.
(A) C57BL/6J mice were treated with 100 mg/kg L-buthionine-sulfoximine (BSO) for 2 hours, the animals were sacrificed, the bone marrow was extracted stained with a panel of antibodies and H2DCFDA (DCF) to analyse ROS in specific LSK, HSC, ST-HSC and LT-HSC populations. (B) Superoxide levels (DCF (mean fluorescence intensity (MFI)) in the specific populations of all animals examined. n=5 in each group. Data shown are means ± SD *P < 0.05

Moreover, the LSK, HSC, ST-HSC and LT-HSC populations all had a significant increase in mitochondrial mass after BSO treatment compared to the control mice (Figure 4.5).
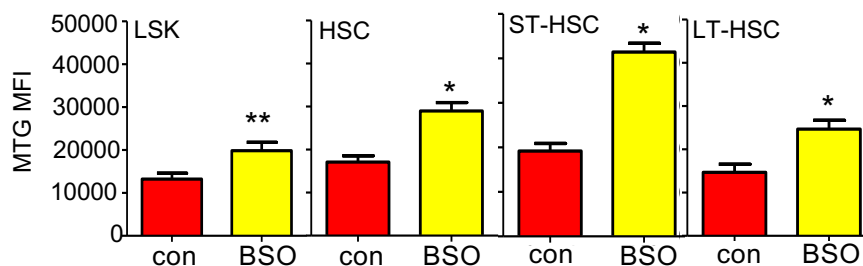
Figure 4.5. BSO induces an increase in mitochondrial content in the haematopoietic stem and progenitor populations.
(A) C57BL/6J mice were treated with 100 mg/kg L-buthionine-sulfoximine (BSO) for 2 hours, the animals were sacrificed, the bone marrow was extracted stained with a panel of antibodies and Mitotracker green (MTG) to analyse mitochondrial content (mitotracker green (mean fluorescence intensity (MFI)) in specific LSK, HSC, ST-HSC and LT-HSC populations n=5 in each group. Data shown are means ± SD *P < 0.05 **P < 0.01

Next, to confirm that ROS was the stimulus for the mitochondrial transfer from the BM microenvironment to the HSC the huNSG model was used. Once engrafted the huNSG mice were treated with BSO for 2 hours, the animals were sacrificed, and the BM was extracted. The human MPP (hMPP) and human HSC (hHSC) were sorted and analysed for mouse mtDNA (Figure 4.6A). The gating used for the sorting was determined by fluorescence minus one and is shown in Figure 4.6B.
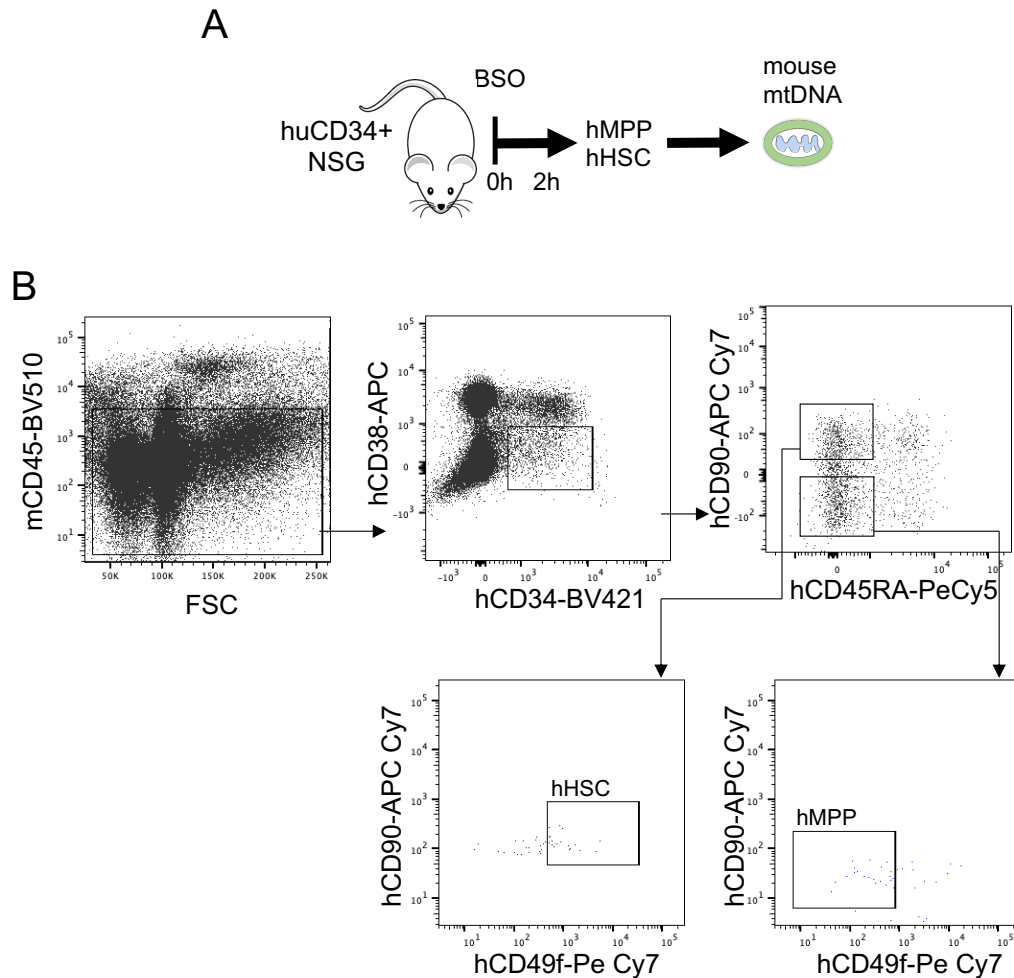
Figure 4.6. Schematic and gating strategy for human MPP and HSC cell populations in huNSG mice.
(A) NSG mice were treated with 25 mg/kg busulfan for 3 days prior to tail-vein injections of human CD34+ cord blood donor cells. The mice were subjected to 100 mg/kg BSO or PBS intraperitoneal injections. After 2 hours the mice were sacrificed, the bone marrow was extracted and stained with a panel of antibodies to isolate and sort specific human HSC and MPP populations by FACS. (B) The gating strategy used is shown.

The BM was also analysed for the presence of human CD45 using flow cytometry. Figure 4.7 confirms equal engraftment of human CD34+ HSCs in recipient NSG mice within both treatment groups.
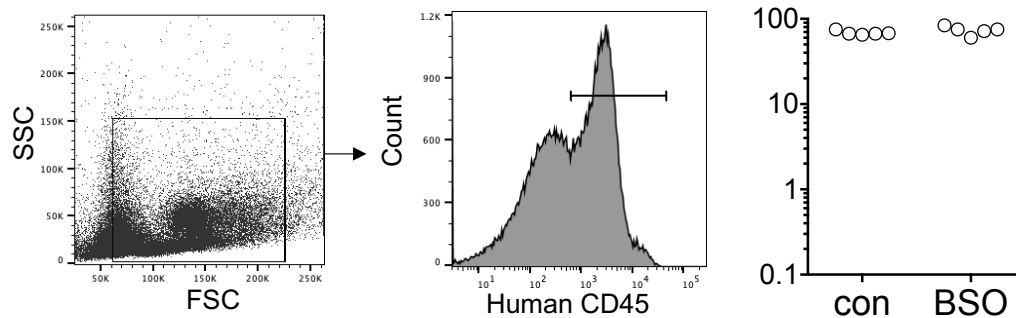
Figure 4.7. Human CD45+ engraftment is seen in the bone marrow of huNSG mouse model.
NSG mice were treated with 25 mg/kg busulfan for 3 days prior to tail-vein injections of human CD34+ cord blood donor cells. The mice were subjected to 100 mg/kg BSO or PBS intraperitoneal injections. After 2 hours the mice were sacrificed, and the bone marrow was extracted. Engraftment was determined by human CD45 expression in the bone marrow detected by flow cytometry analysis. n=5 in each group.

Finally, to determine if intercellular mitochondrial transfer occurred from the mouse BM microenvironment to the HSC in response to elevated ROS alone, species specific mitochondrial analysis was performed. After BSO treatment the BM was extracted and the human MPP and human HSC population were sorted by FACS using the gating strategy shown in Figure 4.6. The DNA was extracted and duplex Taqman qPCR analysis was carried out using species specific probes targeting mitochondrial gene ND1. The Ct values were normalised to human genomic DNA (Tert). Figure 4.8 shows that in the BSO-treated hu-NSG mice, mouse mtDNA is significantly increased in the human MPPs and HSCs. These data show elevated ROS alone causes the transfer of mtDNA from the BM microenvironment to the HSCs.
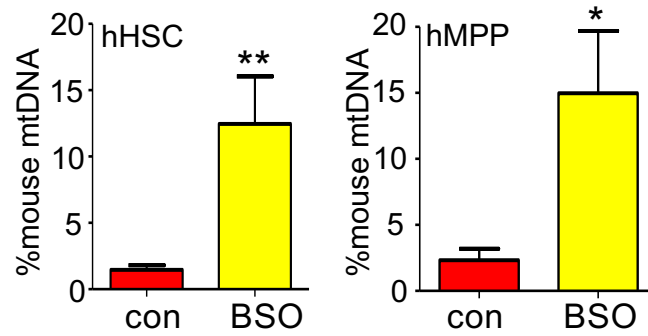
Figure 4.8. Mitochondrial DNA is transferred from the BM microenvironment to the HSC and MPP populations from the huNSG mice in response to BSO treatment.
Human MPP and HSC populations were sorted from the bone marrow of huNSG treated with either BSO or PBS. The DNA was isolated and analysed using species specific Taqman probes targeting ND1 and Tert by qPCR. Mouse or human mitochondrial DNA was measured by $\Delta\Delta Ct$ and normalised to human tert. Data shows the percentage of mouse mitochondria detected in the isolated human cells. Data shown are means ± SD *P < 0.05 **P < 0.01

For further assurance that ROS mediates the LPS-driven increase in mitochondrial content within the HSCs, we used the ROS scavenger N-acetyl-cysteine (NAC) to reduce ROS levels. C57BL/6J mice were pre-treated with NAC for 1 hour before treatment with LPS for 2 hours (Figure 4.9A). Pre-treatment with NAC led to reduced ROS levels in the LSK, HSC, ST-HSC and LT-HSC populations (Figure 4.9B).
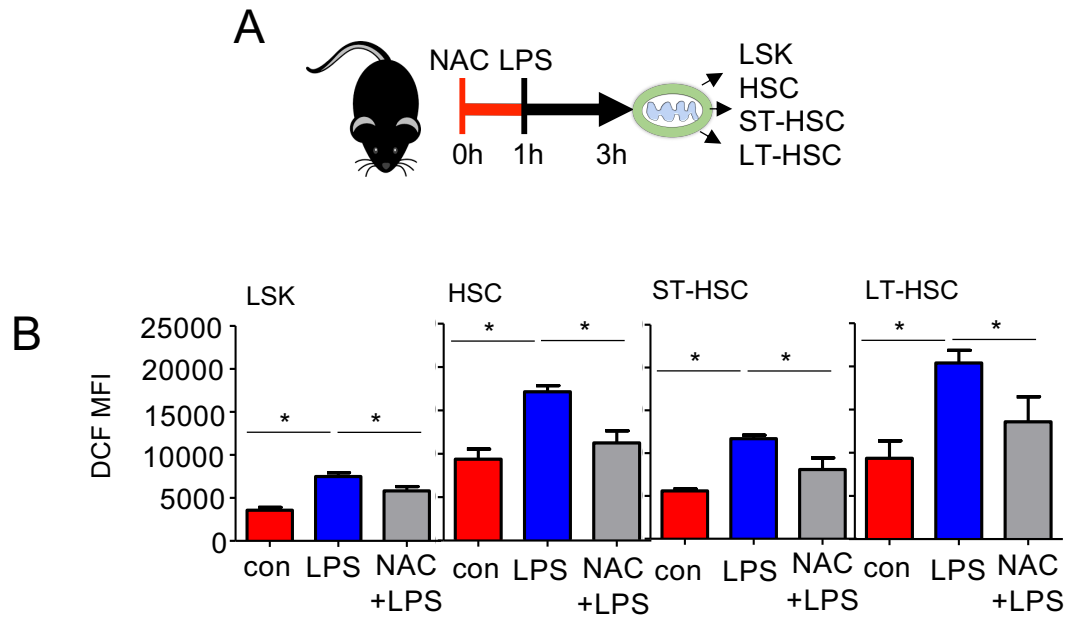
Figure 4.9. NAC reduces the LPS elicited increase in ROS in the haematopoietic stem and progenitor populations.
(A) C57BL/6J mice were pre-treated with 500 mg/kg *N*-acetyl-cysteine (NAC) for 1 hour before treatment with 1 mg/kg LPS for 2 hours. The animals were sacrificed, the bone marrow was extracted stained with a panel of antibodies and H2DCFDA (DCF) to analyse ROS in specific LSK, HSC, ST-HSC and LT-HSC populations. (B) ROS levels (DCF (mean fluorescence intensity (MFI)) in the specific populations of all animals examined. n=5 in each group. Data shown are means ± SD *P < 0.05

Furthermore, NAC treatment inhibited LPS elicited increase in mitochondrial content within the LSK, HSC, ST-HSC and LT-HSC populations (Figure 4.10). Taken together these data suggests that ROS is the stimulus responsible for the transfer of mitochondria to the HSCs during infection.

173
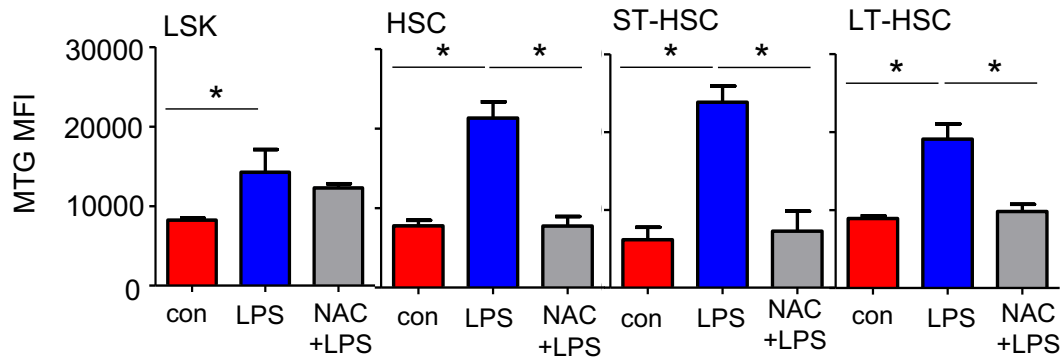
Figure 4.10. NAC reduces the LPS elicited increase in mitochondrial content in the haematopoietic stem and progenitor populations.
C57BL/6J mice were pre-treated with 500 mg/kg *N*-acetyl-cysteine (NAC) for 1 hour before treatment with 1 mg/kg LPS for 2 hours. The animals were sacrificed, the bone marrow was extracted stained with a panel of antibodies and Mitotracker green (MTG) to analyse mitochondrial content (MTG mean flourecence intensity (MFI)) in specific LSK, HSC, ST-HSC and LT-HSC populations n=5 in each group. Data shown are means ± SD *P < 0.05

4.3 NOX2 derived superoxide mediate mitochondrial transfer to the HSC.

To determine if the ROS generated in the BM after bacterial infection was NOX2 derived, we investigated mitochondrial transfer in the CGD or Cybb mouse model. In Cybb mouse the gp91 subunit of NOX2 has been deleted (353) and therefore they cannot produce NOX2 derived superoxide. Wildtype C57BL/6J or Cybb mice were treated with LPS for 2 hours, the BM was extracted and assessed for H_2O_2 production using the Amplex red assay (Figure 4.11A). As expected, there was an increase in H_2O_2 production in the BM of LPS treated mice (Figure 4.11B). Conversely, in the BM of Cybb mice there was no change observed in H_2O_2 production following LPS treatment (Figure 4.11B).
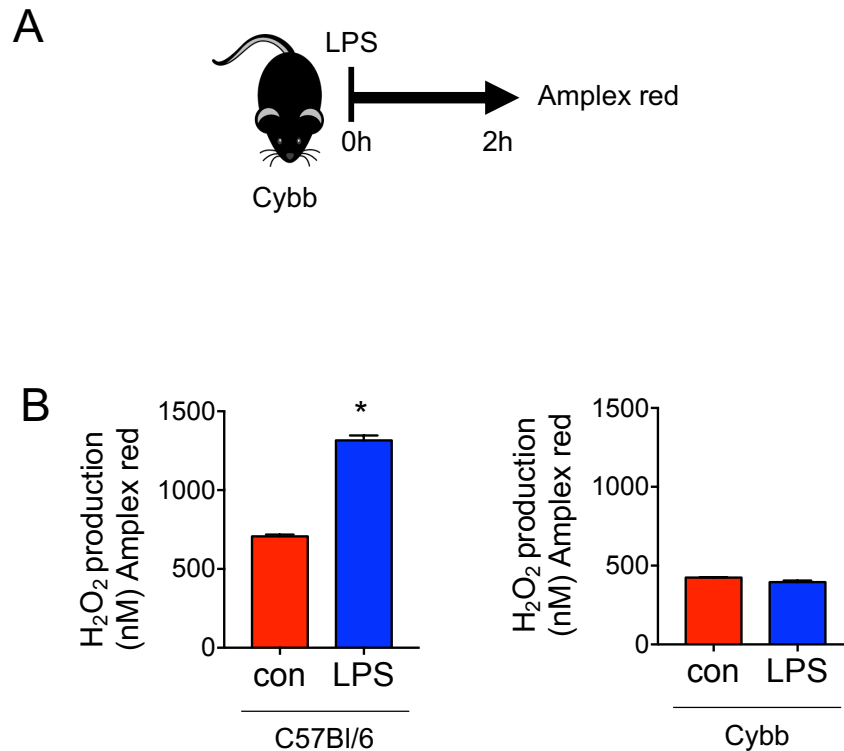
Figure 4.11. LPS induces an increase in H_2O_2 in the bone marrow.
(A) C57Bl/6J mice or Cybb mice were treated with 1 mg/kg LPS or control PBS intraperitoneal injections. After 2 hours the mice were sacrificed, and the bone marrow extracted. (B) 1 x 10^6 bone marrow cells were analysed by Amplex Red assay n=5. Data shown are means ± SD *P < 0.05

Next, to determine if NOX2 derived superoxide was driving the increase in ROS in the HSPC populations ROS levels were measured using the DCF assay. Cybb mice were treated with LPS for 2 hours. The mice were sacrificed, and the haematopoietic cell populations were analysed for mitochondrial content using flow cytometry. The gating strategy to analyse the cell populations of interest is shown in Figure 4.12. All gating was determined using fluorescence minus one controls.
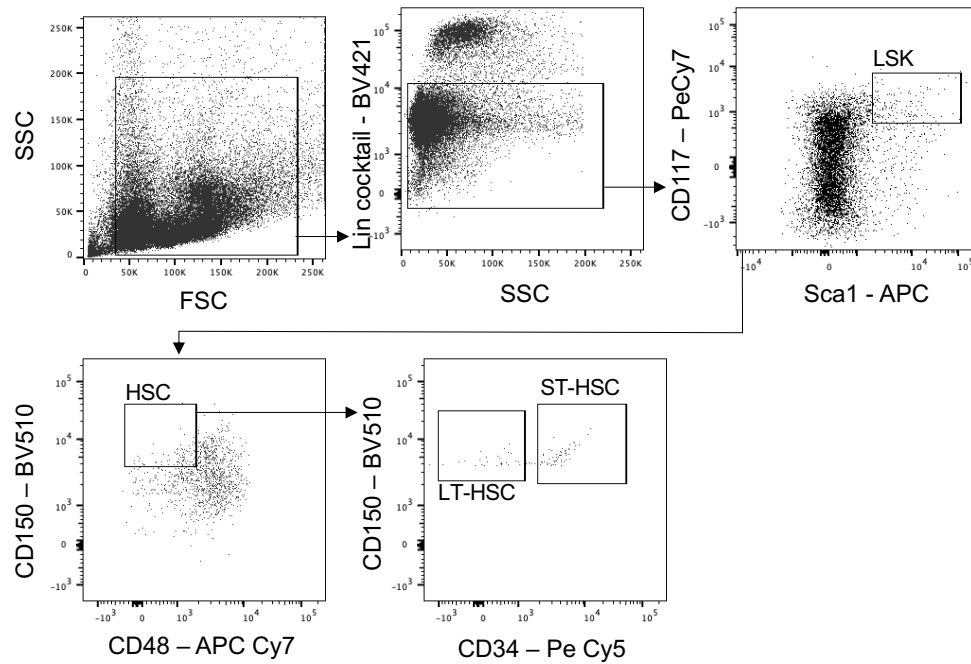
Figure 4.12. Gating strategy for mouse LSK, HSC, ST-HSC and LT-HSC.
Cybb mice were treated with LPS for 2 hours, the animals were sacrificed, and the bone marrow was extracted. The cells were stained with a panel of antibodies to analyse specific LSK, HSC, ST-HSC and LT-HSC populations. The gating strategy used is shown.

Following treatment with LPS for 2 hours, there was no change in the ROS levels (measured by DCF fluorescence) within the LSK, HSC, ST-HSC and LT-HSC populations of the Cybb mice (Figure 4.13).
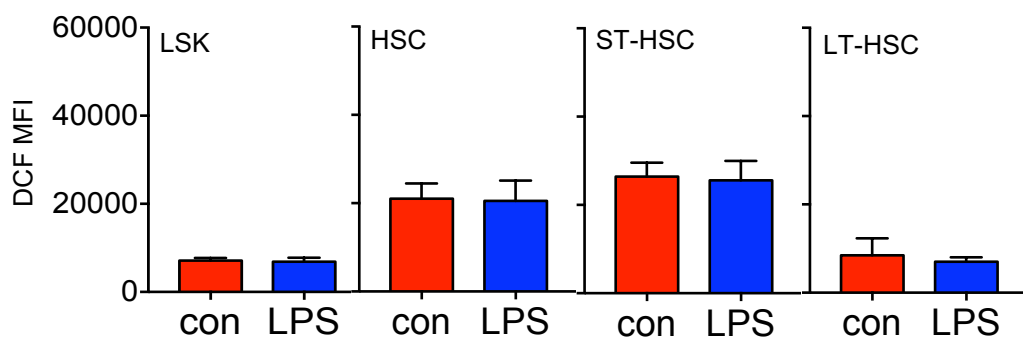
Figure 4.13. HSC ROS levels do not increase in Cybb animals in response to LPS.
Cybb mice were treated with LPS for 2 hours, the animals were sacrificed, and the bone marrow was extracted. The cells were stained with a panel of antibodies and H2DCFDA (DCF) to analyse superoxide levels (DCF (mean fluorescence intensity (MFI)) in specific LSK, HSC, ST-HSC and LT-HSC populations n=5 in each group Data shown are means ± SD

Moreover, Figure 4.14A shows in the Cybb mice the HSPC populations do not have an increased mitochondrial mass after treatment with LPS. To confirm there was no increase in mitochondrial content in the LSK and HSC population in response to LPS, the LSK and HSC population were sorted from control and LPS treated mice and analysed for mtDNA. As expected, there was no increase in mtDNA in both the LSK and HSC population from the LPS treated Cybb mice (Figure 4.14B).
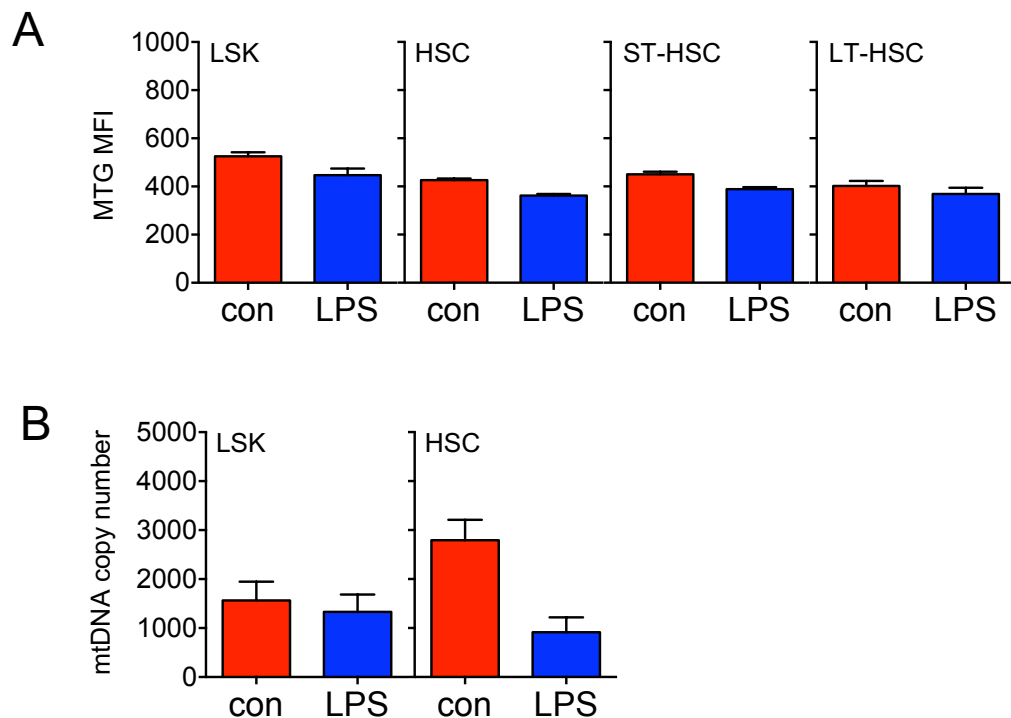
Figure 4.14. HSC mitochondrial content does not increase in Cybb animals in response to LPS.
(A) Cybb mice were treated with LPS for 2 hours, the animals were sacrificed, and the bone marrow was extracted. The cells were stained with a panel of antibodies and Mitotracker Green (MTG) to analyse superoxide levels (MTG (mean fluorescence intensity (MFI)) in specific LSK, HSC, ST-HSC and LT-HSC populations (B) The LSK and HSC populations were sorted from control and LPS treated animals by FACS and analysed for mtDNA by qPCR n=5 in each group. Data shown are means ± SD

Next, to see if exogenous ROS could cause an increase in mitochondrial content in the HSC, Cybb mice were treated with BSO for 2 hours (Figure 4.15A). BSO was confirmed to cause an increase in ROS in the HSC and ST-HSC populations in the Cybb animals (Figure 4.15B).
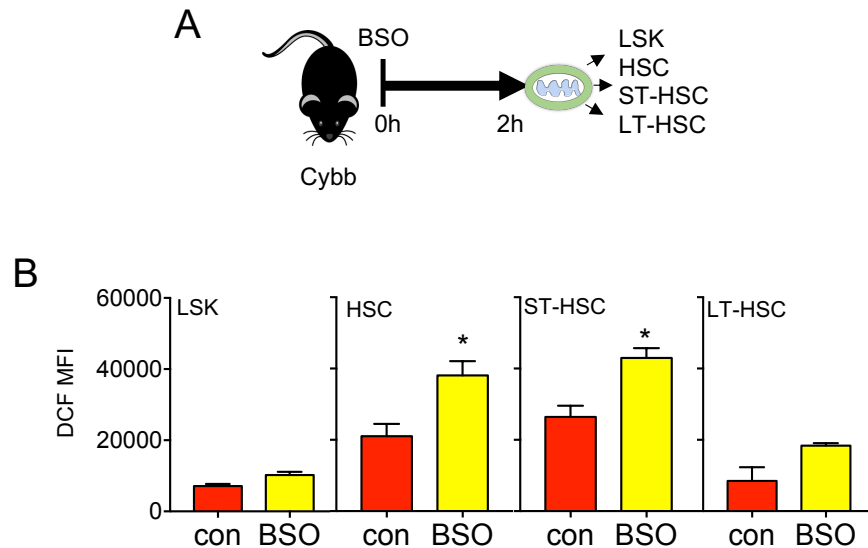
Figure 4.15. HSC ROS levels increase in Cybb animals in response to BSO.
Cybb mice were treated with 100 mg/kg BSO for 2 hours, the animals were sacrificed, and the bone marrow was extracted. (B)The cells were stained with a panel of antibodies and H2DCFDA (DCF) to analyse ROS levels (DCF mean fluorescence intensity (MFI)) in specific LSK, HSC, ST-HSC and LT-HSC populations n=5 in each group. Data shown are means ± SD *P < 0.05

Moreover, unlike LPS there was a significant increase in the mitochondrial content of the LSK, HSC, ST-HSC and LT-HSC populations in the Cybb mice after BSO treatment compared to the control mice (Figure 4.16). Together, these data show NOX2 derived ROS mediates transfer of mitochondria to HSCs during infection.
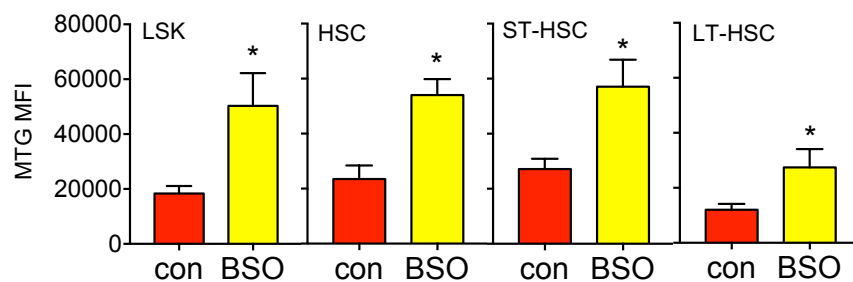
Figure 4.16. HSC mitochondrial content increases in Cybb animals in response to BSO.
Cybb mice were treated with 100 mg/kg BSO for 2 hours, the animals were sacrificed, and the bone marrow was extracted. The cells were stained with a panel of antibodies and Mitotracker Green (MTG) to analyse mitochondrial mass (MTG (mean fluorescence intensity (MFI)) in specific LSK, HSC, ST-HSC and LT-HSC populations n=5 in each group. Data shown are means ± SD *P < 0.05

4.4   BMSCs donate mitochondrial DNA to the HSC during infection

The BM microenvironment is made up of multiple different cell types (354), many of which have been shown to be key in mitochondrial transfer within the BM (41, 302, 324, 349, 352). To establish the cell of the BM which transfers their mitochondria to the HSC during infection I used a co-culture assay which took advantage of the SNP differences in the mtDNA. A TaqMan SNP genotyping assay was designed to detect this difference in ND3 and COX3 mtDNA between PepCboy and CBA mice. TaqMan SNP PCR analysis of PepCboy DNA and CBA DNA with COX3 SNP Taqman probes show positive fluorescence on FAM for CBA cells but negative for PepCboy cells (Figure 4.17A). The ND3 also shows positive fluorescence on FAM for CBA cells but negative for PepCboy cells (Figure 4.17B).
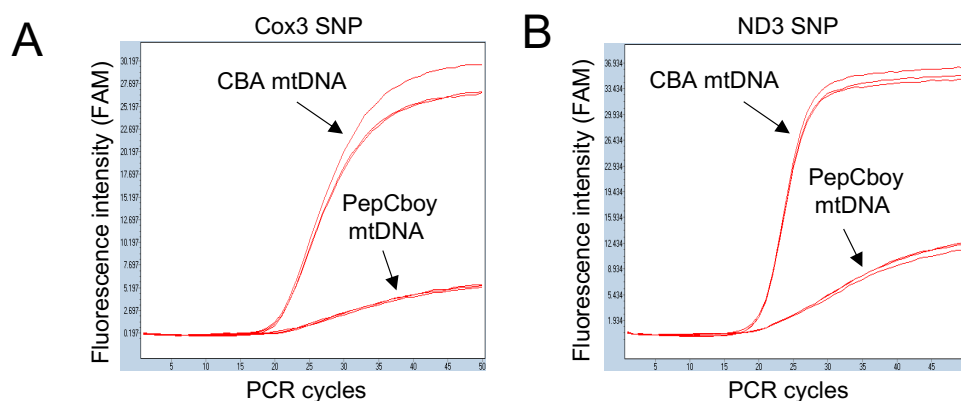
Figure 4.17. TaqMan RT-qPCR analysis of CBA and PepCboy mtDNA.
(A) PCR using COX3 primer shows positive fluorescence on FAM for CBA DNA but negative for PepCboy DNA. (B) Analysis with ND3 primer on FAM shows positive fluorescence for CBA DNA but negative for PepCboy DNA.

To investigate the cell which transferred their mitochondria to the HSC during infection, CBA lineage negative cells were cocultured with PepCboy BM-derived macrophage cells, BM osteoblast or BMSCs for 24 hours with and without H_2O_2. The lineage negative cells were then analysed for PepCboy SNP mtDNA by TaqMan PCR (Figure 4.18).
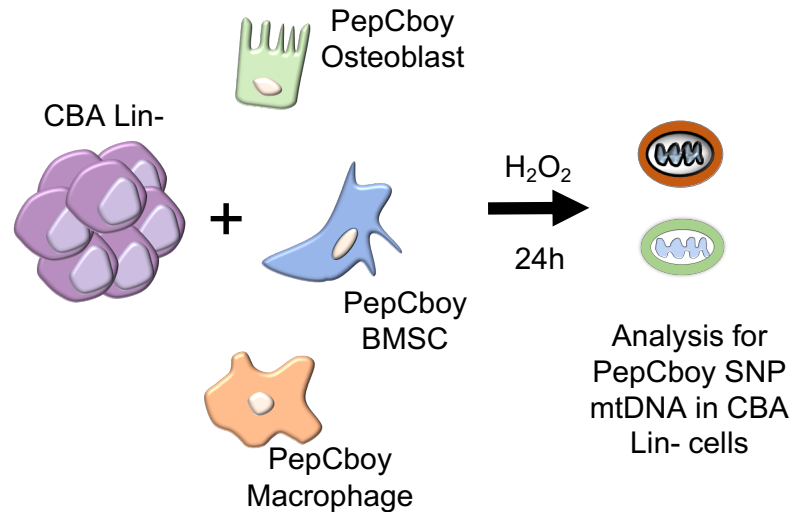
Figure 4.18. Schematic diagram of experimental design.
CBA lineage-negative cells (recipient) were cocultured with PepCboy bone marrow-derived macrophage cells, bone marrow osteoblasts, and BMSCs (donor) for 24 hours with and without H_2O_2. The lineage negative cells were removed and analysed for PepCboy SNP mtDNA in CBA lineage negative cells by TaqMan PCR using ND3 probes.

Figure 4.19 shows that only the BMSCs transferred mtDNA to lineage negative cells when cultured with H_2O_2. There was no transfer of mtDNA observed from the macrophage or osteoblast when cultured in the presence of H_2O_2 (Figure 4.19).
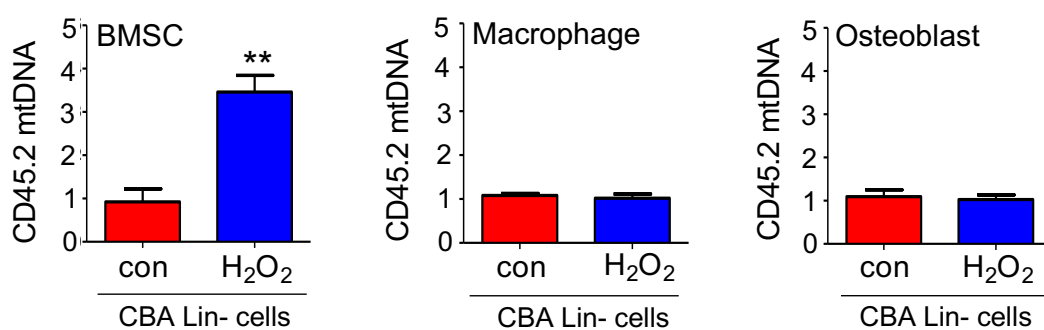
Figure 4.19. BMSCs supply mitochondrial DNA to HSCs in response to elevated H_2O_2.
CBA lineage-negative cells (recipient) were cocultured with PepCboy bone marrow-derived macrophage cells, bone marrow osteoblasts, and BMSCs (donor) for 24 hours with and without H_2O_2. The lineage negative cells were removed and analysed for PepCboy SNP mtDNA in CBA lineage negative cells by TaqMan PCR using ND3 probes. Donor PepCboy mtDNA copy number in CBA lineage negative cells. CBA gDNA was used to standardise mtDNA copy number. Data shown are means ± SD **P < 0.01

Next to determine if mitochondria are transferred from the BMSC to the HSPCs primary mBMSC were transduced with an rLV.EF1.mCherry lentivirus for stable incorporation of mCherry protein tagged mitochondria. Lineage negative cells were transduced with rLV.EF1.AcGFP-Mem9 lentivirus were cultured on the mBMSCs for 24 hours with H_2O_2 and imaged using fluorescence microscopy (Figure 4.20A). BMSC labelled mitochondria transferred to the lineage negative cells in the presence of H_2O_2, quantified by the acquisition of the mCherry fluorescence in the lineage negative cells (Figure 4.20B).
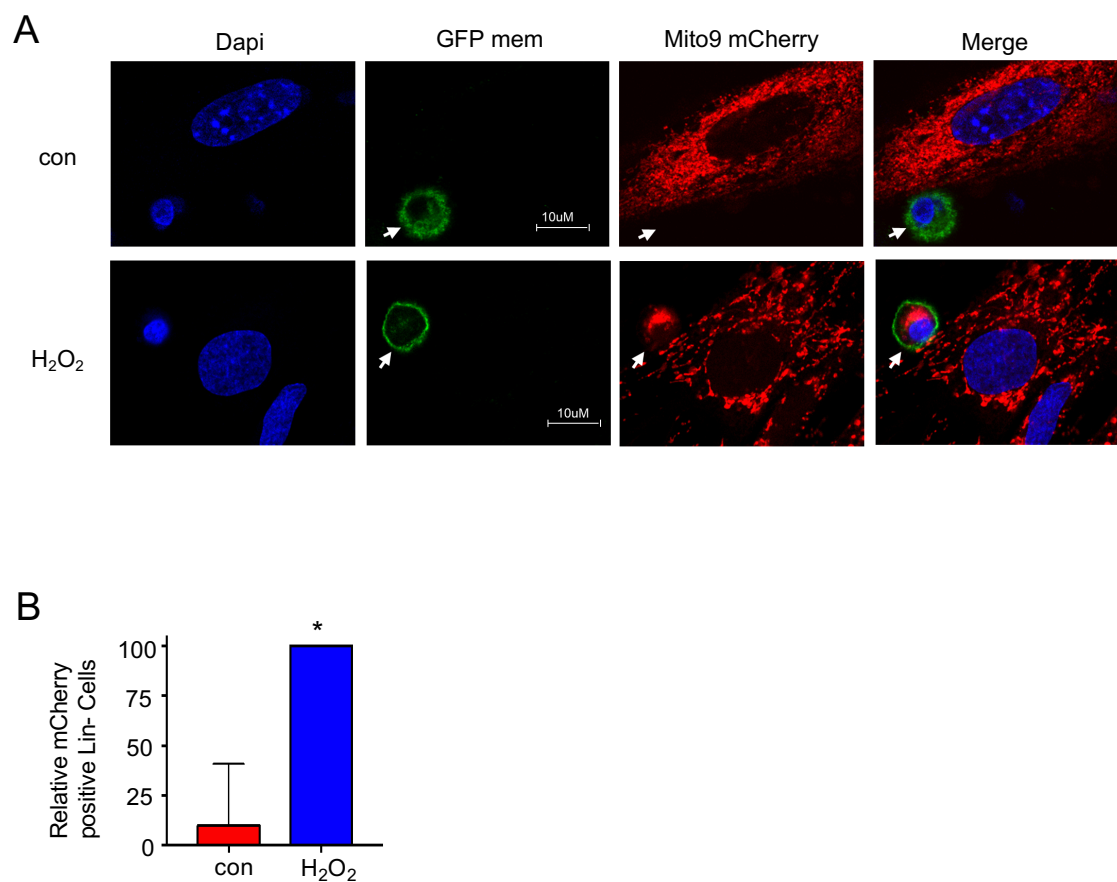
Figure 4.20. BMSCs supply mitochondria to HSCs in response to elevated H_2O_2 treatment.
(A) Representative fluorescent microscopy images of lin- cells (white arrow) lentivirally transduced with the rLV.EF1.AcGFP-Mem9 virus cultured with mBMSCs transduced with rLV.EF1.mCherry-Mito-9 in the absence or presence of 10 µM H_2O_2 for 24 hours. (B) Quantification of rLV.EF1.mCherry-Mito-9 in lin- cells from images shown taken from 3 independent experiments and 20 lineage cells from each experiment. Data shown are means ± SD *P < 0.05

To ensure that the H_2O_2 concentration did not cause lineage negative cell death, cell viability was assessed using the Annexin V assay. No change in apoptosis levels were found in the H_2O_2 treated cells compared to the control (Figure 4.21).
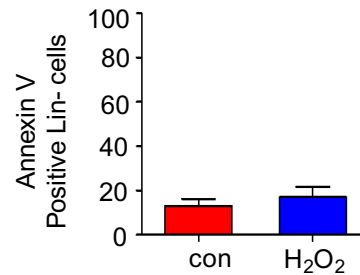
Figure 4.21. H_2O_2 does not cause lineage negative cell death.
Lin- cells were cultured with mBMSCs in the absence or presence of 10 µM H_2O_2 for 24 hours, stained for Annexin V-FITC and analysed by flow cytometry. Data shown are means ± SD

Next, to examine the effects of infection on the BMSC *in vivo* C56BL/6J mice were treated with LPS for 2 hours. The mice were sacrificed, and the BMSCs were analysed for mitochondrial content and ROS using flow cytometry (Figure 4.22A). The gating strategy to analyse the BMSC is shown in Figure 4.36B. The gating was determined using fluorescence minus one controls.
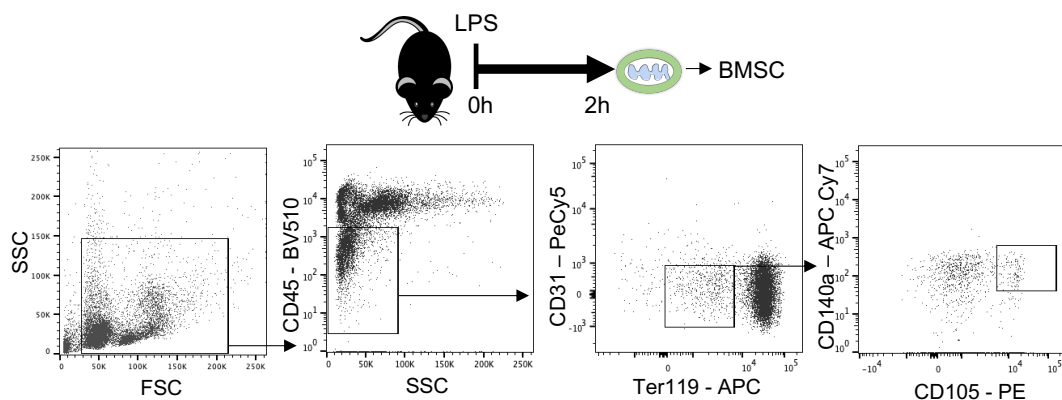
Figure 4.22. Schematic and gating strategy for BMSC.
C57BL/6J mice were treated with 1 mg/kg LPS for 2 hours, the animals were sacrificed, the bone marrow was extracted and stained with a panel of antibodies to analyse the BMSC population. The gating strategy used is shown.

To investigate if infection also induced ROS in the BMSC *in vivo* we analysed ROS levels using DCF. Increased ROS levels were observed in the BMSC from LPS treated mice compared to the control mice (Figure 4.23).
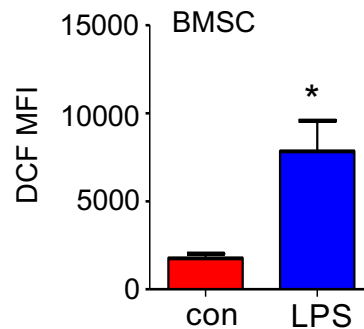
Figure 4.23. LPS induces an increase in ROS levels in the BMSC.
C57BL/6J mice were treated with 1 mg/kg LPS for 2 hours, the animals were sacrificed, the bone marrow was extracted and stained with a panel of antibodies and H2DCFDA (DCF) to analyse ROS (DCF (mean fluorescence intensity (MFI)) in the BMSC population n=5 in each group. Data shown are means ± SD *P < 0.05

Furthermore, after treatment with LPS mitochondrial content was reduced in the BMSC of C57BL/6J mice compared to control animals (Figure 4.24).
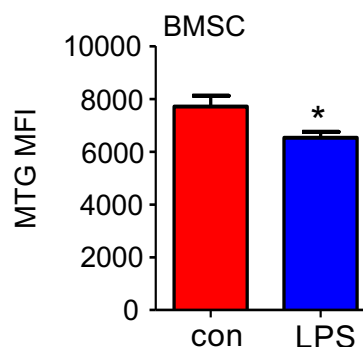
Figure 4.24. LPS induces a decrease in mitochondrial content in the BMSC.
C57BL/6J mice were treated with 1 mg/kg LPS for 2 hours, the animals were sacrificed, the bone marrow was extracted and stained with a panel of antibodies and Mitotracker green (MTG) to analyse the Mitochondrial content (mitotracker green (mean fluorescence intensity (MFI)) in the BMSC population n=5 in each group. Data shown are means ± SD *P < 0.05

To ensure ROS mediates the LPS-driven decrease in mitochondrial content within the BMSCs, we used the ROS scavenger NAC to reduce ROS levels. C57BL/6J mice were pre-treated with NAC for 1 hour before treatment with LPS for 2 hours (Figure 4.25A). As expected, pre-treatment with NAC inhibited the LPS elicited increase in ROS levels in the BMSC (Figure 4.25B).
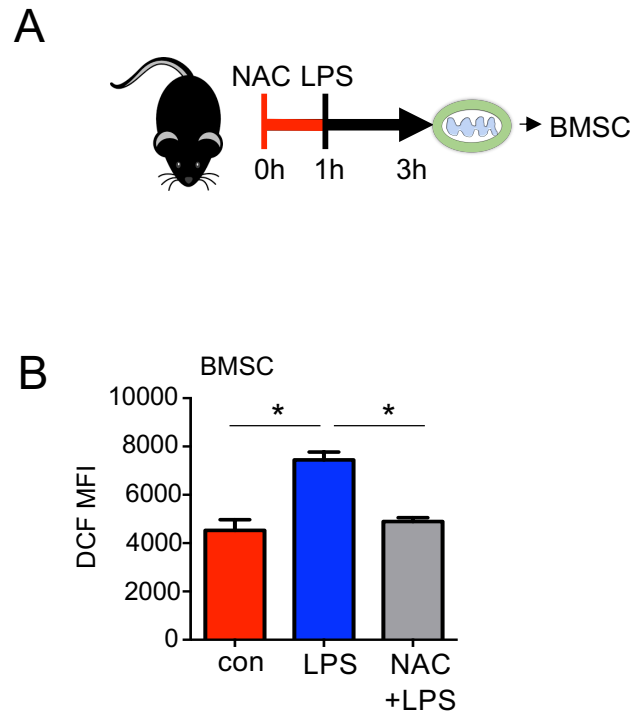
Figure 4.25. NAC reduces the LPS elicited increase in ROS in the haematopoietic stem and progenitor populations.
(A) C57BL/6J mice were pre-treated with 500 mg/kg N-acetyl-cysteine (NAC) for 1 hour before treatment with 1 mg/kg LPS for 2 hours. The animals were sacrificed, the bone marrow was extracted stained with a panel of antibodies and H2DCFDA (DCF) to analyse ROS in the BMSC. (B) ROS levels (DCF (mean fluorescence intensity (MFI)) in the specific populations of all animals examined n=5 in each group. Data shown are means ± SD *P < 0.05

Next, I examined if pre-treatment with NAC had an effect on mitochondrial content in the BMSC. Figure 4.26 shows the reduction in the mitochondrial mass cause by the LPS was inhibited by the addition of NAC. Using both *in vitro* and *in vivo* models, these data show that BMSC provide the mitochondria to the HSC during acute infection.
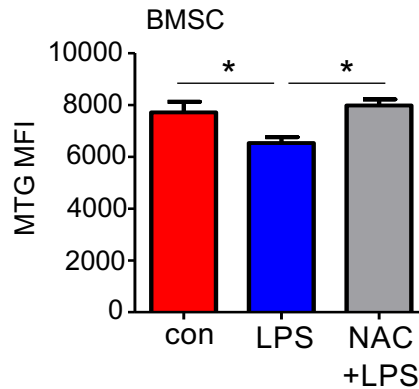
Figure 4.26. NAC inhibits the LPS elicited decrease in mitochondrial content in the BMSC.
C57BL/6J mice were pre-treated with 500 mg/kg *N*-acetyl-cysteine (NAC) for 1 hour before treatment with 1 mg/kg LPS for 2 hours. The animals were sacrificed, the bone marrow was extracted stained with a panel of antibodies and Mitotracker green (MTG) to analyse mitochondrial content (MTG mean fluorescence intensity (MFI)) in the BMSC n=5 in each group. Data shown are means ± SD *P < 0.05

4.5 BM macrophage derived superoxide coordinates mitochondrial increase in the HSCs in response to infection

In the previous sections I found that mitochondria are transferred from the BMSC to the HSC during infection and this transfer is mediated by superoxide. Next I aimed to determine the source of the superoxide following infection. BM macrophages have previously been shown to regulate HSC location (77, 355), erythropoiesis (356, 357) and steady state granulopoiesis (358, 359). However, the full mechanism by which HSCs expansion is regulated by macrophages remains unknown. BM derived macrophages (BMDM) produce H_2O_2 in response to LPS *in vitro* (360). Moreover, selective mutations in the H_2O_2 generating complex of the macrophage, have been shown to be vital in the immune response to infection (233, 361). I therefore investigated the role of BMDM in mediating mitochondrial content during infection.

First, to look at specific macrophage derived H_2O_2 I isolated BMDM from C57BL/6J and Cybb mice. We treated the BMDM with LPS for 30 minutes and analysed the media for H_2O_2 production by the Amplex Red assay (Figure 4.27A). *In vitro*, C57BL/6J BMDM generated increased extracellular H_2O_2 in

response to LPS. In contrast, following LPS treatment the Cybb BMDM had a decreased production of extracellular H_2O_2 compared to the control (Figure 4.27B).
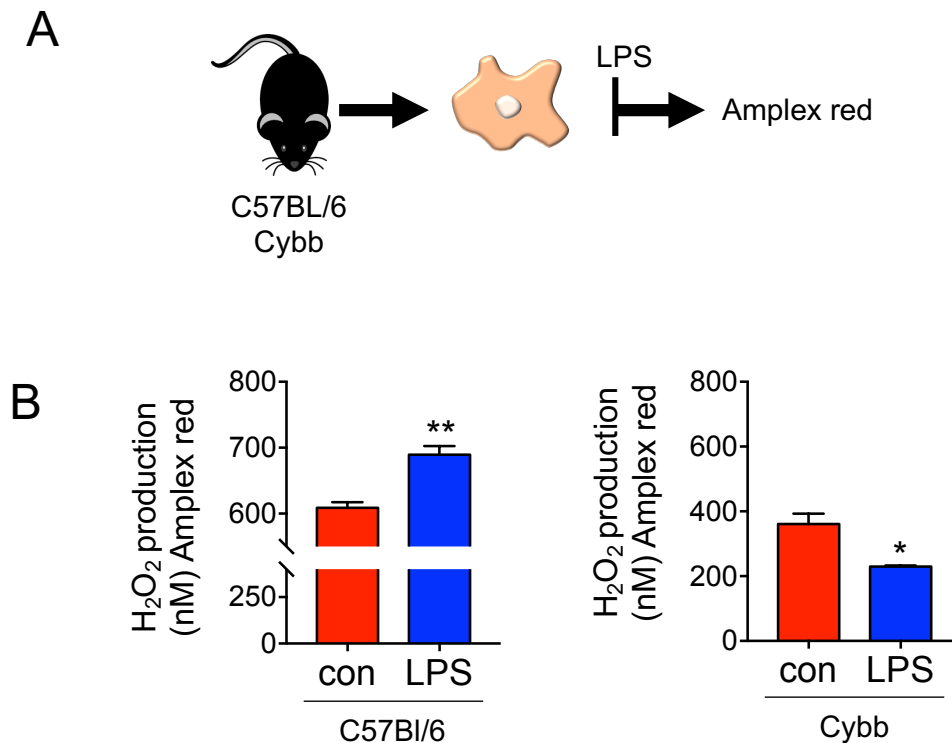
Figure 4.27. Bone marrow derived macrophages produce NOX2 derived H_2O_2 in response to LPS
(A) Bone marrow derived macrophages from C57Bl/6J mice or Cybb mice were treated with 1 μl/ml of LPS for 30 minutes the media was removed and were analysed for H_2O_2 production by Amplex Red assay. (B) H_2O_2 produced by the bone marrow derived macrophages after LPS treatment from C57Bl/6J mice or Cybb mice n=5. Data shown are means ± SD *P < 0.05 **P < 0.01

Next, to examine the effects of infection on the BM macrophage *in vivo* C57BL/6J mice were treated with LPS for 2 hours. The mice were sacrificed, and the BM macrophages were analysed using flow cytometry (Figure 4.28A). The gating strategy to analyse the macrophages is shown in Figure 4.28B. The gating was determined using fluorescence minus one controls. We observed there was a significantly increased number of macrophages in the C57BL/6J mice treated with LPS compared to the control (Figure 4.28B).
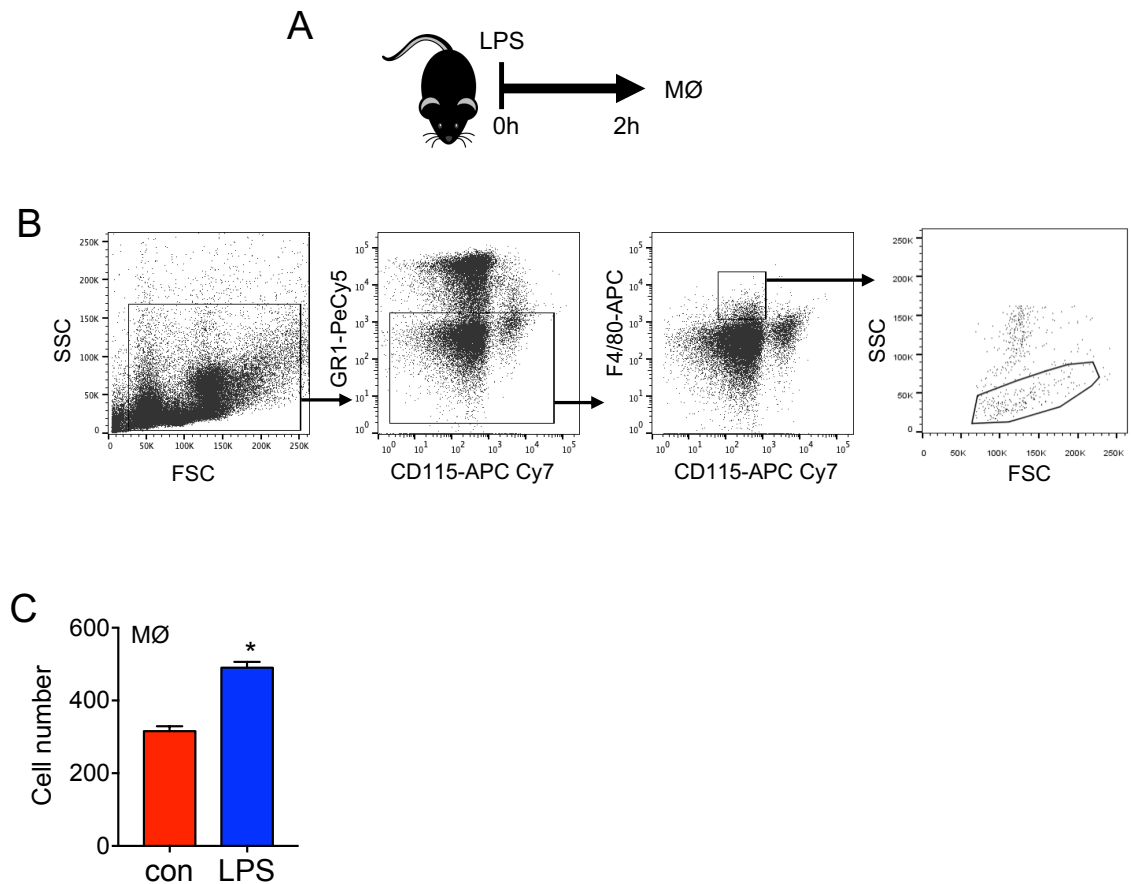
Figure 4.28. Macrophage number increases after LPS infection.
(A) C57Bl/6J mice were treated with 1 mg/kg LPS or control PBS intraperitoneal injections. After 2 hours the mice were sacrificed and the bone marrow extracted. The cells were analysed for GR1, CD115, F4/80 expression to analyse the macrophage population. (B) The gating strategy used is shown. (C) Macrophage cell number after treatment with LPS. Data shown are means ± SD of n=4 in each group. *p<0.05.

Next, to examine if the H_2O_2 produced by the BMDM could stimulate mitochondrial DNA transfer I used a coculture assay which took advantage of the SNP differences in the mtDNA described in Figure 4.17 and 4.18. Instead of using H_2O_2 directly, the co-culture with BMSC and lineage negative cells were stimulated with conditioned media from LPS activated BMDM for 24 hours. The CBA lineage negative cells were isolated and analysed for the presence of PepCboy SNP mtDNA by TaqMan qPCR using ND3 probes (Figure 4.29A).

Conditioned media from LPS activated C57BL/6J macrophages induced mitochondrial transfer from the PepCboy BMSC to the CBA lineage negative cells (Figure 4.29B). No transfer of mtDNA was observed in the coculture cultured with conditioned media from LPS activated Cybb macrophages (Figure 4.29C). Taken together, these results suggest BMDM derived NOX2 superoxide stimulate mitochondrial transfer to the HSPC during infection.
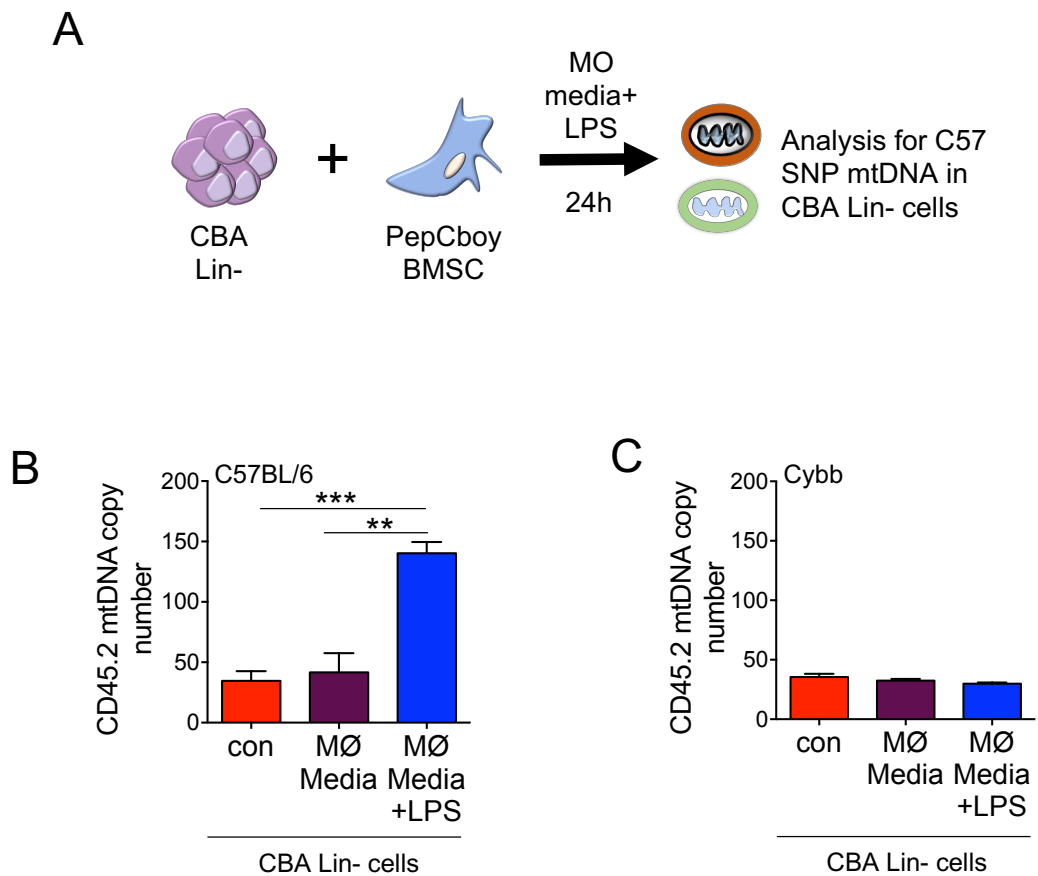
Figure 4.29. Bone marrow macrophage derived H_2O_2 is required for mitochondrial DNA transfer.
CBA lineage negative cells were co-cultured with PepCboy BMSCs for 24 hours with conditioned media from LPS treated C57BL/6J or Cybb bone marrow derived macrophages for 1 hour. The CBA lineage negative cells were removed and analysed for PepCboy by TaqMan qPCR. (B) The mtDNA copy number of PepCboy mtDNA in CBA lineage negative cells after treatment with conditioned media from C57BL/6J bone marrow derived macrophages (B) The mtDNA copy number of PepCboy mtDNA in CBA lineage negative cells after treatment with conditioned media from Cybb bone marrow derived macrophages. Data shown are means ± SD ** $p < 0.01$ *** $p < 0.001$

To investigate the role of BM macrophage derived NOX2 superoxide *in vivo* C57BL/6J mice were injected daily with control or clodronate liposomes for 3 days to deplete the BM macrophages. The animals were then infected with *S. typhimurium* for 72 hours, the mice were sacrificed, and the BM was extracted and analysed using flow cytometry (Figure 4.30).

Figure 4.30. Schematic of experimental design.
Schematic diagram of experimental design. C57BL/6J mice were injected with clodronate liposomes for 3 days prior to *S.typhimurium* infection for 72 hours. The mice were sacrificed, and the bone marrow extracted and analysed for GR1, CD115, F4/80 expression or H2DCFDA, Mitotracker green (MTG), Sca 1, CD117, CD48, CD150 and CD34 expression.

Following *S. typhimurium* infection, to confirm BM macrophages were depleted the number of BM macrophages were assessed using flow cytometry. There was a significant decrease in the number of BM macrophages in the *S. typhimurium* and clodronate treated animals compared to *S. typhimurium* alone (Figure 4.31).
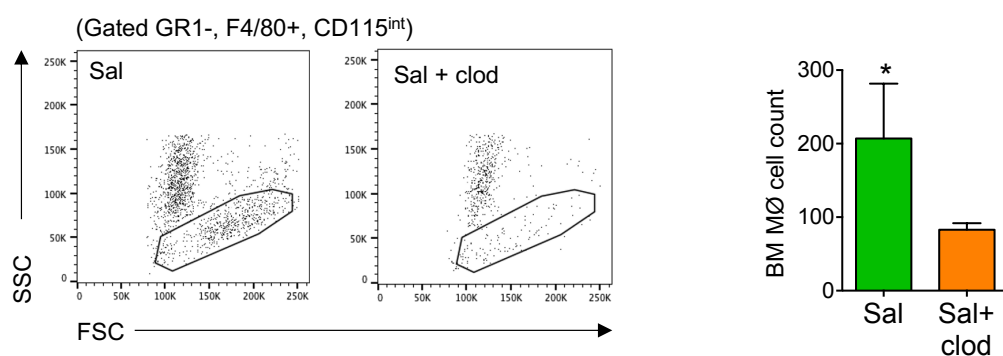
Figure 4.31. Bone marrow macrophages are depleted with clodronate liposomes.
C57BL/6J mice were injected with clodronate liposomes for 3 days prior to *S.typhimurium* infection for 72 hours. The mice were sacrificed and the bone marrow extracted and analysed for GR1, CD115, F4/80 expression. Relative macrophage cell count of *S.typhimurium* infected mice verses clodronate and *S.typhimurium* mice. Data shown are means ± SD of 4 mice in each group *p<0.05

Next, to determine if the absence of macrophages in the BM caused a decrease in ROS in the HSPC populations following infection, ROS levels were measured using the DCF assay. Increases in ROS levels in the LSK, HSC, ST-HSC and LT-HSC were shown to be inhibited in clodronate treated animals inoculated with *S.typhimurium* compared to control (non-clodronate treated) *S.typhimurium* inoculated animals (Figure 4.32).
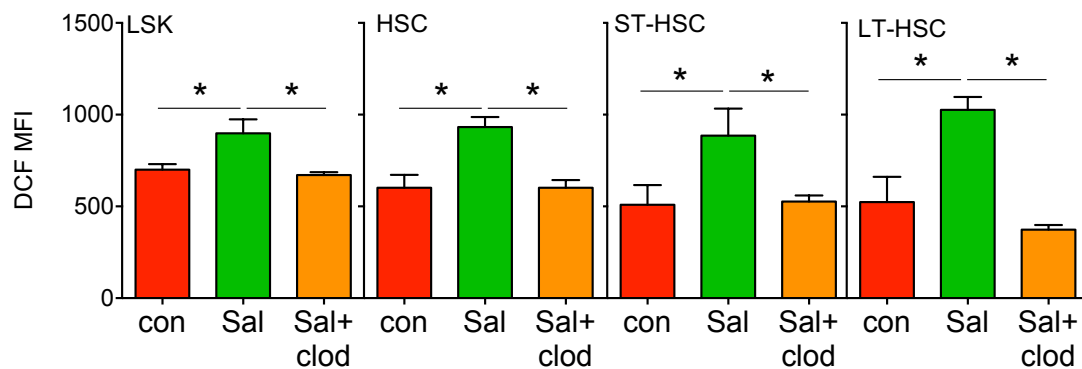
Figure 4.32. Macrophage depletion inhibits HSPC ROS increase in response to infection.
C57BL/6J mice were injected with clodronate liposomes for 3 days prior to *S.typhimurium* infection for 72 hours. The mice were sacrificed and the bone marrow extracted and analysed for H2DCFDA (DCF), Sca 1, CD117, CD48, CD150 and CD34 expression to analyse ROS in specific populations n=4 each group. Data shown are means ± SD *P < 0.05

Furthermore, depletion of macrophages inhibited the *S.typhimurium* elicited increase in mitochondrial content within the LSK, HSC, ST-HSC and LT-HSC populations (Figure 4.33).
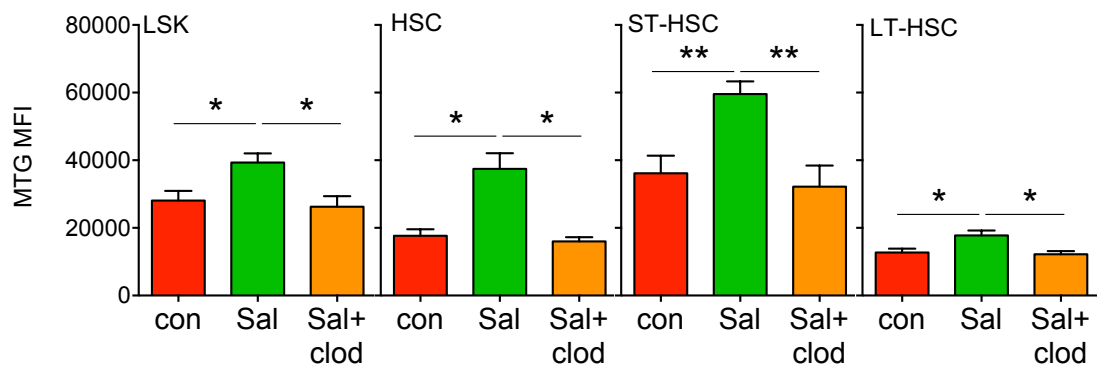
Figure 4.33. Macrophage derived ROS coordinates mitochondrial content increase in the HSC in response to infection.
C57BL/6J mice were injected with clodronate liposomes for 3 days prior to *S.typhimurium* infection for 72 hours. The mice were sacrificed and the bone marrow extracted and analysed for Mitotracker green (MTG), Sca 1, CD117, CD48, CD150 and CD34 expression to analyse mitochondrial content in specific populations n=4 in each group. Data shown are means ± SD *P < 0.05 **P < 0.01

Figure 4.34 confirms an significant increase in cell number of the LSK, HSC, ST-HSC and LT-HSC populations following *S.typhimurium* infection. However, this increase in cell number was not observed in the clodronate treated animals inoculated with *S.typhimurium* (Figure 4.34)*.*
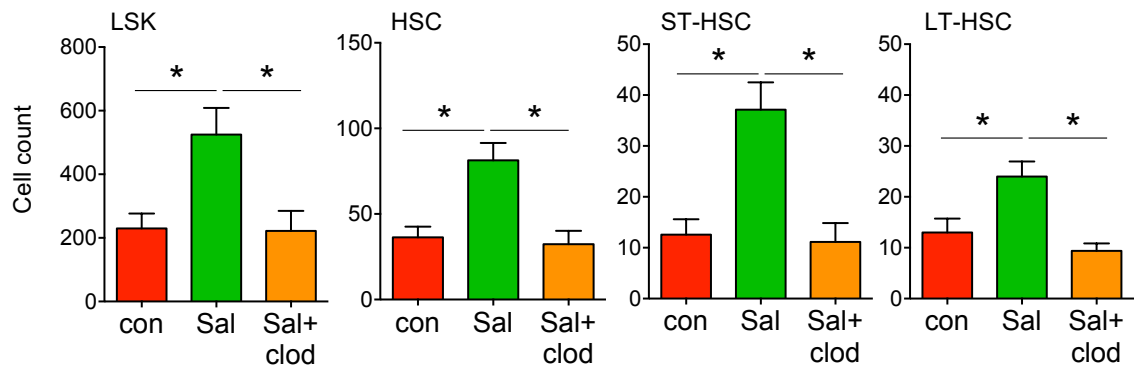
Figure 4.34. Macrophages coordinate HSCs expansion in response to infection.
C57BL/6J mice were injected with clodronate liposomes for 3 days prior to S.typhimurium infection for 72 hours. The mice were sacrificed, the bone marrow extracted and analysed for Sca 1, CD117, CD48, CD150 and CD34 expression to analyse cell number. n=4 in each group. Data shown are means ± SD *P < 0.05

Overall, these data indicate the increase in NOX2 derived superoxide following infection is generated by macrophages and results in transfer of mitochondrial DNA to the HSC. Without macrophages, HSCs do not have an increased ROS and mitochondrial content following *S.typhimurium* infection, limiting the expansion of the HSC.

4.6 Gap junctions regulate the movement of mitochondria from the BMSC to the HSC during infection

I next aimed to establish the mechanism by which mitochondria move from the BMSC to the HSC during infection. Previous literature describing mitochondrial transfer have shown the most commonly reported mechanism of transfer is via TNTs (362). Therefore, to assess if TNTs were facilitating the mitochondrial transfer to the HSCs, I used the TNT inhibitor, Cytochalasin B (CytoB). The maximum dose of intraperitoneal CytoB tolerated was selected to inhibit the formation of TNTs (363). First, C57BL/6J mice were pre-treated with CytoB for 1 hour before treatment with LPS for 2 hours. The mice were sacrificed, and the BM was extracted and assessed by flow cytometry (Figure 4.35A). Figure 4.35B shows LPS caused a significant increase in mitochondrial mass within the LSK, HSC, ST-HSC and LT-HSC populations. Pre-treatment with CytoB did not inhibit the LPS elicited increase in mitochondrial mass. There was a significant increase in mitochondrial content observed in the HSPC populations from animals treated with CytoB and LPS compared to the control animals (Figure 4.35B). It was also observed treatment with CytoB prior to LPS did not inhibit the expansion of the HSPC populations (Figure 4.35C). Taken together, these data suggest TNTs do not directly regulate the movement of mitochondria to the HSC during infection. However, it is not clear if the dose of the inhibitor chosen was sufficient enough to inhibit the TNT's.
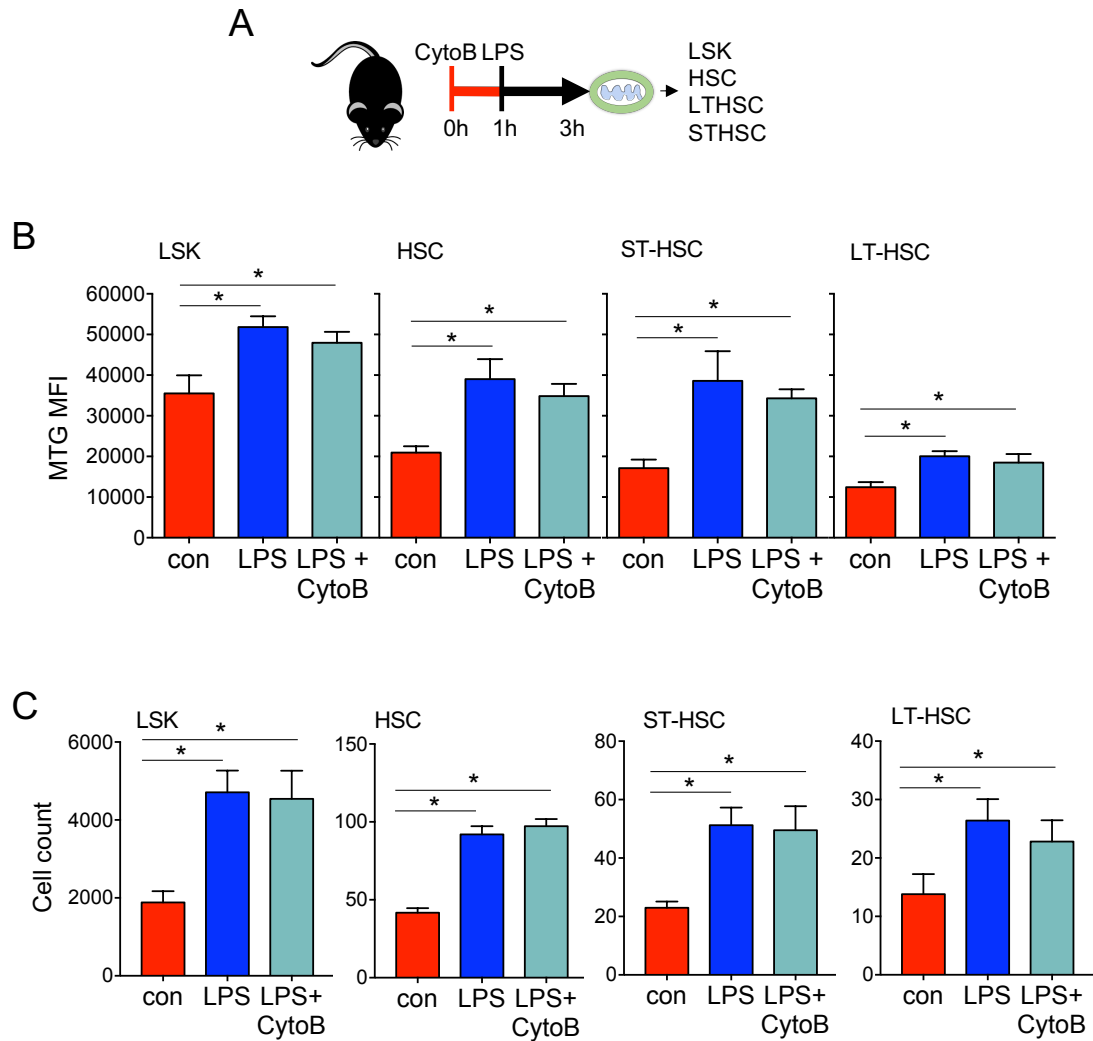
Figure 4.35. Cytochalasin B does not inhibit mitochondrial content increase after LPS treatment.
(A) C57BL/6J mice were pre-treated with 25 mg/kg cytochalasin B (CytoB) for 1 hour before treatment with 1 mg/kg LPS for 2 hours. The animals were sacrificed, the bone marrow was extracted stained with a panel of antibodies and Mitotracker green (MTG). (B) Mitochondrial content (MTG mean fluorescence intensity (MFI)) in specific LSK, HSC, ST-HSC and LT-HSC populations n=5 (C) Cell count of LSK, HSC, ST-HSC and LT-HSC populations n=5 in each group. Data shown are means ± SD *P < 0.05

It has also been reported that intracellular mitochondria transfer can occur through gap junctions (364). To investigate if gap junctions mediate mitochondrial transfer to the HSCs in response to LPS I used the gap junction inhibitor carbenoxolone (CBX). C57BL/6J mice were pre-treated with CBX for 1 hour before treatment with LPS for 2 hours. The mice were sacrificed, and the BM was extracted and assessed by flow cytometry (Figure 4.36A). Pre-treatment with CBX led to reduced mitochondrial content in the LSK, HSC, ST-

HSC and LT-HSC populations compared to LPS treatment alone (Figure 4.36B). Moreover, pre-treatment with CBX inhibited the LPS induced increase in LSK, HSC, ST-HSC and LT-HSC cell number (Figure 4.36C).
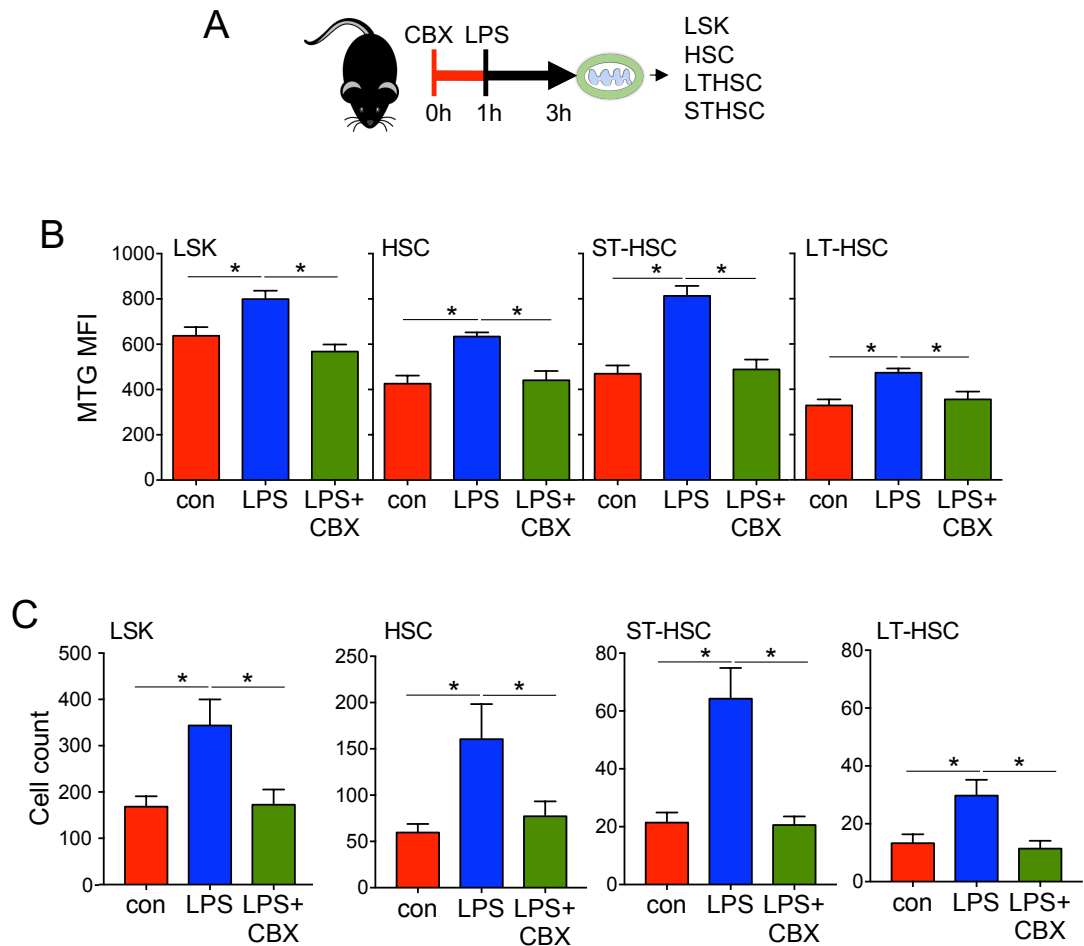
Figure 4.36. Carbenoxolone inhibits mitochondrial content increase after LPS treatment.
(A) C57BL/6J mice were pre-treated with 50 mg/kg carbenoxolone (CBX) for 1 hour before treatment with 1 mg/kg LPS for 2 hours. The animals were sacrificed, the bone marrow was extracted stained with a panel of antibodies and Mitotracker green (MTG). (B) Mitochondrial content (MTG mean fluorescence intensity (MFI)) in specific LSK, HSC, ST-HSC and LT-HSC populations n=5 (C) Cell count of LSK, HSC, ST-HSC and LT-HSC populations n=5 in each group. Data shown are means ± SD *P < 0.05

To determine the functional consequences of the inhibition of mitochondrial content increase caused by the CBX, C57BL/6J mice were treated with control PBS or LPS for 2 hours. The animals were sacrificed, and the BM was extracted and analysed for mitochondrial potential by flow cytometry. Figure

4.37 shows a significant decrease in mitochondrial potential in the CBX and LPS treated LSKs, HSCs and ST-HSCs, compared to the LPS alone. There were no observed changes in mitochondrial potential in the LT-HSCs (Figure 4.37).
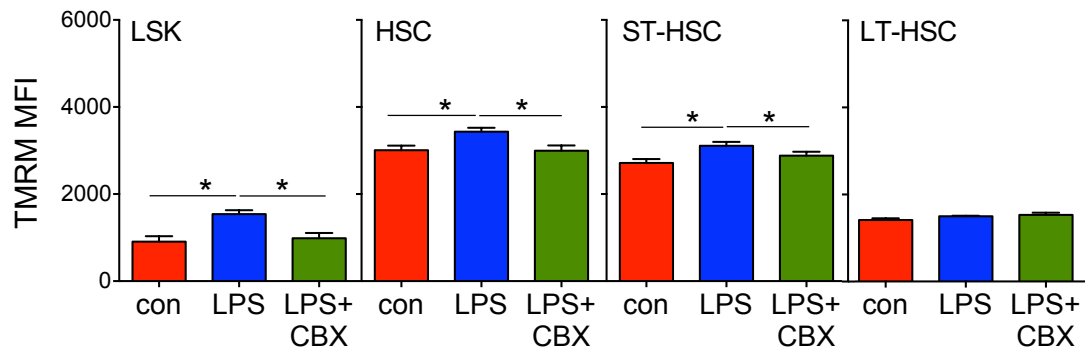
Figure 4.37. Carbenoxolone inhibits increase in mitochondrial potential after LPS treatment.
C57BL/6J mice were pre-treated with 50 mg/kg carbenoxolone (CBX) for 1 hour before treatment with 1 mg/kg LPS for 2 hours. The animals were sacrificed, the bone marrow was extracted, stained with a panel of antibodies and Tetramethylrhodamine, methyl ester (TMRM) to assess mitochondrial health (TMRM mean fluorescence intensity (MFI)) in specific LSK, HSC, ST-HSC and LT-HSC populations n=5 in each group. Data shown are means ± SD *P < 0.05

To confirm that gap junctions are involved in the intercellular communication between BMSCs and HSCs, I used the mobile dye, calcein (365). Calcein enters the cell via gap junction therefore, I stained BMSC with calcein and then cultured these with lineage negative cells. The cocultures were treated with CBX or vehicle and then treated with H_2O_2. Results show there was an increase in calcein dye uptake into the lineage negative cells cultured with BMSC in the presence of H_2O_2 compared to the control treated cultures. Moreover, this uptake of calcein was reduced when the coculture were treated with the gap junction inhibitor CBX (Figure 4.38).
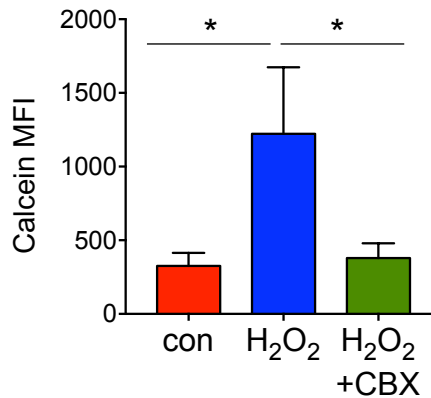
Figure 4.38. Carbenoxolne inhibits the transfer of calcein from BMSC to lineahe negative cells following H_2O_2 treatment.
mBMSC were pretreated with calcein for 30 minutes. Lineage negative cells were then cultured with the calcein stained BMSC and treated with 10 μM H_2O_2 or 50 μM carbenoxolone (CBX) and 10 μM H_2O_2 for 24 hours. The lineage negative cells were removed and analysed for calcein using flow cytometry and mean fluorescence intensity (MFI). *P < 0.05

To determine if CBX had an effect on mitochondrial DNA transfer I used the coculture assay which took advantage of the SNP differences in the mtDNA described in Figure 4.17 and 4.18. Figure 4.39 shows there is a significant decrease in transfer of mtDNA to the lineage negative cells when cultured in the presence of CBX and H_2O_2 compared to H_2O_2 alone.
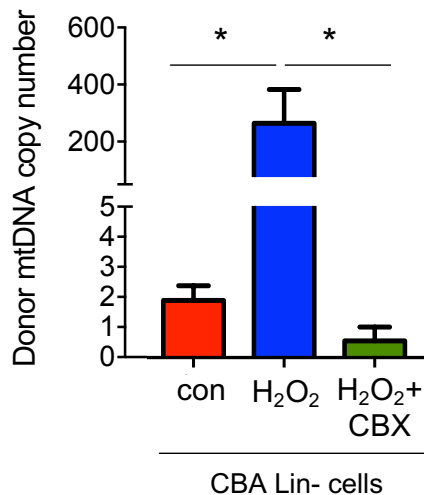
Figure 4.39. Mitochondrial DNA transfer from the BMSC is inhibited by carbenoxolone.
CBA lineage-negative cells (recipient) were cocultured with PepCboy BMSCs (donor) with 10 μM H_2O_2 or carbenoxolone and 10 μM H_2O_2 for 24 hours. The lineage negative cells were removed and analysed for PepCboy SNP mtDNA in CBA lineage negative cells by TaqMan PCR using ND3 probes. PepCboy donor mtDNA copy number in CBA lineage negative cells. CBA gDNA was used to standardise mtDNA copy number. Data shown are means ± SD *P < 0.05

Next, to visualise the block on mitochondrial transfer from the BMSC to the HSPCs, primary mBMSC were transduced with an rLV.EF1.mCherry lentivirus for stable incorporation of mCherry protein tagged mitochondria. Lineage negative cells were stained with CD45-APC and cultured on the mBMSCs for 24 hours with H_2O_2 or H_2O_2 and the CX43 memetic peptide Gap27. The cells were fixed and stained with CX43 (green) and DAPI (blue) and imaged using fluorescence microscopy (Figure 4.40A). BMSC labelled mitochondria transfer to the lineage negative cells was inhibited in the presence of H_2O_2 and Gap27, quantified by the acquisition of the mCherry fluorescence in the lineage negative cells (Figure 4.40B).
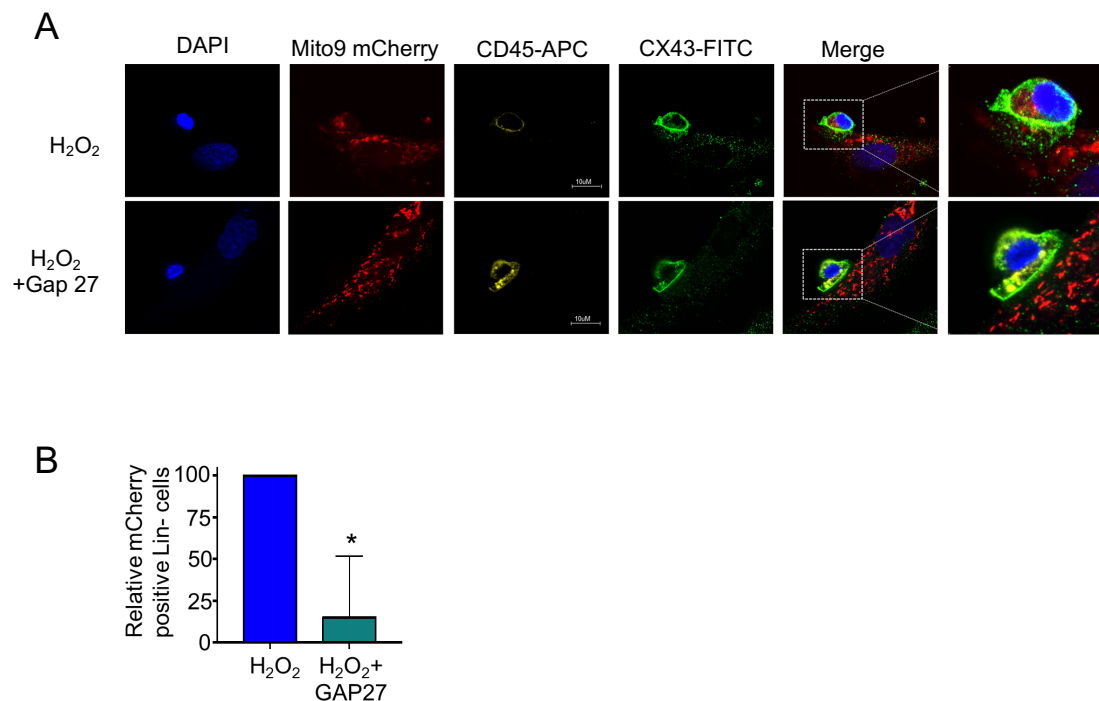
Figure 4.40. Gap junctions regulate mitochondrial transfer from BMSCs to HSCs.
(A) Representative confocal microscopy images of lineage negative cells stained with membrane CD45-APC (yellow) cultured with mBMSCs transduced with rLV.EF1.mCherry-Mito-9 (mitochondria (red)) in cocultured with 10 μM H_2O_2 with and without pretreatment with GAP27 (100 μM). The cells were fixed and stained with DAPI (blue) and CX43 (green) (magnification 63X) (B) Quantification of rLV.EF1.mCherry-Mito-9 in lin- cells from images shown taken from 3 independent experiments and 20 lineage cells from each experiment. Data shown are means ± SD *P < 0.05

To determine if mitochondrial transfer was regulated by CX43 gap junctions I used the coculture assay which took advantage of the SNP differences in the mtDNA described in Figure 4.17 and 4.18. There is a significant decrease in mtDNA transfer to the lineage negative cells when cultured in the presence of GAP27 and H_2O_2 compared to H_2O_2 alone (Figure 4.41). Taken together, using methods to inhibit gap junctions, these results show CX43 gap junctions regulate mitochondrial transfer from the BMSC to the HSC populations in models of acute infection.
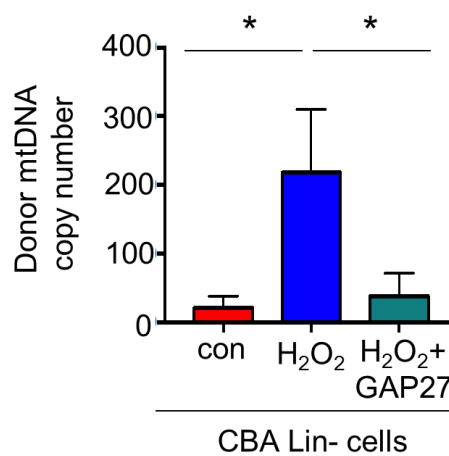
Figure 4.41. Mitochondrial DNA transfer from the BMSC is inhibited by CX43 blocking peptide GAP27.
CBA lineage-negative cells (recipient) were cocultured with PepCboy BMSCs (donor) with 10 μM H_2O_2 alone or 100 μM GAP27 and 10 μM H_2O_2 for 24 hours. The lineage negative cells were removed and analysed for PepCboy SNP mtDNA in CBA lineage negative cells by TaqMan PCR using ND3 probes. Donor PepCboy mtDNA copy number in CBA lineage negative cells. CBA gDNA was used to standardise mtDNA copy number. Data shown are means ± SD *P < 0.05

4.7 ROS activates phosphorylation of AKT to enable mitochondrial transfer by PI3K

Increased ROS levels have previously been shown to be associated with increased signalling of phosphoinositide-3,4,5-trisphosphate (PIP_3) and subsequent activation of phosphoinositide 3-kinase (PI3K) (366, 367). The PIP_3 also activates downstream signalling of the protein kinase AKT (pAKT) which is vital for cell survival (368). Therefore, I next quantified AKT

phosphorylation (S473) in the HSC after treatment with *S.typhimurium* (72 hours) or LPS (2 hours). AKT phosphorylation was significantly elevated in the LSK, HSC, ST-HSC and LT-HSC population after both *S.typhimurium* infection and LPS treatment compared to the untreated control (Figure 4.42A-C).
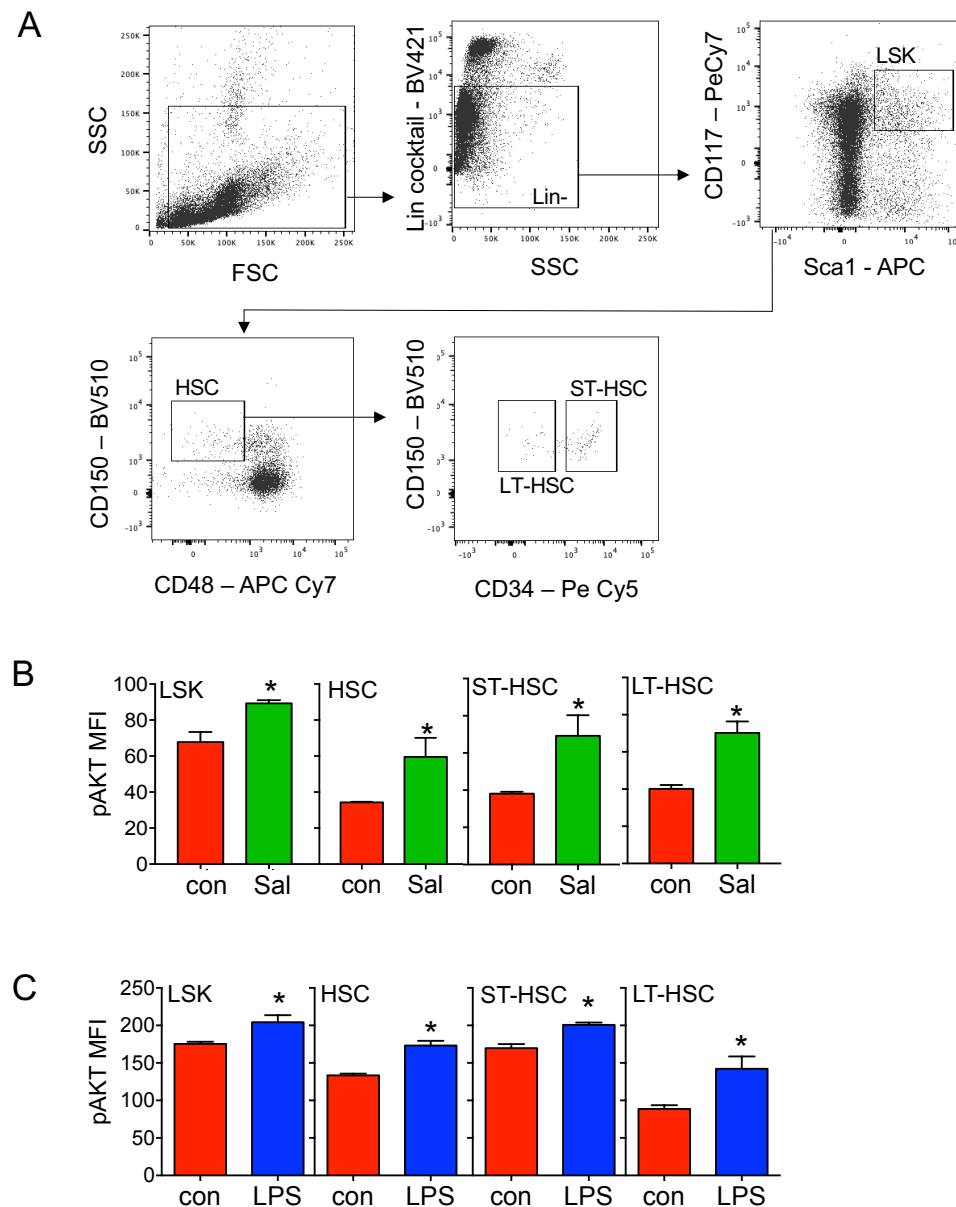
Figure 4.42. pAKT expression is elevated in the haematopoietic stem and progenitor populations after *S.typhimurium* infection and LPS treatment. (A) Gating strategy used is shown (B) C57BL/6J mice were infected with *S.typhimurium* (Sal) for 72 hours, the animals were sacrificed, the bone marrow was extracted and stained with a panel of antibodies. The cells were then fixed and stained with pAKT-PE and assessed by flow cytometry n=6. (C) C57BL/6J mice were treated with LPS for 2 hours, the animals were sacrificed, the bone marrow was extracted and stained with a panel of antibodies. The cells were then fixed and stained with pAKT-PE and assessed by flow cytometry n=5 in each group. Data shown are means ± SD *P < 0.05

Next, to examine the effects of infection on AKT phosphorylation in the BMSC *in vivo* C57BL/6J mice were treated with LPS for 2 hours or infected with *S.typhimurium* for 72 hours. The mice were sacrificed, and the BMSCs were analysed for pAKT expression using flow cytometry. pAKT was significantly increased in the BMSC after both *S.typhimurium* and LPS treatment compared to the untreated control (Figure 4.43A-C).
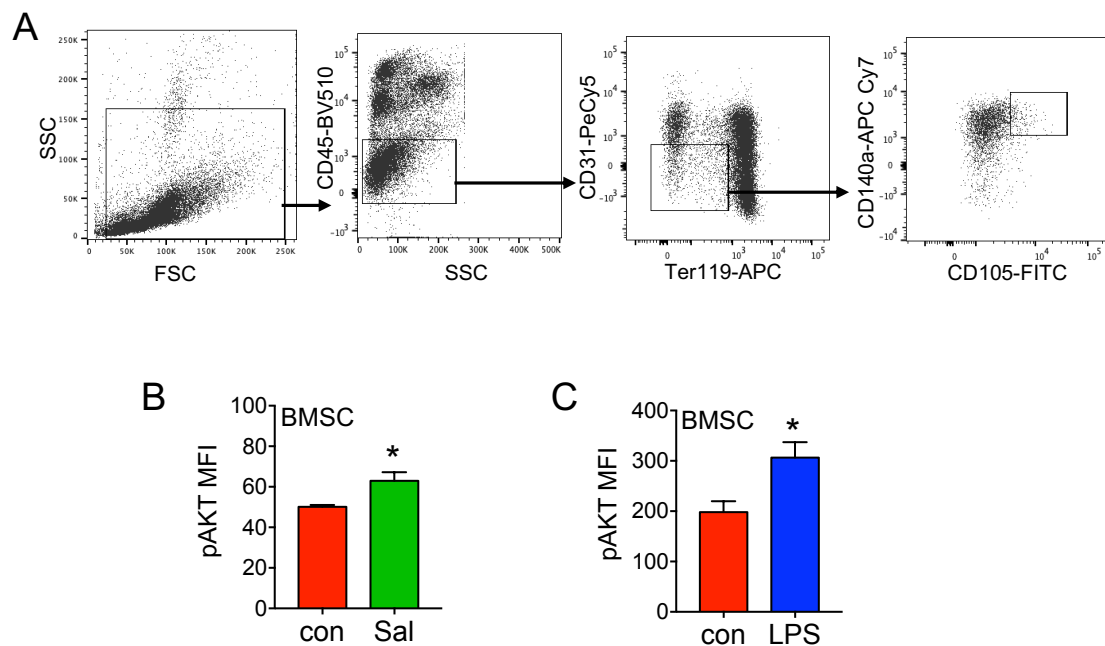
Figure 4.43. pAKT expression is elevated in the BMSC after *S.typhimurium* infection and LPS treatment.
(A) Gating strategy used is shown (B) C57BL/6J mice were infected with *S.typhimurium* (Sal) for 72 hours, the animals were sacrificed, the bone marrow was extracted and stained with a panel of antibodies to analyse the BMSC population. The cell were then fixed and stained with pAKT-PE and assessed by flow cytometry n=6. (C) C57BL/6J mice were treated with LPS for 2 hours, the animals were sacrificed, the bone marrow was extracted and stained with a panel of antibodies to analyse the BMSC population. The cell were then fixed and stained with pAKT-PE and assessed by flow cytometry n=5 in each group. Data shown are means ± SD *P < 0.05

Next, to confirm increased ROS causes AKT phosphorylation *in vivo* C57BL/6J mice were treated with BSO for 2 hours. The mice were sacrificed, and the HSPCs were analysed for pAKT expression using flow cytometry (Figure 4.44A). Figure shows pAKT was significantly increased in the LSK HSC, ST-HSC after BSO treatment compared to the untreated control.
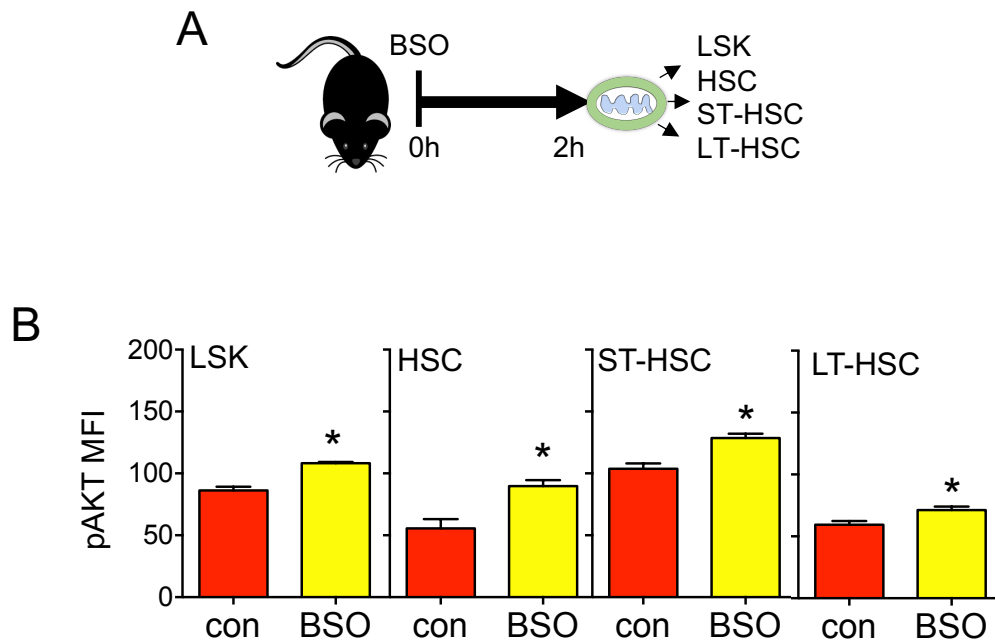
Figure 4.44. BSO induces an increase in pAKT expression in the haematopoietic stem and progenitor populations.
(A) C57BL/6J mice were treated with 100 mg/kg L-buthionine-sulfoximine (BSO) for 2 hours, the animals were sacrificed, the bone marrow was extracted stained with a panel of antibodies and pAKT-PE. (B) pAKT expression (pAKT (mean fluorescence intensity (MFI)) in the specific populations of all animals examined. n=5 in each group. Data shown are means ± SD *P < 0.05

To investigate if ROS also induced pAKT in the BMSC C57BL/6J mice were treated with 100 mg/kg BSO for 2 hours. pAKT was significantly increased in the BMSC after BSO treatment compared to the control untreated mice (Figure 4.45).
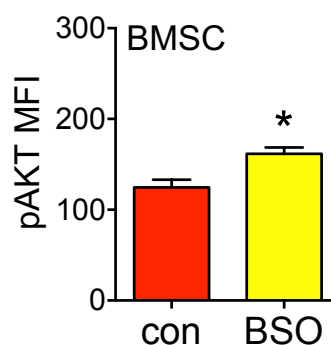
Figure 4.45. BSO induces an increase in pAKT expression in the BMSC.
(A) C57BL/6J mice were treated with 100 mg/kg L-buthionine-sulfoximine (BSO) for 2 hours, the animals were sacrificed, the bone marrow was extracted stained with a panel of antibodies and pAKT-PE. (B) pAKT expression (pAKT (mean fluorescence intensity (MFI)) in all animals examined. n=5 in each group. Data shown are means ± SD *P <0.05

Next, to confirm the increase in phosphorylation of AKT in the HSC I cocultured BMSC and lineage negative cells in the presence of H_2O_2 and assessed phosphorylation of AKT (pAKT-S473) by western blotting. Figure 4.46 shows an increase in AKT phosphorylation in the lineage negative cells when cultured with BMSC in the presence of H_2O_2.
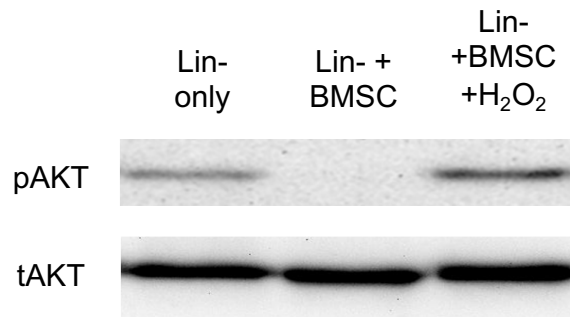
Figure 4.46. pAKT expression is elevated in the lineage negative cells after coculture with BMSC with H_2O_2.
Western bot analysis of lineage negative (lin-) cells co-cultured with mBMSCs. The co-culture was treated with 10 μM H_2O_2 for 30 minutes, the lin- cells were removed and analysed for pAKT expression.

AKT is phosphorylated as part of the PI3K pathway, where PI3K is converted into PIP_3 which binds to AKT (369, 370). AKT is then phosphorylated by mTOR (371) or DNA-dependent protein kinase (372) which initiates full AKT activity. To determine if PI3K had an effect on mitochondrial transfer I used the PI3K delta (PI3Kδ) inhibitor Cal 101. I used the coculture assay which took advantage of the SNP differences in the mtDNA described in Figure 4.17 and 4.18. Figure 4.47 shows there is a significant decrease in mtDNA transfer to the lineage negative cells when cultured in the presence of Cal 101 and H_2O_2 compared to H_2O_2 alone.
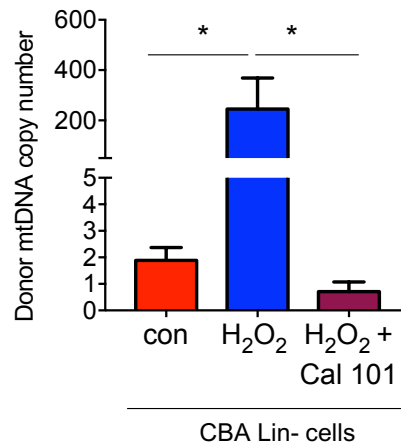
Figure 4.47. Mitochondrial DNA transfer from the BMSC is inhibited by Cal 101.
CBA lineage-negative cells (recipient) were cocultured with PepCboy BMSCs (donor) with 10 µM H_2O_2 or 25 µM Cal 101 and 10 µM H_2O_2 for 24 hours. The lineage negative cells were removed and analysed for PepCboy SNP mtDNA in CBA lineage negative cells by TaqMan PCR using ND3 probes. Donor PepCboy mtDNA copy number in CBA lineage negative cells. CBA gDNA was used to standardise mtDNA copy number. Data shown are means ± SD *P < 0.05

To assess if PI3K inhibition was involved with gap junctions regulation I used the mobile dye, calcein (365). Consistent with previous results, in the presence of H_2O_2 there was an increase in calcein dye uptake into the lineage negative cells compared to the control. However, this uptake of calcein was reduced when the coculture was treated with the PI3Kδ inhibitor Cal 101 prior to H_2O_2 addition (Figure 4.48).
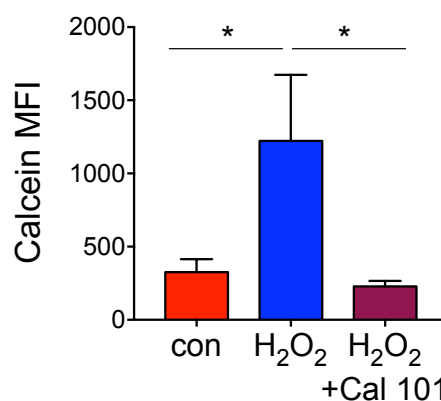
Figure 4.48. Cal 101 inhibits the increase in calcein expression observed following LPS treatment.
mBMSC were pretreated with calcein for 30 minutes. Lineage negative cells were then cultured with the calcein stained BMSC and treated with 10 µM H_2O_2 and 25 µM Cal 101 or 10 µM H_2O_2 alone for 24 hours. The lineage negative cells were removed and analysed for calcein using flow cytometry and mean fluorescence intensity (MFI). *P < 0.05

To investigate if PI3K mediates mitochondrial content increase in the HSCs in response to LPS, C57BL/6J mice were pre-treated with Cal 101 for 1 hour before treatment with LPS for 2 hours. The mice were sacrificed, and the BM was extracted and assessed by flow cytometry (Figure 4.49A). Pre-treatment with Cal 101 led to a reduced mitochondrial content in the LSK, HSC, ST-HSC and LT-HSC populations compared to LPS treatment alone (Figure 4.49B).
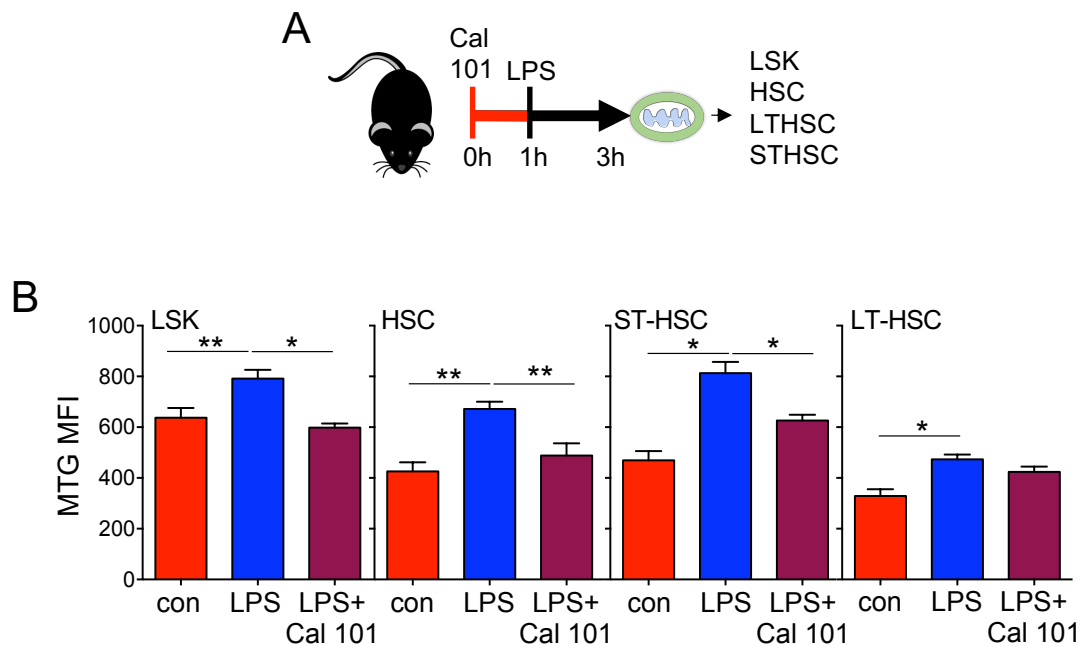
Figure 4.49. Cal 101 inhibits mitochondrial content increase after LPS treatment.
(A) C57BL/6J mice were pre-treated with 30 mg/kg Cal 101 for 1 hour before treatment with 1 mg/kg LPS for 2 hours. The animals were sacrificed, the bone marrow was extracted stained with a panel of antibodies and Mitotracker green (MTG). (B) Mitochondrial content (MTG mean fluorescence intensity (MFI)) in specific LSK, HSC, ST-HSC and LT-HSC populations n=5 in each group. Data shown are means ± SD *P < 0.05 **P < 0.01

Finally, to determine the functional consequences of the inhibition of mitochondrial content increase caused by the Cal 101, C57BL/6J mice were treated with control PBS or LPS for 2 hours. The animals were sacrificed, and the BM was extracted and analysed for mitochondrial potential by flow cytometry. Figure 4.50 shows a significant decrease in mitochondrial potential

in the Cal 101 and LPS treated LSK, HSC and ST-HSCs, compared to the LPS alone. There were no observed changes in mitochondrial potential in the LT-HSC (Figure 4.50). Taken together, these data show PI3K signaling mediates transfer of mitochondrial from BMSCs to HSCs via a pAKT dependent mechanism.
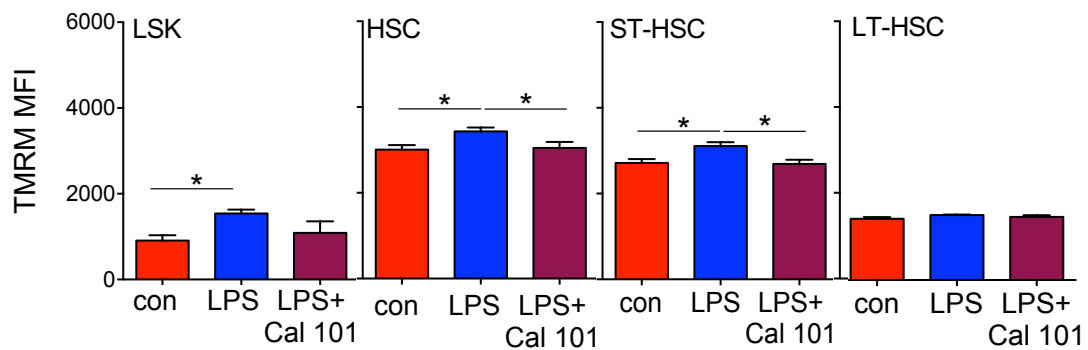
Figure 4.50. Cal 101 inhibits mitochondrial membrane potential increase after LPS treatment.
(A) C57BL/6J mice were pre-treated with 30 mg/kg Cal 101 for 1 hour before treatment with 1 mg/kg LPS for 2 hours. The animals were sacrificed, the bone marrow was extracted stained with a panel of antibodies and Mitotracker green (MTG). (B) Mitochondrial content (MTG mean fluorescence intensity (MFI)) in specific LSK, HSC, ST-HSC and LT-HSC populations n=5 in each group. Data shown are means ± SD *P < 0.05

4.8   Summary

In this chapter I have shown that mitochondria are transferred from the BMSC to the HSC in response to infection. Moreover, I have identified mitochondria move via gap junctions and this is stimulated by NOX2 superoxide, causing oxidative stress in HSC and the BMSC. This elevated superoxide in the BM is generated by the macrophages and facilitates mitochondrial movement to the HSC. Finally, I have identified that the increase in superoxide regulates PI3K activation and subsequent phosphorylation of AKT which drives transfer of mitochondria from the BMSC to the HSC during acute infection.

5 Enhanced free fatty acid uptake via CD36 promotes a metabolic switch to β-oxidation by haematopoietic stem cells in response to bacterial infection

5.1 Introduction

In chapter 3 and 4 I have shown that mitochondria are transferred from the BMSC to the HSC in response to acute infection. I next wanted to examine what fuels the HSCs TCA cycle in response to infection. The TCA cycle integrates many fuels sources including fatty acids, glucose and glutamine to generate ATP and functions as an assembly point for cellular respiration and metabolism (373). The HSC is supported by cells of the BM microenvironment and the BM has a high fat content which increases with age (165). Recent studies have shown, metabolic pathways are central in regulating haematopoiesis, and HSC metabolism can determine cell differentiation or maintenance of quiescence (374). Specifically, FAO has been shown to be utilised to aid self-renewal and differentiation in both committed progenitors and the more primitive HSCs (26). Moreover, the inhibition of FAO can reduce stem cell differentiation capacity (26).

In malignant haematopoiesis, several studies have shown fatty acids are key in fuelling leukaemia. A study by Ye *et al.* 2016 showed there is elevated levels of FFA in the serum of leukaemic mice. Moreover, the LSC induced lipolysis in the BMAT to fuel the LSC by FAO (17). A study from our lab group has also shown that FFA are taken up by AML blasts for increased proliferation due to increased β-oxidation (17, 42). Therefore, I hypothesise that the metabolic switch towards β-oxidation dependency in AML originates from the physiological HSC response to stress and HSC take up FFAs in response to infection.

In this chapter, I will examine acquisition of FFAs by HSCs following *S. typhimurium* or LPS infection. Furthermore, I will investigate the mechanisms regulating fatty acid transport to the HSC and immunometabolic consequences following acute bacterial infection.

5.2   *S.typhimurium* infection drives uptake of long chain fatty acids in the HSC

It has previously been shown FFA levels in the serum are elevated in response to infection (375, 376). To determine if FFA were elevated in models of acute bacterial infection C57BL/6J mice were infected with *S.typhimurium* for 72 hours or treated with LPS for 16 hours. The 16-hour LPS time point was chosen as the cells still have an increased mitochondrial content, an IL 6 response and it just after the cells begin to cycle. Figure 5.1 shows there was an increase in serum FFA levels from *S.typhimurium* and LPS treated mice compared to control mice.
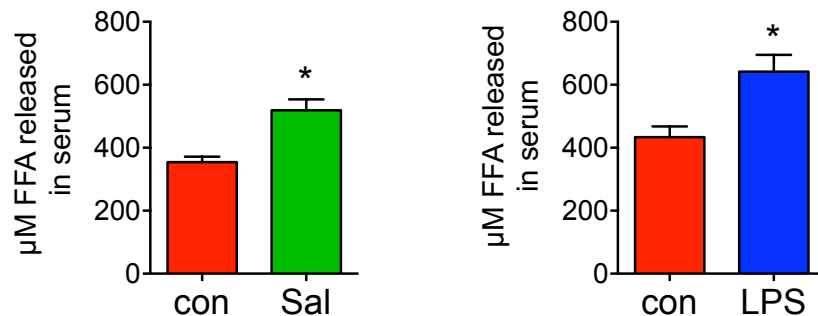
Figure 5.1. Elevated levels of FFA in the serum of *S.typhimurium* and LPS treated mice.
C57BL/6J mice were infected with *S.typhimurium* (Sal) for 72 hours or LPS for 16 hours. Blood was taken from the animals by cardiac puncture and the serum was assessed for levels of FFA. n=5 in each group. Data shown are means ± SD *$P < 0.05$

Next, to investigate if the elevated FFAs following infection were taken up by the haematopoietic cells, I developed a transplant model to track real time fatty acid uptake *in vivo*. PepCboy CD45.1 lineage negative (lin-), CD117 positive (LK) cells were isolated and transduced with a firefly luciferase virus (LK[+FF]). The cells were then transplanted into busulfan treated C57BL/6J CD45.2 animals (Figure 5.2A). Engraftment and transduction of the LK[+FF] cells were monitored using D-luciferin by *in vivo* bioluminescent imaging (Figure 5.2B). 12 weeks post transplantation the CD45.1 LK[+FF] engrafted CD45.2 animals were injected with a probe containing a long chain FFA conjugated to luciferin

molecule (FFA-luc) through a cleavable disulphide bond (Figure 5.2C and D). The probe is stable extracellularly however, once internalised into the cells following lipid uptake, the disulphide bond is cleaved by glutathione. The luciferin molecule reacts with the luciferase and fluorescence can be observed by bioluminescent imaging (377). One week later after the mice had recovered the animals were injected with LPS for 16 hours. Following LPS treatment, there was activation of luciferase in the BM compartment signifying long chain FFA are taken up by haematopoietic cells in response to LPS (Figure 5.2 C and D).
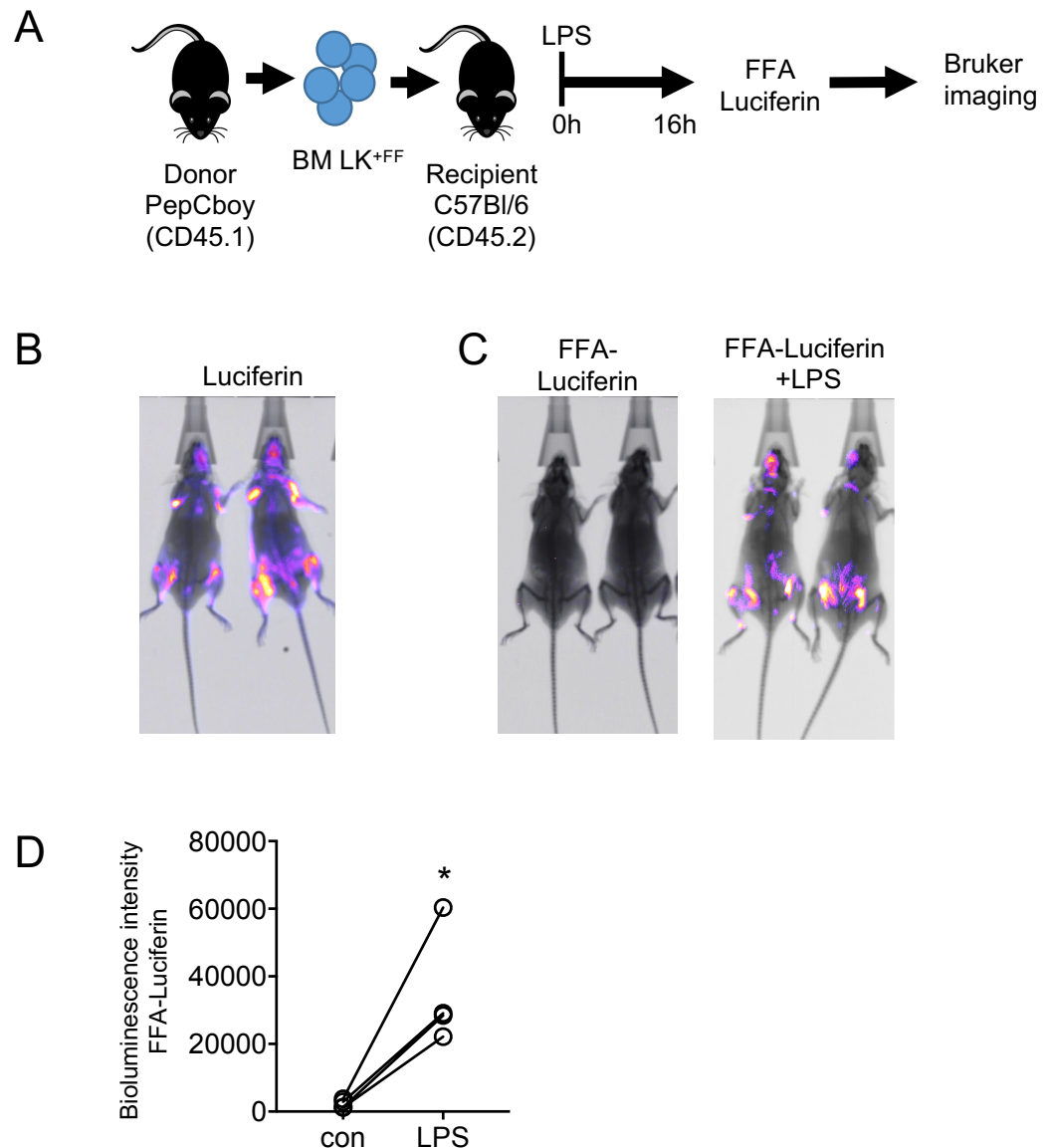
Figure 5.2. Treatment with LPS drives fatty acid uptake in the haematopoietic compartment.
(A) Schematic diagram of the experimental design. PepCboy CD45.1 lineage negative, CD117 positive (LK) cells were isolated and transduced with a firefly luciferase virus (LK^{+FF}) and transplanted into CD45.2 animals. (B) Mice were bioluminescence imaged using luciferin to confirm engraftment. (C) Mice were injected with control PBS for 16 hours then treated with FFA-SS-luc and imaged using bioluminescence (FFA-luciferin). One-week later mice were injected LPS for 16 hours then treated with FFA-SS-luc and imaged using bioluminescence (FFA-luciferin+LPS). Representative images of control and LPS treated mice. (D) Densitometry of the bioluminescent images in (C) to determine fluorescence intensity in vehicle and LPS treated animals. n=4 in each group. Data shown are means ± SD *P < 0.05

To assess the specific HSPC populations with increased lipid content during infection, C57BL/6J mice were infected with *S.typhimurium* for 72 hours. The HSPC populations were analysed for lipid content with a panel of cell surface antibodies and Bodipy 493/503 using flow cytometry (Figure 5.3A). This included all colour compensations and the gating strategy to isolate the specific cell populations of interest is shown in Figure 5.3B. All gating was determined using fluorescence minus one controls.
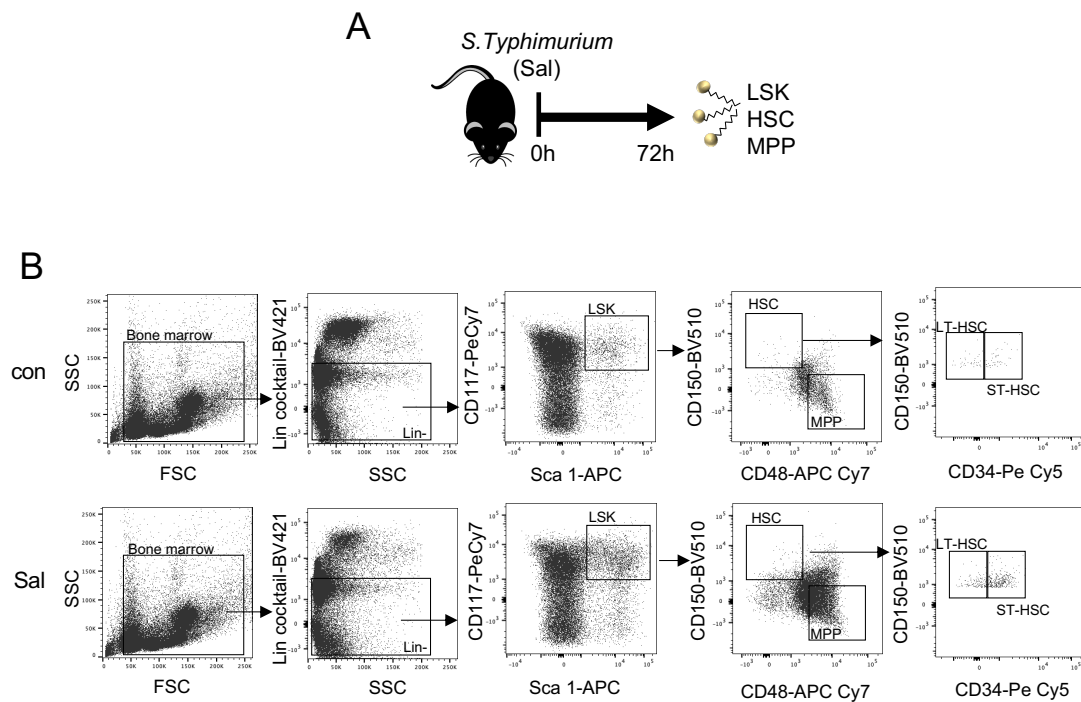
Figure 5.3. Gating strategy for mouse Lin-, LSK, HSC, MPP, ST-HSC and LT-HSC.
(A) C57BL/6J mice were infected with *S.typhimurium* (Sal) for 72 hours, the animals were sacrificed, and the bone marrow was extracted. The cells were stained with a panel of antibodies to analyse specific Lin-, LSK, HSC, MPP, ST-HSC and LT-HSC populations. (B) The gating strategy used is shown.

Figure 5.4 shows that the LSK (Lin- Sca 1+ CD117+), MPPs (Lin- Sca 1+ CD117+ CD150+ CD48+), total HSCs (Lin- Sca 1+ CD117+ CD150+ CD48-), ST-HSCs (Lin- Sca 1+ CD117+ CD150+ CD48- CD34+) and LT-HSCs (Lin- Sca 1+ CD117+ CD150+ CD48- CD34-) (68) populations within the BM all have an increased intracellular neutral lipid staining after *S.typhimurium* infection compared to the control non-infected animals.
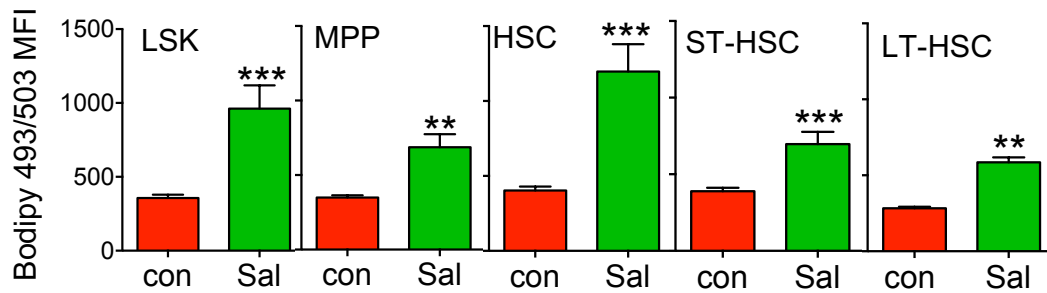
Figure 5.4. *S.typhimurium* induces an increase in lipid content in the haematopoietic populations.
C57BL/6J mice were infected with *S. typhimurium* (Sal) for 72 hours, the animals were sacrificed, the bone marrow was extracted and stained with a panel of antibodies and Bodipy 493/503 to analyse lipid content (Bodipy 493/503 mean fluorescence intensity (MFI)) in specific Lin-, LSK, HSC, MPP, ST-HSC and LT-HSC populations. n=6 in each group. Data shown are means ± SD **P < 0.01 ***P < 0.001

Similarly, following 16 hours of LPS treatment HSPC populations within the BM have an increased lipid content after treatment with LPS (Figure 5.5).
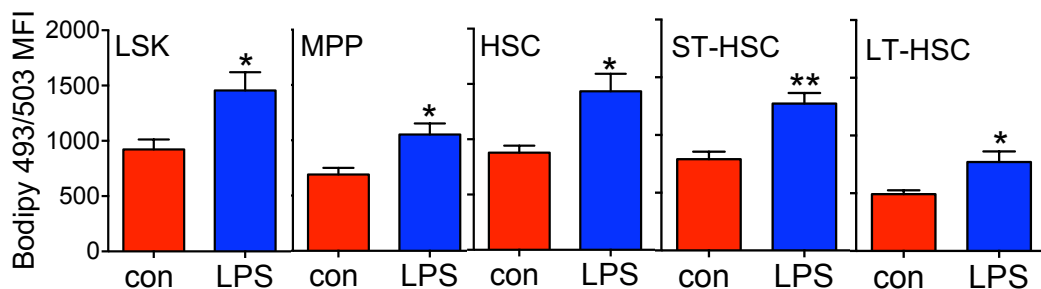
Figure 5.5. LPS induces an increase in lipid content in the haematopoietic populations.
C57BL/6J mice were treated with 1 mg/kg LPS for 16 hours, the animals were sacrificed, the bone marrow was extracted and stained with a panel of antibodies and Bodipy 493/503 to analyse lipid content (Bodipy 493/503 mean fluorescence intensity (MFI)) in specific Lin-, LSK, HSC, MPP, ST-HSC and LT-HSC populations. n=5 Data shown are means ± SD *P <0.05 **P < 0.01

Next, to investigate if the increase in lipid content was due to uptake of FFA, C57BL/6J mice were infected with *S. typhimurium* for 72 hours or treated with LPS for 16 hours. The LK cells were isolated and incubated with Bodipy FL-C12 (a FFA tagged to Bodipy) for 30 minutes. There was an increase in FFA uptake observed in the LK cells from *S.typhimurium* or LPS compared to LKs from untreated mice (Figure 5.6).
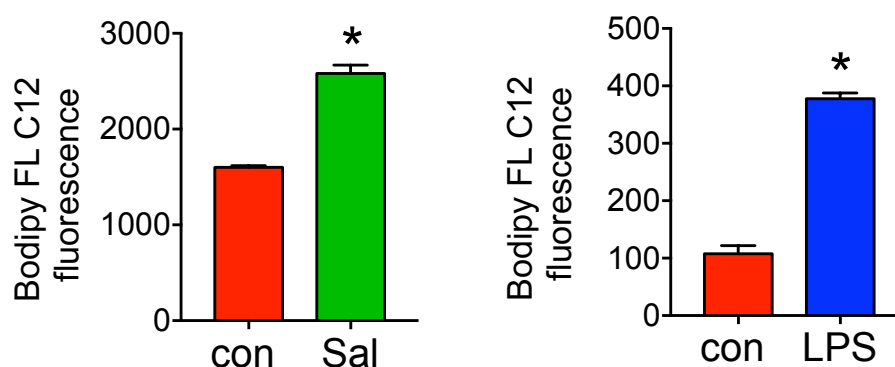
Figure 5.6. LPS and *S.typhimurium* induce an uptake of FFA in the haematopoietic progenitor populations.
C57BL/6J mice were infected with *S.typhimurium* (Sal) for 72 hours or LPS for 16 hours. The animals were sacrificed and the bone marrow extracted. LK cells were isolated and incubated with Bodipy FL-C12 and fluorescence was measured. n=5 in each group Data shown are means ± SD *P < 0.05

To visualise the uptake of FFA LK cells isolated from the BM of control or *S. typhimurium* infected (72 hours) C57BL/6J mice were stained with Bodipy 493/503, Hoechst 33342 and Sca 1-APC membrane stain for 30 minutes and imaged using fluorescence microscopy (Figure 5.7A). LK cells positive for Sca 1-APC membrane stain were then classified as LSKs. LSK cells from *S.typhimurium* infected mice had an increased lipid content quantified by Bodipy 493/503 fluorescence (Figure 5.7B). Taken together these results demonstrates HSPCs take up FFA in response to infection and this leads to an increased lipid content in the cell.

A

Control   S. typhimurium

B
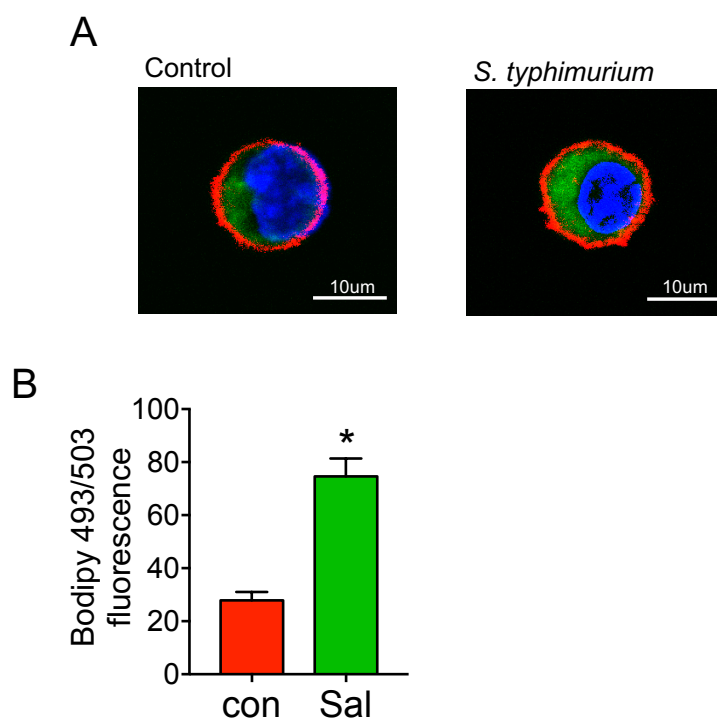
Figure 5.7 *S.typhimurium* infection induces uptake of FFA in LSK cells.
C57BL/6J mice were infected with *S.typhimurium* (Sal) for 72 hours (A)
Representative live cell fluorescent microscopy images of LSK cells isolated from the
mice, Sca 1 membrane stain (red), Bodipy 493/503 (green) and Hoechst 33342
(blue). Data shown are means ± SD of n=5 mice. (B) Quantification of Bodipy 493/503
fluorescence in LSK cells from images shown, 20 LK cells from each mouse in each
condition. Data shown are means ± SD *P < 0.05

5.3   *S.typhimurium* infection increases OCR and dependency on β-oxidation in HSPCs

To understand the metabolic consequences of the increase in FFA in the
HSCs response to infection I used the mitochondrial extracellular flux assay to
measure oxygen consumption. LSKs isolated from *S.typhimurium* (72 hours) or
LPS (16 hours) treated animals had an increased OCR at both basal and
maximal respiration compared to the control LSK cells (Figure 5.8A and B).
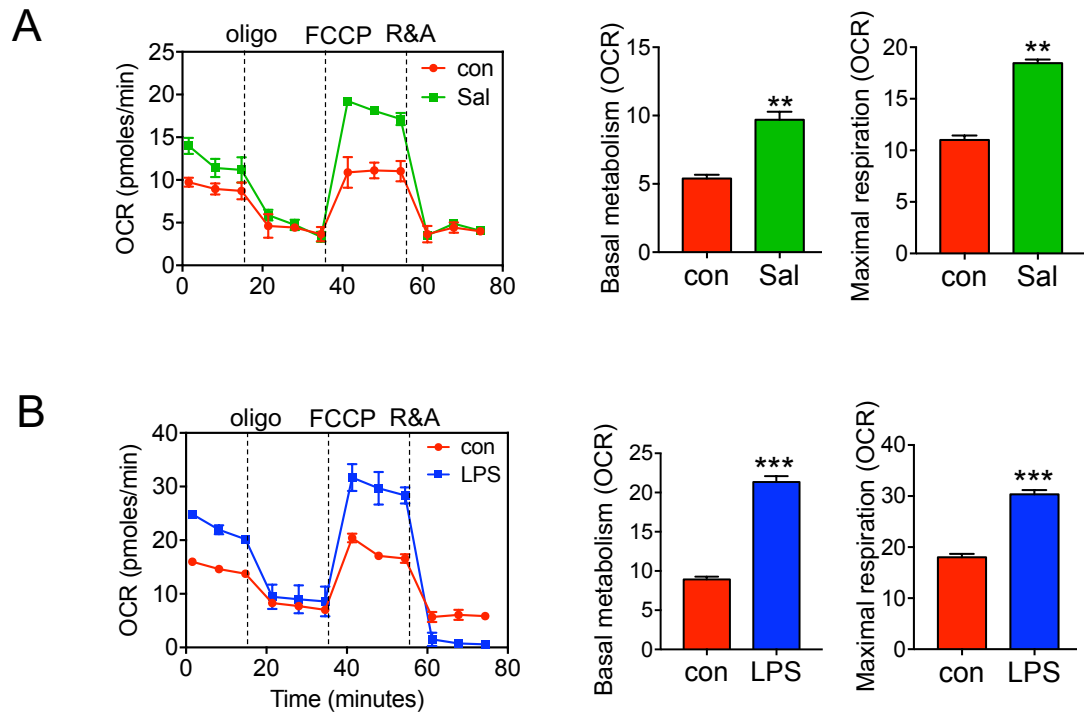
Figure 5.8. LSK have increased OCR levels after LPS treatment or _S.typhimurium_ infection.

(A) C57BL/6J mice were infected with _S.typhimurium_ (Sal) for 72 hours, the animals were sacrificed, the BM was extracted and stained with a panel of antibodies to isolate the LSK population by FACS. Basal (normalised to rotenone) and maximal OCR levels were measured by OCR. n=5 in each group. (B) C57BL/6J mice were treated with PBS or LPS for 2 hours, the animals were sacrificed, the BM was extracted and stained with a panel of antibodies to isolate the LSK population by FACS. Basal (normalised to rotenone) and maximal OCR levels were measured by the extracellular flux assay. n=5 in each group. Data shown are means ± SD **P < 0.01***P < 0.001

To assess the changes in glycolysis after _S.typhimurium_ (72 hours) infection or LPS (16 hours) treatment. I used the extracellular flux assay to analyse ECAR (Figure 5.9A). Whilst there was an increase in basal OCR there was no observed increase in basal glycolysis (ECAR) following _S.typhimurium_ (72 hours) infection or LPS (16 hours) treatment (Figure 5.9B).
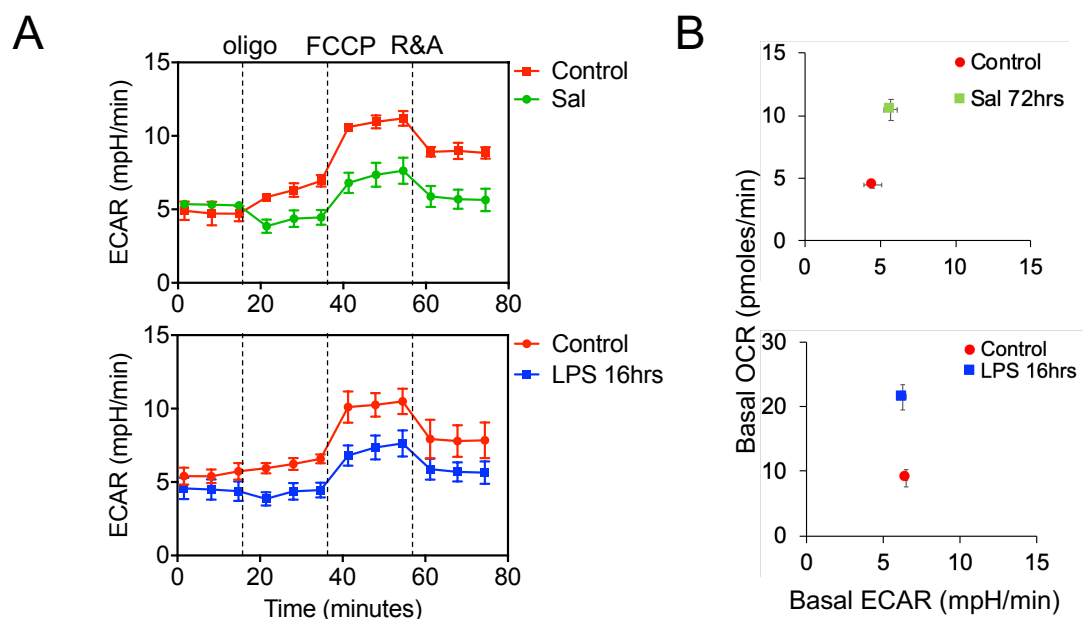
Figure 5.9. LSK have no change in basal glycolysis after LPS treatment or *S.typhimurium* infection.
(A) C57BL/6J mice were infected with *S.typhimurium* (Sal) for 72 hours or treated with LPS for 16 hours, the animals were sacrificed, the bone marrow was extracted and stained with a panel of antibodies to isolate the LSK population by FACS. Glycolysis levels were measured by ECAR. (B) Basal OCR (normalised to rotenone) vs Basal ECAR of LSK after *S.typhimurium* and LPS treatment. n=5 in each group. Data shown are means ± SD

Cells utilise pyruvate, long chain FAs and glutamine as the major substrates to generate ATP to support cellular metabolism. The Seahorse XF Mito Fuel Flex Test uses inhibitors of these pathways to identify the ability of the cell to switch between oxidative pathways, to meet the basal metabolic demands. I used the assay to monitor the contribution of FAO or β-oxidation to maintain basal metabolism in LSKs from LPS (16 hours) treated animals. Figure 5.10 shows, LSK from LPS treated C57BL/6J mice have an increased dependency on FAO as a source of energy compared to LSKs from control mice.
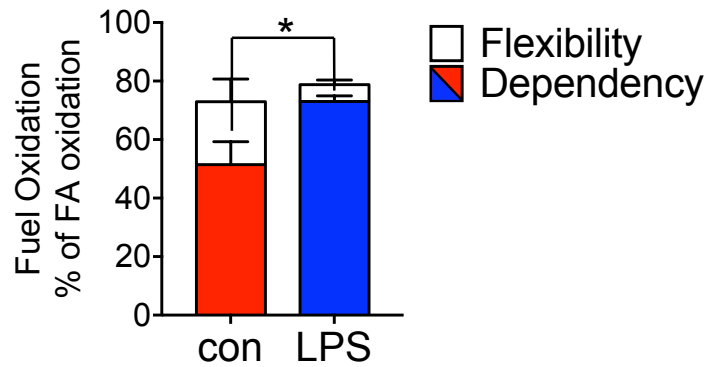
Figure 5.10. LPS treatment drives increased dependency on fatty acid oxidation in the LSK population.
C57BL/6J mice were treated with LPS for 16 hours, the animals were sacrificed, the BM was extracted and stained with a panel of antibodies to isolate the LSK population by FACS. The LSK population was analysed for the reliance on fatty acids to maintain baseline respiration. n=5 in each group. Data shown are means ± SD *P < 0.05

Next, to establish the role of β-oxidation on OCR, C57BL/6J mice were treated with LPS for 16 hours. The animals were sacrificed and the LSKs were isolated by FACS and treated *ex vivo* with an inhibitor of mitochondrial CPT1, etomoxir (ETX) to inhibit β-oxidation. Seahorse XF Mito stress test analysis showed *ex vivo* treatment ETX inhibited the LPS elicited increase in basal and maximal OCR but did not affect the control cells (Figure 5.11A and B).
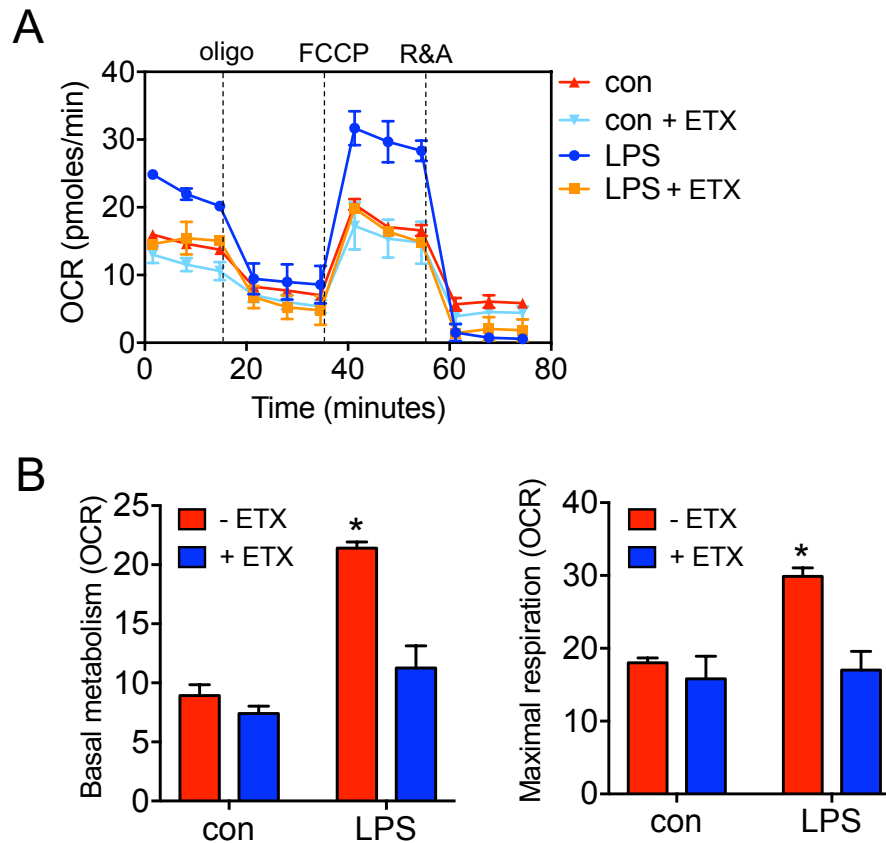
Figure 5.11. LSKs have an increased dependency on β oxidation following LPS treatment.
C57BL/6J mice were treated with LPS for 16 hours, the animals were sacrificed, the bone marrow was extracted and stained with a panel of antibodies to isolate the LSK population by FACS. The LSKs were treated with the β-oxidation inhibitor, etomoxir (ETX) and oxygen consumption rate (OCR) levels were measured by the extracellular flux assay. (B) Basal mitochondrial respiration (normalised to rotenone) of LSK cells from control and LPS treated animals with and without ETX. Maximal mitochondrial respiration LK cells from control and LPS treated animals with and without ETX. Data shown are means ± SD of n=5 mice in each group. *P < 0.05

To understand the importance of β-oxidation in the HSCs response to infection *in vivo,* C57BL/6J mice were pre-treated ETX for 1 hour before administration of S.*typhimurium.* The mice were then treated with ETX daily, 72 hours post *S.typhimurium* administration the animals were scarified and the BM was analysed by flow cytometry (Figure 5.12A). Figure 5.12B shows LSK, HSC, ST-HSC, and LT-HSC cell cycling were all significantly reduced in the ETX and *S.typhimurium* treated animals compared to *S.typhimurium* alone.
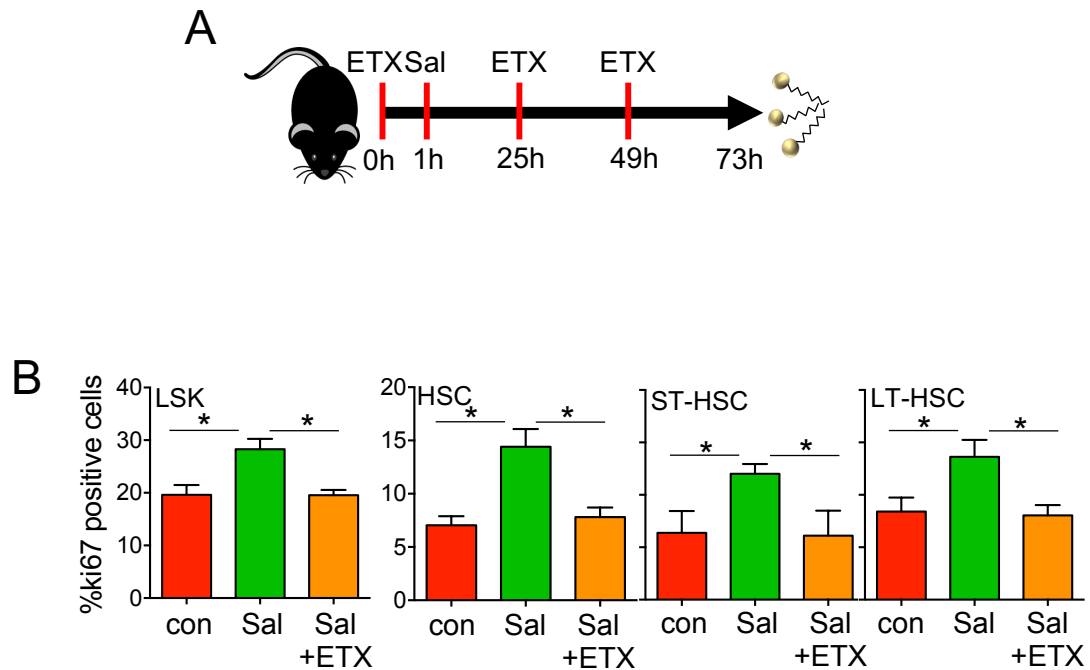
Figure 5.12: Ki67 positive cells following _S. typhimurium_
(A) Schematic of experiment. C57BL/6J mice were infected with _S.typhimurium_ and then 72 h later treated with etoposide (ETX). The BM was extracted, and the expression of Ki67 analysed by flow cytometry. (B) LSK, HSC, ST-HSC and LT-HSC populations were examined for signs of cycling measured by Ki67 positive cells after _S. typhimurium_ and ETX treatment. Data shown are means ± SD of >4 mice in each group *p<0.05.

Next, to examine if the decrease in cell cycling correlated with a decrease in cell number, I examined the cell count per 100,000 BM cells after ETX and S.*typhimurium*. As expected the *S.typhimurium* treated animals had a significant increase in LSK, HSC, ST-HSC and LT-HSC cell number. However, in the ETX and *S.typhimurium* treated group there was no change in HSPC cell count compared to the control (Figure 5.13).
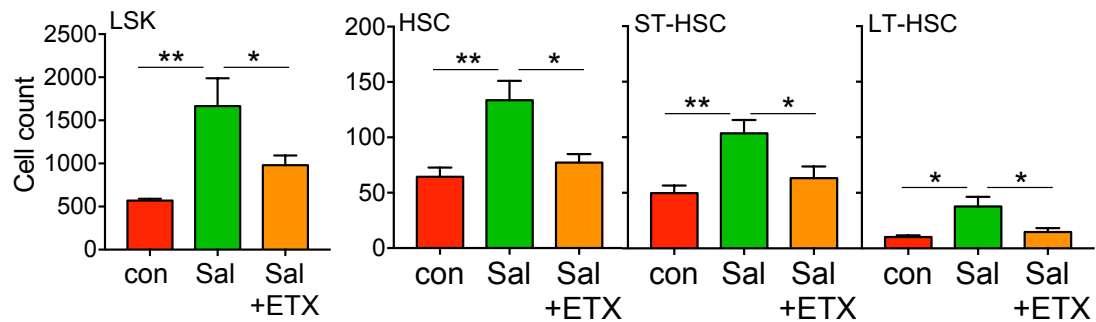
Figure 5.13. Etomoxir inhibits cell number increase after *S.typhimurium* infection.
C57BL/6J mice were infected with *S.typhimurium* (Sal) for 72 hours and Etomoxir (ETX). The BM was extracted, and the cells were analysed for cell count per 100 000 cells by flow cytometry for LSK, HSC, ST-HSC and LT-HSC populations. Data shown are means ± SD of >4 mice in each group *p<0.05 **p<0.01

To confirm the effect of ETX on cell count and cell cycling following *S.typhimurium* infection was not due to a decrease in lipid content in the cell I used Bodipy 493/503 staining. Figure 5.14 shows that lipid content is significantly increased in the LSK, HSC, ST-HSC and LT-HSC in both the *S.typhimurium* alone and ETX and *S.typhimurium* infection compared the control.
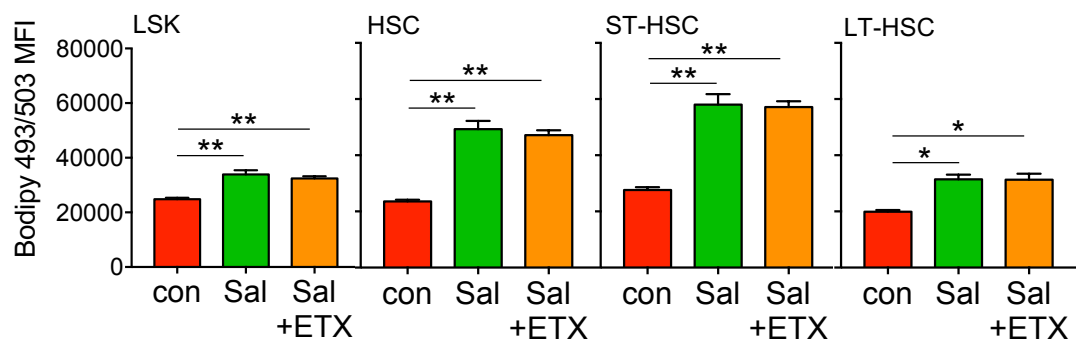
Figure 5.14. Etomoxir does not inhibit lipid content increase in the HSC after *S.typhimurium* infection.
C57BL/6J mice were infected with *S.typhimurium* (Sal) for 72 hours and Etomoxir (ETX). The BM was extracted and stained with a panel of antibodies and Bodipy 493/503 to analyse lipid content (Bodipy 493/503 mean fluorescence intensity (MFI)) in specific LSK, HSC, ST-HSC and LT-HSC populations. Data shown are means ± SD of >4 mice in each group *p<0.05 **p<0.01

To establish the role of β-oxidation on OCR following *S.typhimurium* infection, the LSKs from control and *S.typhimurium* were isolated by FACS and treated *ex vivo* with ETX. Seahorse XF Mito stress test analysis showed *ex vivo* treatment ETX inhibited the *S.typhimurium* induced increase in both basal and maximal OCR. ETX did not affect OCR in the LSKs from control animals (Figure 5.15A and B).
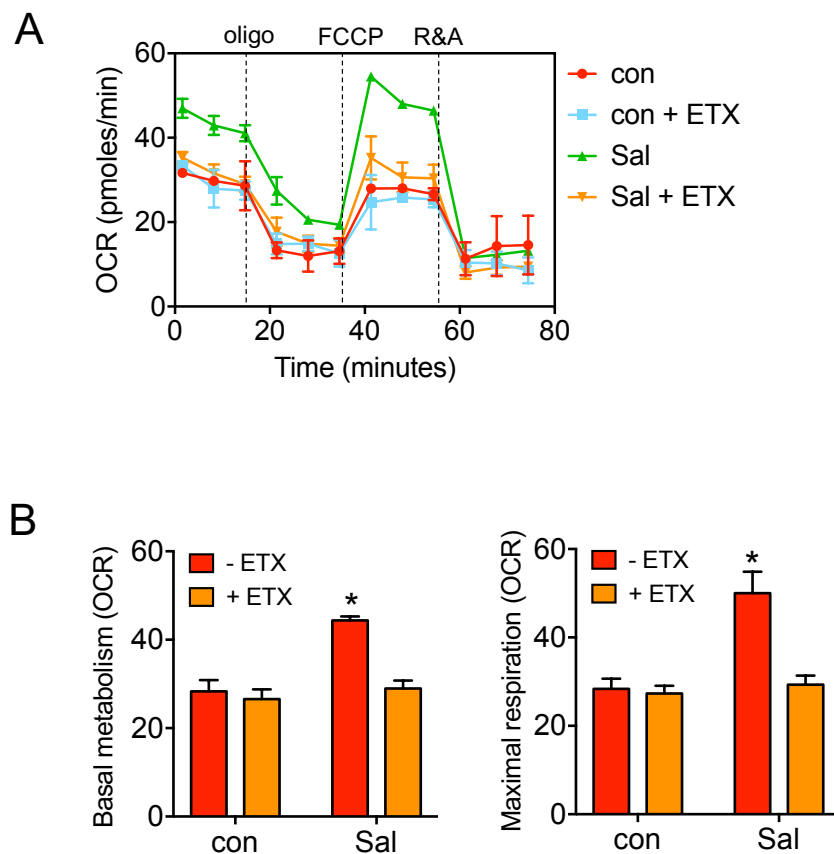
Figure 5.15. LSKs have a decreased OCR following etomoxir and *S.typhimurium* infection.
C57BL/6J mice were infected with *S.typhimurium* (Sal) for 72 hours and etomoxir (ETX). The bone marrow was extracted and stained with a panel of antibodies to isolate the LSK population by FACS. (A) The LSKs were treated with the β-oxidation inhibitor, ETX and oxygen consumption rate (OCR) levels were measured by extracellular flux assay. (B) Basal mitochondrial respiration (normalised to rotenone) of LSK cells from control and LPS treated animals with and without ETX. Maximal mitochondrial respiration LK cells from control and LPS treated animals with and without ETX. Data shown are means ± SD of n>4 mice in each group. *P <0.05

To next determine if ETX inhibited the HSC response to LPS treatment C57BL/6J mice were pre-treated with ETX for 1 hour before 16 hours of LPS treatment. The mice were sacrificed, and the BM was analysed by flow cytometry (Figure 5.16A). ETX inhibited the LPS elicited increase in LSK, HSC and LT-HSC cell cycling (Figure 5.16B). ST-HSC cell cycling was not significantly reduced by ETX pre-treatment compared to LPS alone, however, there was a trend towards a decreased cell cycling (Figure 5.16B).
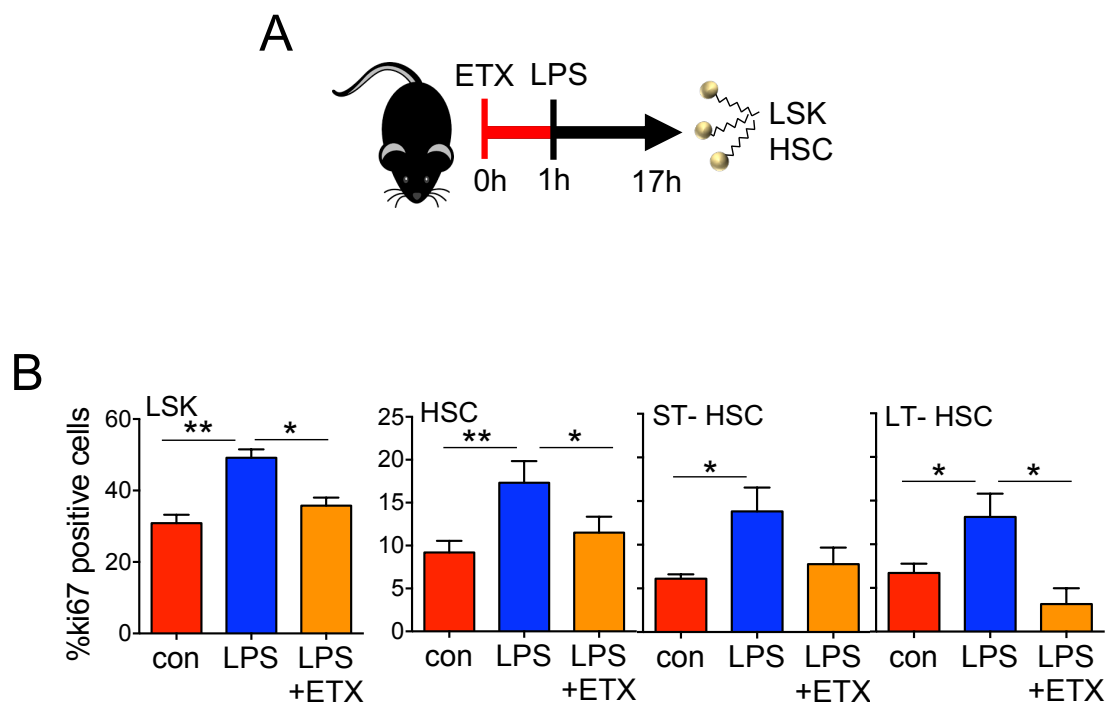
Figure 5.16. Etomoxir inhibits increase in Ki67 positive cells after LPS treatment.
(A) Schematic diagram of experimental design in which C57BL/6J mice were pre-treated with etomoxir (ETX) for 1 hour before LPS treatment (16 hours). The BM was extracted, and the cells were analysed by flow cytometry for Ki67 staining in the LSK, HSC, ST-HSC and LT-HSC populations. (B) Percentage of cycling cells as measured by Ki67 positive cells after and ETX and LPS treatment. Data shown are means ± SD of 5 mice in each group *p<0.05 **p<0.01.

To determine whether ETX pre-treatment before LPS, had an effect on HSPC cell count, the BM was stained with a HSC antibody panel and cell number per 100 000 BM cells was assessed by flow cytometry. Figure 5.17 confirms a significant increase in cell number of the LSK, HSC, ST-HSC and LT-HSC populations following LPS treatment. However, this increase in cell number was not observed in the LPS and ETX treated animals (Figure 5.17).
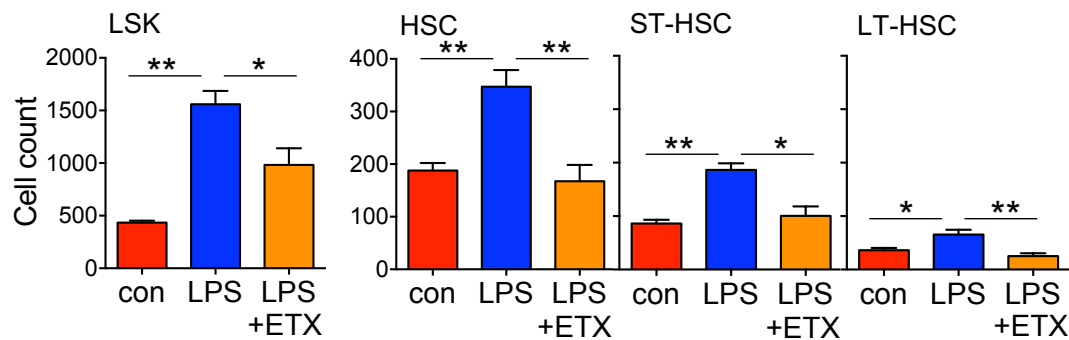
Figure 5.17. Etomoxir inhibits cell number increase after LPS treatment. C57BL/6J mice were pre-treated with etomoxir (ETX) for 1 hour before LPS treatment (16 hours). The BM was extracted, and the cells were analysed for LSK, HSC, ST-HSC and LT-HSC cell number by flow cytometry. Data shown are means ± SD of 5 mice in each group *p<0.05 **p<0.01.

Next, to understand the colony forming ability of the haematopoietic cells after ETX and LPS treatment, C57BL/6J mice were treated with control PBS, LPS alone or ETX and LPS for 16 hours. The animals were sacrificed, the BM was extracted, seeded in a semisolid Methocult for 7 days. Pre-treatment with ETX significant reduced expansion of the granulocyte monocyte progenitor population (GM) compared to LPS treatment alone (Figure 5.18).
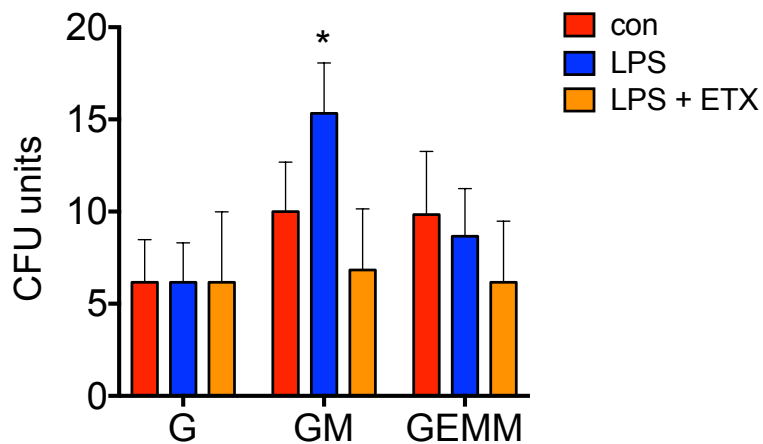
Figure 5.18. Etomoxir inhibits the LPS induced expansion of the granulocyte monocyte progenitor populations.
C57BL/6J mice were pre-treated with etomoxir (ETX) for 1 hour before LPS treatment (16 hours), the animals were sacrificed, the bone marrow was extracted. 1 x 10^4 bone marrow cells were seeded in a semisolid Methocult for 7 days. Granulocytic progenitor (G), granulocyte monocyte progenitor (GM), and granulocyte monocyte megakaryocyte progenitor (GEMM) colonies were then counted. Data shown are means ± SD of n=5 in each group *P < 0.05

ETX is an inhibitor of CPT1 which is located on the inner wall of the outer mitochondrial membrane (378). CPT1 is an enzyme responsible for acyl carnitines formation which is vital for the transportation of fatty acyl chains from the cytosol into the mitochondria, a step which is crucial for FAO (379). Therefore, I next confirmed CPT1A expression was increased on the HSC following LPS treatment. C57BL/6J mice were treated with LPS for 16 hours, the mice were sacrificed, and the HSC population was isolated by FACS. Figure 5.19 shows that HSC from LPS treated mice have a significantly increased expression of CPT1A compared to HSCs from control mice.
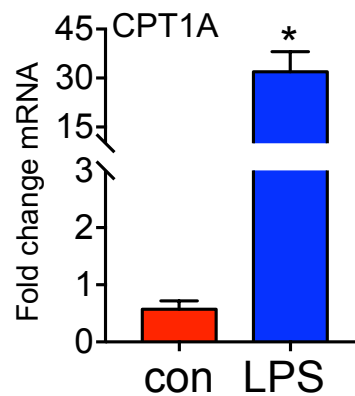
Figure 5.19. CPT1A is upregulated in the HSC at 16 hours post LPS treatment.
C57BL/6J mice were treated with LPS for 16 hours, the animals were sacrificed, the bone marrow was extracted and stained with a panel of antibodies to isolate the HSC population by FACS. RNA was analysed for CPT1A gene expression by qPCR. n=5 in each group. Data shown are means ± SD *P < 0.05

ETX has previously been reported to have off-target effects, when used at high concentrations. These off target effects include inhibition of complex 1 in the mitochondria (380) and induction of severe oxidative stress (381) which could have an effect on the HSC response to infection. Therefore, to investigate the specific function of CPT1A in the haematopoietic compartment following LPS treatment, LK cells were isolated from WT CD45.1 mice and transduced with control KD (LK $^{(con\ KD)}$) or CPT1A KD (LK$^{CPT1A\ KD}$) (Figure 5.20A). Figure 5.20B confirms CPT1A was successfully knocked down on average by 70% in the LK$^{CPT1A\ KD}$. The LK$^{CPT1A\ KD}$ cells were then transplanted into WT CD45.2 mice and 14-weeks post transplantation the animals were treated with LPS for 16 hours (Figure 5.20A). The mice were then sacrificed, the BM was extracted, and stained with CD45.1 PE to monitor engraftment. Figure 5.20C confirms equal engraftment of CD45.1 cells in recipient CD45.2 mice within both treatment groups.
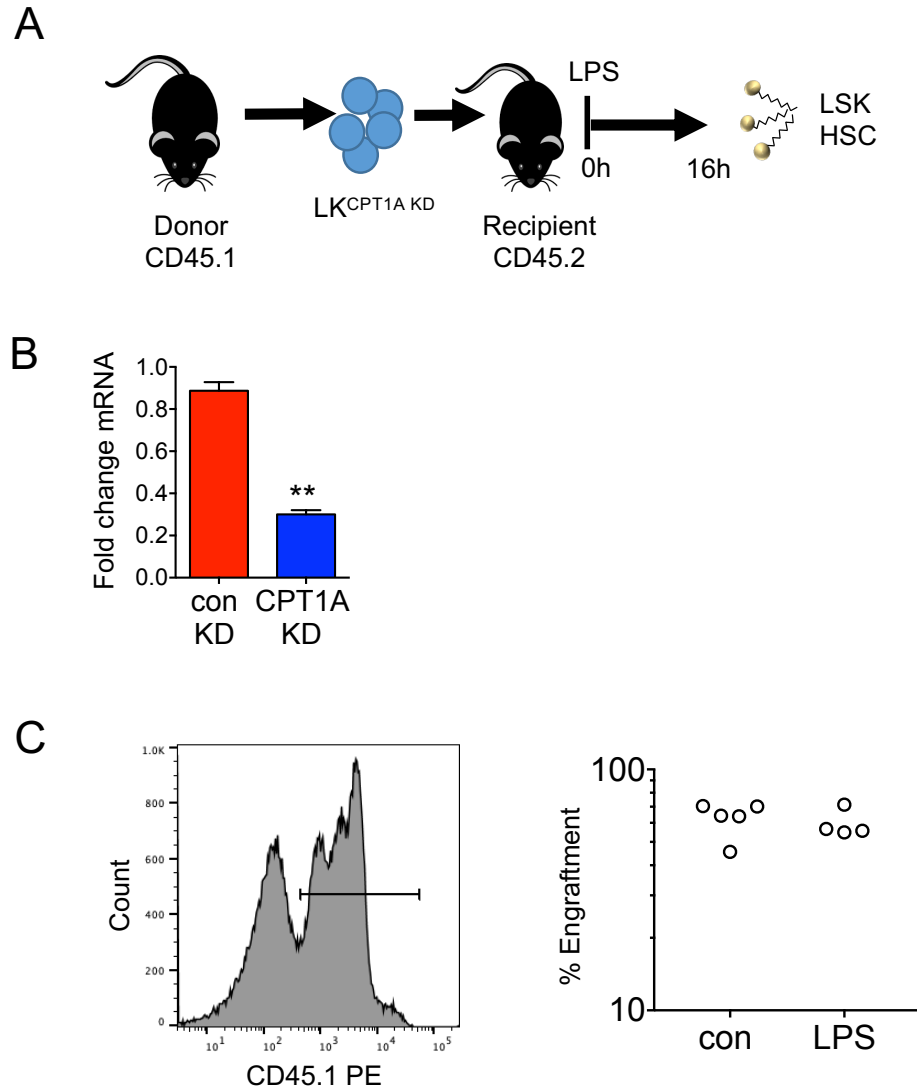
Figure 5.20. CD45.1 engraftment is seen in the bone marrow of transplant mice.
(A) Schematic diagram of the experimental design, CD45.1 lineage negative, CD117 positive (LK) cells were transduced with a CPT1A knockdown lentivirus (LK^CPT1A KD) and transplanted into CD45.2 animals. Post engraftment mice were treated with LPS for 16 hours and the bone marrow assessed by flow cytometry. (B) Relative CPT1A expression in control knockdown (conKD) and CPT1A knockdown (CPT1AKD) LK cells before transplantation. (C) 16 hours post LPS treatment the animals were sacrificed, and the BM was extracted, the cells were analysed by flow cytometry for CD45.1 expression to confirm engraftment. Data shown are means ± SD of >4 mice in each group.

In addition to engraftment the BM was also stained with a panel of antibodies, permeabilised and fixed to assess HSPC cycling by flow cytometry. The gating strategy to identify cell cycling in the specific cell populations of interest is shown in Figure 5.21A. All gating was determined using fluorescence minus

one controls. Figure 5.21B and C shows there was no change in LSK and HSC cell cycling in the LK$^{CPT1A\ KD}$ transplant animals in response to LPS.
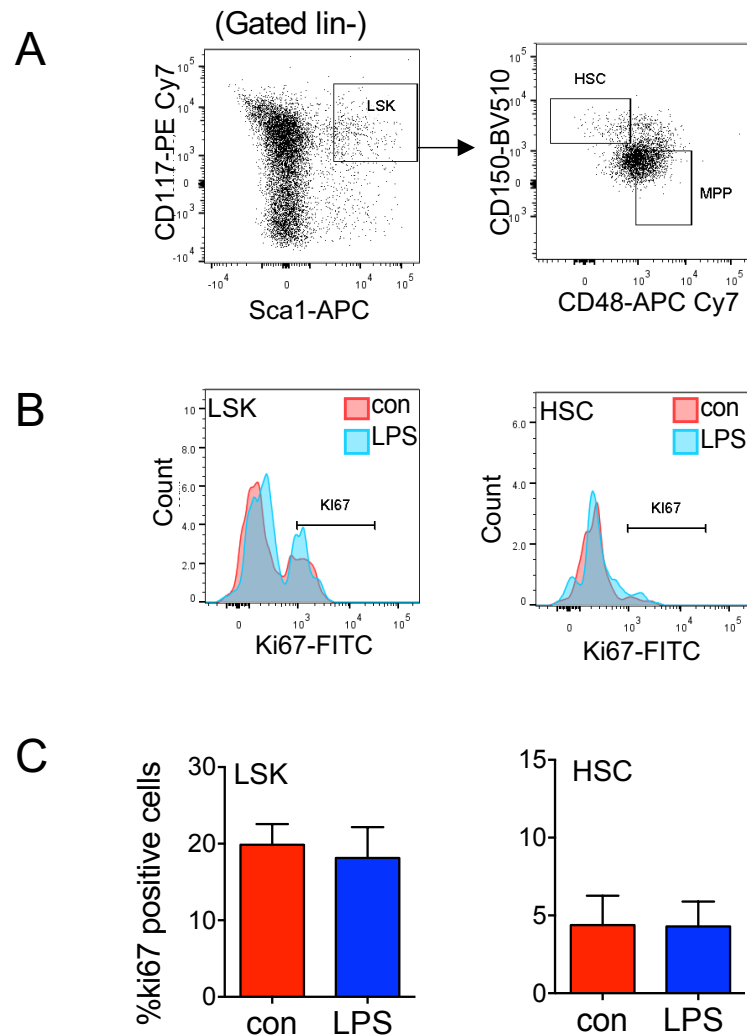
Figure 5.21. Ki67 positive cells increase following LPS treatment is inhibited in the CPT1AKD HSC.
CD45.1 lineage negative, CD117 positive (LK) cells were transduced with a CPT1A knockdown lentivirus (LK$^{CPT1A\ KD}$) and transplanted into CD45.2 animals. Post engraftment mice were treated with LPS for 16 hours and the bone marrow assessed by flow cytometry for percentage of Ki67 positive cells. (A) The gating strategy used is shown. (B) Representative histogram plot of Ki67-FITC expression in the LSK and HSC population. (C) Percentage of cycling cells as measured by Ki67 positive cells. Data shown are means ± SD of >4 mice in each group.

There was also no observed increase in LSK, HSC, ST-HSC and LT-HSC count per BM 100 000 cells in the LPS treated LK$^{CPT1A\ KD}$ transplant animals compared to the control (Figure 5.22).
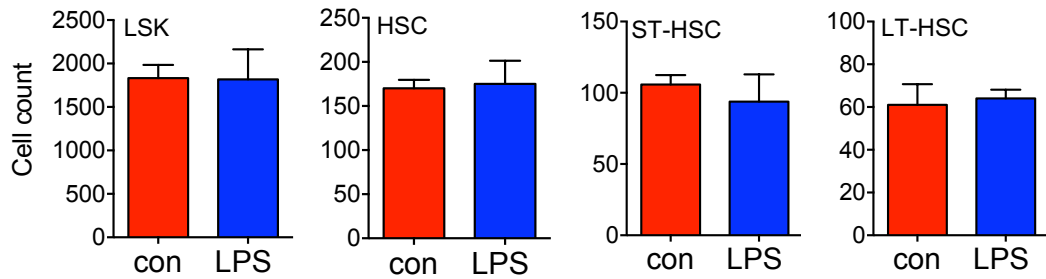
Figure 5.22. CPT1AKD HSC inhibits cell number increase after LPS treatment.
CD45.1 lineage negative, CD117 positive (LK) cells were transduced with a CPT1A knockdown lentivirus (LK$^{CPT1A\ KD}$) and transplanted into CD45.2 animals. Post engraftment mice were treated with LPS for 16 hours and the bone marrow assessed by flow cytometry for cell number per 100 000 cells. Data shown are means ± SD of >4 mice in each group.

To ensure the CPT1A KD did not affect lipid transport into the cell the BM was stained with a panel of antibodies and Bodipy 493/503. Lipid content was significantly increased in the LSK, HSC, ST-HSC and LT-HSC of the LK$^{CPT1A\ KD}$ transplant mice following LPS treatment (Figure 5.23). Together, these results demonstrate HSCs have an increased dependency on β-oxidation for cell cycling and expansion, following infection.
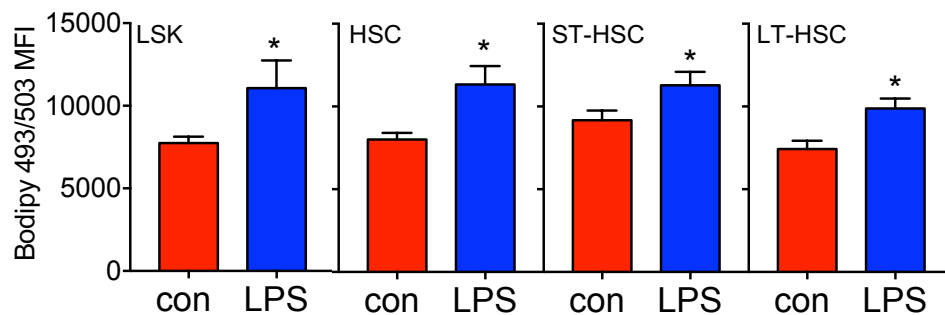
Figure 5.23. CPT1AKD does not inhibit lipid content increase after LPS treatment.
CD45.1 lineage negative, CD117 positive (LK) cells were transduced with a CPT1A knockdown lentivirus (LK$^{CPT1A\ KD}$) and transplanted into CD45.2 animals. Post engraftment mice were treated with LPS for 16 hours. The bone marrow was extracted and stained with a panel of antibodies and Bodipy 493/503 to analyse lipid content (Bodipy 493/503 mean fluorescence intensity (MFI)) in specific LSK, HSC, ST-HSC and LT-HSC populations. Data shown are means ± SD of >4 mice in each group *p<0.05

## 5.4 CD36 regulates uptake of long chain free fatty acid by the HSC in response to infection

I next examined the mechanism regulating the uptake of FFA to the HSC in response to infection. Numerous membrane proteins have been shown to be associated with lipid uptake including fatty acid-binding proteins (FABPs), fatty acid transport proteins (FATPs) which are also known as solute carrier 27 (SLC27). To investigate how FAs are transported into the HSC following LPS treatment or *S.typhimurium* infection, I assessed the gene expression of several membrane proteins known to be involved with lipid trafficking (262). Figure 5.24 shows that mRNA expression of the lipid transporters CD36, Slc27a2, Slc27a4 and Fabp3 were all upregulated in the HSCs isolated from LPS (2 and 16 hours) or *S.typhimurium* (72 hours) treated animals compared to control HSCs. There was no change in the expression of Slc27a5, Fabp1, Fabp4 and LDLR in the HSC from LPS or *S.typhimurium* infected mice. HSC expression of Slc27a1, Fabp5 and Msr1 were downregulated following LPS or *S.typhimurium* treatment (Figure 5.24).
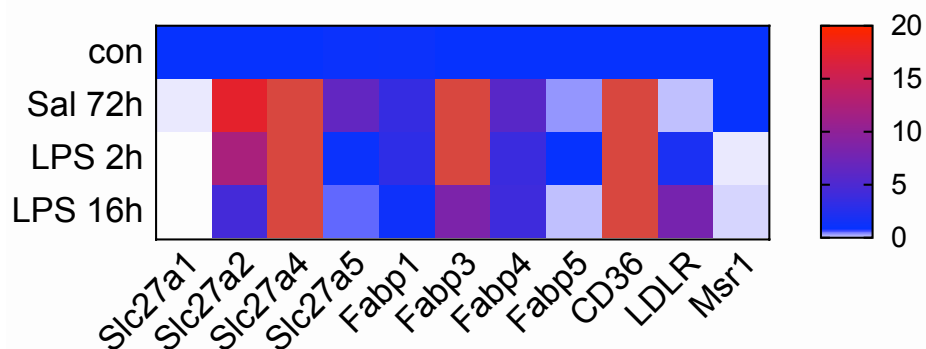
Figure 5.24. Fatty acid transporter genes expression in HSC in response to *S.typhimurium* infection or LPS treatment.
C57BL/6J mice were treated with *S.typhimurium* (72 hours) or LPS for 2 or 16 hours, the animals were sacrificed, the bone marrow was extracted and stained with a panel of antibodies to isolate the HSC population by FACS. RNA was analysed for gene expression of fatty acid transporter genes by qPCR. n=5 in each group.

It has previously been shown, the LSCs take up FFA to support increased proliferation. Furthermore, LSCs expressing the fatty acid transporter CD36 demonstrated high levels of fatty acid oxidation, providing those LSCs with a survival advantage (17). Therefore, I focused on CD36 expression and function in the HSC. To confirm CD36 expression was elevated during infection C57BL/6J mice were infected with *S.typhimurium* for 72 hours or LPS for 16 hours and assessed for CD36 by flow cytometry. Increased protein expression of CD36 was observed in the LSK, HSC, ST-HSC and LT-HSC from both *S.typhimurium* and LPS treated mice compared to the control mice (Figure 5.25A and B). Although still elevated CD36 protein expression (Figure 5.25) was not as significantly elevated compared to the mRNA expression of CD36 (Figure 5.24). One possible explanation for this difference is that levels of mRNA expression do not always translate to protein expression. This may be because of timing of the experiments or the fact I am just observing the membrane expression of CD36 protein using flow cytometry.
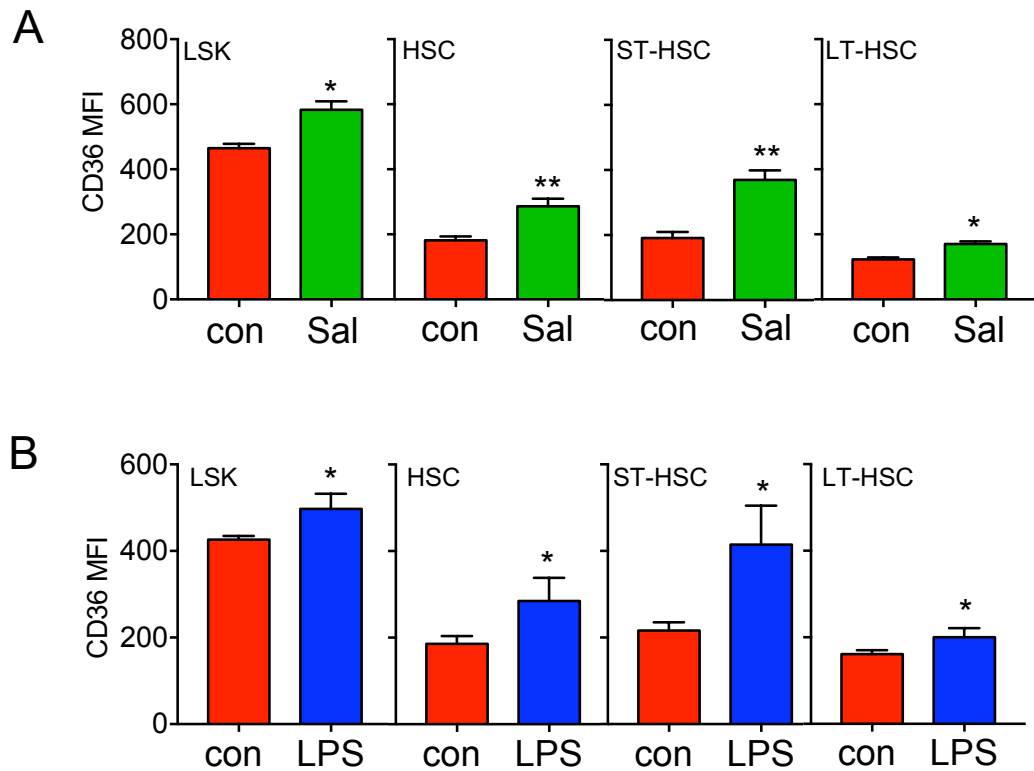
Figure 5.25. CD36 expression in the HSC is elevated after *S.typhimurium* infection or LPS treatment.
(A) C57BL/6J mice were infected with *S.typhimurium* (Sal) for 72 hours, the animals were sacrificed, the bone marrow was extracted and stained with a panel of antibodies to analyse CD36 expression in specific LSK, HSC, ST-HSC and LT-HSC populations. n=6 in each group. (B) C57BL/6J mice were treated with 1 mg/kg LPS for 16 hours, the animals were sacrificed, the bone marrow was extracted stained with a panel of antibodies to analyse CD36 expression in specific populations n=5 in each group. Data shown are means ± SD *P < 0.05 **p<0.01.

To test the importance the role of CD36 in FFA uptake and the impact on HSC expansion following infection, C57BL/6J mice were pre-treated with the CD36 inhibitor sulfosuccinimidyl oleate (SSO) for 1 hour before LPS treatment for 16 hours (Figure 5.26A). Figure 5.26B confirms CD36 expression was inhibited in the LPS and SSO treated mice compared to LPS alone.
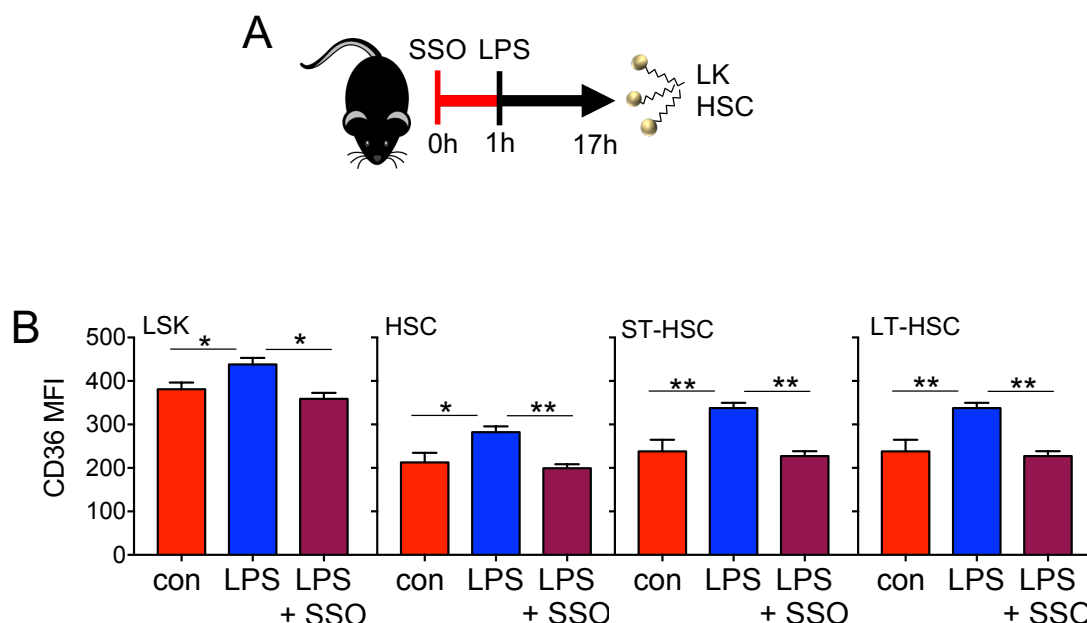
Figure 5.26. Sulfosuccinimidyl oleate inhibits CD36 expression increase after LPS treatment.
(A) Schematic of experimental design. C57BL/6J mice were pre-treated with 40 mg/kg sulfosuccinimidyl oleate (SSO) for 1 hour before treatment with 1 mg/kg LPS for 16 hours. The animals were sacrificed, the bone marrow was extracted stained with a panel of HSC antibodies. (B) CD36 expression (CD36 mean fluorescence intensity (MFI)) in specific LSK, HSC, ST-HSC and LT-HSC populations n=5 in each group. Data shown are means ± SD *P < 0.05 **P < 0.01

I next examined the consequence of CD36 inhibition on lipid content in the HSPCs following infection. SSO pre-treatment inhibited the LPS elicited increase in lipid content within the HSC, ST-HSC and LT-HSC populations (Figure 5.27). In the LSK population lipid content was not significantly reduced by SSO pre-treatment compared to LPS alone, however, there was a trend towards decreased lipid levels (Figure 5.27).
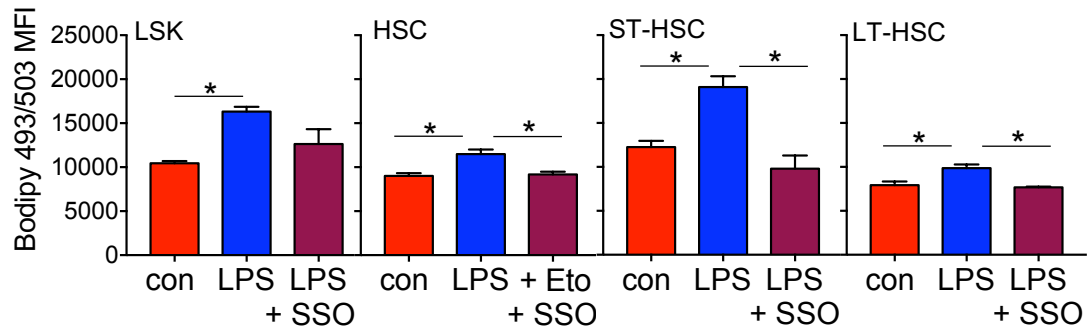
Figure 5.27. Sulfosuccinimidyl oleate inhibits LPS induced increase in lipid content in the HSC.
C57BL/6J mice were pre-treated with 40 mg/kg sulfosuccinimidyl oleate (SSO) for 1 hour before treatment with 1 mg/kg LPS for 16 hours. The animals were sacrificed, the bone marrow was extracted stained with a panel of HSC antibodies and Bodipy 493/503 to analyse lipid content (Bodipy 493/503 mean fluorescence intensity (MFI)) in specific LSK, HSC, ST-HSC and LT-HSC populations. n=5 in each group. Data shown are means ± SD *P < 0.05

To assess if the decrease in lipid content in the HSPCs from the LPS and SSO treated animals was due to a decrease in FA uptake into the cells, the LK population was isolated and incubated with Bodipy FL-C12 for 30 minutes. There was a reduced FFA uptake observed in the LK cells from LPS and SSO treated animals compared to LKs from LPS alone treated mice (Figure 5.28).
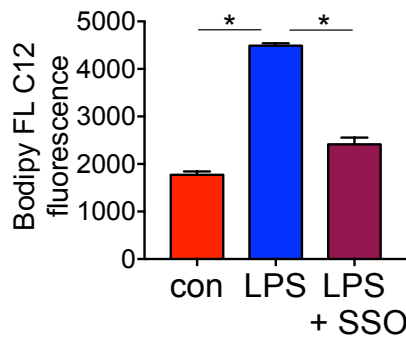
Figure 5.28. Sulfosuccinimidyl oleate inhibits LPS induced fatty acid uptake into the LK cells.
C57BL/6J mice were pre-treated with 40 mg/kg sulfosuccinimidyl oleate (SSO) for 1 hour before treatment with 1 mg/kg LPS for 16 hours. The animals were sacrificed, the bone marrow and LK cells were isolated. The LK cells were incubated with Bodipy FL-C12 and fluorescence was measured. n=5 in each group Data shown are means ± SD *P< 0.05

I next determined if the SSO induced reduction in lipid uptake and subsequent lipid content within the HSPCs following LPS treatment had an effect on cell cycling. Figure 5.29A shows LSK, HSC, ST-HSC, and LT-HSC cell cycling were all significantly reduced in the SSO and LPS treated animals compared to LPS alone.
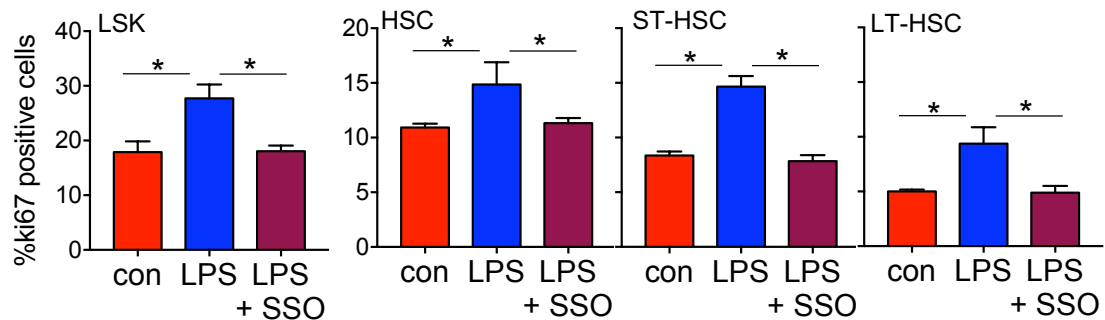
Figure 5.29. Sulfosuccinimidyl oleate inhibits Ki67 positive cell expression in the HSC after LPS treatment.
C57BL/6J mice were pre-treated with 40 mg/kg sulfosuccinimidyl oleate (SSO) for 1 hour before treatment with 1 mg/kg LPS for 16 hours. The animals were sacrificed, the bone marrow was extracted stained with a panel of HSC antibodies and Ki67 to analyse cell cycling. Percentage of cycling cells was measured by Ki67 positive cells after LPS and SSO treatment. n=5 in each group. Data shown are means ± SD *P < 0.05

To examine if the decrease in cell cycling was correlated with a decrease in cell number, I examined the cell count per 100 000 BM cells after SSO and LPS. As previously ovserved, the LPS treated animals had a significant increase in LSK, HSC, ST-HSC and LT-HSC cell number. However, in the SSO and LPS treated mice there was no change in HSPC cell count compared to the control (Figure 5.30).
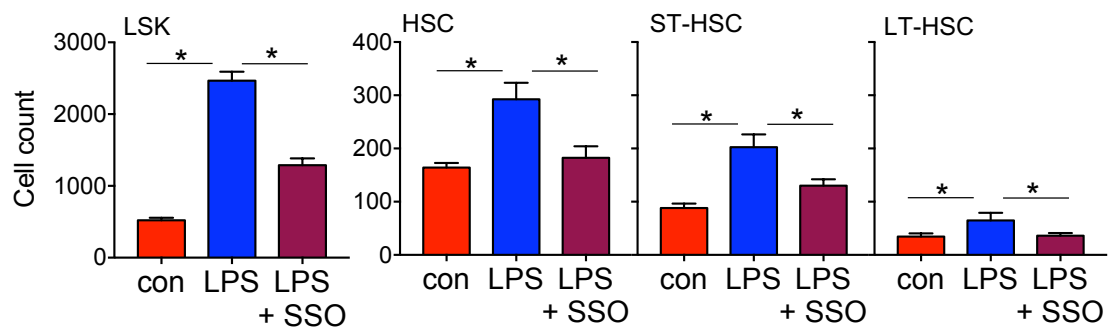
Figure 5.30. Sulfosuccinimidyl oleate inhibits increase in HSC cell count after LPS treatment.
C57BL/6J mice were pre-treated with 40 mg/kg sulfosuccinimidyl oleate (SSO) for 1 hour before treatment with 1 mg/kg LPS for 16 hours. The animals were sacrificed, the bone marrow was extracted assessed by flow cytometry for cell number per 100 000 cells. n=5 in each group. Data shown are means ± SD *P < 0.05

Next, to establish the role of FA uptake on OCR, the LSKs from control, LPS alone and SSO and LPS treatment mice were isolated by FACS. Seahorse XF Mito stress test analysis showed pre-treatment with SSO inhibited the LPS induced increase basal and maximal OCR but did not affect the control cells (Figure 5.31A and B). However, in this experiment the basal respiration was very low and not consistent with multiple previous experiments in the control and LPS treated LSKs. Moreover, the oligomycin was not observed to decrease OCR which is an expected respiration dynamic due to ATP synthase inhibition. This could be due to the wrong oligomycin concentration in the assay or the length of time the LSKs took to sort from the BM for the assay therefore, these results are not reliable.
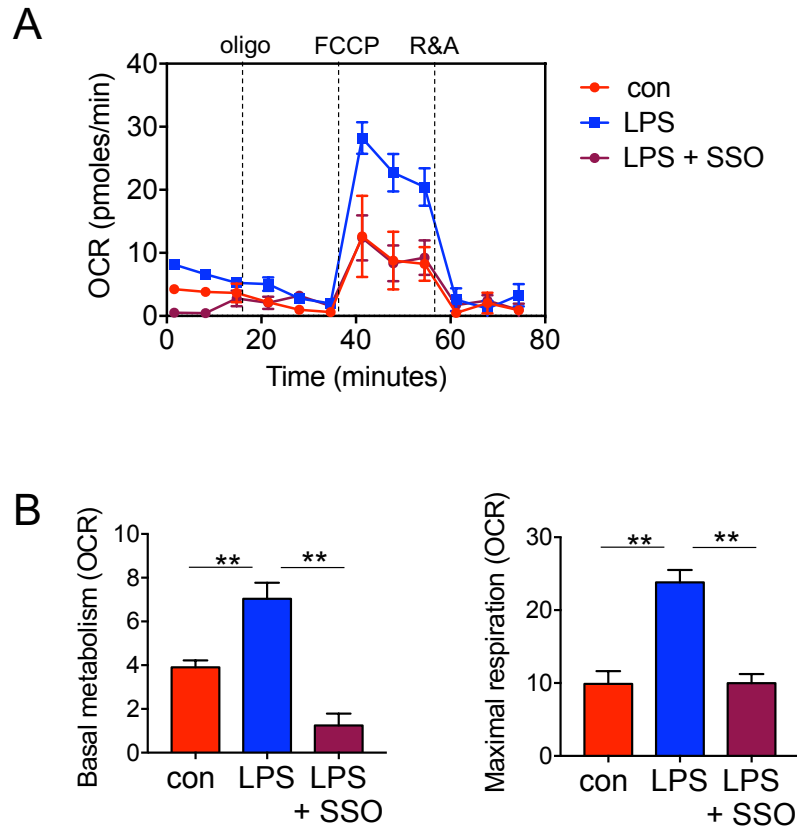
Figure 5.31. LSKs have a reduced OCR following SSO and LPS treatment.
C57BL/6J mice were pre-treated with 40 mg/kg sulfosuccinimidyl oleate (SSO) for 1 hour before treatment with 1 mg/kg LPS for 16 hours. The animals were sacrificed, the bone marrow was extracted and stained with a panel of antibodies to isolate the LSK population by FACS and oxygen consumption rate (OCR) levels were measured by extracellular flux assay. (B) Basal (normalised to rotenone) and maximal mitochondrial respiration of LSK cells from control, LPS or LPS and SSO treated animals. Data shown are means ± SD of n=5 mice in each group. **P < 0.01

To confirm the effects of pharmacological inhibition of CD36 in response to infection was consistent with genetic knockout of CD36 we used CD36 deficient mice (CD36$^{-/-}$). CD36$^{-/-}$ mice or WT CD36$^{+/+}$ mice were treated with LPS for 16 hours (Figure 5.32A). LPS treated WT CD36$^{+/+}$ animals had a significant increase in lipid content in the LSK, HSC, ST-HSC, and LT-HSC compared to the control mice (Figure 5.32B). However, there was no observed increase in lipid levels in the LPS treated CD36$^{-/-}$ mice compared to baseline control CD36$^{-/-}$ mice (Figure 5.32B).
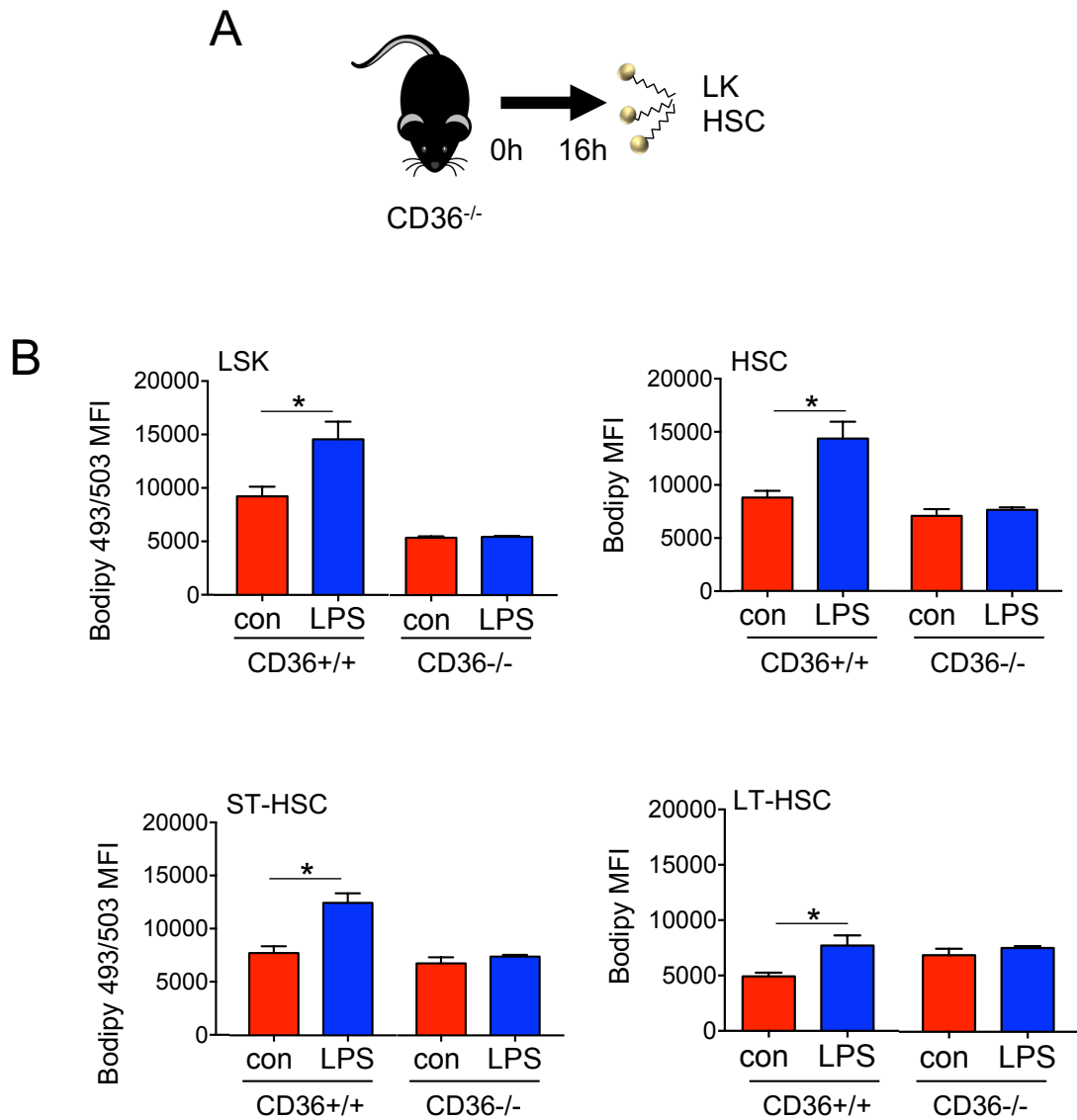
Figure 5.32. CD36^{-/-} mice have reduced lipid content after LPS treatment.
(A) Schematic of experimental design. CD36$^{-/-}$ or WT (CD36$^{+/+}$) mice were treated with 1 mg/kg LPS for 16 hours, the animals were sacrificed, the bone marrow was extracted stained with a panel of antibodies and Bodipy 493/503 (B) Lipid content (Bodipy 493/503 mean fluorescence intensity (MFI)) in specific LSK, HSC, ST-HSC and LT-HSC populations n=5 in each group. Data shown are means ± SD *P < 0.05

Unlike the WT CD36$^{+/+}$ animals, LK cells from LPS treated CD36$^{-/-}$ mice did not have an increased lipid uptake compared to LK cells from control CD36$^{-/-}$ mice (Figure 5.33).
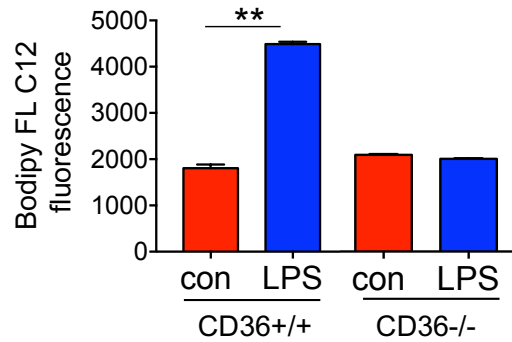
Figure 5.33. CD36$^{-/-}$ mice have reduced fatty acid uptake into the LK cells after LPS treatment.
CD36$^{-/-}$ or WT (CD36$^{+/+}$) mice were treated with 1 mg/kg LPS for 16 hours. The animals were sacrificed, the bone marrow and LK cells were isolated. The LK cells were incubated with Bodipy FL-C12 and fluorescence was measured. n=5 in each group Data shown are means ± SD *P < 0.05

Figure 5.34 shows there was no change in LSK, HSC, ST-HSC, and LT-HSC cell cycling in the CD36$^{-/-}$ mice treated with LPS compared to control untreated CD36$^{-/-}$ mice. In contrast, LPS treated WT CD36$^{+/+}$ animals had a significant increase in HSPC cell cycling compared to control mice (Figure 3.34)
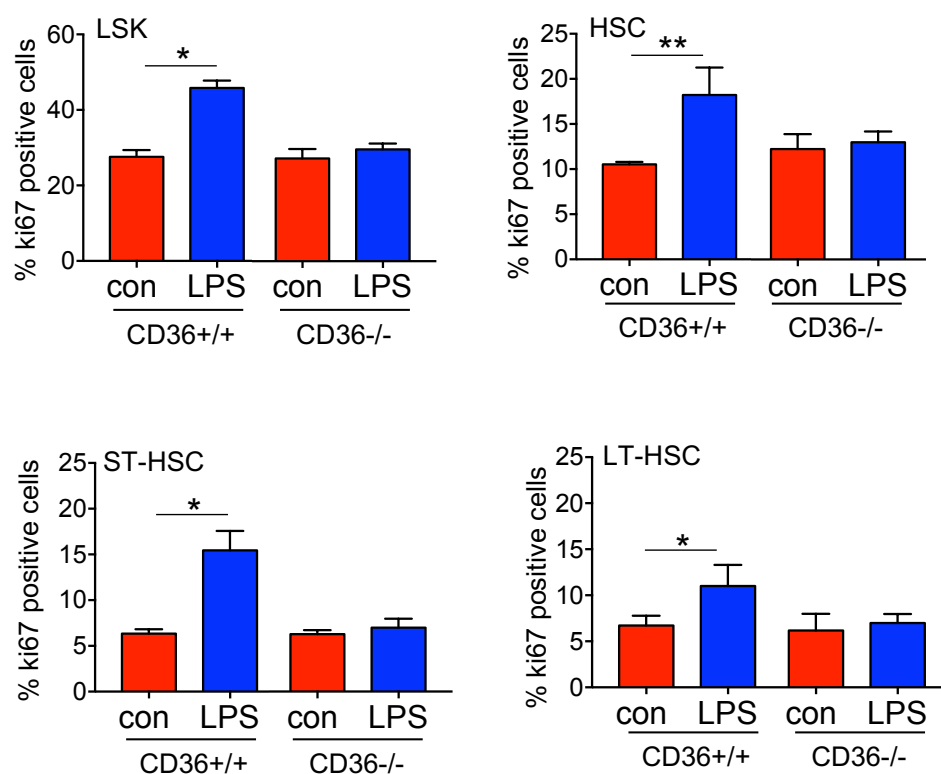
Figure 5.34. CD36$^{-/-}$ mice have reduced HSC cell cycling after LPS treatment.
CD36$^{-/-}$ or WT (CD36$^{+/+}$) mice were treated with 1 mg/kg LPS for 16 hours. The animals were sacrificed, the bone marrow was extracted stained with a panel of HSC antibodies and Ki67 to analyse cell cycling in the LSK, HSC, ST-HSC and LT-HSC population. Percentage of cycling cells was measured by Ki67 positive cells after LPS treatment. n=5 in each group. Data shown are means ± SD *P < 0.05

To monitor the contribution of FAO or β-oxidation in maintaining basal metabolism in CD36$^{-/-}$ mice I used the Seahorse XF Mito Fuel Flex Test. CD36$^{-/-}$ mice were treated with LPS for 16 hours, the mice were sacrificed and the LSK were isolated from the BM by FACS. Figure 5.35 shows, LSK from LPS treated CD36$^{-/-}$ mice have no change in dependency on FAO as a source of energy compared to LSKs from control CD36$^{-/-}$ mice. Moreover, the dependency on FAO as a source of energy in CD36$^{-/-}$ mice is lower than the FAO dependency in WT mice (Figure 5.10 and 5.35).
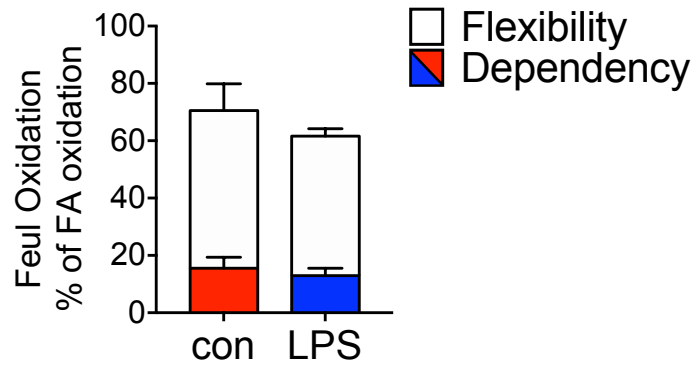
Figure 5.35. CD36^{-/-} mice have a low dependency on fatty acid oxidation in the LSK population.
CD36$^{-/-}$ were treated with LPS for 16 hours, the animals were sacrificed, the bone marrow was extracted and stained with a panel of antibodies to isolate the LSK population by FACS. The LSK population was analysed for the reliance on fatty acids to maintain baseline respiration. n=5 in each group. Data shown are means ± SD

Next, to confirm FFA uptake was impaired in the CD36$^{-/-}$ mice following LPS treatment was specific to the HSPC compartment I used the transplant model to track real time fatty acid uptake *in vivo*. CD36$^{-/-}$ CD45.2 LK cells were isolated and transduced with a firefly luciferase virus (CD36$^{-/-}$ LK^{+FF}). The cells were then transplanted into busulfan treated PepCboy CD45.1 animals (Figure 5.36A). Engraftment and transduction of the CD36$^{-/-}$ LK^{+FF} cells were monitored using D-luciferin by *in vivo* bioluminescent imaging (Figure 5.36B). 14 weeks post transplantation the CD36$^{-/-}$ LK^{+FF} engrafted CD45.1 animals were injected with FFA-luc (Figure 5.36C and D). One-week later, after the mice had recovered the animals were injected with LPS for 16 hours. Following LPS treatment, there was no activation of luciferase in the BM compartment signifying long chain FFA are not taken up by CD36$^{-/-}$ haematopoietic cells in response to LPS (Figure 5.36C and D).
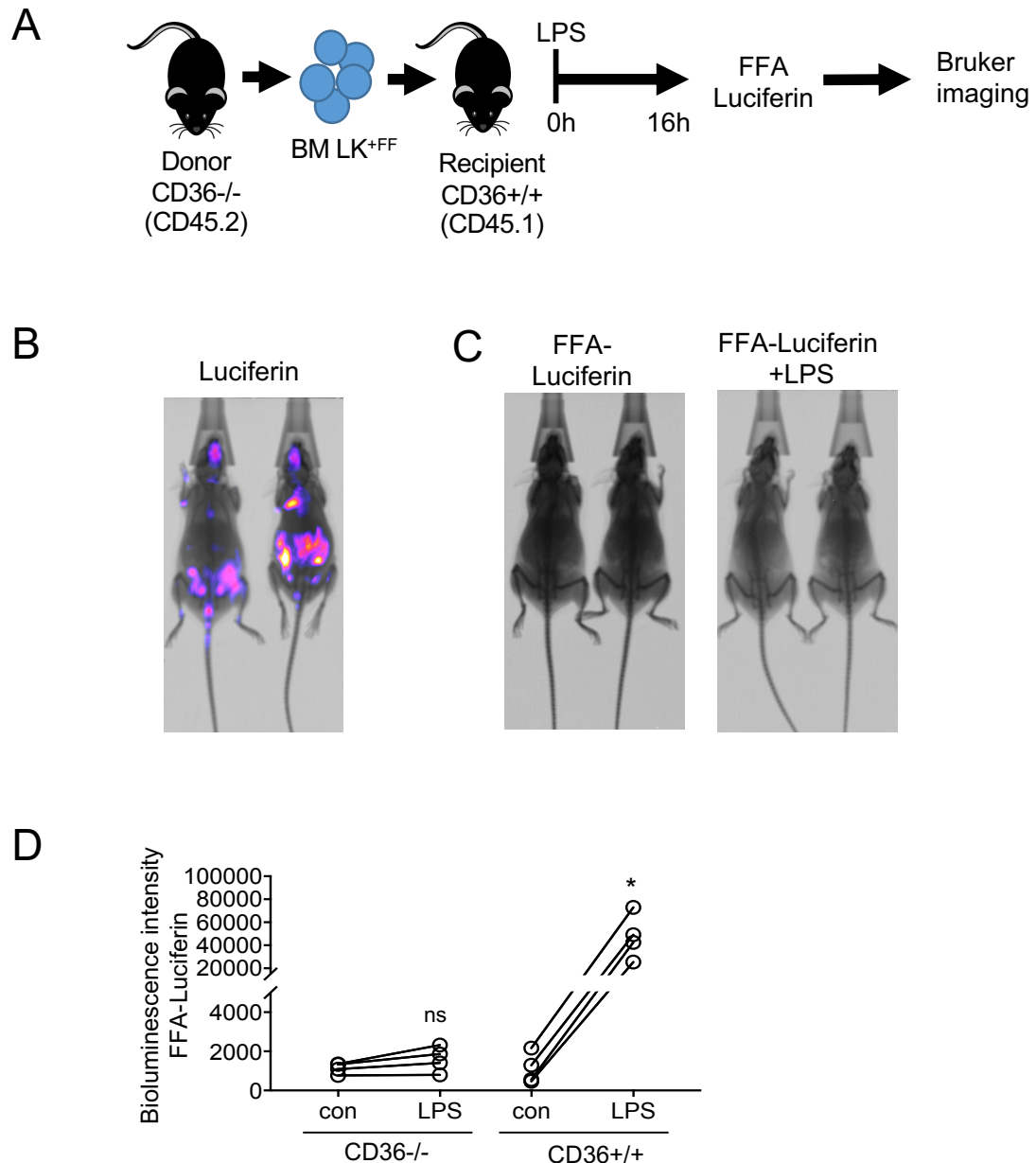
Figure 5.36. Treatment with LPS does not drives fatty acid uptake in the haematopoietic compartment of CD36$^{-/-}$ mice.
(A) Schematic diagram of the experimental design. CD36$^{-/-}$ lineage negative, CD117 positive (LK) cells were isolated and transduced with a firefly luciferase virus (LK^{+FF}) and transplanted into WT (CD36$^{+/+}$) CD45.2 animals. (B) Mice were bioluminescence imaged using luciferin to confirm engraftment. (C) Mice were injected with control PBS for 16 hours then treated with FFA-SS-luc and imaged using bioluminescence (FFA-luciferin). One-week later mice were injected LPS for 16 hours then treated with FFA-SS-luc and imaged using bioluminescence (FFA-luciferin+LPS). Representative images of control and LPS treated mice. (D) Densitometry of the bioluminescent images in (C) to determine fluorescence intensity in vehicle and LPS treated animals. n=4 in each group. Data shown are means ± SD *P < 0.05

To test the importance of CD36 in FFA uptake following *S.typhimurium* infection, WT CD36$^{+/+}$ and CD36$^{-/-}$ were infected with *S.typhimurium* for 72 hours (Figure 3.37A). Figure 5.37B confirms lipid levels were significantly increased in the WT CD36$^{+/+}$ LSK, HSC, ST-HSC and LT-HSC following *S.typhimurium* infection. Surprisingly LSK, HSC, and ST-HSC from *S.typhimurium* treated CD36$^{-/-}$ mice also had an increase in lipid content compared to control mice (Figure 5.37B). CD36 regulates the uptake of long chain FAs, it is expected following infection cells take up long chain FAs as they are more efficient energy source compare to short or medium chain FAs. Bodipy 493/503 staining is a measure of total lipid content in the cell therefore, the increase in lipid content observed in the could be due to an abundance of short or medium chain FAs. There was no difference in LT-HSC lipid levels from control and *S.typhimurium* treated CD36$^{-/-}$ mice (Figure 5.37B).
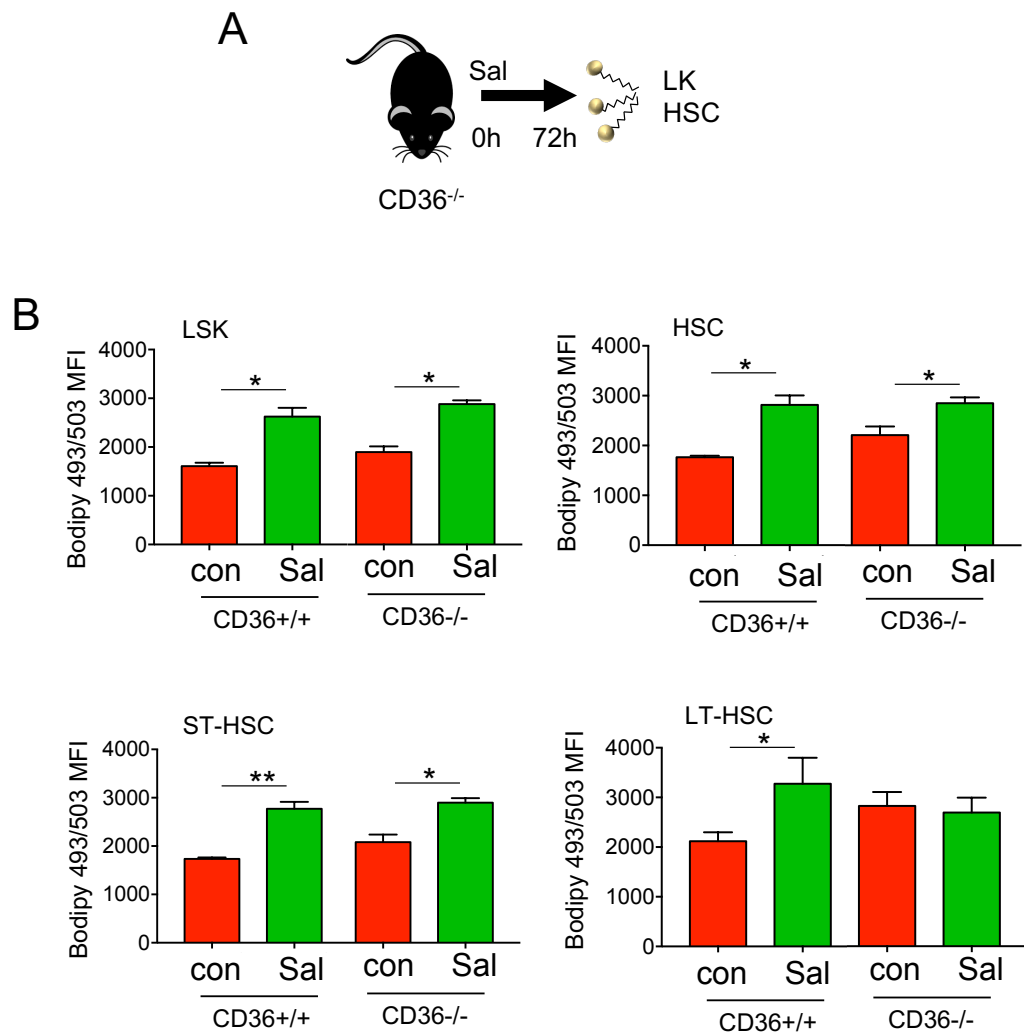
Figure 5.37. Lipid content is elevated in the CD36$^{-/-}$ HSC after *S.typhimurium* infection.
(A) Schematic of experimental design. CD36$^{-/-}$ or WT (CD36$^{+/+}$) mice were infected with *S.typhimurium* (Sal) for 72 hours, the animals were sacrificed, the bone marrow was extracted stained with a panel of antibodies and Bodipy 493/503. (B) Lipid content (Bodipy 493/503 mean fluorescence intensity (MFI)) in specific LSK, HSC, ST-HSC and LT-HSC populations n=6 in each group. Data shown are means ± SD *P < 0.05

Next, to visualise uptake of FFA within the LK cells following infection, LK cells isolated from the BM of control or *S. typhimurium* infected (72 hours) WT CD36$^{+/+}$ and CD36$^{-/-}$ mice. The cells were stained with Bodipy 493/503, Hoechst 33342 and Sca 1-APC membrane stain for 30 minutes and imaged using fluorescence microscopy (Figure 5.38A). LK cells positive for Sca 1-APC membrane stain were classified as LSKs. LSK cells from *S. typhimurium* infected WT CD36$^{+/+}$ mice had an increased lipid content quantified by Bodipy

493/503 fluorescence (Figure 5.38B). However, LSK cells from CD36$^{-/-}$ mice infected with *S. typhimurium* had a significantly reduced lipid content compared to control mice (Figure 5.38B).
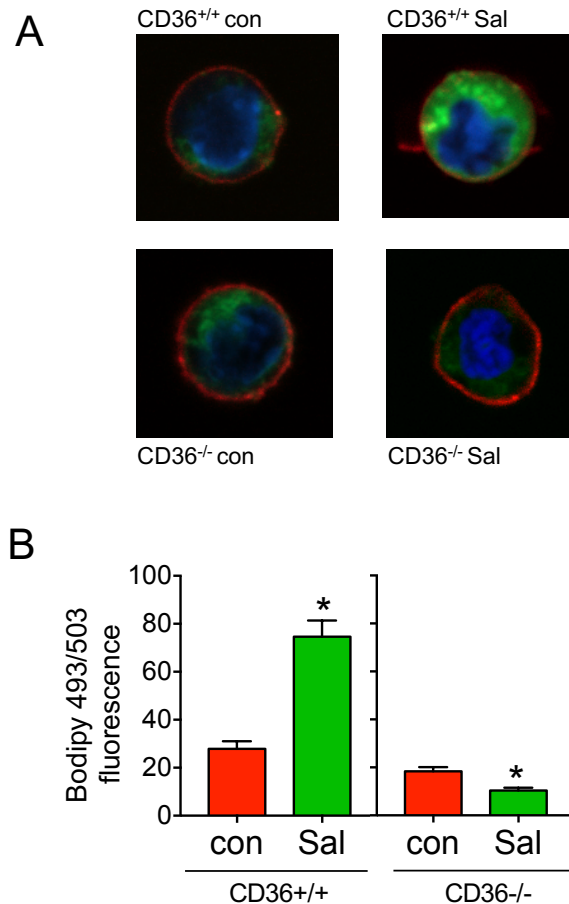
Figure 5.38. Infection with *S.typhimurium* does not drive fatty acid uptake in the LSK of CD36$^{-/-}$ mice.
CD36$^{-/-}$ or WT (CD36$^{+/+}$) mice were infected with *S.typhimurium* (Sal) for 72 hours. (A) Representative live cell fluorescent microscopy images of LK cells isolated from the mice, Sca 1-APC membrane stain (red), Bodipy 493/503 (green) and Hoechst 33342 (blue). Data shown are means ± SD of n=5 mice. (B) Quantification of Bodipy 493/503 fluorescence in LK cells from images shown, 20 LK cells from each mouse in each condition. Data shown are means ± SD *P < 0.05

To understand the importance of CD36 expression on HSPC metabolism in response to infection, LSK from CD36$^{+/+}$ and CD36$^{-/-}$ *S.typhimurium* infected mice were isolated by FACS. Seahorse XF Mito stress test analysis showed, in contrast to WT CD36$^{+/+}$, CD36$^{-/-}$ LSKs from *S.typhimurium* infected mice have no change in basal or maximal OCR compared to CD36$^{-/-}$ LSKs from control mice (Figure 5.39A and B).
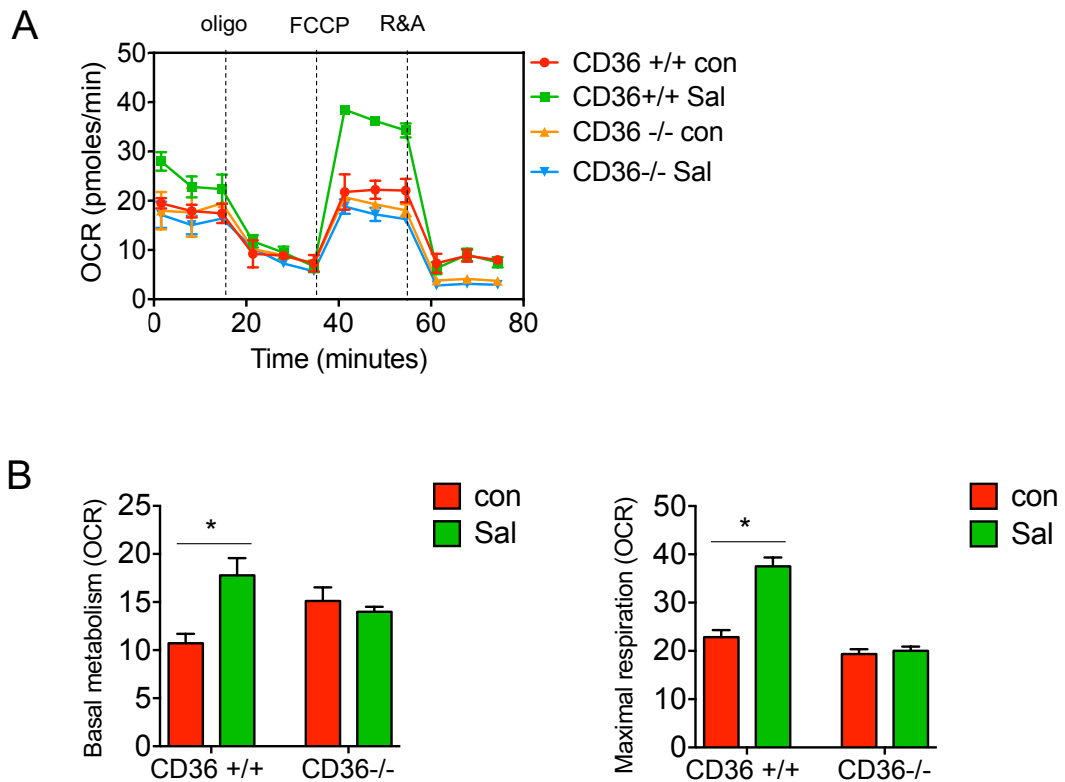
Figure 5.39. LSK from CD36$^{-/-}$ mice do not have increased OCR after S.typhimurium infection.
(A) CD36$^{-/-}$ or WT (CD36$^{+/+}$) mice were infected with *S.typhimurium* (Sal) for 72 hours. The bone marrow was extracted and stained with a panel of antibodies to isolate the LSK population by FACS and OCR levels were measured by the extracellular flux assay. (B) Basal mitochondrial respiration (normalised to rotenone) and maximal mitochondrial respiration of LSK cells from control and *S. typhimurium* treated animals. Data shown are means ± SD of n=6 mice in each group. *P < 0.05

To assess the changes in glycolysis in the WT CD36$^{+/+}$ and CD36$^{-/-}$ mice after *S.typhimurium* (72 hours) infection I used the extracellular flux assay to analyse ECAR (Figure 5.40A). In the WT CD36$^{+/+}$ mice there was an increase in basal OCR but was no observed increase in basal glycolysis (ECAR) following *S. typhimurium* (72 hours) infection (Figure 5.40B). Conversely, CD36$^{-/-}$ LSK have increased basal ECAR but no changes in basal OCR response to *S.typhimurium* infection (Figure 5.40B). Together, these data show that CD36 is essential for the uptake of FFA and subsequent cell cycling in response to infection.
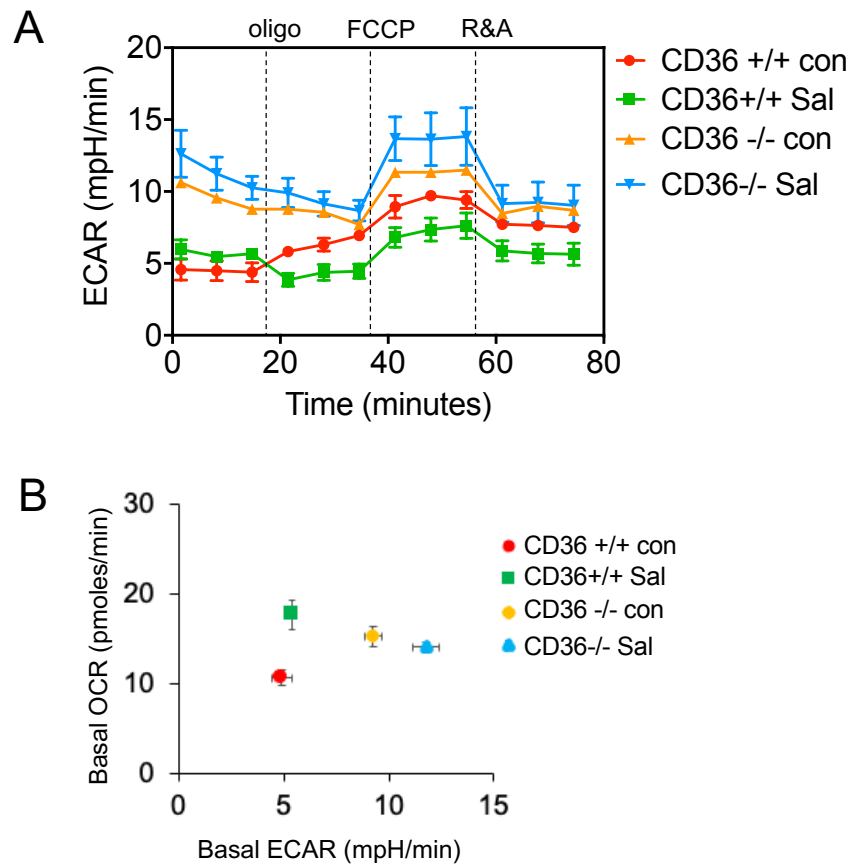
Figure 5.40. LSK from CD36$^{-/-}$ mice have an increased reliance on glycolysis after *S.typhimurium* infection.
(A) CD36$^{-/-}$ or WT (CD36$^{+/+}$) mice were infected with *S.typhimurium* (Sal) for 72 hours. The bone marrow was extracted and stained with a panel of antibodies to isolate the LSK population by FACS. ECAR was measured by the extracellular flux assay. (B) Basal OCR (normalised to rotenone) vs Basal ECAR of CD36$^{-/-}$ and CD36$^{+/+}$ LSKs after *S. typhimurium* infection. Data shown are means ± SD of n=6 mice in each group.

Next, to understand the importance of CD36 specifically in the haematopoietic compartment in response to infection, I used a transplantation model. LK cells from WT CD36$^{+/+}$ (CD45.2) mice were isolated and transplanted into recipient WT (CD45.1) animals, these were termed WT$^{(CD36+/+)}$. LK cells were also isolated from CD36$^{-/-}$ (CD45.2) mice and transplanted into recipient WT (CD45.1) animals, these were termed WT$^{(CD36-/-)}$. 14 weeks post transplantation WT$^{(CD36+/+)}$ and WT$^{(CD36-/-)}$ were infected with *S. typhimurium* for 4 days (Figure 5.41). The longer time point was chosen to assess the differences in the severity of the infection between the WT$^{(-/-CD36)}$ and the WT$^{(+/+CD36)}$ animals after *S. typhimurium* treatment.
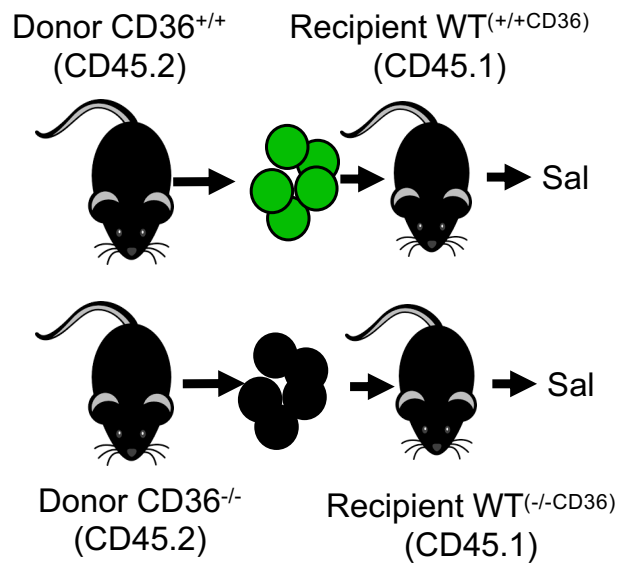
Figure 5.41. Schematic of experimental design.
CD36$^{+/+}$ CD45.2 or CD36$^{-/-}$ CD45.2 lineage negative, CD117 positive cells were isolated and transplanted into WT CD45.1 animals WT$^{(+/+CD36)}$ or WT$^{(-/-CD36)}$. Post engraftment mice were treated with *S. typhimurium* for 96 hours.

WT$^{(-/-CD36)}$ transplanted animals infected with *S. typhimurium* had a significantly increased weight loss compared to WT$^{(+/+CD36)}$ transplanted animals, a hallmark of more advanced *S. typhimurium* infection (Figure 5.42A). WT$^{(-/-CD36)}$ also had enhanced mortality compared to WT$^{(+/+CD36)}$ transplanted animals (4.42B).
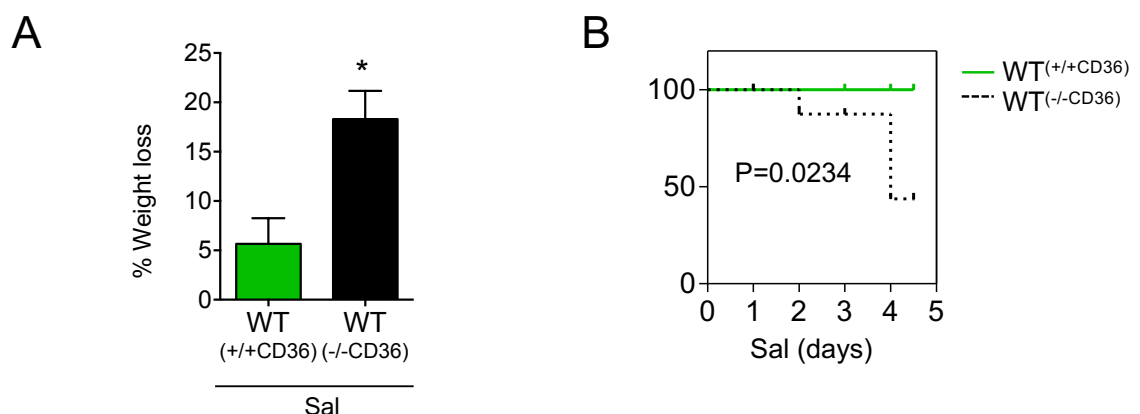
Figure 5.42. WT$^{(-/-CD36)}$ mice have increased weight loss and increased susceptibility to *S.typhimurium* infection.
CD36$^{+/+}$ CD45.2 or CD36$^{-/-}$ CD45.2 lineage negative, CD117 positive cells were isolated and transplanted into WT CD45.1 animals WT$^{(+/+CD36)}$ or WT$^{(-/-CD36)}$. Post engraftment mice were treated with *S.typhimurium* for 96 hours. (A) Percentage weight loss at 96 hours post *S.typhimurium* infection. (B) Kaplan-Meier survival curve. n>5 in each group. Data shown are means ± SD *P < 0.05

To determine engraftment mice were sacrificed, the BM was extracted and stained with CD45.2 FITC for flow cytometry analysis. Figure 5.43 confirms equal engraftment of WT CD36$^{+/+}$ (CD45.2) and CD36$^{-/-}$ (CD45.2) into WT CD45.1 mice.
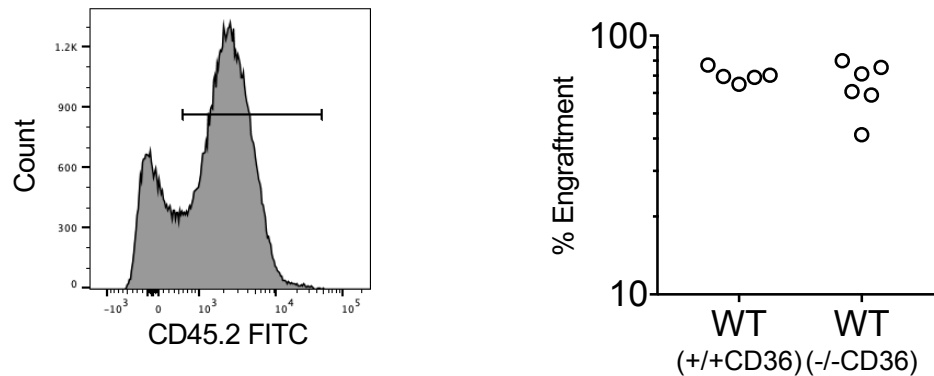
Figure 5.43. CD45.2 cell engraftment is seen in the bone marrow of transplant mice.
CD36$^{+/+}$ CD45.2 or CD36$^{-/-}$ CD45.2 lineage negative, CD117 positive cells were isolated and transplanted into WT CD45.1 animals WT$^{(+/+CD36)}$ or WT$^{(-/-CD36)}$. Post engraftment mice were treated with *S.typhimurium.* 96 hours post *S. typhimurium* treatment the animals were sacrificed, and the BM was extracted, the cells were analysed by flow cytometry for CD45.1 expression to confirm engraftment. n>5 in each group. Data shown are means ± SD

Following 96 hours of *S.typhimurium* infection blood was taken from the WT$^{(+/+CD36)}$ and WT$^{(-/-CD36)}$ mice. The serum was isolated and assessed for levels of FFA. Figure 5.44 shows there was an increase in serum FFA levels from *S.typhimurium* treated WT$^{(-/-CD36)}$ mice compared to *S.typhimurium* treated WT$^{(CD36+/+)}$ mice.
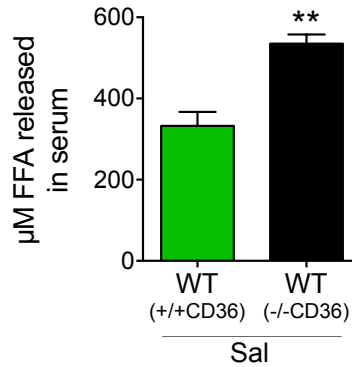
Figure 5.44. Elevated levels of FFA in the serum of WT$^{(-/-CD36)}$ mice following *S.typhimurium* infection.
CD36$^{+/+}$ CD45.2 or CD36$^{-/-}$ CD45.2 lineage negative, CD117 positive cells were isolated and transplanted into WT CD45.1 animals WT $^{(+/+CD36)}$ or WT$^{(-/-CD36)}$. Post engraftment mice were treated with *S.typhimurium* for 96 hours. Blood was taken from the animals by cardiac puncture and the serum was assessed for levels of FFA. n>5 in each group. Data shown are means ± SD **P < 0.01

I next determined the importance of CD36 expression on the haematopoietic compartment on lipid levels following *S.typhimurium* infection. Figure 5.45 show lipid levels were significantly decreased in the WT$^{(-/-CD36)}$ LSK, HSC, ST-HSC, and LT-HSC compared to the WT$^{(+/+CD36)}$ HSPCs following *S.typhimurium* infection.
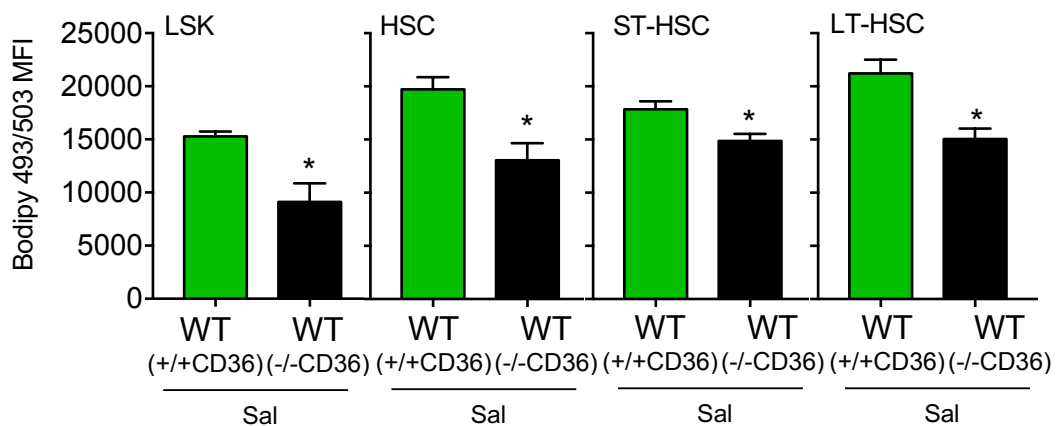
Figure 5.45. WT$^{(-/-CD36)}$ mice have a reduced lipid content in the HSC following *S.typhimurium* infection.
CD36$^{+/+}$ CD45.2 or CD36$^{-/-}$ CD45.2 lineage negative, CD117 positive cells were isolated and transplanted into WT CD45.1 animals WT$^{(+/+CD36)}$ or WT$^{(-/-CD36)}$. Post engraftment mice were treated with *S.typhimurium* for 96 hours. The animals were sacrificed, the bone marrow was extracted stained with a panel of antibodies and Bodipy 493/503. Lipid content (Bodipy 493/503 mean fluorescence intensity (MFI)) was assessed in specific LSK, HSC, ST-HSC and LT-HSC populations by flow cytometry. n>5 in each group. Data shown are means ± SD *P < 0.05

Alongside lipid level quantification, the BM was also stained with a panel of antibodies, permeabilised and fixed to assess cell cycling by flow cytometry. There was a significant decrease in LSK, HSC, ST-HSC and LT-HSC cell cycling from WT$^{(-/-CD36)}$ animals treated with *S.typhimurium* compared to the WT$^{(+/+CD36)}$ HSPC (Figure 5.46).
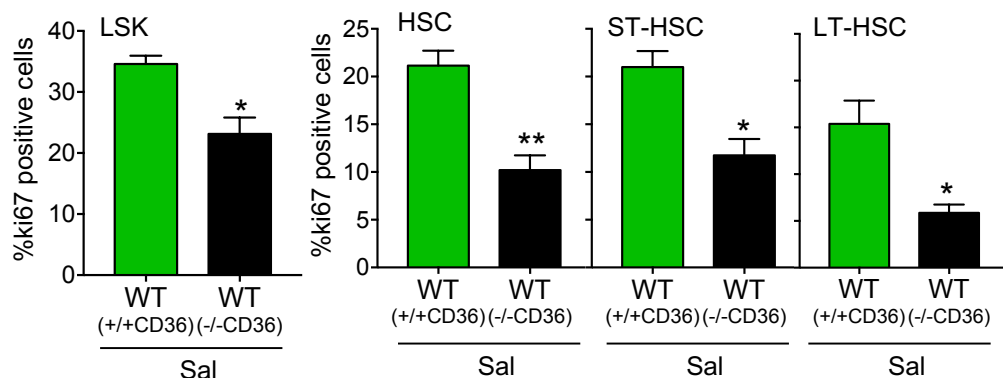
Figure 5.46. WT$^{(-/-CD36)}$ mice have a reduced HSC Ki67 positive expression following *S.typhimurium* infection.
CD36$^{+/+}$ CD45.2 or CD36$^{-/-}$ CD45.2 lineage negative, CD117 positive cells were isolated and transplanted into WT CD45.1 animals WT$^{(+/+CD36)}$ or WT$^{(-/-CD36)}$. Post engraftment mice were treated with *S.typhimurium* for 96 hours. The animals were sacrificed, the bone marrow was extracted stained with a panel of HSC antibodies and Ki67 to analyse cell cycling in the LSK, HSC, ST-HSC and LT-HSC population. Percentage of cycling cells was measured by Ki67 positive cells after *S.typhimurium* treatment. n>5 in each group. Data shown are means ± SD *P < 0.05 **P < 0.01

Finally, to determine if the uptake of FFA in response to infection is specific to HSCs I developed a transplant model in which WT CD45.1 LK cells were isolated and transplanted into CD36$^{-/-}$ mice. Therefore, these animals were CD36 knockout but had a WT haematopoietic system. 14 weeks post transplantation the animals were treated with LPS for 16 hours (Figure 5.47A). The mice were then sacrificed, the BM was extracted, and stained with CD45.1 PE to monitor engraftment. Figure 5.47B and Appendix Figure 8.1 and 8.3 confirms equal engraftment of CD45.1 WT cells in recipient CD45.2 CD36$^{-/-}$ mice within both treatment groups.
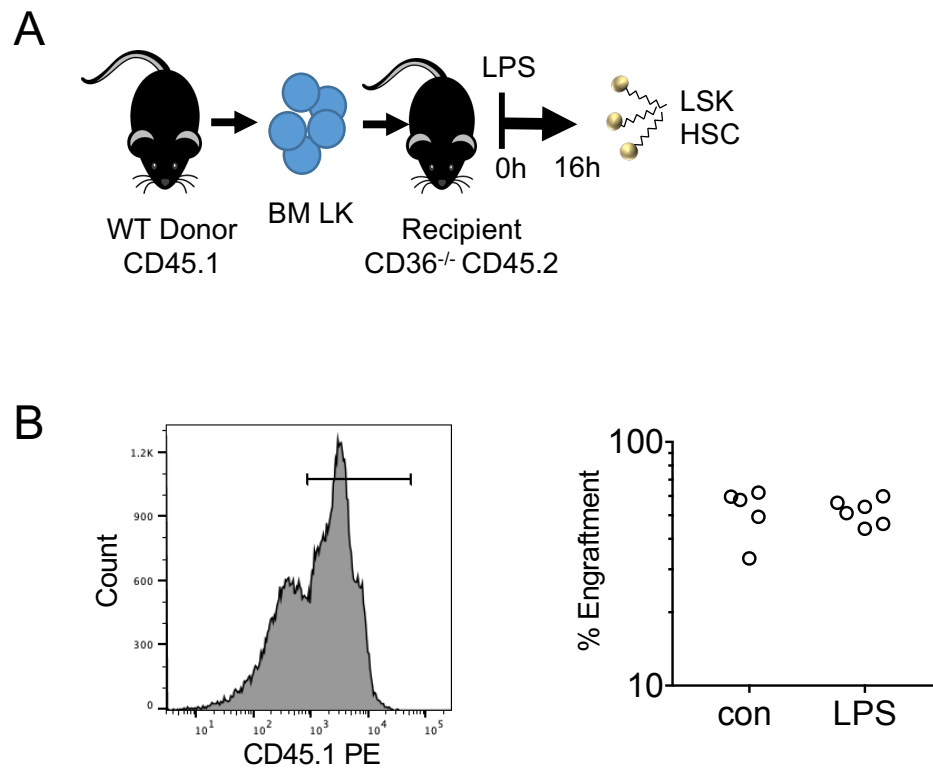
Figure 5.47. CD45.1 cell engraftment is seen in the bone marrow of CD36$^{-/-}$ mice transplanted with CD36$^{+/+}$ LK cells.
(A) Schematic diagram of experimental design. CD36$^{+/+}$ CD45.1 lineage negative, CD117 positive cells were isolated and transplanted into CD36$^{-/-}$ CD45.2 animals. Post engraftment mice were treated with LPS for 16 hours and cells were analysed by flow cytometry. (B) 16 hours post LPS treatment the animals were sacrificed and the bone marrow was extracted, the cells were analysed for CD45.1 expression to confirm engraftment. n>5 in each group. Data shown are means ± SD

I next looked at the effect treatment with LPS had on CD36 expression in the HSPCs from the transplant mice. CD36 expression was elevated in the WT HSC LSK, HSC, ST-HSC and LT-HSC transplanted into CD36$^{-/-}$ mice after treatment with LPS (Figure 5.48).
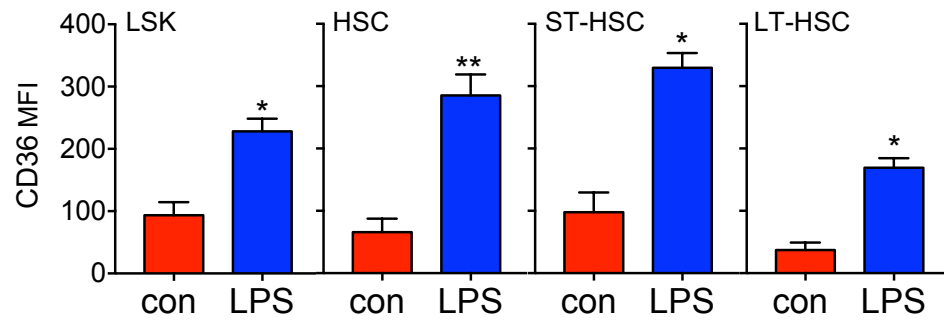
Figure 5.48. CD36 expression is elevated in CD36$^{-/-}$ mice transplanted with CD36$^{+/+}$ LK cells following LPS treatment.
CD36$^{+/+}$ CD45.1 lineage negative, CD117 positive cells were isolated and transplanted into CD36$^{-/-}$ CD45.2 animals. Post engraftment mice were treated with LPS for 16 hours. The animals were sacrificed, the bone marrow was extracted and stained with a panel of antibodies to analyse CD36 expression in specific LSK, HSC, ST-HSC and LT-HSC populations. n>5 in each group. Data shown are means ± SD *P < 0.05 **P < 0.01

Moreover, lipid content within the LSK, HSC, ST-HSC and LT-HSC was significantly increased in the WT CD36$^{+/+}$ into CD36$^{-/-}$ mice in response to LPS treatment. This increase in lipid content observed was similar to the WT response to LPS (Figure 5.49).
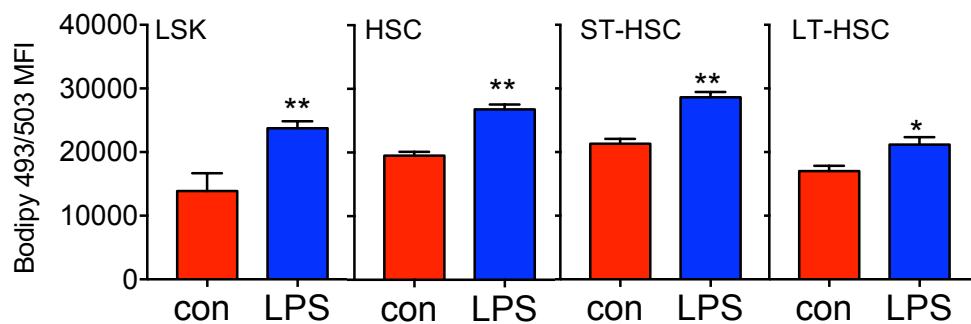
Figure 5.49. LPS induces an increase in lipid content in the haematopoietic populations of the CD36$^{-/-}$ mice transplanted with CD36$^{+/+}$ LK cells.
CD36$^{+/+}$ CD45.1 lineage negative, CD117 positive cells were isolated and transplanted into CD36$^{-/-}$ CD45.2 animals. Post engraftment mice were treated with LPS for 16 hours. The bone marrow was extracted and stained with a panel of antibodies and Bodipy 493/503 to analyse lipid content (Bodipy 493/503 mean fluorescence intensity (MFI)) in specific Lin-, LSK, HSC, ST-HSC and LT-HSC populations. n>5 in each group. Data shown are means ± SD *P < 0.05 **P < 0.01

Next, to determine if the increase in lipid content was due to uptake of FFA, LK cells were isolated from the transplant mice and incubated with Bodipy FL-C12 for 30 minutes. Similar to the WT animal, increased FFA uptake was observed in the LK cells from the LPS treated transplant mice compared to LKs from untreated transplant mice (Figure 5.50).
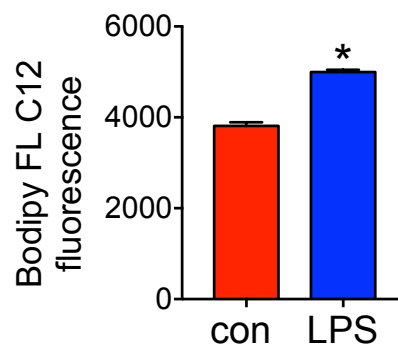
Figure 5.50. LPS induces an uptake of FFA in the haematopoietic progenitor populations of the CD36$^{-/-}$ mice transplanted with CD36$^{+/+}$ LK cells.
CD36$^{+/+}$ CD45.1 lineage negative, CD117 positive (LK) cells were isolated and transplanted into CD36$^{-/-}$ CD45.2 animals. Post engraftment mice were treated with LPS for 16 hours. The animals were sacrificed, and the bone marrow extracted. LK cells were isolated and incubated with Bodipy FL-C12 and fluorescence was measured. n>5 in each group. Data shown are means ± SD *P < 0.05

In addition to engraftment, CD36 expression and lipid content, the BM was also stained with a panel of antibodies, permeabilised and fixed to assess HSPC cycling. Figure 5.51 shows there was increased LSK, HSC, ST-HSC and LT-HSC cell cycling in the transplant animals in response to LPS treatment.
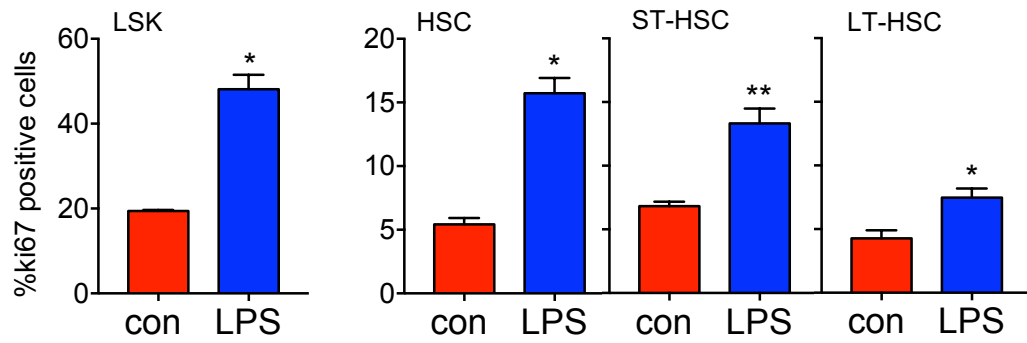
Figure 5.51. LPS increases Ki67 expression in HSC in the CD36$^{-/-}$ mice transplanted with CD36$^{+/+}$ LK cells.
CD36$^{+/+}$ CD45.1 lineage negative, CD117 positive cells were isolated and transplanted into CD36$^{-/-}$ CD45.2 animals. Post engraftment mice were treated with LPS. Following 16 hours of LPS treatment, the animals were sacrificed, and the bone marrow extracted. The bone marrow was stained with a panel of HSC antibodies and Ki67 to analyse cell cycling in the LSK, HSC, ST-HSC and LT-HSC population. Percentage of cycling cells was measured by Ki67 positive cells after LPS treatment. n>5 in each group. Data shown are means ± SD *P < 0.05 **P < 0.01

To investigate if the increase in cell cycling was associated with an increased cell number, HSPC cell count per 100 000 BM cells was assessed by flow cytometry. Comparable to the WT response to infection, Figure 5.52 confirms a significant increase in cell number of LSK, HSC, ST-HSC and LT-HSC populations per 100 000 BM cells following and LPS treatment.
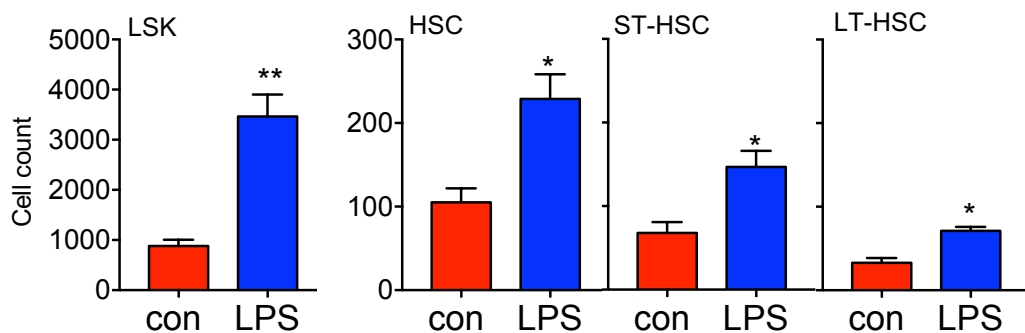
Figure 5.52. LPS increases HSC numbers per 100 000 BM cells counted in CD36-/- mice transplanted with CD36$^{+/+}$ LK cells.
CD36$^{+/+}$ CD45.1 lineage negative, CD117 positive cells were isolated and transplanted into CD36$^{-/-}$ CD45.2 animals. Post engraftment mice were treated with LPS. Following 16 hours of LPS treatment, the animals were sacrificed, the bone marrow was extracted and stained with a panel of antibodies to analyse cell number per 100 000 bone marrow cells in specific LSK, HSC, ST-HSC and LT-HSC populations. n>5 in each group. Data shown are means ± SD *P < 0.05

Next to understand the metabolic changes in the HSPCs from the transplant mice after LPS treatment, I used the mitochondrial extracellular flux assay. LSKs isolated from LPS treated transplant animals had an increased basal and maximal respiration compared to the control LSKs (Figure 5.53A and B).
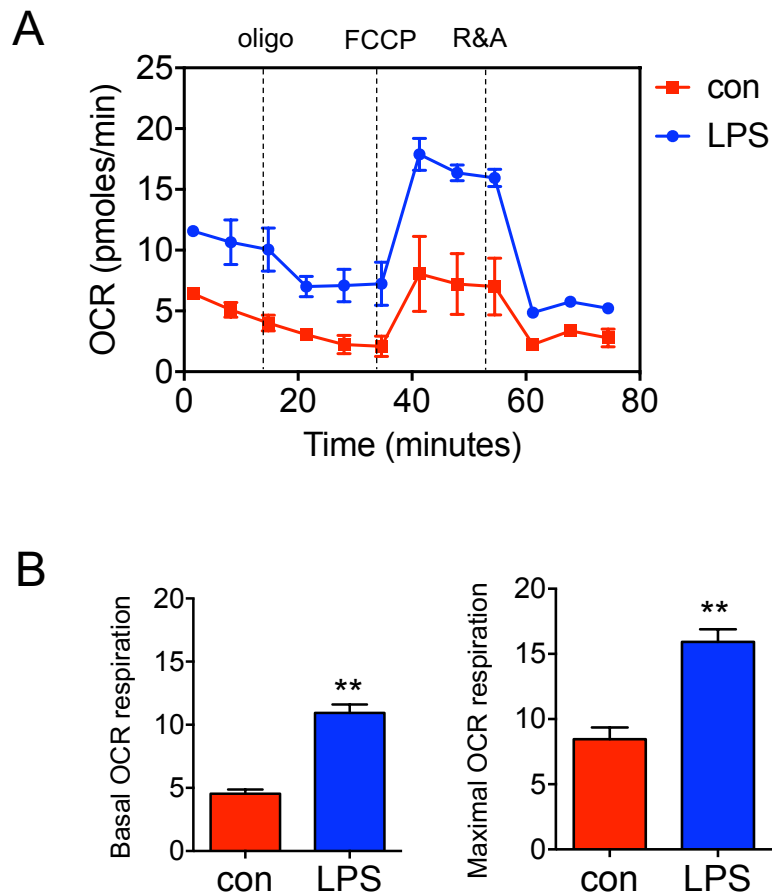
Figure 5.53. LSKs from CD36$^{-/-}$ mice transplanted with CD36$^{+/+}$ LK cells have an increased OCR following LPS infection.
(A) CD36$^{+/+}$ CD45.1 lineage negative, CD117 positive cells were isolated and transplanted into CD36$^{-/-}$ CD45.2 animals. Post engraftment mice were treated with LPS. Following 16 hours of LPS treatment, the animals were sacrificed, the bone marrow was extracted and stained with a panel of antibodies to isolate the LSK population by FACS and OCR levels were measured by extracellular flux assay. (B) Basal mitochondrial respiration (normalised to rotenone) and maximal mitochondrial respiration of LSK cells from control and LPS treated transplant mice. n>5 in each group. Data shown are means ± SD **P < 0.01

Next, to assess glycolysis in the LSK from the control and LPS treated transplant animals, ECAR was measured. Similar to WT animals, glycolysis was not significantly upregulated in the LSKs from the LPS treated transplant animals compared to control transplant animals (Figure 5.54A and B). Together these data show that CD36 on the HSC is essential for the haematopoietic response to infection.
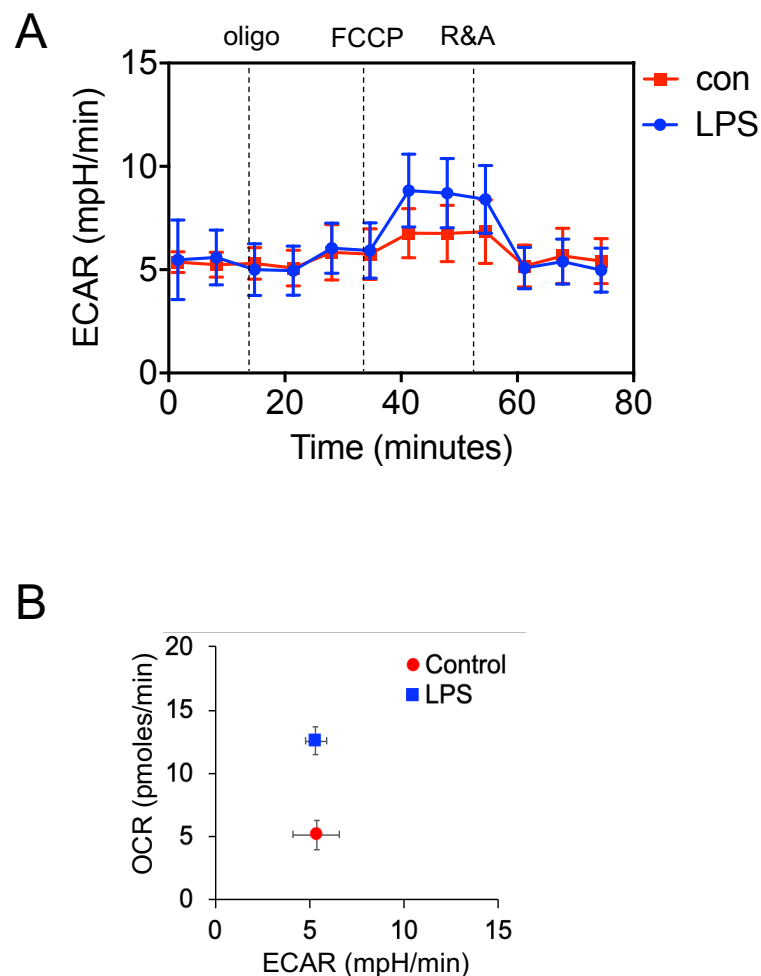
Figure 5.54. LSKs from CD36$^{-/-}$ mice transplanted with CD36$^{+/+}$ LK cells no change in basal ECAR after LPS infection.
(A) CD36$^{+/+}$ CD45.1 lineage negative, CD117 positive cells were isolated and transplanted into CD36$^{-/-}$ CD45.2 animals. Post engraftment mice were treated with LPS. Following 16 hours of LPS treatment, the animals were sacrificed, the bone marrow was extracted and stained with a panel of antibodies to isolate the LSK population by FACS. ECAR was measured by extracellular flux assay (B) Basal OCR (normalised to rotenone) vs basal ECAR of control and LPS treated transplant mice. n>5 in each group. Data shown are means ± SD

5.5   Summary

In the final results chapter of my thesis I have presented data to show HSCs have an increased lipid content following infection. This lipid increase is due to the acquisition of FFA into the cells and causes a metabolic shift in the HSCs towards a dependency on β-oxidation as a source of energy. Moreover, the inhibition of β-oxidation leads to decreased OCR and subsequent reduction of Ki67 positive cells. I have also shown the acquisition of FFA into the HSC is regulated by the membrane fatty acid transporter CD36. Without CD36 expression on the HSC during infection, there is an impaired uptake of FFA and an increased use of glycolysis as the metabolic pathway to generate ATP. There is also a decreased cell cycling which leads to an increased susceptibility to the infection and enhanced mortality. Overall, HSCs take up FFA into the cell via CD36 which leads to an increased dependency on β-oxidation, a process which is critical for the immune response to infection.

6   Discussion and Conclusions

6.1   General discussion

Infectious diseases have been a major selective pressure in mammalian evolution and are still a leading cause of global mortality. Of the top 10 causes of global death in 2019, two are communicable or infectious diseases, diarrhoeal diseases and lower respiratory infections (382). The innate immune response to the challenge of infection must be rapid and robust to generate significant numbers of leukocytes in a short space of time. The most abundant leukocyte found in mammals are neutrophils and they contribute to infection resolution by activation of other lymphocytes, capturing microbes within extracellular traps, phagocytosis and enzyme mediated lysis (383). During infection neutrophil and other immune cell turnover is colossal, there is an increased demand and the haematopoietic system responds by rapidly switching from steady-state haematopoiesis to emergency granulopoiesis (384). This transition involves interactions between both haematopoietic and non-haematopoietic cells of the BM microenvironment including exchange of cytokines and growth factors (385-387). BMSC specifically have previously been shown to support the increased demand for haematopoiesis during inflammatory conditions, preventing HSC exhaustion (388). The change from steady-state to emergency haematopoiesis places substantial metabolic demand on the haematopoietic system.   A better understanding of the metabolic changes in the HSC during normal physiological stress can help in understanding how these processes can become dysregulated in diseases such as ageing and cancer.

In this thesis I have described the process of mitochondrial transfer from BMSC to haematopoietic progenitors to support the innate immune response to acute infection. Additionally, I have identified a mechanism regulating this transfer and subsequent onset of emergency haematopoiesis by an increase in mitochondrial content causing a metabolic change in the HSC before mitochondrial biogenesis can occur. I have also identified a substrate used by the mitochondria during infection, the HSCs take up FFA to support the

257

increased metabolic demand. Moreover, this study established the mechanisms governing the uptake of the FFA into the HSC, without which leads to an enhanced susceptibility to the infection causing mortality.

6.2   Key findings

6.2.1   Mitochondrial transfer in the bone marrow

In this thesis, I have shown mitochondria are trafficked from the BMSC to the HSC during infection, adding to the many cells types which undergo intercellular mitochondrial transfer.

HSCs have previously been shown to be utilise glycolysis as opposed to mitochondrial OXPHOS to meet their energy demands, a metabolic adaptation influenced by their hypoxic niche (245). This preference for glycolysis reflects the low metabolic demands of the quiescent HSC as OXPHOS is the most efficient pathway for energy production (389). The reduced reliance on mitochondrial function in the HSC allows for maintenance of low ROS levels, as HSCs are vulnerable to oxidative stress (351, 390). Furthermore, it has been shown that HSC mitochondria are relatively inactive (287) and ROS associated with mitochondrial activity is lower in the HSC compared to the more committed progenitors (245, 288). This suggests HSCs require a rapid burst of mitochondrial metabolism for differentiation. Whilst it is known that HSCs switch from glycolysis to OXPHOS for the increased energy demand required for differentiation, the mechanisms regulating this switch remains to be elucidated. However, it is probable, the metabolic change is more complex than a switch from one metabolic pathway to another. This metabolic switch in the HSC may have evolved from an increase in energy demand for rapid differentiation in response to exogenous stress. Here I find pathogenic stress initiates an increase in mitochondrial mass within the HSC prompting a metabolic switch to an increased reliance on mitochondrial OXPHOS.

Notably, it has been shown that HSCs undergoing self-renewal need to minimise mitochondrial activity to remain quiescent (247, 286, 391). Moreover, these HSCs have been shown to have a higher long term multilineage reconstituting ability in both primary and secondary transplants compared to HSCs with increased mitochondria membrane potential, indicating mitochondrial biogenesis (392). This may suggest, whilst I find HSCs have an increased mitochondrial mass during infection there may be a subset of HSCs which do not have an increased mitochondrial content to maintain self-renewal and replenish the HSC pool without exhaustion.

Given the supporting data on increased mitochondrial activity in the more committed progenitor cells it would be expected that these cells also have an increased mitochondrial content during infection. However, I find two hours following LPS treatment there is no increase in the mitochondrial content in the committed progenitor populations. Mitochondrial respiration occurs in immune cells however, the rate of consumption is dependent on the specific cells state of reactivity. It has previously been reported that activated immune cells could favour glycolysis due to it generating ATP more rapidly than OXPHOS (393). Moreover, the metabolic profile of the committed progenitors differs from that of the HSCs (247). Therefore, this could be the reason why the more committed progenitors do not have an increased mitochondrial mass following infection.

Intercellular mitochondrial transfer is increasingly becoming recognised as a fundamental process occurring in both malignant and non-malignant tissue. In a malignant setting the mitochondrial trafficking to the tumour cells increases ATP production through enhanced OXPHOS which enables the progression of lung (293), breast (394), melanoma (298) and ovarian (394) cancer. In addition, my lab group has shown that mitochondria are transferred from the BMSC to the AML blasts in a NOX2 dependent manner. The mitochondrial transfer promoted an increase in OXPHOS in the AML and inhibition of NOX2 prevented the transfer of mitochondria decreasing AML survival (41). Moreover, this caused an upregulation of PGC-1α driven mitochondrial biogenesis in the BMSC (395). Non- malignant cells have also been shown to

acquire mitochondria from an adjacent cell. BM derived stromal cells protect against acute injury by mitochondrial transfer to the pulmonary alveoli following LPS treatment (295). In the first chapter of my thesis I established mitochondrial transfer occurs in a non-malignant haematological system following pathogenic stress. Therefore, suggesting that mitochondrial transfer to AML is a process which has been hijacked from the highly evolved normal HSC physiological response to infection. It also provides a paradigm in which other malignant cells, established to be dependent on mitochondrial transfer for survival, have evolved from the non-malignant counterpart which use mitochondrial transfer in response to stress. It is also likely many non-malignant cells which have a strong association with adjacent cells may undergo mitochondrial transfer.

6.2.2   Mitochondrial biogenesis and infection

Importantly in this study I found that this mitochondrial transfer occurred from the BMSC to the HSC before the onset of mitochondrial biogenesis. It has previously been shown the transition from quiescent to active HSCs is inherently associated with increased mitochondrial biogenesis (396-399). During the transition, mitochondrial health is tightly regulated by mitochondrial unfolded protein response (UPR^{mt}). Moreover, SIRT7 a vital component of UPR^{mt} can supress mitochondrial biogenesis to conserve the HSC pool under stress (400). These data highlight the HSCs ability to activate numerous mechanisms to regulate metabolic activity, which is a fundamental determinant of HSC maintenance and cell fate. It also suggests HSCs critically need to increase their mitochondrial mass prior to undergoing differentiation. In context, I find within two hours of LPS infection mitochondrial biogenesis is not upregulated, therefore the mitochondrial transfer to the HSC is vital to increase mitochondrial mass for HSC activation in response to the infection.

Whilst I found biogenesis was not upregulated two hours after infection, I did find PGC-1α mRNA was upregulated. PGC-1α is a co-transcriptional activator which is a central regulator of mitochondrial biogenesis (401). PGC-1α activates various transcription factors including NRF1 and NRF2, which in turn

promotes Tfam expression driving transcription and replication of mtDNA (402). However, PGC-1α has also been highlighted to regulate ROS levels within the cell by elevating the expression of various ROS-detoxifying enzymes. Excess ROS within the cell can cause damage to DNA, lipids and proteins. St-Pierre *et al*. 2003 reported expression of PGC-1α in muscle cells increased the expression of superoxide dismutase 2 (SOD2) and glutathione peroxidase 1 (GPX1), which remove superoxide and hydrogen peroxide respectively (403). Moreover, PGC-1α expression improved cell survival in oxidative stress conditions (404) whilst reduced expression sensitised cells to oxidative stress (405). This suggests the alongside the initiation of mitochondrial biogenesis, the increased expression of PGC-1α seen at 2 hours following LPS infection may be to maximise ATP production whilst preventing oxidative damage in the cell.

Furthermore, there is increasing evidence to suggest PGC1α also regulates the intrinsic properties of the mitochondria, which can impact oxidative metabolism and gene expression changes (401). Mitochondria isolated from muscle cells of transgenic mice ectopically expressing PGC1α had a greater capability for substrate oxidation compare to wild type mice (403). Therefore, the new mitochondria that are imported in the presence of PGC1α following infection, could have different properties including a higher ability to oxidise substrates compared to the original organelles.

6.2.3   BMSC and stressed haematopoiesis

It is becoming more apparent that HSCs heavily rely on the supportive BM microenvironment for HSC maintenance and differentiation. BMSC specifically, can support haematopoiesis through both direct and indirect mechanisms and therefore, are a key component of the HSC cell niche (406). My results contribute to the evidence, I have shown during infection BMSC donate their mitochondria to the HSCs for an increased metabolic capacity. It has also been shown this process occurs from the HSC to the BMSC through CX43 mediated gap junctions (324). The mitochondria were shown to be transferred to the BMSC to modulate ROS within the HSC. However, this

research was a conference abstract therefore, limited conclusions can be made. Nonetheless, it is clear mitochondrial transfer between HSC and the microenvironment is a fundamental process that occurs to support haematopoiesis.

Mitochondrial transfer involving BMSCs has also been reported in many malignant haematopoietic cells including AML (41) and ALL (407) to enhance proliferation and survival. Moreover, AML stimulates mitochondrial biogenesis in BMSCs ensuring the BMSCs remain a viable, continual source of mitochondria (408). Although not researched in this thesis, I believe a similar process occurs in BMSCs following infection to ensure a constant supply of mitochondria to the HSC. Taken together the BMSC is a key supportive cell in both malignant and non-malignant haematopoiesis.

6.2.4   ROS and infection

It has been well reported that ROS production is rapidly increased in response to infection. This acts to facilitate clearance of the pathogen and activate signalling cascades associated with cell proliferation and inflammation (409, 410). The two sources of ROS which have been well characterised during host cell- microbial interaction are the mitochondrial electron transport chain and membrane associated NOX complex. The NOX complexes are typically associated with phagocytic cells which have a rapid respiratory burst mechanism to generate ROS (411). NOX machinery has also been found in numerous non-phagocytic cell types including epithelial and endothelial cells (412, 413). NOX2 specifically, located on monocytes/macrophages is vital in the immune response to bacterial infection and defects in the enzyme leads to CGD (233). It has been shown that BM microenvironment myeloid cell derived NOX2 ROS plays a crucial role in facilitating emergency granulopoiesis during infection (414). Moreover, it is known that NOX2 activation is crucial for microbial management, however the direct mechanism linking the initiation of the complex and pathogen elimination is not yet clear. In this study I have shown the production of NOX2 derived ROS by the macrophages increases oxidative stress in BMSC and the HSC driving mitochondrial transfer.

Moreover, mitochondrial transfer from the BMSC to the HSC was reduced in mice with the inability for phagocytic NOX2 production. Overall this suggest that NOX2 derived ROS is vital for the immune response to acute infection.

6.2.5 Macrophages in the HSC niche

Macrophages play a significant defensive role in combatting infection by responding to systemic signals via expression of many cytokines and chemokines (415). Many studies have shown that macrophages also play a key role in the regulation of HSCs. Tissue specific BM macrophages promote HSC retention by regulating osteolineage cells and BMSCs, thus antagonising the SNS-mediated inhibition of HSC retention in the BM (77, 355, 356, 416). *In vivo* depletion of macrophages using genetic models or clodronate-loaded liposomes promotes the mobilization of HSPCs into the blood (355). Furthermore, BM CD169^{+} macrophages promote the retention of HSCs in the BM by inducing the expression of CXCL12 (77). Moreover, a rare population of macrophages that are α-smooth muscle actin positive, localized adjacent to HSCs, may protect HSCs from exhaustion by limiting the production of ROS under stress (417). My research shows in the absence of macrophages there is a significant decrease in macrophage generated NOX2 ROS following infection. This leads to a reduction of mitochondrial mass and subsequent block on cell number increase within the HSPC populations. Therefore, regulation of HSC mitochondrial content by production of NOX2 derived ROS can be added to the list of key roles of the macrophage during acute infection.

6.2.6 Gap junctions; the mitochondrial transporter

Mitochondria have previously been shown to be transferred intercellularly by TNTs (293, 394, 418, 419), extracellular vesicles (296) and gap junctions (295). During infection I found mitochondria was transferred from the BMSC to the HSC via CX43 mediated gap junction. The gap junction inhibitor CBX and the CX43 memetic peptide Gap27 reduce mitochondrial transfer between BMSC and the HSCs. Interestingly, whilst AML is the malignant counterpart to

the HSPCs the mechanism of mitochondrial transfer differed. Transfer of mitochondria from the BMSC to the AML was shown to be facilitated by TNTs and inhibition of TNT formation by CytoB blocked this mitochondrial transfer (41). I found that inhibition of TNT formation by CytoB has no effect on mitochondrial content in the HSC. This could be due to the HSC residing in close proximity to the BMSC within the niche allowing for gap junction formation between these cells (420). CytoB is commonly used for inhibiting TNTs however it works by inhibiting actin therefore is not specific to inhibiting the formation of TNTs. Thus, mitochondria could move through TNTs to the HSC however the gap junction's formation is the critical mechanism in regulating mitochondrial transfer during infection.

Gap junctions are plasma membrane channels that allow for the direct interchange of cytoplasmic components between adjacent cells (319). They enable the exchange of small molecules including ions, second messengers (e.g. Ca^{2+}, IP_3, cAMP), metabolites, individual amino acids and short peptides through a regulated gate (320). This raises the question during infection what else moves between the BMSC and the HSC besides mitochondria? To further understand the physiological response to infection, it would be interesting to determine the extent of the transfer between HSC and BMSC. Unfortunately, this was not in the scope of my PhD but hopefully will be investigated in the future.

It has been reported that mitochondrial transfer is bi-directional and mitochondria transfer from T-ALL cells to BMSC via TNTs (421). This transfer was found to reduce levels of ROS in the T-ALL cells. This was similar to Golan *et al.* 2016, where mitochondria were transferred to the BMSCs to modulate ROS within the HSC (324). High levels of mitochondrial ROS have been associated with dysfunctional mitochondria (422) therefore in these studies the transferred mitochondria could be dysfunctional. It would be interesting to investigate if HSCs are exporting dysfunctional mitochondria during infection to aid in cellular proliferation.

6.2.7 PI3K and infection

PI3Ks are a family of lipid kinases key in mediating many intracellular signalling cascades involved in proliferation and survival (423). PI3Ks are comprised of a catalytic subunit and a regulatory subunit, the regulatory subunit stabilises and blocks the catalytic subunit (424). PI3K phosphorylates phosphoinositide and produces phosphoinositide-3,4,5-trisphosphate (PIP_3), this then recruits the downstream signalling factor protein kinase AKT (368). Previous studies have shown increased ROS is linked to an increased PIP_3 signalling and subsequent AKT signalling (367). PI3Ks have also been shown to modulate NOX complex's by regulation of Rac activity (425). In my thesis I have shown that phosphorylated AKT (pAKT) is upregulated in the BMSCs and the HSCs following acute infection and ROS alone can cause this upregulation.

Moreover, I find PI3K regulates the movement of mitochondria from the BMSCs to the HSC. Inhibition of PI3Kδ by Cal 101, significantly reduces mitochondrial transfer and leads to a dysfunctional immune response to acute infection. Cal 101 is also used as a second line drug in the treatment of chronic lymphocytic leukaemia (CLL) (426). It was reported however, Cal 101 caused serious adverse effects including death, mostly due to infection (427). This suggests inhibition of mitochondrial transfer may have been the cause of the increased susceptibility to infection.

6.2.8 Fatty acid uptake

In the past several years, the metabolic requirements for HSC function have been investigated (245, 428-431). However, many studies have focused on glycolysis and the maintenance of HSCs under normal conditions and the contribution of lipid metabolism under stress has not been fully appreciated. The HSC energy requirements during differentiation and expansion following infection is vast and requires a rapid and efficient energy production.

For optimal use of all substrates available and to optimise energy requirements cells can reprogramme protein localisation, turnover and gene expression (432). The first stage in nutrient homeostasis is uptake of the nutrient by the cells, which often involves many specific membrane receptors. This is followed by a downstream network of proteins for intracellular nutrient traffic or signal transduction (433). Long chain fatty acids are a common nutrient found in the diet and a major source of energy for many cells (434, 435). Fatty acids can also regulate the expression of genes by transcription factors such as peroxisome proliferator-activated receptors (PPARs) (436, 437) which regulate numerous metabolic genes (438) and FoxO1 (439) important for adapting to low nutrient availability (440). The liver and adipocyte tissue are the only tissues which possess the ability for de *novo* fatty acid synthesis, all other cells depend on fatty acid uptake for their metabolic needs (441). This emphasises the physiological importance of fatty acid uptake into cells. In this study I have identified that HSCs take up FFA in response to acute infection and this uptake is critical to the immune response.

FFA uptake is now commonly recognised as an essential process, sustaining cell metabolism in both malignant and non-malignant cells. In a non-malignant setting, quiescent HSCs have a high rate of fatty acid oxidation, and inhibition of fatty acid oxidation leads to HSC dysfunction (26). Furthermore, in malignant cells FFA are used as a major energy source in ovarian (442) and prostate cancers (443). This process is similar to observations in AML, FFAs are taken up by the AML blasts to enhancing proliferation through a mechanism which increases β-oxidation in the blast (42). This, therefore, suggests that FFA uptake by AML is again a process which has been hijacked from the normal physiological response to stress.

6.2.9   Metabolic switch during infection

When HSCs undergo differentiation in response to stress, I have shown there is a metabolic switch towards mitochondrial OXPHOS which is associated with elevated ROS. The question still remains what fuels the TCA cycle in response to infection. Single cell gene expression analysis has shown that FAO plays a

crucial role in HSC expansion (335). FAO has also been associated with HSC maintenance via the PML-Peroxisome proliferator-activated receptor delta (PPARδ) pathway by regulating asymmetric division (26). Inhibition of FAO causes HCSs to undergo symmetric divisions leading to HSC exhaustion and depletion of the stem cell pool (26). FAO has also been shown to be pertinent in sustaining ATP production in breast epithelial cells when contact is lost with the extracellular matrix (444). Therefore, this suggests increased ATP production by FAO may protect HSCs following differentiation when contact is lost with the BM niche. Moreover, a recent study has shown when mice undergo short term starvation there is a decrease in the number of HSC (445). This data further suggested HSC differentiation is reliant on FAO as a loss in HSC number may be attributed to an increased FAO during starvation causing, the HSC to undergo differentiation initiating a loss of the HSC pool.

It has not yet been investigated if FAO is the preferred metabolic pathway in HSC differentiation. Models using *Drosophila* have demonstrated FAO is critical for the differentiation of blood cell progenitors and the progenitors are unable to differentiate in the absence of FAO (446). Interestingly it has been reported that muscle stem cells (447), endothelial precursors (448), intestinal stem cells (449) and neural stem cells (450) all have a metabolic dependence on FAO. In this study I add HSCs to the list of cells that are dependent on FAO metabolism. I show during infection HSCs take up FFA this in turn causes a rapid shift from baseline, quiescent glycolytic metabolism to increased dependency on FAO. Furthermore, mitochondria are the main site for FAO where the fatty acids are broken down to generate ATP (451). This suggests the imported mitochondria in the HSC following infection could be using the acquired fatty acids to fuel FAO.

6.2.10 CD36; the fatty acid transporter

In this thesis I have reported HSCs take up FFA during infection and this is through upregulation of the fatty acid translocase or CD36 located on the cell surface. CD36 is a scavenger receptor class B family of proteins involved in metabolism, immunity, angiogenesis and atherosclerosis (452). It is a

membrane glycoprotein which is present on, mononuclear phagocytes, platelets, hepatocytes, myocytes, adipocytes, and other haematopoietic cells (453). CD36 binds and facilitates the transport of long chain fatty acids and can function as a regulator of these processes (454, 455).

In the past few years CD36 has been studied considerably for its role in mediating fatty acid uptake and subsequent oxidation in the pathophysiology of the liver (456) and the heart (457) associated with dysregulated fatty acid metabolism (458). Moreover, the presence of CD36 on pluripotent stem cell derived cardiomyocytes was found to be a marker of maturation and can be used to define more mature cells (459). This suggests during infection upregulation of CD36 could be used as a marker of HSC differentiation. In fact, because CD36 is expressed on numerous cell types, and the plurality of the disease phenotypes related to CD36 function, to study CD36 function in HSCs I decided to develop the transplant model system. This model used CD36 knockout on HSCs transplanted into wild type animals, rather than using CD36 global knockout animals for this study. In context, I find cell-autonomous requirement of CD36 upregulated in the HSCs facilitates fatty acid uptake, allowing HSC expansion and enabling the immune response to infection.

CD36 has also been implicated in adipocyte differentiation, upregulation of CD36 was correlated with enhanced differentiation and adipogenesis and silencing of CD36 impaired these processes (453). This could suggest if there is upregulation of CD36 on the adipocytes following infection this could function to increase adipogenesis, creating more adipocytes for the release of FFAs. However, due to the lack of ability to look at adipocytes in the bone marrow I was unable to study this but hopefully this can be investigated in the future.

CD36 has numerous functions other than fatty acid uptake including recognition and internalisation of pathogens. Macrophages deficient of CD36 have demonstrated a reduced *Staphylococcus aureus* (*S.aureus*) internalisation and a marked reduction in IL 12 and tumour necrosis factor-α and production (460). This resulted in an inability to clear the *S.aureus* causing

the presence of the bacteria in the bloodstream (460). This data complicates the interpretation of the survival studies in the transplant CD36$^{-/-}$ mice in terms of the role of HSC FAO. As this is a transplant model in which the haematopoietic system is CD36 knockout there would be a number of tissue macrophages which remained WT however they also would also be CD36 deficient macrophages in the model. Therefore, the impaired response to infection may also be due to CD36 knockout macrophages inability to respond to the pathogenic stress. However, in this model during infection we do see an activation of glycolysis in the HSC which is not seen in control cells suggesting the cells are actively trying to generate ATP. Moreover, it has been found at early stages of infection with malaria wild type mice have a higher circulatory proinflammatory cytokines and lower anti-inflammatory cytokines than CD36 knockout mice. However, at later stages of infection the inflammatory profile was comparable between wildtype and CD36 knockout mice. I do find HSCs have an increased CD36 expression which facilitates fatty acid uptake into the cells following infection. However, to test the specific effect of fatty acid uptake in the HSC following infection, I would need a mouse model in which is CD36 could be knocked out in only the HSCs prior to infection.

Notably following infection, the gene expression of numerous fatty acid transporters were up-regulated. Long chain fatty acid rapidly diffuse across the phospholipid membrane (461) and this is regulated by many integral or membrane associated proteins (462, 463). The fatty acid transporter proteins (Slc27a1, Slc27a4, Slc27a5) (265, 266) are located on the plasma membrane and function by coupling fatty acid uptake to the first reaction in FA utilisation (263, 463). During infection I find SCL27A4 is upregulated in the HSC during infection and therefore may play a role in the trafficking of FFA into the cell. FA binding proteins (Fabp1, Fabp3, Fabp4, Fabp5) are also known to be important in fatty acid transport (264). FABPs are the plasma membrane isoforms of the mitochondrial aspartate aminotransferase which is an enzyme involved in maintaining the cytoplasmic/mitochondrial NADH/NAD ratios (464). Following infection, I find that FABP3 is upregulated in the HSC, this could be a result of cellular redox shuttling to regulate oxidative metabolism. It is interesting to note AML utilises FABP4 to support the survival and proliferation

of the malignant cells (42) however, I did not find FABP4 to be upregulated in the HSC during infection. It is also highly likely there is more than one channel through which fatty acids can be transported into the HSC. However, due to time restraints I was unable to look at the specific role of these transporters found to be upregulated following infection during my PhD.

6.3   Limitations

Despite the results attained in this thesis, and the progress made in understanding the HSC response to infection there are a number of limitations which should be considered. The number of mice used in each experiment was relatively low, this was to keep in line with the 3Rs (Replacement, Reduction and Refinement) to perform more humane animal research. An increased number of mice may have led to increased significance in the data sets.

Another of the main limitations in this study is the difficultly in assessing the true HSC. A lot of the metabolic work was focused on the LSK or the LK, this was due to the difficulty in sorting a large number of HSCs from the BM. I also encountered problems with availability of the sorter and breakdown of the equipment. The length of time the cells are out of the microenvironment could also affect the metabolic capacity of these cells. Therefore, the study would have greatly benefited from technology to rapidly isolate true HSCs from the BM.

Preferably, the isolation of BMSCs from both mouse and humans could have been more specific. Mouse BMSC were isolated from the adherent population of the BM and characterised as CD45, Ter119 and CD31 negative, CD140a and CD105 positive BMSC therefore very heterogeneous population. It would be interesting to investigate the specific BMSC population that transferred mitochondria to the HSC. Improved techniques in single cell sequencing has found there are many different types of BMSCs (141, 142) it would be interesting to isolate these populations and analyse mitochondrial transfer to the HSC. I was also unable to look at whether *in vivo* BMSC donate their

mitochondria to the HSC during infection. It would be of interest to use a model in which the BMSCs specifically have a fluorescent tag on the mitochondria and see if following infection, the HSC acquire the tagged mitochondria. However, even with this model the tag or mRNA for the tag could be being transferred and not the mitochondria themselves.

Many interpretations in this study have been drawn based on inhibition by pharmacological agents. This can be a concern due to non-specific off target effects even at steady state haematopoiesis. Where possible I have tried to use genetic approach's either a knockout model or knockdown by shRNA to complement the work using pharmacological agents. However, this was not possible in every case due to limitations of mouse models or shRNA viruses available.

Another limitation is that the majority of the work was undertaken in mouse models to represent the true microenvironment. However, it is difficult to know how translatable these processes are to humans. It is almost impossible to study the microenvironment interactions with the HSC during infection in humans, therefore the mouse is the closest model available we can use to understand the physiologic processes occurring in humans. The NSG mouse model used was also subject to limitations. NSG mice are severely immunocompromised allowing the engraftment of human cells without rejection. However, the lack of functional B and T cells would undoubtedly have an effect on the response to infection. To circumnavigate this issue, I used both *in vivo* and *in vitro* models to support the conclusion that HSCs acquire mitochondria from the BMSC following infection.

It has been shown by many groups investigating stem cells under inflammation that HSC marker expression is changed upon acute inflammation. This makes the HSC population difficult to analyse when gating flow cytometry data. To combat this, I used the additional marker CD34 to gate for the quiescent HSC compartment and the conclusions were drawn on the HSCs.

The body's response to LPS and *Salmonella* infection differs, whole bacterial cells secrete many virulence factors and activate numerous TLRs and PRR to regulate the immune response whilst LPS alone activates a TLR4 immune response. Therefore, LPS alone may not be truly representative of a bacterial infection, however, it is useful in assessing the kinetics of the host response to infection. To try and assess the same phase of the inflammatory response between LPS and *Salmonella* on fatty acid uptake I used a time point which had similar IL 6 expression in the serum.

6.4   Future work

Although the main aims and objectives of this studied were accomplished, there are a few areas which can be developed in the future. Firstly, the functionality of the HSC after infection would be of interest. Low mitochondrial membrane potential and activity have been shown to be key features of the self-renewing human and murine HSCs (392, 465). These HSC also possess higher multilineage reconstituting capacity long-term in both primary and secondary transplantations (392). I have shown HSCs have an increased OCR and mitochondrial potential during infection, however it would be interesting to perform secondary transplantation with these HSCs and assess their reconstitution capacity and if they exhibit any have any lineage skewing.

I find during infection there is a switch within the HSC from glycolytic metabolism towards OXPHOS and β-oxidation. I showed this occurred by seahorse metabolic analysis however to understand the significance of this switch and the transcriptional change regulating this, it would need to be confirmed by more sophisticated biochemical and molecular characterizations such as RNA sequencing or single cell RNA sequencing.

In this study I did not look at the source of the FFA during infection. BM adipose tissue (MAT) function as an energy source and an endocrine organ which accounts for around 70% of the BM in humans (109). Furthermore, the number of BM adipocytes increase in both human and mice with age (108, 466). These adipocytes have been implicated in many processes including regulation of

272

the haematopoietic niche (121), inflammation (467), osteoporosis (468) and bone metabolism (469). Moreover BM adipocytes support the proliferation of numerous tumours including AML (42), multiple myeloma (470) and metastatic solid tumours (471). Therefore, understanding the role of BM adipocytes in supporting the mammalian response to infection remains an important question.

CD36 deficient mice haave a different metabolic profile to wildtype mice it would be interesting to investigate if this affects the differentiation ability of CD36 deficient HSCs at both steady state and during infection. It would also help to determine if the HSC defects are reflected in the number of functional myeloid cells already at steady state or specifically found during infection. This could be achieved by transplanting control or LPS treated CD36 knockout HSCs and testing their multilineage reconstitution potentials.

In this thesis I have underlined the process of FFA uptake and mitochondrial transfer to the HSC as the physiological immune response to infection, these techniques can now be applied for use in conditions of stress. It would be interesting to see if and how these processes are dysregulated in ageing, obesity, in adipocyte rich areas, chronic or repeated infection and whether these processes are specific to the HSC.

6.5   Conclusions

Overall in my thesis I have reported that mitochondrial transfer and FFA uptake to the HSC forms part of the complex system modulating how HSCs differentiate and sustain haematopoiesis during stress. This process initiates a switch within the HSCs from baseline glycolytic metabolism towards OXPHOS and β-oxidation to facilitate proliferation and differentiation. The mitochondrial transfer occurs early on in the immune response before the transcriptional changes for mitochondrial biogenesis transpires, in a system evolved to support the rapid requirement for the granulocytic response to infection. Moreover, macrophage derived NOX2 ROS acts as the mediator of mitochondrial transfer from the microenvironment to the HSC. Mechanistically, the ROS facilitates the opening of CX43 gap junctions and is regulated by PI3K activation, allowing mitochondrial transfer from the BMSCs to the HSCs. In addition, at a later stage of infection transcriptional changes in the HSC, initiate upregulation of the fatty acid transporter CD36 facilitating the uptake of FFAs. Furthermore, without mitochondrial transfer or FFA uptake HSCs cannot switch from glycolysis to OXPHOS and β-oxidation and therefore do not enter the cell cycle. This leads to an increased susceptibility and mortality to infection. Taken together, the increased mitochondria acquired from the BMSCs may provide the extra machinery to metabolise the acquired fatty acids. The combination of OXPHOS and FAO have the ability to provide HSC with huge amounts of ATP which can be used for rapid proliferation following infection. Overall, these data provide new insights into the metabolic changes occurring in the haematopoietic system which underpin immune cell expansion in the mammalian response to acute infection.

7   References

1.   Fliedner TM, Graessle D, Paulsen C, Reimers K. Structure and function of bone marrow hemopoiesis: mechanisms of response to ionizing radiation exposure. Cancer Biother Radiopharm. 2002;17(4):405-26.
2.   Blood cell formation | biochemistry | Britannica.com.
3.   Kwak HJ, Liu P, Bajrami B, Xu Y, Park SY, Nombela-Arrieta C, et al. Myeloid cell-derived reactive oxygen species externally regulate the proliferation of myeloid progenitors in emergency granulopoiesis. Immunity. 2015;42(1):159-71.
4.   Ogawa M, Porter PN, Nakahata T. Renewal and commitment to differentiation of hemopoietic stem cells (an interpretive review). Blood. 1983;61(5):823-9.
5.   Wu JY, Scadden DT, Kronenberg HM. Role of the osteoblast lineage in the bone marrow hematopoietic niches. J Bone Miner Res. 2009;24(5):759-64.
6.   Calvi LM, Link DC. The hematopoietic stem cell niche in homeostasis and disease. Blood. 2015;126(22):2443-51.
7.   Weiss L, Geduldig U. Barrier cells: stromal regulation of hematopoiesis and blood cell release in normal and stressed murine bone marrow. Blood. 1991;78(4):975-90.
8.   Jagannathan-Bogdan M, Zon LI. Hematopoiesis. Development. 2013;140(12):2463-7.
9.   Orkin SH, Zon LI. Hematopoiesis: an evolving paradigm for stem cell biology. Cell. 2008;132(4):631-44.
10.   Ogawa M, LaRue AC, Mehrotra M. Hematopoietic stem cells are pluripotent and not just "hematopoietic". Blood Cells Mol Dis. 2013;51(1):3-8.
11.   Glatman Zaretsky A, Engiles JB, Hunter CA. Infection-induced changes in hematopoiesis. J Immunol. 2014;192(1):27-33.
12.   Doulatov S, Notta F, Laurenti E, Dick JE. Hematopoiesis: a human perspective. Cell Stem Cell. 2012;10(2):120-36.
13.   McCulloch EA, Till JE. The Radiation Sensitivity of Normal Mouse Bone Marrow Cells, Determined by Quantitative Marrow Transplantation into Irradiated Mice. Radiation Research. 1960;13(1):115-.
14.   Weissman IL. Clonal origins of the hematopoietic system: the single most elegant experiment. J Immunol. 2014;192(11):4943-4.
15.   BECKER AJ, McCULLOCH EA, TILL JE. Cytological demonstration of the clonal nature of spleen colonies derived from transplanted mouse marrow cells. Nature. 1963;197:452-4.
16.   Kosan C, Godmann M. Genetic and Epigenetic Mechanisms That Maintain Hematopoietic Stem Cell Function. Stem Cells Int. 2016;2016:5178965-.
17.   Ye H, Adane B, Khan N, Sullivan T, Minhajuddin M, Gasparetto M, et al. Leukemic Stem Cells Evade Chemotherapy by Metabolic Adaptation to an Adipose Tissue Niche. Cell Stem Cell. 2016;19(1):23-37.
18.   Ng AP, Alexander WS. Haematopoietic stem cells: past, present and future. Cell Death Discov. 2017;3:17002.
19.   Velten L, Haas SF, Raffel S, Blaszkiewicz S, Islam S, Hennig BP, et al. Human haematopoietic stem cell lineage commitment is a continuous process. Nature Cell Biology. 2017;19(4):271-81.
20.   Fulop GM, Phillips RA. The scid mutation in mice causes a general defect in DNA repair. Nature. 1990;347(6292):479-82.
21.   Mosier DE, Gulizia RJ, Baird SM, Wilson DB. Transfer of a functional human immune system to mice with severe combined immunodeficiency. Nature. 1988;335(6187):256-9.
22.   Ishikawa F. Modeling normal and malignant human hematopoiesis in vivo through newborn NSG xenotransplantation. Int J Hematol. 2013;98(6):634-40.

23.   Audige A, Rochat MA, Li D, Ivic S, Fahrny A, Muller CKS, et al. Long-term leukocyte reconstitution in NSG mice transplanted with human cord blood hematopoietic stem and progenitor cells. BMC Immunol. 2017;18(1):28.

24.   Sarkaria SM, Decker M, Ding L. Bone Marrow Micro-Environment in Normal and Deranged Hematopoiesis: Opportunities for Regenerative Medicine and Therapies. Bioessays. 2018;40(3).

25.   Kumar R, Godavarthy PS, Krause DS. The bone marrow microenvironment in health and disease at a glance. Journal of Cell Science. 2018;131(4):jcs201707.

26.   Ito K, Carracedo A, Weiss D, Arai F, Ala U, Avigan DE, et al. A PML-PPAR-delta pathway for fatty acid oxidation regulates hematopoietic stem cell maintenance. Nat Med. 2012;18(9):1350-8.

27.   Morrison SJ, Scadden DT. The bone marrow niche for haematopoietic stem cells. Nature. 2014;505(7483):327-34.

28.   Görgens A, Radtke S, Möllmann M, Cross M, Dürig J, Horn PA, et al. Revision of the human hematopoietic tree: granulocyte subtypes derive from distinct hematopoietic lineages. Cell Rep. 2013;3(5):1539-52.

29.   Laurenti E, Göttgens B. From haematopoietic stem cells to complex differentiation landscapes. Nature. 2018;553(7689):418-26.

30.   Shafat MS, Gnaneswaran B, Bowles KM, Rushworth SA. The bone marrow microenvironment - Home of the leukemic blasts. Blood reviews. 2017;31(5):277-86.

31.   Tavassoli M, Crosby WH. Bone marrow histogenesis: a comparison of fatty and red marrow. Science. 1970;169(3942):291-3.

32.   Gurevitch O, Slavin S, Feldman AG. Conversion of red bone marrow into yellow - Cause and mechanisms. Med Hypotheses. 2007;69(3):531-6.

33.   Zhao E, Xu H, Wang L, Kryczek I, Wu K, Hu Y, et al. Bone marrow and the control of immunity. Cell Mol Immunol. 2012;9(1):11-9.

34.   Agarwala S, Tamplin OJ. Neural Crossroads in the Hematopoietic Stem Cell Niche. Trends in Cell Biology. 2018;28(12):987-98.

35.   Pino AM, Miranda M, Figueroa C, Rodriguez JP, Rosen CJ. Qualitative Aspects of Bone Marrow Adiposity in Osteoporosis. Front Endocrinol (Lausanne). 2016;7:139.

36.   Brandi ML. Microarchitecture, the key to bone quality. Rheumatology (Oxford). 2009;48 Suppl 4:iv3-8.

37.   Cordeiro-Spinetti E, Taichman RS, Balduino A. The bone marrow endosteal niche: how far from the surface? J Cell Biochem. 2015;116(1):6-11.

38.   Islam A, Glomski C, Henderson ES. Bone lining (endosteal) cells and hematopoiesis: a light microscopic study of normal and pathologic human bone marrow in plastic-embedded sections. Anat Rec. 1990;227(3):300-6.

39.   Compston JE. Bone marrow and bone: a functional unit. J Endocrinol. 2002;173(3):387-94.

40.   Jung WC, Levesque JP, Ruitenberg MJ. It takes nerve to fight back: The significance of neural innervation of the bone marrow and spleen for immune function. Semin Cell Dev Biol. 2017;61:60-70.

41.   Marlein CR, Zaitseva L, Piddock RE, Robinson SD, Edwards DR, Shafat MS, et al. NADPH oxidase-2 derived superoxide drives mitochondrial transfer from bone marrow stromal cells to leukemic blasts. Blood. 2017;130(14):1649-60.

42.   Shafat MS, Oellerich T, Mohr S, Robinson SD, Edwards DR, Marlein CR, et al. Leukemic blasts program bone marrow adipocytes to generate a protumoral microenvironment. Blood. 2017;129(10):1320-32.

43.   Sison EA, Brown P. The bone marrow microenvironment and leukemia: biology and therapeutic targeting. Expert Rev Hematol. 2011;4(3):271-83.

44.   Tamma R, Ribatti D. Bone Niches, Hematopoietic Stem Cells, and Vessel Formation. Int J Mol Sci. 2017;18(1):151.

45.   Guerrouahen BS, Al-Hijji I, Tabrizi AR. Osteoblastic and vascular endothelial niches, their control on normal hematopoietic stem cells, and their consequences on the development of leukemia. Stem Cells Int. 2011;2011:375857-.

46.   Boulais PE, Frenette PS. Making sense of hematopoietic stem cell niches. Blood. 2015;125(17):2621-9.

47.   Schofield R. The relationship between the spleen colony-forming cell and the haemopoietic stem cell. Blood cells. 1978;4(1-2):7-25.

48.   Schepers K, Campbell TB, Passegué E. Normal and leukemic stem cell niches: insights and therapeutic opportunities. Cell Stem Cell. 2015;16(3):254-67.

49.   Lucas D. The Bone Marrow Microenvironment for Hematopoietic Stem Cells. Adv Exp Med Biol. 2017;1041:5-18.

50.   Lo Celso C, Fleming HE, Wu JW, Zhao CX, Miake-Lye S, Fujisaki J, et al. Live-animal tracking of individual haematopoietic stem/progenitor cells in their niche. Nature. 2009;457(7225):92-6.

51.   Mendelson A, Frenette PS. Hematopoietic stem cell niche maintenance during homeostasis and regeneration. Nature Medicine. 2014;20(8):833-46.

52.   Morrison SJ, Scadden DT. The bone marrow niche for haematopoietic stem cells. Nature. 2014;505(7483):327-34.

53.   Lucas D. The Bone Marrow Microenvironment for Hematopoietic Stem Cells. 10412017. p. 5-18.

54.   Bone Marrow, Thymus And Blood: Changes Across The Lifespan. Aging health. 2009;5(3):385-93.

55.   McCulloch EA, Till JE. The radiation sensitivity of normal mouse bone marrow cells, determined by quantitative marrow transplantation into irradiated mice. Radiat Res. 1960;13:115-25.

56.   Till JE, Mc CE. A direct measurement of the radiation sensitivity of normal mouse bone marrow cells. Radiat Res. 1961;14:213-22.

57.   Becker AJ, Mc CE, Till JE. Cytological demonstration of the clonal nature of spleen colonies derived from transplanted mouse marrow cells. Nature. 1963;197:452-4.

58.   Seita J, Weissman IL. Hematopoietic stem cell: self-renewal versus differentiation. Wiley Interdiscip Rev Syst Biol Med. 2010;2(6):640-53.

59.   McGuire VA, Arthur JS. Stress-induced haematopoietic stem cell proliferation: new roles for p38α and purine metabolism. Stem Cell Investig. 2016;3:64.

60.   Muller-Sieburg CE, Whitlock CA, Weissman IL. Isolation of two early B lymphocyte progenitors from mouse marrow: a committed pre-pre-B cell and a clonogenic Thy-1-lo hematopoietic stem cell. Cell. 1986;44(4):653-62.

61.   Spangrude GJ, Heimfeld S, Weissman IL. Purification and characterization of mouse hematopoietic stem cells. Science. 1988;241(4861):58-62.

62.   Rossi DJ, Seita J, Czechowicz A, Bhattacharya D, Bryder D, Weissman IL. Hematopoietic stem cell quiescence attenuates DNA damage response and permits DNA damage accumulation during aging. Cell Cycle. 2007;6(19):2371-6.

63.   Uchida N, Weissman IL. Searching for hematopoietic stem cells: evidence that Thy-1.1lo Lin- Sca-1+ cells are the only stem cells in C57BL/Ka-Thy-1.1 bone marrow. J Exp Med. 1992;175(1):175-84.

64.   Ikuta K, Weissman IL. Evidence that hematopoietic stem cells express mouse c-kit but do not depend on steel factor for their generation. Proc Natl Acad Sci U S A. 1992;89(4):1502-6.

65.   Smith LG, Weissman IL, Heimfeld S. Clonal analysis of hematopoietic stem-cell differentiation in vivo. Proceedings of the National Academy of Sciences of the United States of America. 1991;88(7):2788-92.

66.   Osawa M, Hanada K, Hamada H, Nakauchi H. Long-term lymphohematopoietic reconstitution by a single CD34-low/negative hematopoietic stem cell. Science. 1996;273(5272):242-5.

67.   Morrison SJ, Weissman IL. The long-term repopulating subset of hematopoietic stem cells is deterministic and isolatable by phenotype. Immunity. 1994;1(8):661-73.

68.   Walter D, Lier A, Geiselhart A, Thalheimer FB, Huntscha S, Sobotta MC, et al. Exit from dormancy provokes DNA-damage-induced attrition in haematopoietic stem cells. Nature. 2015;520(7548):549-52.

69.   Challen GA, Boles N, Lin KK, Goodell MA. Mouse hematopoietic stem cell identification and analysis. Cytometry A. 2009;75(1):14-24.

70.   Marlein CR, Rushworth SA. Bone Marrow. eLS: John Wiley & Sons, Ltd: Chichester.; 2018.

71.   Challen GA, Boles N, Lin KK-Y, Goodell MA. Mouse hematopoietic stem cell identification and analysis. Cytometry A. 2009;75(1):14-24.

72.   Hirayama D, Iida T, Nakase H. The Phagocytic Function of Macrophage-Enforcing Innate Immunity and Tissue Homeostasis. Int J Mol Sci. 2017;19(1):92.

73.   Aderem A, Underhill DM. Mechanisms of phagocytosis in macrophages. Annu Rev Immunol. 1999;17:593-623.

74.   Mosser DM, Edwards JP. Exploring the full spectrum of macrophage activation. Nat Rev Immunol. 2008;8(12):958-69.

75.   McCabe A, MacNamara KC. Macrophages: Key regulators of steady-state and demand-adapted hematopoiesis. Exp Hematol. 2016;44(4):213-22.

76.   Winkler IG, Sims NA, Pettit AR, Barbier V, Nowlan B, Helwani F, et al. Bone marrow macrophages maintain hematopoietic stem cell (HSC) niches and their depletion mobilizes HSCs. Blood. 2010;116(23):4815-28.

77.   Chow A, Lucas D, Hidalgo A, Méndez-Ferrer S, Hashimoto D, Scheiermann C, et al. Bone marrow CD169+ macrophages promote the retention of hematopoietic stem and progenitor cells in the mesenchymal stem cell niche. J Exp Med. 2011;208(2):261-71.

78.   Asada N, Takeishi S, Frenette PS. Complexity of bone marrow hematopoietic stem cell niche. International Journal of Hematology. 2017;106(1):45-54.

79.   Wickramasinghe SN, Porwit A, Erber WN. Normal bone marrow cells: Development and cytology. Blood and Bone Marrow Pathology. 2011:19-44.

80.   Stein GS, Lian JB, van Wijnen AJ, Stein JL, Montecino M, Javed A, et al. Runx2 control of organization, assembly and activity of the regulatory machinery for skeletal gene expression. Oncogene. 2004;23(24):4315-29.

81.   Komori T, Yagi H, Nomura S, Yamaguchi A, Sasaki K, Deguchi K, et al. Targeted disruption of Cbfa1 results in a complete lack of bone formation owing to maturational arrest of osteoblasts. Cell. 1997;89(5):755-64.

82.   Rutkovskiy A, Stenslokken KO, Vaage IJ. Osteoblast Differentiation at a Glance. Med Sci Monit Basic Res. 2016;22:95-106.

83.   Xie Y, Yin T, Wiegraebe W, He XC, Miller D, Stark D, et al. Detection of functional haematopoietic stem cell niche using real-time imaging. Nature. 2009;457(7225):97-101.

84.   Taichman RS, Emerson SG. Human osteoblasts support hematopoiesis through the production of granulocyte colony-stimulating factor. The Journal of experimental medicine. 1994;179(5):1677-82.

85.   Calvi LM, Adams GB, Weibrecht KW, Weber JM, Olson DP, Knight MC, et al. Osteoblastic cells regulate the haematopoietic stem cell niche. Nature. 2003;425(6960):841-6.

86.   Zhang J, Niu C, Ye L, Huang H, He X, Tong W-G, et al. Identification of the haematopoietic stem cell niche and control of the niche size. Nature. 2003;425(6960):836-41.

87.   Adams GB, Martin RP, Alley IR, Chabner KT, Cohen KS, Calvi LM, et al. Therapeutic targeting of a stem cell niche. Nat Biotechnol. 2007;25(2):238-43.

88.   Visnjic D, Kalajzic I, Gronowicz G, Aguila HL, Clark SH, Lichtler AC, et al. Conditional ablation of the osteoblast lineage in Col2.3deltatk transgenic mice. J Bone Miner Res. 2001;16(12):2222-31.

89.   Visnjic D, Kalajzic Z, Rowe DW, Katavic V, Lorenzo J, Aguila HL. Hematopoiesis is severely altered in mice with an induced osteoblast deficiency. Blood. 2004;103(9):3258-64.

90.   Kunisaki Y, Bruns I, Scheiermann C, Ahmed J, Pinho S, Zhang D, et al. Arteriolar niches maintain haematopoietic stem cell quiescence. Nature. 2013;502(7473):637-43.

91.   Nombela-Arrieta C, Pivarnik G, Winkel B, Canty KJ, Harley B, Mahoney JE, et al. Quantitative imaging of haematopoietic stem and progenitor cell localization and hypoxic status in the bone marrow microenvironment. Nature Cell Biology. 2013;15(5):533-43.

92.   Calvi LM. Osteolineage cells and regulation of the hematopoietic stem cell. Best Pract Res Clin Haematol. 2013;26(3):249-52.

93.   Boyle WJ, Simonet WS, Lacey DL. Osteoclast differentiation and activation. Nature. 2003;423(6937):337-42.

94.   Miyamoto T, Suda T. Differentiation and function of osteoclasts. Keio J Med. 2003;52(1):1-7.

95.   Mansour A, Abou-Ezzi G, Sitnicka E, Jacobsen SE, Wakkach A, Blin-Wakkach C. Osteoclasts promote the formation of hematopoietic stem cell niches in the bone marrow. J Exp Med. 2012;209(3):537-49.

96.   Wanjare M, Kusuma S, Gerecht S. Perivascular cells in blood vessel regeneration. Biotechnol J. 2013;8(4):434-47.

97.   Lindahl P, Johansson BR, Levéen P, Betsholtz C. Pericyte loss and microaneurysm formation in PDGF-B-deficient mice. Science. 1997;277(5323):242-5.

98.   Mancini ML, Terzic A, Conley BA, Oxburgh LH, Nicola T, Vary CP. Endoglin plays distinct roles in vascular smooth muscle cell recruitment and regulation of arteriovenous identity during angiogenesis. Dev Dyn. 2009;238(10):2479-93.

99.   Sacchetti B, Funari A, Michienzi S, Di Cesare S, Piersanti S, Saggio I, et al. Self-Renewing Osteoprogenitors in Bone Marrow Sinusoids Can Organize a Hematopoietic Microenvironment. Cell. 2007;131(2):324-36.

100.   Méndez-Ferrer S, Michurina TV, Ferraro F, Mazloom AR, MacArthur BD, Lira SA, et al. Mesenchymal and haematopoietic stem cells form a unique bone marrow niche. Nature. 2010;466(7308):829-34.

101.   Oswald J, Boxberger S, Jorgensen B, Feldmann S, Ehninger G, Bornhauser M, et al. Mesenchymal stem cells can be differentiated into endothelial cells in vitro. Stem Cells. 2004;22(3):377-84.

102.   Rafii S, Shapiro F, Pettengell R, Ferris B, Nachman RL, Moore MA, et al. Human bone marrow microvascular endothelial cells support long-term proliferation and differentiation of myeloid and megakaryocytic progenitors. Blood. 1995;86(9):3353-63.

103.   Winkler IG, Barbier V, Nowlan B, Jacobsen RN, Forristal CE, Patton JT, et al. Vascular niche E-selectin regulates hematopoietic stem cell dormancy, self renewal and chemoresistance. Nature Medicine. 2012;18(11):1651-7.

104.   Yao L, Yokota T, Xia L, Kincade PW, McEver RP. Bone marrow dysfunction in mice lacking the cytokine receptor gp130 in endothelial cells. Blood. 2005;106(13):4093-101.

105.   Ulyanova T, Scott LM, Priestley GV, Jiang Y, Nakamoto B, Koni PA, et al. VCAM-1 expression in adult hematopoietic and nonhematopoietic cells is controlled by tissue-inductive signals and reflects their developmental origin. Blood. 2005;106(1):86-94.

106. Ding L, Saunders TL, Enikolopov G, Morrison SJ. Endothelial and perivascular cells maintain haematopoietic stem cells. Nature. 2012;481(7382):457-62.

107. Itkin T, Gur-Cohen S, Spencer JA, Schajnovitz A, Ramasamy SK, Kusumbe AP, et al. Distinct bone marrow blood vessels differentially regulate haematopoiesis. Nature. 2016;532(7599):323-8.

108. Horowitz MC, Berry R, Holtrup B, Sebo Z, Nelson T, Fretz JA, et al. Bone marrow adipocytes. Adipocyte. 2017;6(3):193-204.

109. Cawthorn WP, Scheller EL, Learman BS, Parlee SD, Simon BR, Mori H, et al. Bone marrow adipose tissue is an endocrine organ that contributes to increased circulating adiponectin during caloric restriction. Cell Metab. 2014;20(2):368-75.

110. Attané C, Estève D, Chaoui K, Iacovoni JS, Corre J, Moutahir M, et al. Human Bone Marrow Is Comprised of Adipocytes with Specific Lipid Metabolism. Cell Rep. 2020;30(4):949-58.e6.

111. Justesen J, Stenderup K, Ebbesen EN, Mosekilde L, Steiniche T, Kassem M. Adipocyte tissue volume in bone marrow is increased with aging and in patients with osteoporosis. Biogerontology. 2001;2(3):165-71.

112. Scheller EL, Doucette CR, Learman BS, Cawthorn WP, Khandaker S, Schell B, et al. Region-specific variation in the properties of skeletal adipocytes reveals regulated and constitutive marrow adipose tissues. Nat Commun. 2015;6:7808.

113. Yeung DK, Griffith JF, Antonio GE, Lee FK, Woo J, Leung PC. Osteoporosis is associated with increased marrow fat content and decreased marrow fat unsaturation: a proton MR spectroscopy study. J Magn Reson Imaging. 2005;22(2):279-85.

114. Bredella MA, Torriani M, Ghomi RH, Thomas BJ, Brick DJ, Gerweck AV, et al. Vertebral bone marrow fat is positively associated with visceral fat and inversely associated with IGF-1 in obese women. Obesity (Silver Spring). 2011;19(1):49-53.

115. Doucette CR, Horowitz MC, Berry R, MacDougald OA, Anunciado-Koza R, Koza RA, et al. A High Fat Diet Increases Bone Marrow Adipose Tissue (MAT) But Does Not Alter Trabecular or Cortical Bone Mass in C57BL/6J Mice. J Cell Physiol. 2015;230(9):2032-7.

116. Meunier P, Aaron J, Edouard C, Vignon G. Osteoporosis and the replacement of cell populations of the marrow by adipose tissue. A quantitative study of 84 iliac bone biopsies. Clin Orthop Relat Res. 1971;80:147-54.

117. Naveiras O, Nardi V, Wenzel PL, Hauschka PV, Fahey F, Daley GQ. Bone-marrow adipocytes as negative regulators of the haematopoietic microenvironment. Nature. 2009;460(7252):259-63.

118. Lecka-Czernik B. Marrow fat metabolism is linked to the systemic energy metabolism. Bone. 2012;50(2):534-9.

119. Martin S, Parton RG. Lipid droplets: a unified view of a dynamic organelle. Nat Rev Mol Cell Biol. 2006;7(5):373-8.

120. Granneman JG, Moore HP. Location, location: protein trafficking and lipolysis in adipocytes. Trends Endocrinol Metab. 2008;19(1):3-9.

121. Zhou BO, Yu H, Yue R, Zhao Z, Rios JJ, Naveiras O, et al. Bone marrow adipocytes promote the regeneration of stem cells and haematopoiesis by secreting SCF. Nat Cell Biol. 2017;19(8):891-903.

122. Mattiucci D, Maurizi G, Izzi V, Cenci L, Ciarlantini M, Mancini S, et al. Bone marrow adipocytes support hematopoietic stem cell survival. J Cell Physiol. 2018;233(2):1500-11.

123. Pittenger MF, Mackay AM, Beck SC, Jaiswal RK, Douglas R, Mosca JD, et al. Multilineage potential of adult human mesenchymal stem cells. Science (New York, NY). 1999;284(5411):143-7.

124. Bianco P, Robey PG, Simmons PJ. Mesenchymal Stem Cells: Revisiting History, Concepts, and Assays. Cell Stem Cell. 2008;2(4):313-9.

125.   Bianco P, Cao X, Frenette PS, Mao JJ, Robey PG, Simmons PJ, et al. The meaning, the sense and the significance: translating the science of mesenchymal stem cells into medicine. Nat Med. 2013;19(1):35-42.
126.   Sacchetti B, Funari A, Remoli C, Giannicola G, Kogler G, Liedtke S, et al. No Identical "Mesenchymal Stem Cells" at Different Times and Sites: Human Committed Progenitors of Distinct Origin and Differentiation Potential Are Incorporated as Adventitial Cells in Microvessels. Stem Cell Reports. 2016;6(6):897-913.
127.   Dominici M, Le Blanc K, Mueller I, Slaper-Cortenbach I, Marini FC, Krause DS, et al. Minimal criteria for defining multipotent mesenchymal stromal cells. The International Society for Cellular Therapy position statement. Cytotherapy. 2006;8(4):315-7.
128.   Lymperi S, Ferraro F, Scadden DT. The HSC niche concept has turned 31. Annals of the New York Academy of Sciences. 2010;1192(1):12-8.
129.   Ding L, Saunders TL, Enikolopov G, Morrison SJ. Endothelial and perivascular cells maintain haematopoietic stem cells. Nature. 2012;481(7382):457-62.
130.   Ding L, Morrison SJ. Haematopoietic stem cells and early lymphoid progenitors occupy distinct bone marrow niches. Nature. 2013;495(7440):231-5.
131.   Anthony BA, Link DC. Regulation of hematopoietic stem cells by bone marrow stromal cells. Trends Immunol. 2014;35(1):32-7.
132.   Langley KE, Bennett LG, Wypych J, Yancik SA, Liu XD, Westcott KR, et al. Soluble stem cell factor in human serum. Blood. 1993;81(3):656-60.
133.   Pesce M, Di Carlo A, De Felici M. The c-kit receptor is involved in the adhesion of mouse primordial germ cells to somatic cells in culture. Mech Dev. 1997;68(1-2):37-44.
134.   Shin JY, Hu W, Naramura M, Park CY. High c-Kit expression identifies hematopoietic stem cells with impaired self-renewal and megakaryocytic bias. The Journal of experimental medicine. 2014;211(2):217-31.
135.   Barker JE. Sl/Sld hematopoietic progenitors are deficient in situ. Exp Hematol. 1994;22(2):174-7.
136.   Schajnovitz A, Itkin T, D'Uva G, Kalinkovich A, Golan K, Ludin A, et al. CXCL12 secretion by bone marrow stromal cells is dependent on cell contact and mediated by connexin-43 and connexin-45 gap junctions. Nat Immunol. 2011;12(5):391-8.
137.   Sugiyama T, Kohara H, Noda M, Nagasawa T. Maintenance of the hematopoietic stem cell pool by CXCL12-CXCR4 chemokine signaling in bone marrow stromal cell niches. Immunity. 2006;25(6):977-88.
138.   Greenbaum A, Hsu YM, Day RB, Schuettpelz LG, Christopher MJ, Borgerding JN, et al. CXCL12 in early mesenchymal progenitors is required for haematopoietic stem-cell maintenance. Nature. 2013;495(7440):227-30.
139.   Mendez-Ferrer S, Lucas D, Battista M, Frenette PS. Haematopoietic stem cell release is regulated by circadian oscillations. Nature. 2008;452(7186):442-7.
140.   Shin JY, Hu W, Naramura M, Park CY. High c-Kit expression identifies hematopoietic stem cells with impaired self-renewal and megakaryocytic bias. J Exp Med. 2014;211(2):217-31.
141.   Jin P, Liu S, Bae H, Zhao Y, Shi R, Chen J, et al. Characterization of BMSC subpopulations by using novel single cell sequencing technology. Cytotherapy. 2018;20(5):S41-S2.
142.   Liu S, Stroncek DF, Zhao Y, Chen V, Shi R, Chen J, et al. Single cell sequencing reveals gene expression signatures associated with bone marrow stromal cell subpopulations and time in culture. Journal of Translational Medicine. 2019;17(1):23.
143.   Tokoyoda K, Egawa T, Sugiyama T, Choi BI, Nagasawa T. Cellular niches controlling B lymphocyte behavior within bone marrow during development. Immunity. 2004;20(6):707-18.

144.	Mendez-Ferrer S, Michurina TV, Ferraro F, Mazloom AR, Macarthur BD, Lira SA, et al. Mesenchymal and haematopoietic stem cells form a unique bone marrow niche. Nature. 2010;466(7308):829-34.

145.	Omatsu Y, Sugiyama T, Kohara H, Kondoh G, Fujii N, Kohno K, et al. The essential functions of adipo-osteogenic progenitors as the hematopoietic stem and progenitor cell niche. Immunity. 2010;33(3):387-99.

146.	Wu J, Zhang W, Ran Q, Xiang Y, Zhong JF, Li SC, et al. The Differentiation Balance of Bone Marrow Mesenchymal Stem Cells Is Crucial to Hematopoiesis. Stem Cells Int. 2018;2018:1-13.

147.	Taniguchi Ishikawa E, Gonzalez-Nieto D, Ghiaur G, Dunn SK, Ficker AM, Murali B, et al. Connexin-43 prevents hematopoietic stem cell senescence through transfer of reactive oxygen species to bone marrow stromal cells. Proc Natl Acad Sci U S A. 2012;109(23):9071-6.

148.	Reya T, Morrison SJ, Clarke MF, Weissman IL. Stem cells, cancer, and cancer stem cells. Nature. 2001;414(6859):105-11.

149.	Boraschi D, Aguado MT, Dutel C, Goronzy J, Louis J, Grubeck-Loebenstein B, et al. The gracefully aging immune system. Sci Transl Med. 2013;5(185):185ps8.

150.	Gavazzi G, Krause KH. Ageing and infection. Lancet Infect Dis. 2002;2(11):659-66.

151.	Ramos-Casals M, García-Carrasco M, Brito MP, López-Soto A, Font J. Autoimmunity and geriatrics: clinical significance of autoimmune manifestations in the elderly. Lupus. 2003;12(5):341-55.

152.	Linton PJ, Dorshkind K. Age-related changes in lymphocyte development and function. Nature Immunology. 2004;5(2):133-9.

153.	Hartsock RJ, Smith EB, Petty CS. Normal variations with aging of the amount of hematopoietic tissue in bone marrow from the anterior iliac crest. A study made from 177 cases of sudden death examined by necropsy. Am J Clin Pathol. 1965;43:326-31.

154.	Ganguly P, El-Jawhari JJ, Giannoudis PV, Burska AN, Ponchel F, Jones EA. Age-related Changes in Bone Marrow Mesenchymal Stromal Cells: A Potential Impact on Osteoporosis and Osteoarthritis Development. Cell Transplant. 2017;26(9):1520-9.

155.	Villeda SA, Luo J, Mosher KI, Zou B, Britschgi M, Bieri G, et al. The ageing systemic milieu negatively regulates neurogenesis and cognitive function. Nature. 2011;477(7362):90-4.

156.	Ergen AV, Boles NC, Goodell MA. Rantes/Ccl5 influences hematopoietic stem cell subtypes and causes myeloid skewing. Blood. 2012;119(11):2500-9.

157.	Chambers SM, Boles NC, Lin KY, Tierney MP, Bowman TV, Bradfute SB, et al. Hematopoietic fingerprints: an expression database of stem cells and their progeny. Cell Stem Cell. 2007;1(5):578-91.

158.	de Haan G, Van Zant G. Dynamic changes in mouse hematopoietic stem cell numbers during aging. Blood. 1999;93(10):3294-301.

159.	Rossi DJ, Bryder D, Zahn JM, Ahlenius H, Sonu R, Wagers AJ, et al. Cell intrinsic alterations underlie hematopoietic stem cell aging. Proc Natl Acad Sci U S A. 2005;102(26):9194-9.

160.	Geiger H, de Haan G, Florian MC. The ageing haematopoietic stem cell compartment. Nat Rev Immunol. 2013;13(5):376-89.

161.	Wang J, Sun Q, Morita Y, Jiang H, Gross A, Lechel A, et al. A differentiation checkpoint limits hematopoietic stem cell self-renewal in response to DNA damage. Cell. 2012;148(5):1001-14.

162.	Sun D, Luo M, Jeong M, Rodriguez B, Xia Z, Hannah R, et al. Epigenomic profiling of young and aged HSCs reveals concerted changes during aging that reinforce self-renewal. Cell Stem Cell. 2014;14(5):673-88.

163.   Young K, Eudy E, Bell R, Loberg M, Stearns T, Velten L, et al. Hematopoietic Stem and Progenitor Cell Aging is Initiated at Middle Age Through Decline in Local Insulin-Like Growth Factor 1 (IGF1). bioRxiv. 2020:2020.07.11.198846.

164.   Kollman C, Howe CW, Anasetti C, Antin JH, Davies SM, Filipovich AH, et al. Donor characteristics as risk factors in recipients after transplantation of bone marrow from unrelated donors: the effect of donor age. Blood. 2001;98(7):2043-51.

165.   Griffith JF. Age-Related Changes in the Bone Marrow. Current Radiology Reports. 2017;5(6):24.

166.   Allart-Vorelli P, Porro B, Baguet F, Michel A, Cousson-Gelie F. Haematological cancer and quality of life: a systematic literature review. Blood Cancer J. 2015;5:e305.

167.   Ramanarayanan J, Dunford LM, Baer MR, Sait SN, Lawrence W, McCarthy PL. Chronic myeloid leukemia after treatment of lymphoid malignancies: response to imatinib mesylate and favorable outcomes in three patients. Leuk Res. 2006;30(6):701-5.

168.   Rajkumar SV, Kumar S. Multiple Myeloma: Diagnosis and Treatment. Mayo Clin Proc. 2016;91(1):101-19.

169.   Kuppers R. The biology of Hodgkin's lymphoma. Nat Rev Cancer. 2009;9(1):15-27.

170.   Manier S, Sacco A, Leleu X, Ghobrial IM, Roccaro AM. Bone marrow microenvironment in multiple myeloma progression. J Biomed Biotechnol. 2012;2012:157496.

171.   Rashidi A, Uy GL. Targeting the microenvironment in acute myeloid leukemia. Curr Hematol Malig Rep. 2015;10(2):126-31.

172.   Chiarini F, Lonetti A, Evangelisti C, Buontempo F, Orsini E, Cappellini A, et al. Advances in understanding the acute lymphoblastic leukemia bone marrow microenvironment: From biology to therapeutic targeting. Biochim Biophys Acta. 2016;1863(3):449-63.

173.   Crompot E, Van Damme M, Pieters K, Vermeersch M, Perez-Morga D, Mineur P, et al. Extracellular vesicles of bone marrow stromal cells rescue chronic lymphocytic leukemia B cells from apoptosis, enhance their migration and induce gene expression modifications. Haematologica. 2017;102(9):1594-604.

174.   Aristizábal JA, Chandia M, Del Cañizo MC, Sánchez-Guijo F. [Bone marrow microenvironment in chronic myeloid leukemia: implications for disease physiopathology and response to treatment]. Rev Med Chil. 2014;142(5):599-605.

175.   Estey E, Dohner H. Acute myeloid leukaemia. Lancet. 2006;368(9550):1894-907.

176.   Lane SW, Scadden DT, Gilliland DG. The leukemic stem cell niche: current concepts and therapeutic opportunities. Blood. 2009;114(6):1150-7.

177.   Kumar CC. Genetic abnormalities and challenges in the treatment of acute myeloid leukemia. Genes Cancer. 2011;2(2):95-107.

178.   Juliusson G, Lazarevic V, Horstedt AS, Hagberg O, Hoglund M, Swedish Acute Leukemia Registry G. Acute myeloid leukemia in the real world: why population-based registries are needed. Blood. 2012;119(17):3890-9.

179.   Rashidi A, DiPersio JF. Targeting the leukemia-stroma interaction in acute myeloid leukemia: rationale and latest evidence. Ther Adv Hematol. 2016;7(1):40-51.

180.   Zhou HS, Carter BZ, Andreeff M. Bone marrow niche-mediated survival of leukemia stem cells in acute myeloid leukemia: Yin and Yang. Cancer Biol Med. 2016;13(2):248-59.

181.   Lopes MR, Pereira JK, de Melo Campos P, Machado-Neto JA, Traina F, Saad ST, et al. De novo AML exhibits greater microenvironment dysregulation compared to AML with myelodysplasia-related changes. Sci Rep. 2017;7:40707.

182.   Korn C, Méndez-Ferrer S. Myeloid malignancies and the microenvironment. Blood. 2017;129(7):811-22.

183.   Burger JA, Ghia P, Rosenwald A, Caligaris-Cappio F. The microenvironment in mature B-cell malignancies: a target for new treatment strategies. Blood. 2009;114(16):3367-75.
184.   Peled A, Tavor S. Role of CXCR4 in the pathogenesis of acute myeloid leukemia. Theranostics. 2013;3(1):34-9.
185.   Cho BS, Kim HJ, Konopleva M. Targeting the CXCL12/CXCR4 axis in acute myeloid leukemia: from bench to bedside. Korean J Intern Med. 2017;32(2):248-57.
186.   Karpova D, Ritchey JK, Holt MS, Abou-Ezzi G, Monlish D, Batoon L, et al. Continuous blockade of CXCR4 results in dramatic mobilization and expansion of hematopoietic stem and progenitor cells. Blood. 2017;129(21):2939-49.
187.   Kessans MR, Gatesman ML, Kockler DR. Plerixafor: a peripheral blood stem cell mobilizer. Pharmacotherapy. 2010;30(5):485-92.
188.   Marlein CR, Zaitseva L, Rushworth SA. Pulling the plug - halting cancer's theft of mitochondria. Oncoscience. 2017;4(11-12):173-4.
189.   Tower J. Stress and stem cells. Wiley Interdiscip Rev Dev Biol. 2012;1(6):789-802.
190.   Stearns SC. Hoffman, A. A. and Parsons, P. A. 1991. Evolutionary Genetics and Environmental Stress. Oxford University Press. paper .ix + 284 pp., illus. ISBN: 0-19-854081-7. Journal of Evolutionary Biology. 1994;7(5):634-5.
191.   Zhao JL, Baltimore D. Regulation of stress-induced hematopoiesis. Curr Opin Hematol. 2015;22(4):286-92.
192.   Goldstein S. Longevity, senescence and the genome. American Journal of Human Genetics. 1992;50(2):451-.
193.   van Deursen JM. The role of senescent cells in ageing. Nature. 2014;509(7501):439-46.
194.   Hellmich C, Moore JA, Bowles KM, Rushworth SA. Bone Marrow Senescence and the Microenvironment of Hematological Malignancies. Frontiers in Oncology. 2020;10(230).
195.   Kirkwood TB. Understanding the odd science of aging. Cell. 2005;120(4):437-47.
196.   Pritz T, Weinberger B, Grubeck-Loebenstein B. The aging bone marrow and its impact on immune responses in old age. Immunol Lett. 2014;162(1 Pt B):310-5.
197.   Cho J, Hur JH, Walker DW. The role of mitochondria in Drosophila aging. Exp Gerontol. 2011;46(5):331-4.
198.   Mansell E, Sigurdsson V, Deltcheva E, Brown J, James C, Miharada K, et al. Mitochondrial Potentiation Ameliorates Age-Related Heterogeneity in Hematopoietic Stem Cell Function. Cell Stem Cell. 2020.
199.   Salmon AB, Richardson A, Pérez VI. Update on the oxidative stress theory of aging: does oxidative stress play a role in aging or healthy aging? Free Radic Biol Med. 2010;48(5):642-55.
200.   Tower J. Hsps and aging. Trends Endocrinol Metab. 2009;20(5):216-22.
201.   Ganz T, Nemeth E. Hepcidin and disorders of iron metabolism. Annu Rev Med. 2011;62:347-60.
202.   López-Otín C, Blasco MA, Partridge L, Serrano M, Kroemer G. The hallmarks of aging. Cell. 2013;153(6):1194-217.
203.   Rossi DJ, Jamieson CH, Weissman IL. Stems cells and the pathways to aging and cancer. Cell. 2008;132(4):681-96.
204.   Flach J, Bakker ST, Mohrin M, Conroy PC, Pietras EM, Reynaud D, et al. Replication stress is a potent driver of functional decline in ageing haematopoietic stem cells. Nature. 2014;512(7513):198-202.
205.   Welch JS, Ley TJ, Link DC, Miller CA, Larson DE, Koboldt DC, et al. The origin and evolution of mutations in acute myeloid leukemia. Cell. 2012;150(2):264-78.

206.   Jaiswal S, Fontanillas P, Flannick J, Manning A, Grauman PV, Mar BG, et al. Age-Related Clonal Hematopoiesis Associated with Adverse Outcomes. New England Journal of Medicine. 2014;371(26):2488-98.

207.   Busque L, Mio R, Mattioli J, Brais E, Blais N, Lalonde Y, et al. Nonrandom X-inactivation patterns in normal females: lyonization ratios vary with age. Blood. 1996;88(1):59-65.

208.   Bonnet D, Dick JE. Human acute myeloid leukemia is organized as a hierarchy that originates from a primitive hematopoietic cell. Nature Medicine. 1997;3(7):730-7.

209.   Corces-Zimmerman MR, Hong WJ, Weissman IL, Medeiros BC, Majeti R. Preleukemic mutations in human acute myeloid leukemia affect epigenetic regulators and persist in remission. Proc Natl Acad Sci U S A. 2014;111(7):2548-53.

210.   Shlush LI, Zandi S, Mitchell A, Chen WC, Brandwein JM, Gupta V, et al. Identification of pre-leukaemic haematopoietic stem cells in acute leukaemia. Nature. 2014;506(7488):328-33.

211.   Zaretsky AG, Engiles JB, Hunter CA. Infection-Induced Changes in Hematopoiesis. The Journal of Immunology. 2014;192(1):27-33.

212.   Pascutti MF, Erkelens MN, Nolte MA. Impact of Viral Infections on Hematopoiesis: From Beneficial to Detrimental Effects on Bone Marrow Output. Front Immunol. 2016;7:364-.

213.   Kolb-Maurer A, Weissinger F, Kurzai O, Maurer M, Wilhelm M, Goebel W. Bacterial infection of human hematopoietic stem cells induces monocytic differentiation. FEMS Immunology & Medical Microbiology. 2004;40(2):147-53.

214.   Chou DB, Sworder B, Bouladoux N, Roy CN, Uchida AM, Grigg M, et al. Stromal-derived IL-6 alters the balance of myeloerythroid progenitors during Toxoplasma gondii infection. J Leukoc Biol. 2012;92(1):123-31.

215.   Glatman Zaretsky A, Silver JS, Siwicki M, Durham A, Ware CF, Hunter CA. Infection with Toxoplasma gondii alters lymphotoxin expression associated with changes in splenic architecture. Infect Immun. 2012;80(10):3602-10.

216.   Shi X, Zhang P, Sempowski GD, Shellito JE. Thymopoietic and bone marrow response to murine Pneumocystis pneumonia. Infect Immun. 2011;79(5):2031-42.

217.   King KY, Goodell MA. Inflammatory modulation of HSCs: viewing the HSC as a foundation for the immune response. Nat Rev Immunol. 2011;11(10):685-92.

218.   Bogeska R, Kaschutnig P, Fawaz M, Mikecin A-M, Büchler-Schäff M, Paffenholz S, et al. Hematopoietic stem cells fail to regenerate following inflammatory challenge. bioRxiv. 2020:2020.08.01.230433.

219.   Esplin BL, Shimazu T, Welner RS, Garrett KP, Nie L, Zhang Q, et al. Chronic exposure to a TLR ligand injures hematopoietic stem cells. J Immunol. 2011;186(9):5367-75.

220.   Maldonado RF, Sá-Correia I, Valvano MA. Lipopolysaccharide modification in Gram-negative bacteria during chronic infection. FEMS Microbiol Rev. 2016;40(4):480-93.

221.   Al-Harrasi A, Hussain H, Csuk R, Khan HY. Chapter 3 - Biological Activities of Boswellic Acids. In: Al-Harrasi A, Hussain H, Csuk R, Yar Khan H, editors. Chemistry and Bioactivity of Boswellic Acids and Other Terpenoids of the Genus Boswellia: Elsevier; 2019. p. 67-109.

222.   Rietschel ET, Kirikae T, Schade FU, Mamat U, Schmidt G, Loppnow H, et al. Bacterial endotoxin: molecular relationships of structure to activity and function. The FASEB Journal. 1994;8(2):217-25.

223.   Alexander C, Rietschel ET. Bacterial lipopolysaccharides and innate immunity. Journal of endotoxin research. 2001;7(3):167-202.

224.   Nemzek JA, Hugunin KMS, Opp MR. Modeling sepsis in the laboratory: merging sound science with animal well-being. Comp Med. 2008;58(2):120-8.

225.   Feasey NA, Dougan G, Kingsley RA, Heyderman RS, Gordon MA. Invasive non-typhoidal salmonella disease: an emerging and neglected tropical disease in Africa. Lancet. 2012;379(9835):2489-99.

226.   Broz P, Ohlson MB, Monack DM. Innate immune response to Salmonella typhimurium, a model enteric pathogen. Gut Microbes. 2012;3(2):62-70.

227.   Haraga A, Ohlson MB, Miller SI. Salmonellae interplay with host cells. Nat Rev Microbiol. 2008;6(1):53-66.

228.   Medzhitov R. Toll-like receptors and innate immunity. Nat Rev Immunol. 2001;1(2):135-45.

229.   Takizawa H, Fritsch K, Kovtonyuk LV, Saito Y, Yakkala C, Jacobs K, et al. Pathogen-Induced TLR4-TRIF Innate Immune Signaling in Hematopoietic Stem Cells Promotes Proliferation but Reduces Competitive Fitness. Cell Stem Cell. 2017;21(2):225-40.e5.

230.   Griendling KK, Sorescu D, Ushio-Fukai M. NAD(P)H oxidase: role in cardiovascular biology and disease. Circ Res. 2000;86(5):494-501.

231.   Singel KL, Segal BH. NOX2-dependent regulation of inflammation. Clin Sci (Lond). 2016;130(7):479-90.

232.   Segal BH, Veys P, Malech H, Cowan MJ. Chronic granulomatous disease: lessons from a rare disorder. Biol Blood Marrow Transplant. 2011;17(1 Suppl):S123-31.

233.   Pizzolla A, Hultqvist M, Nilson B, Grimm MJ, Eneljung T, Jonsson IM, et al. Reactive oxygen species produced by the NADPH oxidase 2 complex in monocytes protect mice from bacterial infections. J Immunol. 2012;188(10):5003-11.

234.   Grimm MJ, Vethanayagam RR, Almyroudis NG, Dennis CG, Khan AN, D'Auria AC, et al. Monocyte- and macrophage-targeted NADPH oxidase mediates antifungal host defense and regulation of acute inflammation in mice. J Immunol. 2013;190(8):4175-84.

235.   Rada B, Leto TL. Oxidative innate immune defenses by Nox/Duox family NADPH oxidases. Contrib Microbiol. 2008;15:164-87.

236.   DeBerardinis RJ, Thompson CB. Cellular metabolism and disease: what do metabolic outliers teach us? Cell. 2012;148(6):1132-44.

237.   Bonora M, Patergnani S, Rimessi A, De Marchi E, Suski JM, Bononi A, et al. ATP synthesis and storage. Purinergic Signal. 2012;8(3):343-57.

238.   Kumari A. Chapter 1 - Glycolysis. In: Kumari A, editor. Sweet Biochemistry: Academic Press; 2018. p. 1-5.

239.   Hui S, Ghergurovich JM, Morscher RJ, Jang C, Teng X, Lu W, et al. Glucose feeds the TCA cycle via circulating lactate. Nature. 2017;551(7678):115-8.

240.   Kennedy EP, Lehninger AL. Oxidation of fatty acids and tricarboxylic acid cycle intermediates by isolated rat liver mitochondria. J Biol Chem. 1949;179(2):957-72.

241.   Kumari A. Chapter 2 - Citric Acid Cycle. In: Kumari A, editor. Sweet Biochemistry: Academic Press; 2018. p. 7-11.

242.   Lenaz G, Genova ML. Structure and organization of mitochondrial respiratory complexes: a new understanding of an old subject. Antioxid Redox Signal. 2010;12(8):961-1008.

243.   Walker JE. The regulation of catalysis in ATP synthase. Curr Opin Struct Biol. 1994;4(6):912-8.

244.   Ferguson SJ. ATP synthase: from sequence to ring size to the P/O ratio. Proc Natl Acad Sci U S A. 2010;107(39):16755-6.

245.   Simsek T, Kocabas F, Zheng J, Deberardinis RJ, Mahmoud AI, Olson EN, et al. The distinct metabolic profile of hematopoietic stem cells reflects their location in a hypoxic niche. Cell stem cell. 2010;7(3):380-90.

246.   Ito K, Suda T. Metabolic requirements for the maintenance of self-renewing stem cells. Nat Rev Mol Cell Biol. 2014;15(4):243-56.

247.	Takubo K, Nagamatsu G, Kobayashi CI, Nakamura-Ishizu A, Kobayashi H, Ikeda E, et al. Regulation of glycolysis by Pdk functions as a metabolic checkpoint for cell cycle quiescence in hematopoietic stem cells. Cell Stem Cell. 2013;12(1):49-61.
248.	Kiel MJ, Yilmaz OH, Iwashita T, Terhorst C, Morrison SJ. SLAM family receptors distinguish hematopoietic stem and progenitor cells and reveal endothelial niches for stem cells. Cell. 2005;121(7):1109-21.
249.	Luo ST, Zhang DM, Qin Q, Lu L, Luo M, Guo FC, et al. The Promotion of Erythropoiesis via the Regulation of Reactive Oxygen Species by Lactic Acid. Sci Rep. 2017;7:38105.
250.	Horton EdS, Beisel WR. The Metabolic Responses to Stress and Physical Activity. (US) NAP, editor. Institute of Medicine (US) Committee on Military Nutrition Research1994.
251.	Hensley CT, Faubert B, Yuan Q, Lev-Cohain N, Jin E, Kim J, et al. Metabolic Heterogeneity in Human Lung Tumors. Cell. 2016;164(4):681-94.
252.	Nielsen TS, Jessen N, Jørgensen JO, Møller N, Lund S. Dissecting adipose tissue lipolysis: molecular regulation and implications for metabolic disease. J Mol Endocrinol. 2014;52(3):R199-222.
253.	Kolditz C-I, Langin D. Adipose tissue lipolysis. Current Opinion in Clinical Nutrition & Metabolic Care. 2010;13(4):377-81.
254.	Porter RK, Brand MD. Mitochondrial proton conductance and H+/O ratio are independent of electron transport rate in isolated hepatocytes. Biochem J. 1995;310 (Pt 2):379-82.
255.	Qu Q, Zeng F, Liu X, Wang QJ, Deng F. Fatty acid oxidation and carnitine palmitoyltransferase I: emerging therapeutic targets in cancer. Cell Death Dis. 2016;7:e2226.
256.	Casals N, Zammit V, Herrero L, Fadó R, Rodríguez-Rodríguez R, Serra D. Carnitine palmitoyltransferase 1C: From cognition to cancer. Prog Lipid Res. 2016;61:134-48.
257.	Zaugg K, Yao Y, Reilly PT, Kannan K, Kiarash R, Mason J, et al. Carnitine palmitoyltransferase 1C promotes cell survival and tumor growth under conditions of metabolic stress. Genes Dev. 2011;25(10):1041-51.
258.	Harjes U, Kalucka J, Carmeliet P. Targeting fatty acid metabolism in cancer and endothelial cells. Crit Rev Oncol Hematol. 2016;97:15-21.
259.	Saltiel AR, Kahn CR. Insulin signalling and the regulation of glucose and lipid metabolism. Nature. 2001;414(6865):799-806.
260.	Hotamisligil GS. Inflammation and metabolic disorders. Nature. 2006;444(7121):860-7.
261.	Furuhashi M, Hotamisligil GS. Fatty acid-binding proteins: role in metabolic diseases and potential as drug targets. Nature Reviews Drug Discovery. 2008;7(6):489-503.
262.	Veglia F, Tyurin VA, Blasi M, De Leo A, Kossenkov AV, Donthireddy L, et al. Fatty acid transport protein 2 reprograms neutrophils in cancer. Nature. 2019;569(7754):73-8.
263.	Black PN, DiRusso CC. Yeast acyl-CoA synthetases at the crossroads of fatty acid metabolism and regulation. Biochim Biophys Acta. 2007;1771(3):286-98.
264.	Berk PD, Potter BJ, Sorrentino D, Stump D, Kiang CL, Zhou SL, et al. Hepatocellular fatty acid uptake is mediated by a plasma membrane fatty acid binding protein closely related to mitochondrial glutamic oxaloacetic transaminase. Ann N Y Acad Sci. 1990;585:379-85.
265.	Doege H, Stahl A. Protein-mediated fatty acid uptake: novel insights from in vivo models. Physiology (Bethesda). 2006;21:259-68.
266.	Stahl A. A current review of fatty acid transport proteins (SLC27). Pflugers Arch. 2004;447(5):722-7.

267. Abumrad N, Coburn C, Ibrahimi A. Membrane proteins implicated in long-chain fatty acid uptake by mammalian cells: CD36, FATP and FABPm. Biochim Biophys Acta. 1999;1441(1):4-13.

268. Black PN, Sandoval A, Arias-Barrau E, DiRusso CC. Targeting the fatty acid transport proteins (FATP) to understand the mechanisms linking fatty acid transport to metabolism. Immunol Endocr Metab Agents Med Chem. 2009;9(1):11-7.

269. Furuhashi M, Ishimura S, Ota H, Miura T. Lipid Chaperones and Metabolic Inflammation. International Journal of Inflammation. 2011;2011:642612.

270. Daviet L, McGregor JL. Vascular biology of CD36: roles of this new adhesion molecule family in different disease states. Thromb Haemost. 1997;78(1):65-9.

271. Janssen KP, Rost R, Eichinger L, Schleicher M. Characterization of CD36/LIMPII homologues in Dictyostelium discoideum. J Biol Chem. 2001;276(42):38899-910.

272. Pepino MY, Kuda O, Samovski D, Abumrad NA. Structure-function of CD36 and importance of fatty acid signal transduction in fat metabolism. Annu Rev Nutr. 2014;34:281-303.

273. Abumrad NA, Goldberg IJ. CD36 actions in the heart: Lipids, calcium, inflammation, repair and more? Biochim Biophys Acta. 2016;1861(10):1442-9.

274. Kim TT, Dyck JR. The role of CD36 in the regulation of myocardial lipid metabolism. Biochim Biophys Acta. 2016;1861(10):1450-60.

275. Glatz JF, Nabben M, Heather LC, Bonen A, Luiken JJ. Regulation of the subcellular trafficking of CD36, a major determinant of cardiac fatty acid utilization. Biochim Biophys Acta. 2016;1861(10):1461-71.

276. Glatz JFC, Luiken JJFP. Dynamic role of the transmembrane glycoprotein CD36 (SR-B2) in cellular fatty acid uptake and utilization. Journal of lipid research. 2018;59(7):1084-93.

277. Hale JS, Otvos B, Sinyuk M, Alvarado AG, Hitomi M, Stoltz K, et al. Cancer stem cell-specific scavenger receptor CD36 drives glioblastoma progression. Stem Cells. 2014;32(7):1746-58.

278. Tabe Y, Yamamoto S, Saitoh K, Sekihara K, Monma N, Ikeo K, et al. Bone Marrow Adipocytes Facilitate Fatty Acid Oxidation Activating AMPK and a Transcriptional Network Supporting Survival of Acute Monocytic Leukemia Cells. Cancer Res. 2017;77(6):1453-64.

279. Tabe Y, Harada M, Miyamae Y, Mogushi K, Kazuno S, Fujimura T, et al. Bone Marrow Adipocyte-Derived Free Fatty Acids Induce Gene Signature Linking Transcription with Metabolic Changes That Contribute to Survival of Acute Monocytic Leukemia Cells. Blood. 2014;124:1013-.

280. Masarwi M, DeSchiffart A, Ham J, Reagan MR. Multiple Myeloma and Fatty Acid Metabolism. JBMR Plus. 2019;3(3):e10173-e.

281. Jacobson J, Duchen MR. Interplay between mitochondria and cellular calcium signalling. Molecular and Cellular Biochemistry. 2004;256(1):209-18.

282. Gray MW. Mitochondrial evolution. Cold Spring Harb Perspect Biol. 2012;4(9):a011403-a.

283. Friedman JR, Nunnari J. Mitochondrial form and function. Nature. 2014;505(7483):335-43.

284. Sato M, Sato K. Maternal inheritance of mitochondrial DNA by diverse mechanisms to eliminate paternal mitochondrial DNA. Biochim Biophys Acta. 2013;1833(8):1979-84.

285. Chan DC. Mitochondria: dynamic organelles in disease, aging, and development. Cell. 2006;125(7):1241-52.

286. Warr MR, Passegué E. Metabolic makeover for HSCs. Cell Stem Cell. 2013;12(1):1-3.

287. Norddahl GL, Pronk CJ, Wahlestedt M, Sten G, Nygren JM, Ugale A, et al. Accumulating mitochondrial DNA mutations drive premature hematopoietic aging

phenotypes distinct from physiological stem cell aging. Cell Stem Cell. 2011;8(5):499-510.

288.   Inoue S, Noda S, Kashima K, Nakada K, Hayashi J, Miyoshi H. Mitochondrial respiration defects modulate differentiation but not proliferation of hematopoietic stem and progenitor cells. FEBS Lett. 2010;584(15):3402-9.

289.   Ludin A, Gur-Cohen S, Golan K, Kaufmann KB, Itkin T, Medaglia C, et al. Reactive oxygen species regulate hematopoietic stem cell self-renewal, migration and development, as well as their bone marrow microenvironment. Antioxid Redox Signal. 2014;21(11):1605-19.

290.   Liang R, Arif T, Kalmykova S, Kasianov A, Lin M, Menon V, et al. Restraining Lysosomal Activity Preserves Hematopoietic Stem Cell Quiescence and Potency. Cell Stem Cell. 2020;26(3):359-76.e7.

291.   Hinge A, He J, Bartram J, Javier J, Xu J, Fjellman E, et al. Asymmetrically Segregated Mitochondria Provide Cellular Memory of Hematopoietic Stem Cell Replicative History and Drive HSC Attrition. Cell Stem Cell. 2020;26(3):420-30.e6.

292.   Chen H, Chan DC. Mitochondrial dynamics--fusion, fission, movement, and mitophagy--in neurodegenerative diseases. Hum Mol Genet. 2009;18(R2):R169-76.

293.   Spees JL, Olson SD, Whitney MJ, Prockop DJ. Mitochondrial transfer between cells can rescue aerobic respiration. Proc Natl Acad Sci U S A. 2006;103(5):1283-8.

294.   Ahmad T, Mukherjee S, Pattnaik B, Kumar M, Singh S, Rehman R, et al. Miro1 regulates intercellular mitochondrial transport & enhances mesenchymal stem cell rescue efficacy. EMBO J. 2014;33(9):994-1010.

295.   Islam MN, Das SR, Emin MT, Wei M, Sun L, Westphalen K, et al. Mitochondrial transfer from bone-marrow-derived stromal cells to pulmonary alveoli protects against acute lung injury. Nat Med. 2012;18(5):759-65.

296.   Hayakawa K, Esposito E, Wang X, Terasaki Y, Liu Y, Xing C, et al. Transfer of mitochondria from astrocytes to neurons after stroke. Nature. 2016;535(7613):551-5.

297.   Moschoi R, Imbert V, Nebout M, Chiche J, Mary D, Prebet T, et al. Protective mitochondrial transfer from bone marrow stromal cells to acute myeloid leukemic cells during chemotherapy. Blood. 2016;128(2):253-64.

298.   Tan AS, Baty JW, Dong LF, Bezawork-Geleta A, Endaya B, Goodwin J, et al. Mitochondrial genome acquisition restores respiratory function and tumorigenic potential of cancer cells without mitochondrial DNA. Cell Metab. 2015;21(1):81-94.

299.   Griessinger E, Moschoi R, Biondani G, Peyron JF. Mitochondrial Transfer in the Leukemia Microenvironment. Trends Cancer. 2017;3(12):828-39.

300.   Torralba D, Baixauli F, Sánchez-Madrid F. Mitochondria Know No Boundaries: Mechanisms and Functions of Intercellular Mitochondrial Transfer. Front Cell Dev Biol. 2016;4:107.

301.   Liu K, Ji K, Guo L, Wu W, Lu H, Shan P, et al. Mesenchymal stem cells rescue injured endothelial cells in an in vitro ischemia-reperfusion model via tunneling nanotube like structure-mediated mitochondrial transfer. Microvasc Res. 2014;92:10-8.

302.   Jackson MV, Morrison TJ, Doherty DF, McAuley DF, Matthay MA, Kissenpfennig A, et al. Mitochondrial Transfer via Tunneling Nanotubes is an Important Mechanism by Which Mesenchymal Stem Cells Enhance Macrophage Phagocytosis in the In Vitro and In Vivo Models of ARDS. Stem Cells. 2016;34(8):2210-23.

303.   Rustom A, Saffrich R, Markovic I, Walther P, Gerdes HH. Nanotubular highways for intercellular organelle transport. Science. 2004;303(5660):1007-10.

304.   Abounit S, Zurzolo C. Wiring through tunneling nanotubes--from electrical signals to organelle transfer. J Cell Sci. 2012;125(Pt 5):1089-98.

305.   Astanina K, Koch M, Jüngst C, Zumbusch A, Kiemer AK. Lipid droplets as a novel cargo of tunnelling nanotubes in endothelial cells. Sci Rep. 2015;5:11453.

306.   Onfelt B, Nedvetzki S, Benninger RK, Purbhoo MA, Sowinski S, Hume AN, et al. Structurally distinct membrane nanotubes between human macrophages support long-distance vesicular traffic or surfing of bacteria. J Immunol. 2006;177(12):8476-83.

307.   Bénard M, Schapman D, Lebon A, Monterroso B, Bellenger M, Le Foll F, et al. Structural and functional analysis of tunneling nanotubes (TnTs) using gCW STED and gconfocal approaches. Biol Cell. 2015;107(11):419-25.

308.   Bukoreshtliev NV, Wang X, Hodneland E, Gurke S, Barroso JF, Gerdes HH. Selective block of tunneling nanotube (TNT) formation inhibits intercellular organelle transfer between PC12 cells. FEBS Lett. 2009;583(9):1481-8.

309.   Hirokawa N, Takemura R. Molecular motors and mechanisms of directional transport in neurons. Nat Rev Neurosci. 2005;6(3):201-14.

310.   Hollenbeck PJ, Saxton WM. The axonal transport of mitochondria. J Cell Sci. 2005;118(Pt 23):5411-9.

311.   Pilling AD, Horiuchi D, Lively CM, Saxton WM. Kinesin-1 and Dynein are the primary motors for fast transport of mitochondria in Drosophila motor axons. Mol Biol Cell. 2006;17(4):2057-68.

312.   Yasuda K, Park HC, Ratliff B, Addabbo F, Hatzopoulos AK, Chander P, et al. Adriamycin nephropathy: a failure of endothelial progenitor cell-induced repair. Am J Pathol. 2010;176(4):1685-95.

313.   Cho YM, Kim JH, Kim M, Park SJ, Koh SH, Ahn HS, et al. Mesenchymal stem cells transfer mitochondria to the cells with virtually no mitochondrial function but not with pathogenic mtDNA mutations. PLoS One. 2012;7(3):e32778.

314.   Willms E, Cabañas C, Mäger I, Wood MJA, Vader P. Extracellular Vesicle Heterogeneity: Subpopulations, Isolation Techniques, and Diverse Functions in Cancer Progression. Front Immunol. 2018;9:738-.

315.   Mittelbrunn M, Sánchez-Madrid F. Intercellular communication: diverse structures for exchange of genetic information. Nat Rev Mol Cell Biol. 2012;13(5):328-35.

316.   Maas SLN, Breakefield XO, Weaver AM. Extracellular Vesicles: Unique Intercellular Delivery Vehicles. Trends Cell Biol. 2017;27(3):172-88.

317.   Phinney DG, Di Giuseppe M, Njah J, Sala E, Shiva S, St Croix CM, et al. Mesenchymal stem cells use extracellular vesicles to outsource mitophagy and shuttle microRNAs. Nat Commun. 2015;6:8472.

318.   Caivano A, Laurenzana I, De Luca L, La Rocca F, Simeon V, Trino S, et al. High serum levels of extracellular vesicles expressing malignancy-related markers are released in patients with various types of hematological neoplastic disorders. Tumour Biol. 2015;36(12):9739-52.

319.   Kelsell DP, Dunlop J, Hodgins MB. Human diseases: clues to cracking the connexin code? Trends Cell Biol. 2001;11(1):2-6.

320.   Lampe PD, Lau AF. The effects of connexin phosphorylation on gap junctional communication. Int J Biochem Cell Biol. 2004;36(7):1171-86.

321.   Lampe PD, Lau AF. Regulation of gap junctions by phosphorylation of connexins. Arch Biochem Biophys. 2000;384(2):205-15.

322.   Goodenough DA, Paul DL. Gap junctions. Cold Spring Harb Perspect Biol. 2009;1(1):a002576.

323.   Li H, Wang C, He T, Zhao T, Chen Y-Y, Shen Y-L, et al. Mitochondrial Transfer from Bone Marrow Mesenchymal Stem Cells to Motor Neurons in Spinal Cord Injury Rats via Gap Junction. Theranostics. 2019;9(7):2017-35.

324.   Golan K, Wellendorf A, Takihara Y, Kumari A, Khatib-Massalha E, Kollet O, et al. Mitochondria Transfer from Hematopoietic Stem and Progenitor Cells to Pdgfrα+/Sca-1-/CD48dim BM Stromal Cells Via CX43 Gap Junctions and AMPK

Signaling Inversely Regulate ROS Generation in Both Cell Populations. Blood. 2016;128(22):5-.

325. Gumpert AM, Varco JS, Baker SM, Piehl M, Falk MM. Double-membrane gap junction internalization requires the clathrin-mediated endocytic machinery. FEBS Lett. 2008;582(19):2887-92.

326. Antanavičiūtė I, Rysevaitė K, Liutkevičius V, Marandykina A, Rimkutė L, Sveikatienė R, et al. Long-distance communication between laryngeal carcinoma cells. PLoS One. 2014;9(6):e99196.

327. Piehl M, Lehmann C, Gumpert A, Denizot JP, Segretain D, Falk MM. Internalization of large double-membrane intercellular vesicles by a clathrin-dependent endocytic process. Mol Biol Cell. 2007;18(2):337-47.

328. Seahorse XF Cell Mito Stress Test Kit, 2020 [Available from: https://www.agilent.com/en/product/cell-analysis/real-time-cell-metabolic-analysis/xf-assay-kits-reagents-cell-assay-media/seahorse-xf-cell-mito-stress-test-kit-740885.

329. Seahorse XF Mito Fuel Flex Test Kit, 2020 [Available from: https://www.agilent.com/en/product/cell-analysis/real-time-cell-metabolic-analysis/xf-assay-kits-reagents-cell-assay-media/seahorse-xf-mito-fuel-flex-test-kit-740888.

330. Gonzalez-Hunt CP, Rooney JP, Ryde IT, Anbalagan C, Joglekar R, Meyer JN. PCR-Based Analysis of Mitochondrial DNA Copy Number, Mitochondrial DNA Damage, and Nuclear DNA Damage. Curr Protoc Toxicol. 2016;67:20.11.1-20.11.25.

331. McCracken MN, George BM, Kao KS, Marjon KD, Raveh T, Weissman IL. Normal and Neoplastic Stem Cells. Cold Spring Harb Symp Quant Biol. 2016;81:1-9.

332. Zhao JL, Baltimore D. Regulation of stress-induced hematopoiesis. Curr Opin Hematol. 2015;22(4):286-92.

333. Nombela-Arrieta C, Pivarnik G, Winkel B, Canty KJ, Harley B, Mahoney JE, et al. Quantitative imaging of haematopoietic stem and progenitor cell localization and hypoxic status in the bone marrow microenvironment. Nature cell biology. 2013;15(5):533-43.

334. Vannini N, Girotra M, Naveiras O, Nikitin G, Campos V, Giger S, et al. Specification of haematopoietic stem cell fate via modulation of mitochondrial activity. Nat Commun. 2016;7:13125.

335. Ito K, Turcotte R, Cui J, Zimmerman SE, Pinho S, Mizoguchi T, et al. Self-renewal of a purified Tie2+ hematopoietic stem cell population relies on mitochondrial clearance. Science. 2016;354(6316):1156-60.

336. de Almeida MJ, Luchsinger LL, Corrigan DJ, Williams LJ, Snoeck HW. Dye-Independent Methods Reveal Elevated Mitochondrial Mass in Hematopoietic Stem Cells. Cell Stem Cell. 2017;21(6):725-9.e4.

337. Ivanov AV, Bartosch B, Isaguliants MG. Oxidative Stress in Infection and Consequent Disease. Oxid Med Cell Longev. 2017;2017:3496043.

338. Xiao B, Deng X, Zhou W, Tan EK. Flow Cytometry-Based Assessment of Mitophagy Using MitoTracker. Front Cell Neurosci. 2016;10:76.

339. Agnello M, Morici G, Rinaldi AM. A method for measuring mitochondrial mass and activity. Cytotechnology. 2008;56(3):145-9.

340. Goodell MA, Rosenzweig M, Kim H, Marks DF, DeMaria M, Paradis G, et al. Dye efflux studies suggest that hematopoietic stem cells expressing low or undetectable levels of CD34 antigen exist in multiple species. Nat Med. 1997;3(12):1337-45.

341. Petursson SR, Chervenick PA, Wu B. Megakaryocytopoiesis and granulopoiesis after murine cytomegalovirus infection. J Lab Clin Med. 1984;104(3):381-90.

342. Dahl R, Walsh JC, Lancki D, Laslo P, Iyer SR, Singh H, et al. Regulation of macrophage and neutrophil cell fates by the PU.1:C/EBPalpha ratio and granulocyte colony-stimulating factor. Nat Immunol. 2003;4(10):1029-36.

343.	Pietras EM, Warr MR, Passegué E. Cell cycle regulation in hematopoietic stem cells. J Cell Biol. 2011;195(5):709-20.

344.	Dong LF, Kovarova J, Bajzikova M, Bezawork-Geleta A, Svec D, Endaya B, et al. Horizontal transfer of whole mitochondria restores tumorigenic potential in mitochondrial DNA-deficient cancer cells. Elife. 2017;6.

345.	Nakano A, Harada T, Morikawa S, Kato Y. Expression of leukocyte common antigen (CD45) on various human leukemia/lymphoma cell lines. Acta Pathol Jpn. 1990;40(2):107-15.

346.	Jafri S, Moore SD, Morrell NW, Ormiston ML. A sex-specific reconstitution bias in the competitive CD45.1/CD45.2 congenic bone marrow transplant model. Sci Rep. 2017;7(1):3495.

347.	Yu X, Gimsa U, Wester-Rosenlöf L, Kanitz E, Otten W, Kunz M, et al. Dissecting the effects of mtDNA variations on complex traits using mouse conplastic strains. Genome Res. 2009;19(1):159-65.

348.	Challen GA, Boles NC, Chambers SM, Goodell MA. Distinct hematopoietic stem cell subtypes are differentially regulated by TGF-beta1. Cell Stem Cell. 2010;6(3):265-78.

349.	Morrison TJ, Jackson MV, Cunningham EK, Kissenpfennig A, McAuley DF, O'Kane CM, et al. Mesenchymal Stromal Cells Modulate Macrophages in Clinically Relevant Lung Injury Models by Extracellular Vesicle Mitochondrial Transfer. Am J Respir Crit Care Med. 2017;196(10):1275-86.

350.	Ho TT, Warr MR, Adelman ER, Lansinger OM, Flach J, Verovskaya EV, et al. Autophagy maintains the metabolism and function of young and old stem cells. Nature. 2017;543(7644):205-10.

351.	Suda T, Takubo K, Semenza GL. Metabolic regulation of hematopoietic stem cells in the hypoxic niche. Cell Stem Cell. 2011;9(4):298-310.

352.	Brestoff JR, Wilen CB, Moley JR, Li Y, Zou W, Malvin NP, et al. Intercellular Mitochondria Transfer to Macrophages Regulates White Adipose Tissue Homeostasis and Is Impaired in Obesity. Cell Metabolism. 2020.

353.	Pollock JD, Williams DA, Gifford MA, Li LL, Du X, Fisherman J, et al. Mouse model of X-linked chronic granulomatous disease, an inherited defect in phagocyte superoxide production. Nat Genet. 1995;9(2):202-9.

354.	Shafat MS, Gnaneswaran B, Bowles KM, Rushworth SA. The bone marrow microenvironment - Home of the leukemic blasts. Blood reviews. 2017;31(5):277-86.

355.	Winkler IG, Sims NA, Pettit AR, Barbier V, Nowlan B, Helwani F, et al. Bone marrow macrophages maintain hematopoietic stem cell (HSC) niches and their depletion mobilizes HSCs. Blood. 2010;116(23):4815-28.

356.	Chow A, Huggins M, Ahmed J, Hashimoto D, Lucas D, Kunisaki Y, et al. CD169(+) macrophages provide a niche promoting erythropoiesis under homeostasis and stress. Nature medicine. 2013;19(4):429-36.

357.	Ramos P, Casu C, Gardenghi S, Breda L, Crielaard BJ, Guy E, et al. Macrophages support pathological erythropoiesis in polycythemia vera and beta-thalassemia. Nature medicine. 2013;19(4):437-45.

358.	Casanova-Acebes M, Pitaval C, Weiss LA, Nombela-Arrieta C, Chevre R, N AG, et al. Rhythmic modulation of the hematopoietic niche through neutrophil clearance. Cell. 2013;153(5):1025-35.

359.	Gordy C, Pua H, Sempowski GD, He YW. Regulation of steady-state neutrophil homeostasis by macrophages. Blood. 2011;117(2):618-29.

360.	Zhao G, Yu R, Deng J, Zhao Q, Li Y, Joo M, et al. Pivotal role of reactive oxygen species in differential regulation of lipopolysaccharide-induced prostaglandins production in macrophages. Molecular pharmacology. 2013;83(1):167-78.

361.	Bustamante J, Arias AA, Vogt G, Picard C, Galicia LB, Prando C, et al. Germline CYBB mutations that selectively affect macrophages in kindreds with X-

linked predisposition to tuberculous mycobacterial disease. Nature immunology. 2011;12(3):213-21.

362.   Paliwal S, Chaudhuri R, Agrawal A, Mohanty S. Regenerative abilities of mesenchymal stem cells through mitochondrial transfer. Journal of Biomedical Science. 2018;25(1):31.

363.   Trendowski M, Zoino JN, Christen TD, Acquafondata C, Fondy TP. Preparation, In Vivo Administration, Dose-Limiting Toxicities, and Antineoplastic Activity of Cytochalasin B. Transl Oncol. 2015;8(4):308-17.

364.   Osswald M, Jung E, Sahm F, Solecki G, Venkataramani V, Blaes J, et al. Brain tumour cells interconnect to a functional and resistant network. Nature. 2015;528(7580):93-8.

365.   Juul MH, Rivedal E, Stokke T, Sanner T. Quantitative determination of gap junction intercellular communication using flow cytometric measurement of fluorescent dye transfer. Cell Adhes Commun. 2000;7(6):501-12.

366.   Connor KM, Subbaram S, Regan KJ, Nelson KK, Mazurkiewicz JE, Bartholomew PJ, et al. Mitochondrial H2O2 regulates the angiogenic phenotype via PTEN oxidation. J Biol Chem. 2005;280(17):16916-24.

367.   Covey TM, Edes K, Fitzpatrick FA. Akt activation by arachidonic acid metabolism occurs via oxidation and inactivation of PTEN tumor suppressor. Oncogene. 2007;26(39):5784-92.

368.   Kwon J, Lee S-R, Yang K-S, Ahn Y, Kim YJ, Stadtman ER, et al. Reversible oxidation and inactivation of the tumor suppressor PTEN in cells stimulated with peptide growth factors. Proceedings of the National Academy of Sciences of the United States of America. 2004;101(47):16419-24.

369.   Hemmings BA, Restuccia DF. PI3K-PKB/Akt pathway. Cold Spring Harb Perspect Biol. 2012;4(9):a011189-a.

370.   Alessi DR, James SR, Downes CP, Holmes AB, Gaffney PR, Reese CB, et al. Characterization of a 3-phosphoinositide-dependent protein kinase which phosphorylates and activates protein kinase Balpha. Curr Biol. 1997;7(4):261-9.

371.   Sarbassov DD, Guertin DA, Ali SM, Sabatini DM. Phosphorylation and regulation of Akt/PKB by the rictor-mTOR complex. Science. 2005;307(5712):1098-101.

372.   Feng J, Park J, Cron P, Hess D, Hemmings BA. Identification of a PKB/Akt hydrophobic motif Ser-473 kinase as DNA-dependent protein kinase. J Biol Chem. 2004;279(39):41189-96.

373.   Anderson NM, Mucka P, Kern JG, Feng H. The emerging role and targetability of the TCA cycle in cancer metabolism. Protein & Cell. 2018;9(2):216-37.

374.   Ito K, Ito K. Hematopoietic stem cell fate through metabolic control. Exp Hematol. 2018;64:1-11.

375.   Zu L, He J, Jiang H, Xu C, Pu S, Xu G. Bacterial Endotoxin Stimulates Adipose Lipolysis via Toll-Like Receptor 4 and Extracellular Signal-regulated Kinase Pathway. Journal of Biological Chemistry. 2009;284(9):5915-26.

376.   Farshtchi D, Lewis VJ. Effects of three bacterial infections on serum lipids of rabbits. J Bacteriol. 1968;95(5):1615-21.

377.   Henkin AH, Cohen AS, Dubikovskaya EA, Park HM, Nikitin GF, Auzias MG, et al. Real-time noninvasive imaging of fatty acid uptake in vivo. ACS Chem Biol. 2012;7(11):1884-91.

378.   Kruszynska YT, Stanley H, Sherratt A. Glucose kinetics during acute and chronic treatment of rats with 2[6(4-chloro-phenoxy) hexyl]oxirane-2-carboxylate, etomoxir. Biochemical Pharmacology. 1987;36(22):3917-21.

379.   Dai J, Liang K, Zhao S, Jia W, Liu Y, Wu H, et al. Chemoproteomics reveals baicalin activates hepatic CPT1 to ameliorate diet-induced obesity and hepatic steatosis. Proceedings of the National Academy of Sciences. 2018;115(26):E5896.

380.   Yao CH, Liu GY, Wang R, Moon SH, Gross RW, Patti GJ. Identifying off-target effects of etomoxir reveals that carnitine palmitoyltransferase I is essential for cancer cell proliferation independent of β-oxidation. PLoS Biol. 2018;16(3):e2003782.

381.   O'Connor RS, Guo L, Ghassemi S, Snyder NW, Worth AJ, Weng L, et al. The CPT1a inhibitor, etomoxir induces severe oxidative stress at commonly used concentrations. Scientific Reports. 2018;8(1):6289.

382.   World Health Organization. The top 10 causes of death 2020 [Available from: https://www.who.int/en/news-room/fact-sheets/detail/the-top-10-causes-of-death.

383.   Brinkmann V, Reichard U, Goosmann C, Fauler B, Uhlemann Y, Weiss DS, et al. Neutrophil extracellular traps kill bacteria. Science (New York, NY). 2004;303(5663):1532-5.

384.   Manz MG, Boettcher S. Emergency granulopoiesis. Nature reviews Immunology. 2014;14(5):302-14.

385.   Herault A, Binnewies M, Leong S, Calero-Nieto FJ, Zhang SY, Kang YA, et al. Myeloid progenitor cluster formation drives emergency and leukaemic myelopoiesis. Nature. 2017;544(7648):53-8.

386.   Boettcher S, Manz MG. Regulation of Inflammation- and Infection-Driven Hematopoiesis. Trends in immunology. 2017;38(5):345-57.

387.   Silberstein L, Goncalves KA, Kharchenko PV, Turcotte R, Kfoury Y, Mercier F, et al. Proximity-Based Differential Single-Cell Analysis of the Niche to Identify Stem/Progenitor Cell Regulators. Cell Stem Cell. 2016;19(4):530-43.

388.   Ziegler P, Boettcher S, Takizawa H, Manz MG, Brummendorf TH. LPS-stimulated human bone marrow stroma cells support myeloid cell development and progenitor cell maintenance. Annals of hematology. 2016;95(2):173-8.

389.   Papa L, Djedaini M, Hoffman R. Mitochondrial Role in Stemness and Differentiation of Hematopoietic Stem Cells. Stem Cells Int. 2019;2019:4067162-.

390.   Ito K, Hirao A, Arai F, Matsuoka S, Takubo K, Hamaguchi I, et al. Regulation of oxidative stress by ATM is required for self-renewal of haematopoietic stem cells. Nature. 2004;431(7011):997-1002.

391.   Yu WM, Liu X, Shen J, Jovanovic O, Pohl EE, Gerson SL, et al. Metabolic regulation by the mitochondrial phosphatase PTPMT1 is required for hematopoietic stem cell differentiation. Cell Stem Cell. 2013;12(1):62-74.

392.   Vannini N, Girotra M, Naveiras O, Nikitin G, Campos V, Giger S, et al. Specification of haematopoietic stem cell fate via modulation of mitochondrial activity. Nature Communications. 2016;7(1):13125.

393.   Pfeiffer T, Schuster S, Bonhoeffer S. Cooperation and competition in the evolution of ATP-producing pathways. Science. 2001;292(5516):504-7.

394.   Pasquier J, Guerrouahen BS, Al Thawadi H, Ghiabi P, Maleki M, Abu-Kaoud N, et al. Preferential transfer of mitochondria from endothelial to cancer cells through tunneling nanotubes modulates chemoresistance. J Transl Med. 2013;11:94.

395.   Marlein CR, Zaitseva L, Piddock RE, Raso-Barnett L, Scott MA, Ingham CJ, et al. PGC-1alpha driven mitochondrial biogenesis in stromal cells underpins mitochondrial trafficking to leukemic blasts. Leukemia. 2018;32(9):2073-7.

396.   Mohrin M, Widjaja A, Liu Y, Luo H, Chen D. The mitochondrial unfolded protein response is activated upon hematopoietic stem cell exit from quiescence. Aging Cell. 2018;17(3):e12756.

397.   Qian P, He XC, Paulson A, Li Z, Tao F, Perry JM, et al. The Dlk1-Gtl2 Locus Preserves LT-HSC Function by Inhibiting the PI3K-mTOR Pathway to Restrict Mitochondrial Metabolism. Cell Stem Cell. 2016;18(2):214-28.

398.   Chen C, Liu Y, Liu R, Ikenoue T, Guan KL, Liu Y, et al. TSC-mTOR maintains quiescence and function of hematopoietic stem cells by repressing mitochondrial biogenesis and reactive oxygen species. J Exp Med. 2008;205(10):2397-408.

399.   Mantel C, Messina-Graham S, Broxmeyer HE. Upregulation of nascent mitochondrial biogenesis in mouse hematopoietic stem cells parallels upregulation of

CD34 and loss of pluripotency: a potential strategy for reducing oxidative risk in stem cells. Cell Cycle. 2010;9(10):2008-17.

400.   Naka K, Muraguchi T, Hoshii T, Hirao A. Regulation of reactive oxygen species and genomic stability in hematopoietic stem cells. Antioxid Redox Signal. 2008;10(11):1883-94.

401.   Austin S, St-Pierre J. PGC1α and mitochondrial metabolism – emerging concepts and relevance in ageing and neurodegenerative disorders. Journal of Cell Science. 2012;125(21):4963-71.

402.   Virbasius JV, Scarpulla RC. Activation of the human mitochondrial transcription factor A gene by nuclear respiratory factors: a potential regulatory link between nuclear and mitochondrial gene expression in organelle biogenesis. Proc Natl Acad Sci U S A. 1994;91(4):1309-13.

403.   St-Pierre J, Lin J, Krauss S, Tarr PT, Yang R, Newgard CB, et al. Bioenergetic analysis of peroxisome proliferator-activated receptor gamma coactivators 1alpha and 1beta (PGC-1alpha and PGC-1beta) in muscle cells. J Biol Chem. 2003;278(29):26597-603.

404.   Valle I, Álvarez-Barrientos A, Arza E, Lamas S, Monsalve M. PGC-1α regulates the mitochondrial antioxidant defense system in vascular endothelial cells. Cardiovascular Research. 2005;66(3):562-73.

405.   St-Pierre J, Drori S, Uldry M, Silvaggi JM, Rhee J, Jäger S, et al. Suppression of reactive oxygen species and neurodegeneration by the PGC-1 transcriptional coactivators. Cell. 2006;127(2):397-408.

406.   García-García A, de Castillejo CLF, Méndez-Ferrer S. BMSCs and hematopoiesis. Immunology Letters. 2015;168(2):129-35.

407.   Burt R, Dey A, Aref S, Aguiar M, Akarca A, Bailey K, et al. Activated stromal cells transfer mitochondria to rescue acute lymphoblastic leukemia cells from oxidative stress. Blood. 2019;134(17):1415-29.

408.   Marlein CR, Zaitseva L, Piddock RE, Raso-Barnett L, Scott MA, Ingham CJ, et al. PGC-1α driven mitochondrial biogenesis in stromal cells underpins mitochondrial trafficking to leukemic blasts. Leukemia. 2018;32(9):2073-7.

409.   Sareila O, Kelkka T, Pizzolla A, Hultqvist M, Holmdahl R. NOX2 complex-derived ROS as immune regulators. Antioxid Redox Signal. 2011;15(8):2197-208.

410.   Lau AT, Wang Y, Chiu JF. Reactive oxygen species: current knowledge and applications in cancer research and therapeutic. J Cell Biochem. 2008;104(2):657-67.

411.   Leto TL, Morand S, Hurt D, Ueyama T. Targeting and regulation of reactive oxygen species generation by Nox family NADPH oxidases. Antioxid Redox Signal. 2009;11(10):2607-19.

412.   Boots AW, Hristova M, Kasahara DI, Haenen GR, Bast A, van der Vliet A. ATP-mediated activation of the NADPH oxidase DUOX1 mediates airway epithelial responses to bacterial stimuli. J Biol Chem. 2009;284(26):17858-67.

413.   Mo Y, Wan R, Chien S, Tollerud DJ, Zhang Q. Activation of endothelial cells after exposure to ambient ultrafine particles: the role of NADPH oxidase. Toxicol Appl Pharmacol. 2009;236(2):183-93.

414.   Kwak H-J, Liu P, Bajrami B, Xu Y, Park S-Y, Nombela-Arrieta C, et al. Myeloid cell-derived reactive oxygen species externally regulate the proliferation of myeloid progenitors in emergency granulopoiesis. Immunity. 2015;42(1):159-71.

415.   Arango Duque G, Descoteaux A. Macrophage cytokines: involvement in immunity and infectious diseases. Front Immunol. 2014;5:491-.

416.   Christopher MJ, Rao M, Liu F, Woloszynek JR, Link DC. Expression of the G-CSF receptor in monocytic cells is sufficient to mediate hematopoietic progenitor mobilization by G-CSF in mice. The Journal of experimental medicine. 2011;208(2):251-60.

417.   Ludin A, Itkin T, Gur-Cohen S, Mildner A, Shezen E, Golan K, et al. Monocytes-macrophages that express α-smooth muscle actin preserve primitive hematopoietic cells in the bone marrow. Nature immunology. 2012;13:1072.

418.   Lou E, Fujisawa S, Morozov A, Barlas A, Romin Y, Dogan Y, et al. Tunneling nanotubes provide a unique conduit for intercellular transfer of cellular contents in human malignant pleural mesothelioma. PLoS One. 2012;7(3):e33093.

419.   Lu J, Zheng X, Li F, Yu Y, Chen Z, Liu Z, et al. Tunneling nanotubes promote intercellular mitochondria transfer followed by increased invasiveness in bladder cancer cells. Oncotarget. 2017;8(9):15539-52.

420.   Scadden DT. Nice neighborhood: emerging concepts of the stem cell niche. Cell. 2014;157(1):41-50.

421.   Wang J, Liu X, Qiu Y, Shi Y, Cai J, Wang B, et al. Cell adhesion-mediated mitochondria transfer contributes to mesenchymal stem cell-induced chemoresistance on T cell acute lymphoblastic leukemia cells. J Hematol Oncol. 2018;11(1):11.

422.   Sun Q, Zhong W, Zhang W, Zhou Z. Defect of mitochondrial respiratory chain is a mechanism of ROS overproduction in a rat model of alcoholic liver disease: role of zinc deficiency. Am J Physiol Gastrointest Liver Physiol. 2016;310(3):G205-14.

423.   Liu P, Cheng H, Roberts TM, Zhao JJ. Targeting the phosphoinositide 3-kinase pathway in cancer. Nat Rev Drug Discov. 2009;8(8):627-44.

424.   Ito Y, Hart JR, Ueno L, Vogt PK. Oncogenic activity of the regulatory subunit p85β of phosphatidylinositol 3-kinase (PI3K). Proceedings of the National Academy of Sciences. 2014;111(47):16826-9.

425.   Hawkins PT, Davidson K, Stephens LR. The role of PI3Ks in the regulation of the neutrophil NADPH oxidase. Biochem Soc Symp. 2007(74):59-67.

426.   Furman RR, Sharman JP, Coutre SE, Cheson BD, Pagel JM, Hillmen P, et al. Idelalisib and rituximab in relapsed chronic lymphocytic leukemia. N Engl J Med. 2014;370(11):997-1007.

427.   ClinicalTrial.gov. Dose Escalation Study of CAL-101 in Select Relapsed or Refractory Hematologic Malignancies 2020 [Available from: https://clinicaltrials.gov/ct2/show/NCT00710528.

428.   Nakada D, Saunders TL, Morrison SJ. Lkb1 regulates cell cycle and energy metabolism in haematopoietic stem cells. Nature. 2010;468(7324):653-8.

429.   Takubo K, Goda N, Yamada W, Iriuchishima H, Ikeda E, Kubota Y, et al. Regulation of the HIF-1alpha level is essential for hematopoietic stem cells. Cell Stem Cell. 2010;7(3):391-402.

430.   Gan B, Hu J, Jiang S, Liu Y, Sahin E, Zhuang L, et al. Lkb1 regulates quiescence and metabolic homeostasis of haematopoietic stem cells. Nature. 2010;468(7324):701-4.

431.   Gurumurthy S, Xie SZ, Alagesan B, Kim J, Yusuf RZ, Saez B, et al. The Lkb1 metabolic sensor maintains haematopoietic stem cell survival. Nature. 2010;468(7324):659-63.

432.   Desvergne B, Michalik L, Wahli W. Transcriptional regulation of metabolism. Physiol Rev. 2006;86(2):465-514.

433.   Zaid H, Antonescu CN, Randhawa VK, Klip A. Insulin action on glucose transporters through molecular switches, tracks and tethers. Biochem J. 2008;413(2):201-15.

434.   Silveira LR, Fiamoncini J, Hirabara SM, Procópio J, Cambiaghi TD, Pinheiro CH, et al. Updating the effects of fatty acids on skeletal muscle. J Cell Physiol. 2008;217(1):1-12.

435.   Prentki M, Madiraju SR. Glycerolipid metabolism and signaling in health and disease. Endocr Rev. 2008;29(6):647-76.

436. Schroeder F, Petrescu AD, Huang H, Atshaves BP, McIntosh AL, Martin GG, et al. Role of fatty acid binding proteins and long chain fatty acids in modulating nuclear receptors and gene transcription. Lipids. 2008;43(1):1-17.

437. Yang J, Sambandam N, Han X, Gross RW, Courtois M, Kovacs A, et al. CD36 deficiency rescues lipotoxic cardiomyopathy. Circ Res. 2007;100(8):1208-17.

438. Madrazo JA, Kelly DP. The PPAR trio: regulators of myocardial energy metabolism in health and disease. J Mol Cell Cardiol. 2008;44(6):968-75.

439. Nahlé Z, Hsieh M, Pietka T, Coburn CT, Grimaldi PA, Zhang MQ, et al. CD36-dependent regulation of muscle FoxO1 and PDK4 in the PPAR delta/beta-mediated adaptation to metabolic stress. J Biol Chem. 2008;283(21):14317-26.

440. Gross DN, van den Heuvel AP, Birnbaum MJ. The role of FoxO in the regulation of metabolism. Oncogene. 2008;27(16):2320-36.

441. Su X, Abumrad NA. Cellular fatty acid uptake: a pathway under construction. Trends in endocrinology and metabolism: TEM. 2009;20(2):72-7.

442. Ladanyi A, Mukherjee A, Kenny HA, Johnson A, Mitra AK, Sundaresan S, et al. Adipocyte-induced CD36 expression drives ovarian cancer progression and metastasis. Oncogene. 2018;37(17):2285-301.

443. Liu Y. Fatty acid oxidation is a dominant bioenergetic pathway in prostate cancer. Prostate Cancer Prostatic Dis. 2006;9(3):230-4.

444. Schafer ZT, Grassian AR, Song L, Jiang Z, Gerhart-Hines Z, Irie HY, et al. Antioxidant and oncogene rescue of metabolic defects caused by loss of matrix attachment. Nature. 2009;461(7260):109-13.

445. Takakuwa T, Nakashima Y, Koh H, Nakane T, Nakamae H, Hino M. Short-Term Fasting Induces Cell Cycle Arrest in Immature Hematopoietic Cells and Increases the Number of Naïve T Cells in the Bone Marrow of Mice. Acta Haematol. 2019;141(3):189-98.

446. Tiwari SK, Toshniwal AG, Mandal S, Mandal L. Fatty acid β-oxidation is required for the differentiation of larval hematopoietic progenitors in Drosophila. Elife. 2020;9.

447. Ryall JG, Dell'Orso S, Derfoul A, Juan A, Zare H, Feng X, et al. The NAD(+)-dependent SIRT1 deacetylase translates a metabolic switch into regulatory epigenetics in skeletal muscle stem cells. Cell Stem Cell. 2015;16(2):171-83.

448. Wong BW, Wang X, Zecchin A, Thienpont B, Cornelissen I, Kalucka J, et al. The role of fatty acid β-oxidation in lymphangiogenesis. Nature. 2017;542(7639):49-54.

449. Chen L, Vasoya RP, Toke NH, Parthasarathy A, Luo S, Chiles E, et al. HNF4 Regulates Fatty Acid Oxidation and Is Required for Renewal of Intestinal Stem Cells in Mice. Gastroenterology. 2020;158(4):985-99.e9.

450. Knobloch M, Pilz G-A, Ghesquière B, Kovacs WJ, Wegleiter T, Moore DL, et al. A Fatty Acid Oxidation-Dependent Metabolic Shift Regulates Adult Neural Stem Cell Activity. Cell Rep. 2017;20(9):2144-55.

451. Kunau W-H, Dommes V, Schulz H. β-Oxidation of fatty acids in mitochondria, peroxisomes, and bacteria: A century of continued progress. Progress in Lipid Research. 1995;34(4):267-342.

452. Febbraio M, Hajjar DP, Silverstein RL. CD36: a class B scavenger receptor involved in angiogenesis, atherosclerosis, inflammation, and lipid metabolism. The Journal of Clinical Investigation. 2001;108(6):785-91.

453. Christiaens V, Van Hul M, Lijnen HR, Scroyen I. CD36 promotes adipocyte differentiation and adipogenesis. Biochimica et Biophysica Acta (BBA) - General Subjects. 2012;1820(7):949-56.

454. Abumrad NA, el-Maghrabi MR, Amri EZ, Lopez E, Grimaldi PA. Cloning of a rat adipocyte membrane protein implicated in binding or transport of long-chain fatty acids that is induced during preadipocyte differentiation. Homology with human CD36. The Journal of biological chemistry. 1993;268(24):17665-8.

455.   Endemann G, Stanton LW, Madden KS, Bryant CM, White RT, Protter AA. CD36 is a receptor for oxidized low density lipoprotein. The Journal of biological chemistry. 1993;268(16):11811-6.

456.   Zhou J, Febbraio M, Wada T, Zhai Y, Kuruba R, He J, et al. Hepatic fatty acid transporter Cd36 is a common target of LXR, PXR, and PPARgamma in promoting steatosis. Gastroenterology. 2008;134(2):556-67.

457.   Ma X, Bacci S, Mlynarski W, Gottardo L, Soccio T, Menzaghi C, et al. A common haplotype at the CD36 locus is associated with high free fatty acid levels and increased cardiovascular risk in Caucasians. Hum Mol Genet. 2004;13(19):2197-205.

458.   Love-Gregory L, Sherva R, Sun L, Wasson J, Schappe T, Doria A, et al. Variants in the CD36 gene associate with the metabolic syndrome and high-density lipoprotein cholesterol. Hum Mol Genet. 2008;17(11):1695-704.

459.   Poon EN-Y, Luo X-l, Webb SE, Yan B, Zhao R, Wu SCM, et al. The cell surface marker CD36 selectively identifies matured, mitochondria-rich hPSC-cardiomyocytes. Cell Research. 2020;30(7):626-9.

460.   Stuart LM, Deng J, Silver JM, Takahashi K, Tseng AA, Hennessy EJ, et al. Response to Staphylococcus aureus requires CD36-mediated phagocytosis triggered by the COOH-terminal cytoplasmic domain. Journal of Cell Biology. 2005;170(3):477-85.

461.   Simard JR, Pillai BK, Hamilton JA. Fatty acid flip-flop in a model membrane is faster than desorption into the aqueous phase. Biochemistry. 2008;47(35):9081-9.

462.   Schwenk RW, Luiken JJ, Bonen A, Glatz JF. Regulation of sarcolemmal glucose and fatty acid transporters in cardiac disease. Cardiovasc Res. 2008;79(2):249-58.

463.   Ehehalt R, Füllekrug J, Pohl J, Ring A, Herrmann T, Stremmel W. Translocation of long chain fatty acids across the plasma membrane--lipid rafts and fatty acid transport proteins. Mol Cell Biochem. 2006;284(1-2):135-40.

464.   Stump DD, Zhou SL, Berk PD. Comparison of plasma membrane FABP and mitochondrial isoform of aspartate aminotransferase from rat liver. Am J Physiol. 1993;265(5 Pt 1):G894-902.

465.   Umemoto T, Hashimoto M, Matsumura T, Nakamura-Ishizu A, Suda T. Ca(2+)-mitochondria axis drives cell division in hematopoietic stem cells. J Exp Med. 2018;215(8):2097-113.

466.   Moerman EJ, Teng K, Lipschitz DA, Lecka-Czernik B. Aging activates adipogenic and suppresses osteogenic programs in mesenchymal marrow stroma/stem cells: the role of PPAR-γ2 transcription factor and TGF-β/BMP signaling pathways. Aging Cell. 2004;3(6):379-89.

467.   Bluher M. Adipose tissue inflammation: a cause or consequence of obesity-related insulin resistance? Clin Sci (Lond). 2016;130(18):1603-14.

468.   Ambrosi TH, Scialdone A, Graja A, Gohlke S, Jank A-M, Bocian C, et al. Adipocyte Accumulation in the Bone Marrow during Obesity and Aging Impairs Stem Cell-Based Hematopoietic and Bone Regeneration. Cell Stem Cell. 2017;20(6):771-84.e6.

469.   Zhang K, Wang C, Chen Y, Ji X, Chen X, Tian L, et al. Preservation of high-fat diet-induced femoral trabecular bone loss through genetic target of TNF-alpha. Endocrine. 2015;50(1):239-49.

470.   Caers J, Deleu S, Belaid Z, De Raeve H, Van Valckenborgh E, De Bruyne E, et al. Neighboring adipocytes participate in the bone marrow microenvironment of multiple myeloma cells. Leukemia. 2007;21(7):1580-4.

471.   Gazi E, Gardner P, Lockyer NP, Hart CA, Brown MD, Clarke NW. Direct evidence of lipid translocation between adipocytes and prostate cancer cells with imaging FTIR microspectroscopy. J Lipid Res. 2007;48(8):1846-56.

8   Appendix

Table 8.1. KiCqStart® SybrGreen Primers used in qPCR analysis.

Gene Name	Forward Primer 5'-3'	Reverse Primer 5'-3'
GAPDH	CTTTTGCGTCGCCAG	TTGATGGCAACAATATCCAC
PGC1a	TCCTCTTCAAGATCCTGTTAC	CACATACAAGGGAGAATTGC
PGC1b	AAGAACTTCAGACGTGAGAG	TCAAAGCGCTTCTTTAGTTC
TFAM	GACCTCGTTCAGCATATAAC	ACAAGCTTCAATTTTCCCTG
NRF1	AAACAAAGGGTTTCATGGAC	GGTACGAGTGAGCTATACTG
NRF2	GAGATAGTTACCATTGACCAG	GACCATTGTTTCCTGTTCTG
tfb1m	TTTACAATCCCAGGAAAAGC	GAATAACATTCCAAGCCCTC
tfb2m	TTAGAAAAGTCAAAGCACGG	GTACTCAGTGAACGTAAATGG
DNM1l	GATTCAATCCGTGATGAGTATG	TAAGTAACCTATTCAGGGTCC
Opa1	CATGGATCTGAAAGTGACAAG	AAGATTTCTTGAGCTTCCTG
MFN1	AACTCCAGAAAGCATAAAGC	TGAAACTCCTGTAATCTTGC
MFN2	GTCATACCACCAATTGCTTC	TCACAGTCTTGACACTCTTC
Slc27a1	CAAGTACAATTGCACGGTAG	GTGAACTCCTCCCAGATG
Slc27a2	AAGAAGTGAATGTGTATGGC	GTTTTCTTTGATCTTGAGGGAG
Slc27a4	CTCAGCTATCTGTGAGATCC	GAGCTTATCGTTAAAACCCTTG
Slc27a5	CTTGTATGTGGGTGAAATCC	CACATAGTTCATTAAGCCCAC
Fabp1	AAATCAAACTCACCATCACC	GATTGTGTCTCCATTGAGTTC
Fabp3	AAACTCATCCTGACTCTCAC	AAAATGTCAGAGGGGAAAAC
Fabp4	GTAAATGGGGATTTGGTCAC	TATGATGCTCTTCACCTTCC
Fabp5	ATGAAAGAGCTAGGAGTAGG	TACAAGAGAACACAGTCGTC
CD36	CATTTGCAGGTCTATCTACG	CAATGTCTAGCACACCATAAG
Msr1	GCGGATCAAGATCACTATAAC	GGTGAAAGGTCTTTTAAGGAG
LDLR	CATCTTCTTCCCTATTGCAC	ATGCTGTTGATGTTCTTCAG
CPT1A	GGGAGGAATACATCTACCTG	GAAGACGAATAGGTTTGAGTTC

Table 8.2. Taqman® assays used for mouse and human mtDNA assessment.

| Taqman® assay	Target Gene	Fluorophore	Assay Specifics
Human mtDNA	ND1	FAM	Hs02596873_S1 ND1
Mouse mtDNA	ND1	VIC	Mm04225274_S1 ND1
Human gDNA	Telomerase reverse transcriptase (TERT)	VIC	Taqman® copy number reference assay human
Mouse gDNA	Telomerase reverse transcriptase (TERT)	VIC	Taqman® copy number reference assay human
Custom TaqMan® COX3 Assay	COX3_9348snp	VIC/FAM	ANNKVUR
Custom TaqMan® ND3 Assay	ND3_9461snp	VIC/FAM	ANPRPEN

Table 8.3. Life technologies Primers used in PCR analysis.

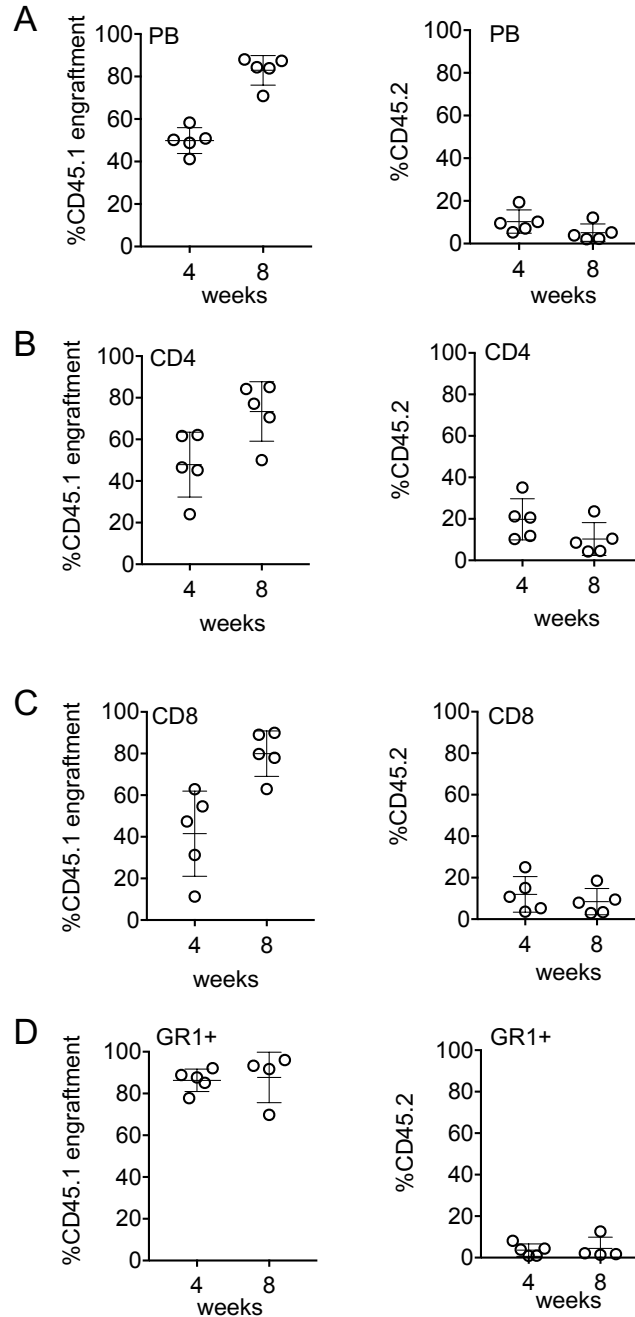| Target	Forward Primer	Reverse Primer
COX3 and ND3_1	GGCTACTGGATTCCATGGACTCC	TGTGTTCATTCATATGCTAGGCCT
COX3 and ND3_2	TGGTTCTACATTCTTCATGGCTACTGG	TTTTGTGTTCATTCATATGCTAGGCCT
ND4_1	ACACTTCTATGACAAACCGACGAA	GGAGCTTCAACATGGGCTTTTGG
ND4_2	AACCAGCCTAACACTTCTATGACAA	GCAATTGGAGCTTCAACATGGGC
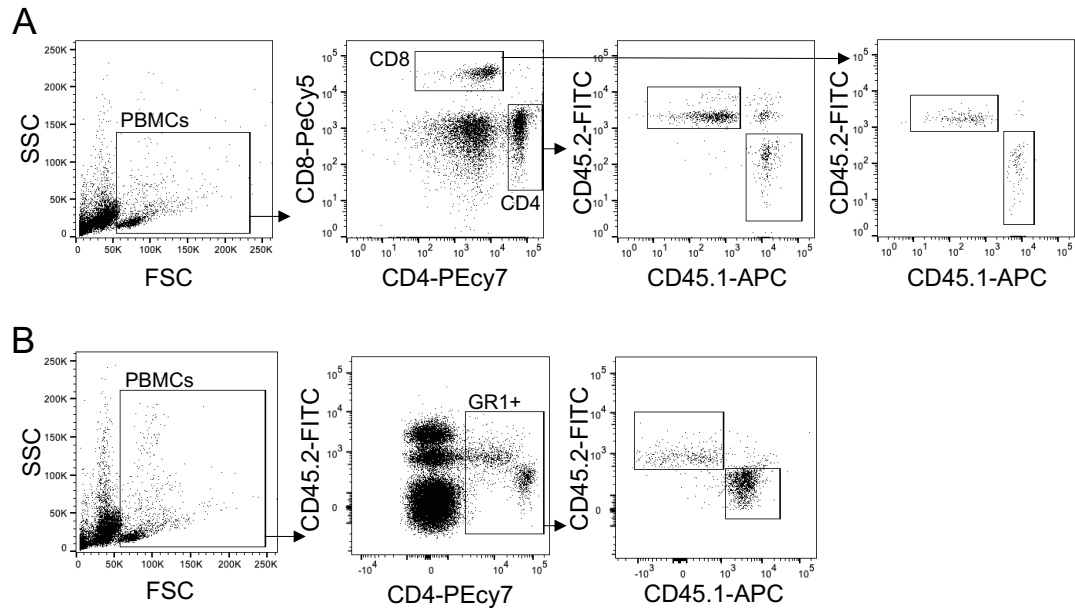
Figure 8.1. Gating strategy for CD4, CD8 and GR1 positive cells.
C57BL/6J mice were treated with 25 mg/kg busulfan for 3 days prior to tail-vein injections of PepcBoy lineage negative, CD117 positive donor cells. The peripheral blood was monitored at 4 weeks and 8 weeks after transplantation and assessed by flow cytometry. (A) The gating strategy for CD4 and CD8 cells is shown. (B) The gating strategy for GR1+ cells is shown.
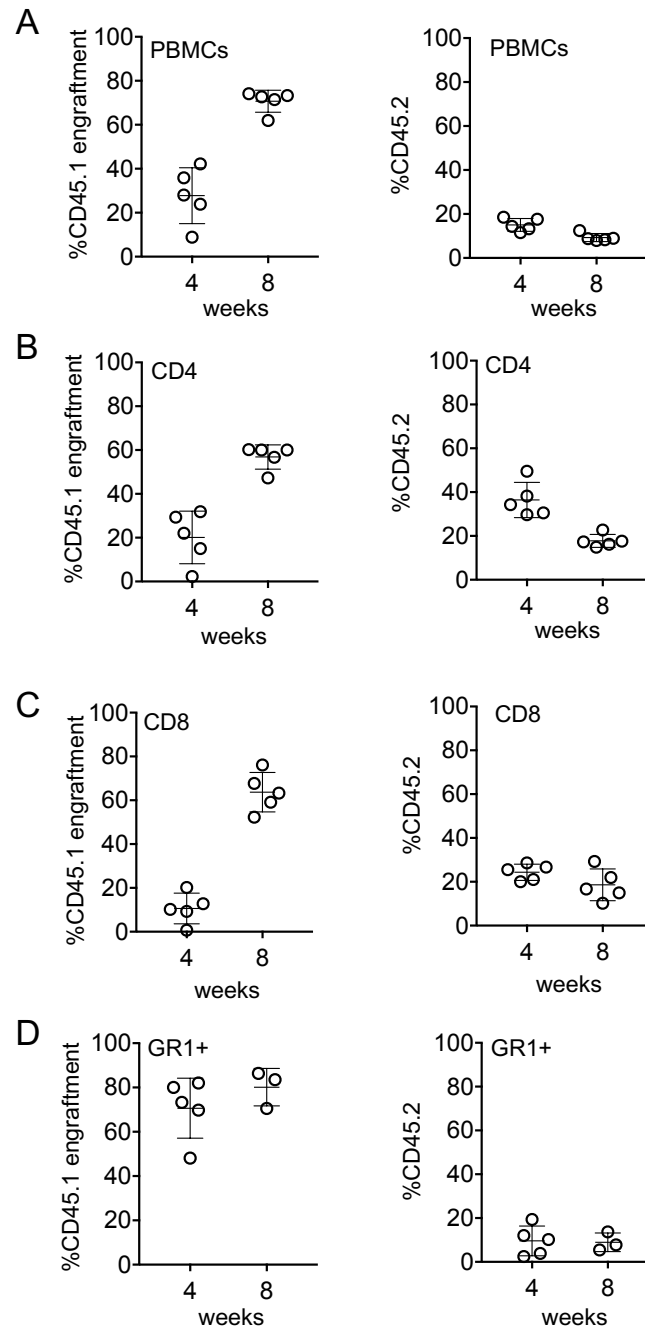
Figure 8.2. CD45.1 engraftment in the peripheral blood of CD45.2 C57BL/6J animals.

C57BL/6J mice were treated with 25 mg/kg busulfan for 3 days prior to tail-vein injections of PepcBoy lineage negative, CD117 positive donor cells. The peripheral blood was monitored at 4 weeks and 8 weeks after transplantation and assessed by flow cytometry. (A) Engraftment was determined by percentage of CD45.1-APC expression on the lymphocytes in the peripheral blood (PB) detected by flow cytometry analysis. Percentage of CD45.2-FITC expressing lymphocytes in the PB. (B) Percentage of CD45.1-APC positive cells in the CD4-PeCy7 positive population. Percentage of CD45.2-FITC positive cells in the CD4-PeCy7 positive population. (C) Percentage of CD45.1-APC positive cells in the CD8-PeCy5 positive population. Percentage of CD45.2-FITC positive cells in the CD8-PeCy5 positive population. (D) Percentage of CD45.1-APC positive cells in the GR1-PeCy5 positive population. Percentage of CD45.2-FITC positive cells in the GR1-PeCy5 positive population.

Figure 8.3. CD45.1 engraftment in the peripheral blood of CD45.2 CD36$^{-/-}$ animals.

CD36$^{-/-}$ mice were treated with 25 mg/kg busulfan for 3 days prior to tail-vein injections of PepcBoy lineage negative, CD117 positive donor cells. The peripheral blood was monitored at 4 weeks and 8 weeks after transplantation and assessed by flow cytometry. (A) Engraftment was determined by percentage of CD45.1-APC expression on the lymphocytes in the peripheral blood (PB) detected by flow cytometry analysis. Percentage of CD45.2-FITC expressing lymphocytes in the PB. (B) Percentage of CD45.1-APC positive cells in the CD4-PeCy7 positive population. Percentage of CD45.2-FITC positive cells in the CD4-PeCy7 positive population. (C) Percentage of CD45.1-APC positive cells in the CD8-PeCy5 positive population. Percentage of CD45.2-FITC positive cells in the CD8-PeCy5 positive population. (D) Percentage of CD45.1-APC positive cells in the GR1-PeCy5 positive population. Percentage of CD45.2-FITC positive cells in the GR1-PeCy5 positive population.